Distribution Agreement

In presenting this thesis or dissertation as a partial fulfillment of the requirements for an advanced degree from Emory University, I hereby grant to Emory University and its agents the non-exclusive license to archive, make accessible, and display my thesis or dissertation in whole or in part in all forms of media, now or hereafter known, including display on the world wide web. I understand that I may select some access restrictions as part of the online submission of this thesis or dissertation. I retain all ownership rights to the copyright of the thesis or dissertation. I also retain the right to use in future works (such as articles or books) all or part of this thesis or dissertation.

Signature:

_____ _____

Jennifer K. Truong Date

ROLES FOR BILE TRANSPORTERS IN THE PATHOGENESIS AND TREATMENT OF LIVER AND INTESTINAL DISEASES

By

Jennifer K. Truong
Doctor of Philosophy

Graduate Division of Biological and Biomedical Science
Biochemistry, Cell and Developmental Biology

_____
Paul A. Dawson, PhD
Advisor

_____
Michael H. Koval, PhD
Committee Member

_____
Jennifer Q. Kwong, PhD
Committee Member

_____
Andrew S. Neish, MD
Committee Member

_____
Eric A. Ortlund, PhD
Committee Member

Accepted:

_____ _____
Kimberly J. Arriola, MPH, PhD
Dean of the James T. Laney School of Graduate Studies

_____
Date

ROLES FOR BILE TRANSPORTERS IN THE PATHOGENESIS AND TREATMENT OF LIVER AND INTESTINAL DISEASES

By

Jennifer K. Truong

B.S., Boston College, 2014

Advisor: Paul A. Dawson, PhD

An abstract of

A dissertation submitted to the faculty of the

James T. Laney School of Graduate Studies of Emory University

in partial fulfillment of the requirements for the degree of

Doctor of Philosophy

In Graduate Division of Biological and Biomedical Science

Biochemistry, Cell and Developmental Biology

2022

Abstract

ROLES FOR BILE TRANSPORTERS IN THE PATHOGENESIS AND TREATMENT OF LIVER AND INTESTINAL DISEASES

By Jennifer K. Truong

The detergent properties of bile acids (BAs) are essential to facilitate dietary fat digestion and absorption. However, BAs are also important for cholesterol homeostasis, hepatic bile formation, biliary lipid excretion, and as signaling molecules to regulate lipid and glucose metabolism. Disruption of BA enterohepatic cycling and signaling is associated with the pathogenesis or progression of liver, gastrointestinal and metabolic diseases. Conversely, novel treatments targeting BA transport and signaling represent new therapeutic opportunities for those disorders. In the studies that follow we used cell-based and knockout mouse models to investigate the relationship of BA hydrophobicity and BA-associated injury, and to elucidate the therapeutic mechanism of actions of the cholehepatic drug *nor*Ursodeoxycholic acid (*nor*UDCA) and BA enterohepatic circulation blockers. The BA pool is more hydrophilic and cytoprotective in mice versus humans, partially limiting translational of findings in mouse model to hydrophobic BA-associated injury in patients. We generated mice lacking *Cyp2c70*, the murine liver enzyme responsible for the synthesis of 6-hydroxylated hydrophilic BAs. We show that *Cyp2c70* KO mice have a more human-like hydrophobic BA pool composition and develop cholestatic liver disease. The liver disease in *Cyp2c70* KO mice can be effectively treated using an ileal apical sodium-dependent BA transporter inhibitor, which reduced the total hepatic BA burden. The bile acid analog, *no*rUrsodeoxycholic acid (*nor*UDCA) is in late-stage clinical development to treat liver disease. However, the molecular mechanisms responsible for its potent therapeutic ability to induce a protective bicarbonate-rich bile flow (hypercholeresis) had not been identified. We show that *nor*UDCA-stimulation of bile flow does not require the major BA transporters, and *nor*UDCA directly stimulates the Ca^{2+}-activated Cl^- channel TMEM16A to induce biliary bicarbonate secretion. The hepatocellular damage by cytotoxic BAs is a primary contributor to the pathogenesis of cholestatic liver injury. However, less is known about the response of other tissues to cytotoxic BAs. We explored the consequences of BA accumulation in an *Ostα* KO mouse model of intestinal BA stasis and used BA-based therapies to investigate the mechanisms of ileal injury. These studies collectively provide additional mechanistic understanding of BA's role in the pathogenesis and treatment of hepatobiliary and gastrointestinal disease.

ROLES FOR BILE TRANSPORTERS IN THE PATHOGENESIS AND TREATMENT OF LIVER AND INTESTINAL DISEASES

By

Jennifer K. Truong

B.S., Boston College, 2014

Advisor: Paul A. Dawson, PhD

A dissertation submitted to the Faculty of the

James T. Laney School of Graduate Studies of Emory University

in partial fulfillment of the requirements for the degree of

Doctor of Philosophy

In Graduate Division of Biological and Biomedical Science

Biochemistry, Cell and Developmental Biology

2022

Acknowledgements

I would first like to thank Dr. Paul Dawson for his guidance, patience, and mentorship throughout my graduate studies. I never expected to do my Ph.D. on bile acids, but after my rotation, it was abundantly clear an opportunity to learn and train with Paul would be invaluable to my development as a scientist. I had a "non-traditional path" in academia, and I am unequivocally appreciative of Paul's support throughout my science exploration (even if it meant a short hiatus from bile acids). I hope that throughout my career I continue to hold myself, and others I mentor, to the same high standards with the kindness Paul has shown me the past four years. I would also like to thank Dr. Saul Karpen, who has largely contributed and provided support throughout my studies, and all the members of the lab for their comradely and love of desserts (special shout out to Anu, Caroline, Jianing, Ashley and Kim for all the mice and emotional support during my research). Thank you to my thesis committee members: Dr. Mike Koval, Dr. Jen Kwong, Dr. Andrew Neish, and Dr. Eric Ortlund who helped guide my research during the time of COVID isolation and virtual interaction.

I would not be here without the sacrifice of my parents, who immigrated to the United States to give me a better education; this degree is for all of us. I have been incredibly lucky to have crossed paths with countless mentors from Collegiate Directions Inc., Boston College and Mitobridge who have helped me improve as a scientist and more importantly, become a better person. Thank you to Matt, Eric, Kal, and Domi who have written numerous support letters and encouraged me to pursue (and stay in) graduate school, especially during the times I thought I could not do it.

Many thanks to my friends and loved ones who have been there through it all with me. Kim and Jacky who have been the best long-distance support (and therapists) for the past decade.

Chris, thank you for reminding me to always find the positives and to be a life-long learner. Dr. Maria and Dr. Jesse who have listened, cried and ate through Atlanta with me the past 4 years – I truly would not have made it through without both of you and I am looking forward to our future reunions.

Finally, my deepest gratitude goes to any and everyone who has shared a drink with me at the bar after a rough day in lab and made everything leading up to this possible. Cheers to bile acids!

TABLE OF CONTENTS

TABLE OF FIGURES

TABLE OF TABLES

Chapter 1: Introduction to Bile Acid Metabolism and Scope of Dissertation

This chapter is adapted from below with permission from Elsevier Science:

Truong, J. K., & Dawson, P.A. (2021) Bile Acid Metabolism. In N. Ridgway & R. McLeod (Eds). *Biochemistry of Lipids, Lipoproteins and Membranes* (pp. 395-428). Elsevier Science.

Abbreviations

ASBT: Apical sodium-dependent bile acid transporter

ABC: ATP binding cassette

AKR1C2: Aldo-keto reductase 1C2 (AKR1C2; 3α-hydroxysteroid dehydrogenase)

AKR1C4: Aldo-keto reductase 1C4 (AKR1C4; 3α-hydroxysteroid dehydrogenase)

AKR1D1: Aldo-keto reductase 1D1 (AKR1D1; Δ4-3-oxosteroid 5β-reductase)

BAAT: Bile acid: amino acid *N*-acyltransferase

BSEP: Bile salt export pump

CAR: Constitutive androsterone receptor

CMC: Critical micellar concentration

CREB: cAMP response element-binding protein

CTX: Cerebrotendinous xanthomatosis

CYP27A1: Sterol 27-hydroxylase

CYP46A1: Cholesterol 24-hydroxylase

CYP7A1: Cholesterol 7α-hydroxylase

CYP7B1: Oxysterol 7α-hydroxylase

CYP8B1: Sterol 12α-hydroxylase

FATP5: Fatty acid transport protein 5 (SLC27A5)

FXR: Farnesoid X receptor

GLP-1: Glucagon-like peptide-1

HSD3B7: 3β-Hydroxy-Δ5-C27-steroid oxidoreductase

IBABP: Ileal bile acid binding protein

MRP: Multidrug resistance protein

NTCP: Na^+-taurocholate-cotransporting polypeptide

OATP: Organic anion transporting polypeptide

OST: Organic solute transporter

PXR: Pregnane X receptor

VDR: Vitamin D receptor

Introduction

Bile acids have long captured the interest of chemists and biochemists. Over the past 200 years, much has been learnt regarding the structure, physical properties, metabolism and function of these essential detergents and signalling molecules. Bile acids are stable and indigestible molecules that perform a variety of indispensable functions in the liver and gastrointestinal tract. Although best known for their ability to form micelles and facilitate absorption of lipids in the gut, the physiological functions of bile acids extend well beyond their role as simple detergents. The major functions of bile acids include: (1) inducing bile flow and hepatic secretion of biliary lipids (phospholipid and cholesterol); (2) digestion and absorption of dietary fats, cholesterol and fat-soluble vitamins; (3) regulation of cholesterol homoeostasis; (4) signaling via nuclear and G-protein-coupled receptors to regulate bile acid, lipid and energy homeostasis; and (5) regulating the composition of the gut microbiome.

Bile acids are amphipathic compounds possessing a characteristic four-ring perhydrocyclopentanophenanthrene nucleus and a carbon side chain attached to the D ring (Figure 1). Synthesis of bile acid from cholesterol is an evolutionarily conserved biological process in vertebrates and functions to convert cholesterol, a hydrophobic membrane lipid into water-soluble derivatives that are excreted into bile (1). As a group, these molecules are called ‘bile salts’ or ‘bile acids’ and are included in the ST category (sterol lipids: bile acids and derivatives) in the LIPID MAPS Lipid comprehensive classification system (http://www.lipidmaps.org/). In nature, bile salts consist mainly of sulphate conjugates of bile alcohols and of taurine (or glycine) amino-acyl amidated conjugates of bile acids (2, 3). Conjugation with these hydrophilic moieties yields molecules that are membrane-impermeable, an essential property that allows bile salts to be concentrated in bile and maintained at high

concentration in the lumen of the small intestine. Most bile salts can be assigned to one of three general classes, based on the type of terminal polar group (alcohol vs acid) and the length of their side chain (27-carbon vs 24-carbon). The three major classes are 27-carbon (C-27) bile alcohols, C-27 bile acids and 24-carbon (C-24) bile acids. The general structure of their steroid nucleus, side chain and position of their hydroxyl groups are shown in Figure 1. This chapter focuses on C-24 bile acids (with a five carbon side chain and carboxyl group at the C-24 position), which are the predominant form of bile salts in humans and most mammals (4).

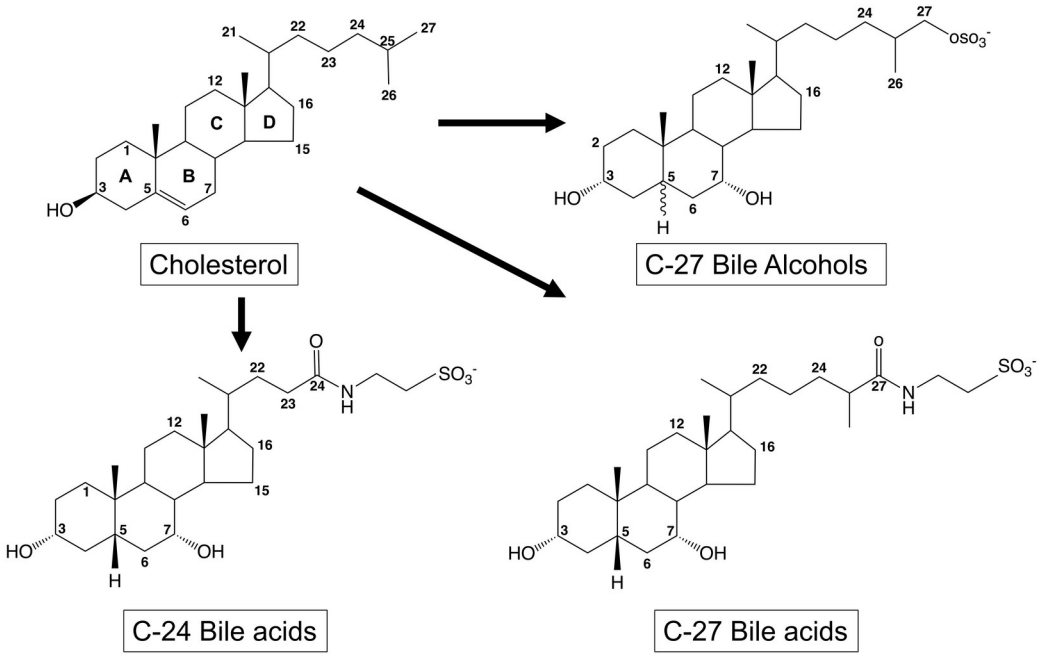

Figure 1. Major classes of bile acids.

Cholesterol is converted to C-27 bile alcohols (shown as the sulphate conjugate), C-27 bile acids (shown as the taurine conjugate) and C-24 bile acids (shown as the taurine conjugate). The default structure is shown with 3α- and 7α-hydroxyl groups for all three classes.

Bile Acid Structure and Physical Properties

Cholesterol is a C-27 sterol with a hydroxyl group at the C-3 position, a double bond at the C-5/6 position, and a steroid nucleus consisting of four fused carbon rings (designated A, B, C and D). During its conversion to bile acids, cholesterol undergoes changes that include hydroxylation at the C-7 position, shortening of the 8-carbon isooctane side chain to a 5-carbon isopentanoic acid side chain, epimerization of the C-3 hydroxyl group to a 3α conformation, and reduction of the double bond to yield a structure in which the A and B rings are oriented in a cis configuration almost perpendicular to one another. The products, typically called 5β bile acids, are the major bile acid species in mammals. However, C-24 bile acids with their A and B rings in a trans configuration (called 5α, allo or planar bile acids) have been identified in lower vertebrates, some mammalian species, and in humans during fetal/neonatal development and certain disease states. A comparison of the structure of cholesterol and a common bile acid, cholic acid, is shown in Figure 2 (5, 6). For bile acids, the carboxyl group at the C-24 position and hydroxyl groups on the steroid rings often reside on the same side of the molecule, thereby forming a hydrophilic surface that opposes the hydrophobic face. As a result, bile acids are amphipathic molecules and may have potent detergent properties.

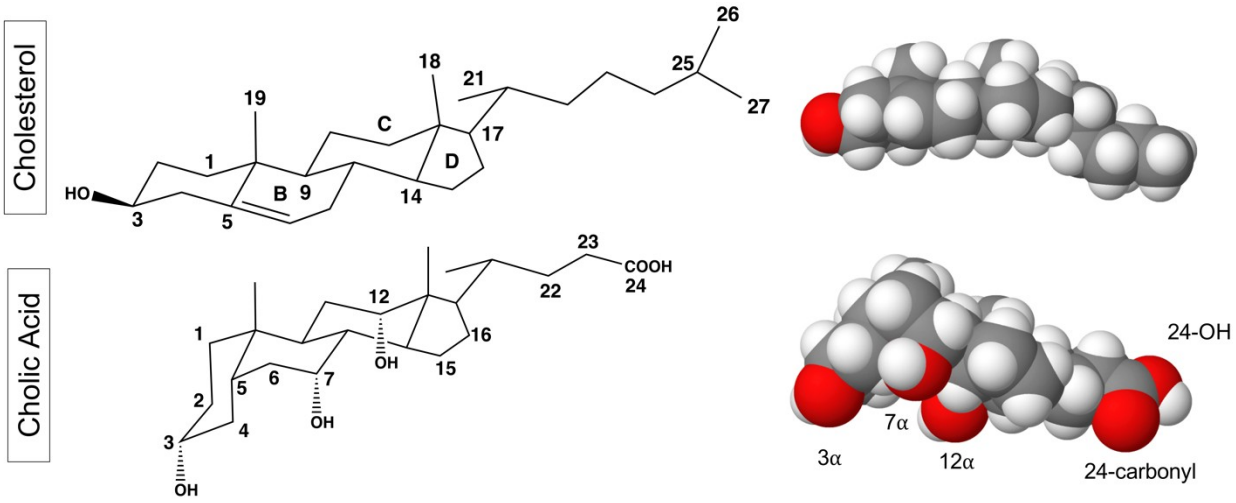

Figure 2. Structural comparison of cholesterol and C-24 bile acids.

(Left) In the pathway for bile acid synthesis, the stereo-configuration of the cholesterol steroid ring structure is altered, and the side chain is shortened. (Right) Space-filling models of cholesterol and cholic acid are shown, with carbon atoms indicated in grey, hydrogen atoms in white and oxygen atoms in red.

Bile acids are amphipathic molecules with the hydroxyl groups aligning to form a hydrophilic surface opposing the hydrophobic face of the carbon steroid nucleus (2, 3). The names, position of the hydroxyl groups and relative hydrophilicity/hydrophobicity of the major bile acids commonly found in mammals are shown in Figure 3. In Chapter 2, we discuss in more detail the differences in bile acid composition in murine species compared to humans and their influence on translational research.

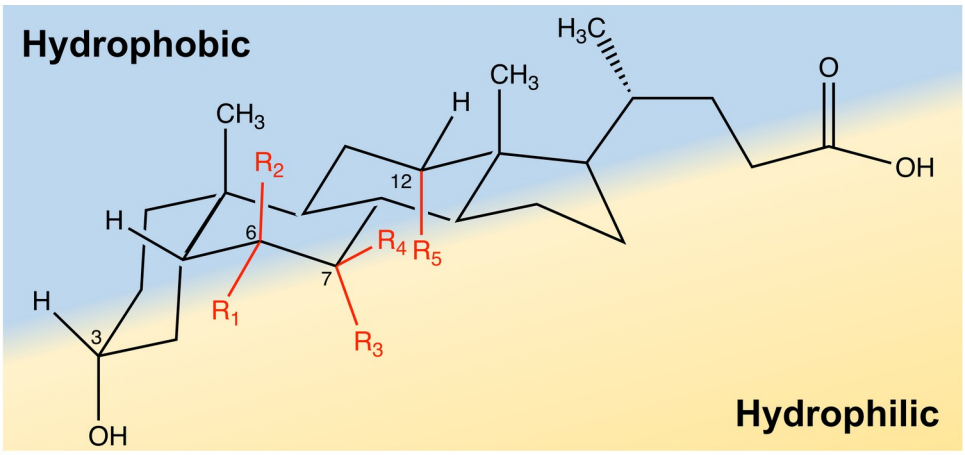

Hydrophilic

Hydrophobic

Bile acid		R1 6α	R2 6β	R3 7α	R4 7β	R5 12α
ω-muricholic acid	ωMCA	OH	H	H	OH	H
β-muricholic acid	βMCA	H	OH	H	OH	H
α-muricholic acid	αMCA	H	OH	OH	H	H
ursodeoxycholic acid	UDCA	H	H	H	OH	H
cholic acid	CA	H	H	OH	H	OH
chenodeoxycholic acid	CDCA	H	H	OH	H	H
deoxycholic acid	DCA	H	H	H	H	OH
lithocholic acid	LCA	H	H	H	H	H

Figure 3. Structure and relative hydrophobicity of the common bile acids in humans and mice.

Hydroxyl groups that are oriented in the α-orientation are located below the steroid nucleus and are axial to the plane of the steroid nucleus. Hydroxyl groups that are in the β-orientation are located above the steroid nucleus and are equatorial to the plane of the steroid nucleus.

The molecular structure of an individual bile acid species determines its physical properties, metabolism, signaling potential and function. For example, the aqueous solubility of a bile acid is influenced by the position, orientation, and number of hydroxyl groups. Their hydrophilicity decreases (hydrophobicity increases) as the structures progress from trihydroxy bile acids, such as cholic acid and muricholic acid, to the monohydroxy bile acid lithocholic acid. The side chain of bile acids is typically linked by a covalent bond to an amino acid, taurine or glycine. Amino acyl conjugation affects the aqueous solubility of bile acids, with taurine conjugates being more soluble than glycine conjugates, which in turn are more soluble than unconjugated bile acids (7). The solubility of bile acids will depend on their ionization state, which is a function of their pKa (acid dissociation constant; degree of ionization), and their aggregation state. The pKa values for bile acids range from ~5 for unconjugated bile acids to ~3.8 for glycine conjugates, and less than 2 for taurine conjugates.

As a result, a significant fraction of unconjugated bile acids is protonated and insoluble under the pH conditions present in the small intestine during digestion (pH values of approximately 6–7), whereas most conjugated bile acids will be ionized and present in aqueous solution as sodium salts. The critical micellar concentration (CMC) is the threshold in aqueous solution bile acid molecules will stack to form macromolecular aggregates or micelles. *In vivo*, bile acids complex preferentially with other polar lipids to form mixed micelles. As with aqueous solubility, bile acid structure affects the CMC, size of the micelle that forms, and number of bile acid molecules per micelle. In this regard, the hydrophobic nature of the human bile acid pool composition (predominantly CA and CDCA) is advantageous for forming micelles and facilitating lipid absorption. In contrast, the major bile acid in mouse bile, MCA is a relatively poor detergent and increases resistance to body weight gain with high fat diets (8). In fact, the

capacity of the bile acid-containing micelle to incorporate other lipids varies directly with bile acid hydrophobicity, such that micelles containing hydrophobic bile acids, are able to incorporate more cholesterol than micelles containing hydrophilic bile acids, which are relatively poor detergents.

Hydrophobicity is not only an indicator of lipid solubility, but it is also a predictor of cytotoxicity. More hydrophobic bile acids such as DCA and LCA have been linked to many cytotoxic diseases (9-11). While hydrophilic bile acids like UDCA promote bile flow and efflux and are used for therapeutic purposes, hydrophobic bile acids tend to cause ER stress, DNA damage, and oxidative stress (12-15). Hydrophobicity is also a marker for bile acid cell signaling and dictates bile acid interaction with and activation of receptors (16). Beyond their micelle and signaling roles, bile acids also have antimicrobial properties and serve to protect the gut mucosa (16, 17) and maintain the intestinal barrier (16, 18).

Biosynthesis of Bile Acids

Hepatic bile acid synthesis is the major pathway for cholesterol catabolism. In species such as humans and hamsters, only a minor fraction of newly synthesized cholesterol is used directly for hepatic bile acid synthesis (2, 19-21). Most is drawn from the large hepatic pool that includes lipoprotein-derived cholesterol, thereby linking the pathways for hepatic metabolism of lipoproteins and cholesterol with bile acid biosynthesis. In a 70-kg human, approximately 0.5 g of cholesterol is converted to bile acids each day (~7 mg per day per kg body weight) to balance the loss of bile acids in the feces (22). This accounts for more than 90% of the catabolism of cholesterol (vs approximately 10% for steroid biosynthesis), and fecal loss of bile acids accounts for almost half of all the cholesterol eliminated from the body each day. In mice, approximately

1.25 mg of cholesterol is converted to bile acids each day (~50 mg per day per kg body weight), and accounts for a similar fraction of the daily whole body loss of cholesterol.

Biosynthetic Pathway

Bile acids synthesized by the hepatocyte are called primary bile acids to distinguish them from secondary bile acids, which are metabolic products formed through a variety of reactions carried out by the gut microbiota. Bile acid synthesis is a complex process requiring 17 distinct enzymatic reactions and movement of intermediates between multiple compartments of the cell, including the cytosol, endoplasmic reticulum (ER), mitochondria and peroxisomes. Cytosolic carrier proteins and membrane transporters are thought to mediate the movement of biosynthetic intermediates through these cell compartments. For example, the ATP-binding cassette (ABC) transporter ABCD3 transports C-27 bile acid intermediates into the peroxisome for subsequent side chain shortening. However, with a few such exceptions, the mechanisms responsible for intracellular transport of bile acid biosynthetic intermediates remain largely uncharacterized. It was originally thought that bile acids were synthesized by one major pathway, called the 'classical' or neutral (CYP7A1) pathway that favors biosynthesis of the primary bile acid cholic acid (23). However, subsequent studies culminated in the discovery of an 'alternative' or acidic (CYP27A1) pathway that favors biosynthesis of the primary bile acid chenodeoxycholic acid in humans and 6-hydroxylated bile acid species such as muricholic acid and hyocholic acid in mice and rats. Two additional pathways have also been delineated, the Yamasaki and 25-hydroxylation pathways, although their contribution to bile acid synthesis in healthy adults is thought to be minor (24). The major steps and chemical modifications in the classical and

alternative pathways for bile acid biosynthesis in humans are summarized in Figure 4. The biosynthetic enzymes that carry out those reactions are listed in Table 1.

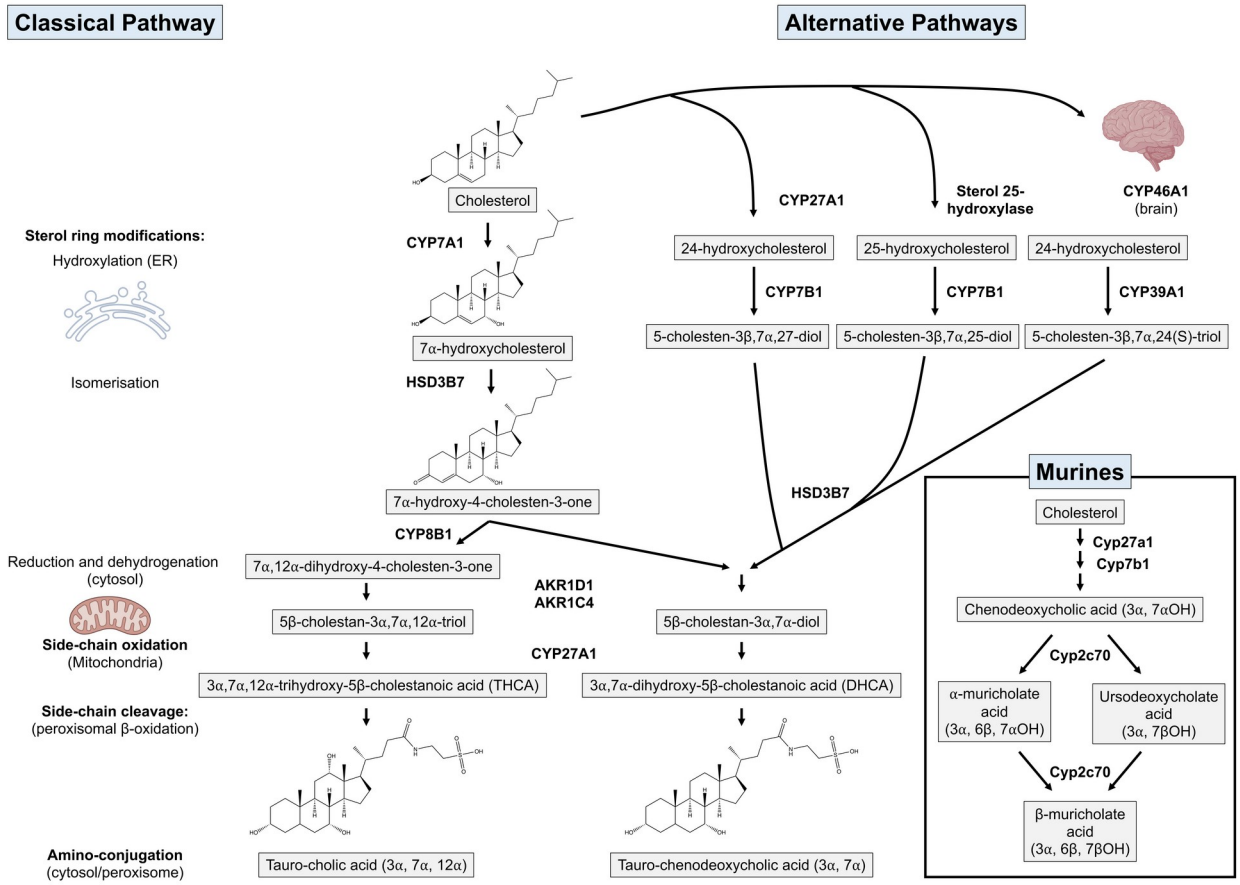

Figure 4. Major pathways for bile acid synthesis in humans.

The major classical (also called neutral) pathway for bile acid synthesis begins with cholesterol 7α-hydroxylase (CYP7A1). Bile acid intermediates synthesized via this pathway are substrates for the sterol 12α-hydroxylase (CYP8B1), the rate-determining step in production of cholic acid. In the minor alternative (also called acidic) pathway for bile acid synthesis, cholesterol is first hydroxylated on its side chain by sterol 27-hydroxylase (CYP27A1), sterol 25-hydroxylase or sterol 24-hydroxylase (CYP46A1). Subsequent hydroxylation of the steroid nucleus is catalyzed by oxysterol 7α-hydroxylase (CYP7B1) or to a lesser extent by the distinct oxysterol 7α-hydroxylase, CYP39A1. The classical and alternative pathways converge at the enzymatic step

for isomerization of the steroid ring. The alternative pathway preferentially produces chenodeoxycholic acid. After side chain oxidation and cleavage, bile acids are amino acyl-amidated to taurine or glycine. (*Inset*) In murine species, the cytochrome P450 Cyp2c70 converts chenodeoxycholic acid to α-muricholic acid, ursodeoxycholic acid, and β-muricholic acid.

Table 1. Enzymes of the Classical (Neutral) and Alternative (Acidic) Pathways for Bile Acid Synthesis

	Enzyme	Symbol	MW	Tissue	Organelle	Human Disease	Mouse KO
1	Cholesterol 7α-hydroxylase	*CYP7A1*	57,660	Liver	ER	Yes	Yes
2	Sterol 27-hydroxylase	*CYP27A1*	56,900	Many	Mito	Yes	Yes
3	Cholesterol 24-hydroxylase	*CYP46A1*	56,821	Brain-enriched	ER	No	Yes
4	Cholesterol 25-hydroxylase	*CH25H*	31,700	Many	ER	No	Yes
5	Oxysterol 7α-hydroxylase	*CYP7B1*	58,255	Liver-enriched	ER	Yes	Yes
6	Oxysterol 7α-hydroxylase	*CYP39A1*	54,129	Many	ER	No	No
7	3β-Hydroxy-Δ5-C27 steroid oxidoreductase	*HSD3B7*	40,929	Many	ER	Yes	Yes
8	Sterol 12α-	*CYP8B1*	58,078	Liver	ER	No	Yes

	hydroxylase						
9	Δ4-3-*o*xosteroid 5β-reductase	*AKR1D1*	37,377	Many	Cytosol	Yes	No
10	3α-*h*ydroxysteroid dehydrogenase	*AKR1C4*	37,095	Many	Cytosol	No	No
11	Cytochrome P450 2C70	*Cyp2c70*	56,157	Liver	ER	NA	Yes
12	Very long chain acyl CoA synthetase; VLCS	*SLC27A2*	70,312	Liver, gut	Perox	No	Yes
13	Bile acid CoA synthetase; FATP5; BACS	*SLC27A5*	70,312	Liver	PM/ER/Perox	Yes	Yes
14	α-Methylacyl-CoA racemase; peroxisomal multifunctional enzyme 2	*AMACR*	42,359	Liver, kidney	Perox/Mito	Yes	Yes
15	Enoyl-CoA	*EHHADH*	79,494	Many	Perox/Mito	Yes	Yes

	hydratase/3-hydroxy CoA dehydrogenase	*;*					
16	Branched-chain acyl CoA oxidase	*ACOX2*	76,826	Many	Perox	Yes	No
17	D-bifunctional protein; 17β-hydroxysteroid dehydrogenase IV	*HSD17B4*	78,686	Many	Perox	Yes	Yes
18	Thiolase sterol carrier protein 2	*SCP2*	58,993	Liver-enriched	Perox	Yes	Yes
19	Bile acid CoA: Amino acid *N*-acyltransferase	*BAAT*	46,296	Liver	Perox, Cyto	Yes	No
20	Cytochrome P450 2A12	*Cyp2a12*	56,179	Liver	ER	NA	Yes

Cyto, cytosol; ER, endoplasmic reticulum; KO, knockout; Mito, mitochondria; NA, not applicable; PM, plasma membrane; Perox, peroxisome.

In the classical pathway, modification of the steroid rings precedes side chain cleavage and is initiated by the hepatic enzyme cholesterol 7α-hydroxylase (CYP7A1). In the alternative pathway, the side chain of cholesterol is modified before the steroid ring structure is altered. The first step in the alternative pathway involves hydroxylation of the cholesterol side chain by one of several different enzymes that are present in liver and extra-hepatic tissues, such as the brain and lungs (Figure 4). After hydroxylation of the cholesterol side chain by C-24, C-25 or C-27 sterol hydroxylases, the products undergo C-7 hydroxylation by distinct oxysterol 7α-hydroxylases, including CYP7B1 and to a lesser extent CYP39A1. Of these alternative hydroxylation pathways, C-27 hydroxylation carried out by mitochondrial sterol 27-hydroxylase (CYP27A1) is quantitatively most important for bile acid synthesis. CYP27A1 is ubiquitously expressed, and 27-hydroxylation may be a general mechanism for removal of cholesterol from cells such as macrophages. Although the 24-hydroxylation pathway is only a minor contributor to bile acid synthesis, conversion of cholesterol to 24S-hydroxycholesterol by the brain-specific cholesterol 24-hydroxylase (CYP46A1) is the major mechanism for cholesterol elimination from the brain. In that pathway, cholesterol is converted to an oxysterol product (24S-hydroxycholesterol) capable of crossing the blood–brain barrier and entering the systemic circulation, where it is carried on lipoprotein particles to the liver for catabolism to bile acids. It should also be noted that the substrate specificity of CYP46A1 is not limited to cholesterol, and the enzyme may also function in metabolism of neurosteroids or even drugs in the central nervous system (25).

In the classical pathway, CYP7A1, an ER-bound microsomal cytochrome P450 enzyme, is rate limiting for bile acid synthesis. The 7α-hydroxylation of cholesterol by human CYP7A1 is one of the fastest reactions known for a mammalian P450. Although cholesterol is the major

in vivo substrate, in vitro studies have shown that CYP7A1 can bind and hydroxylate cholesterol, cholest-4-en-3-one and oxysterols such as 25-hydroxycholesterol and 27-hydroxycholesterol. Insight to the catalytic mechanism and substrate specificity of CYP7A1, and other cytochrome P450 sterol hydroxylases, comes from resolution of the human CYP7A1 structure by X-ray crystallography (26). The structure revealed a typical mammalian P450 fold with the sequence organized into four β-pleated sheets and 12 α-helices, which form the core around the haem prosthetic group. With regard to enzyme mechanism, analysis of the ligand bound structures indicated that the hydrophobic side chain of the sterol substrate enters the active site first. Based on these analyses, the authors propose a model by which CYP7A1 is embedded in the outer leaflet of the ER membrane with its active site facing toward the inner leaflet. The cholesterol substrate sits in the inner leaflet of the membrane with its 3β-hydroxy group facing the ER lumen and its side chain extending toward the outer leaflet. Following changes in the membrane lipid composition or protein conformation, cholesterol enters the substrate access channel of CYP7A1 and moves into close proximity of the heme group in the active site. In the cytochrome P450 structures solved to date, this cholesterol orientation (side chain near the heme) is a general feature of the mammalian P450 enzymes that hydroxylate sterol substrates (CYP11A1, CYP46A1, CYP7A1).

Following 7α-hydroxylation, the next step for bile acid biosynthesis in the classical pathway is catalyzed by the enzyme 3β-hydroxy-Δ5-C27-steroid oxidoreductase (HSD3B7). This reaction converts 7α-hydroxycholesterol to 7α-hydroxy-4-cholestene-3-one (often abbreviated as C4), which is a common precursor for cholic acid and chenodeoxycholic acid and is measured as a biomarker of hepatic bile acid synthesis. In the subsequent step, 7α-hydroxy-4-cholestene-3-one can be hydroxylated by the microsomal cytochrome P450 enzyme sterol 12α-hydroxylase

(CYP8B1) or proceed directly to steroid ring isomerization/saturation, which is catalyzed by Δ4-3-oxosteroid 5β-reductase (aldo-keto reductase 1D1; AKR1D1), and reduction of the 3-oxo group to a 3α-alcohol by 3α-hydroxysteroid dehydrogenase (aldo-keto reductase 1C4; AKR1C4). These are the final steps of the steroid ring structure modifications. If 7α-hydroxy-4-cholestene-3-one is first hydroxylated by CYP8B1, the 7α,12α-hydroxy-4-cholestene-3-one product is converted in subsequent steps to a trihydroxy bile acid (cholic acid). In contrast, bypassing the step catalyzed by CYP8B1 leads to formation of a dihydroxy bile acid. Indeed, CYP8B1 is a major determinant of the ratio of cholic acid to chenodeoxycholic acid in the bile acid pool of humans. In murine species (Figure 4, insert), CYP8B1 controls the ratio of cholic acid to muricholic acid, because chenodeoxycholic acid is further metabolized to muricholic acid by a distinct 6-hydroxylation reaction. In this fashion, CYP8B1 plays a critical role in determining the chemical and functional properties of the bile acid pool. Cytochrome P450 Cyp2c70 was recently identified as the enzyme responsible for synthesis of murine primary 6-hydroxylated bile acids, as a result, hydrophilic and less injurious muricholates (MCAs) constitute almost half of the circulating BA pool in mice (27-30). Cyp2c70 functions as both a 6β-hydroxylase and C-7 epimerase to convert chenodeoxycholic acid to β-muricholic acid. In the major pathway, Cyp2c70 first 6-hydroxylates chenodeoxycholic acid (3α,7α hydroxy) to yield α-muricholic acid (3α, 6β, 7α hydroxy) as an intermediate and then epimerizing the hydroxyl group at the C-7 position to produce the major murine primary bile acid β-muricholic acid (3α, 6β,7β hydroxy). As a minor pathway, Cyp2c70 can also convert chenodeoxycholic acid (3α,7α hydroxy) to ursodeoxycholic acid (3α,7β hydroxy) as an intermediate before hydroxylating the 6 position to yield β-muricholic acid (3α, 6β,7β hydroxy) (31). In contrast, MCAs are not present in the BA pool of humans, who lack *Cyp2c70* or a gene that performs a similar enzymatic function. In

Chapter 2, we characterize a *Cyp2c70* KO mouse model which develops features of neonatal cholestasis as a result of the more injurious, human-like BA composition. In our studies, we tested whether blocking bile acid return to the liver to interrupt the enterohepatic circulation would be protective in *Cyp2c70* KO mice and investigated the predicted cytotoxicity of the humanized BA pool composition.

The classical and alternative biosynthetic pathways converge at the isomerization step catalysed by HSD3B7, converting the 7α-hydroxylated intermediates to their 3-oxo, Δ4 forms. Although oxysterol products of the alternative pathway's early hydroxylation reactions are substrates for CYP8B1, these precursors preferentially bypass sterol 12α-hydroxylation and proceed directly to the steroid ring isomerisation and saturation reactions in vivo. As such, the alternative pathway favours synthesis of chenodeoxycholic acid or its 6-hydroxylated products over cholic acid. Following the steroid ring modifications, β-oxidation and shortening of the side chain by three carbon atoms occurs in peroxisomes (Figure 4). The di- and trihydroxycoprostanoic acid derivatives formed from cholesterol are activated to their corresponding CoA-thioesters by very-long-chain acyl-CoA synthetase (VLCS; SLC27A2; FATP2) and bile acid CoA synthase (BACS; SLC27A5; FATP5). After transport into peroxisomes by ABCD3, these CoA-thioester intermediates are converted to their respective (25*S*)-isomers by α-methylacyl-CoA racemase (AMACR) or enoyl-CoA hydratase/3-hydroxy CoA dehydrogenase (EHHADH; L-Bifunctional protein; peroxisomal multifunctional enzyme-1). This is an indispensable step for bile acid synthesis because the subsequent enzyme, branched-chain acyl-CoA oxidase (ACOX2), accepts only (*S*)-isomers as substrates. D-bifunctional protein (HSD17B4) then catalyses the subsequent hydration and dehydrogenation reactions prior to side chain cleavage by thiolase 2/sterol carrier protein 2. Finally, the CoA-

thioester bile acids are conjugated to glycine or taurine in a reaction catalysed by bile acid-CoA:amino acid *N*-acyltransferase (BAAT). There are multiple enzymes with bile acid-CoA ligase activity capable of producing bile acid CoA-thioesters (32). During bile acid biosynthesis, there appears to be redundancy where the C-27 bile acid-CoA thioester intermediate is synthesized by very-long-chain acyl-CoA synthetase (VLCS; SLC27A2) and/or bile acid CoA synthase (BACS; SLC27A5). In contrast, VLCS (SLC27A2) does not recognize the C-24 bile acids and only BACS (SLC27A5) is used to generate CoA-thioesters of the unconjugated C-24 bile acids returning to the liver in the enterohepatic circulation. Regardless of the source of the bile acid-CoA thioester, this step is considered rate limiting in bile acid amidation. The subsequent conjugation step mediated by BAAT is remarkably efficient, as more than 98% of bile acids secreted by the liver into bile are amidated to taurine or glycine. For bile acid conjugation, the vertebrate genome encodes multiple genes, BAAT and BAATP1, which arose by tandem duplication and subsequent reciprocal gene loss. As a result, most species including humans retain only a single functional gene with bile acid coenzyme A: amino acid N-acyltransferase activity (33). In most species, taurine is the amino acid primarily used for conjugation. However in mammals, bile acids may also be amino acylated with glycine in addition to taurine (34). In humans, the ratio of glycine to taurine-conjugated bile acid in the bile acid pool is approximately three-to-one, whereas in mice, bile acids are almost exclusively conjugated to taurine. Indeed, the taurine/glycine conjugation pattern varies considerably between different mammalian species, ranging from almost exclusively taurine in the rat, mouse, sheep and dog, to glycine greater than taurine in the pig, hamster, guinea pig, and human, to exclusively glycine in the rabbit. This specificity is controlled by the BAAT enzyme and, to a lesser degree, availability of the taurine precursor. As noted above, taurine conjugated bile acids

have a lower pKa than their respective glycine conjugates and are more likely to remain ionised, soluble and membrane-impermeant. However, both the glycine and taurine amide linkages are relatively resistant to cleavage by the pancreatic carboxypeptidases that would be encountered by bile acids in the digestive process, as compared to other amino acids. As such, the evolutionary and functional significance underlying selection of taurine or glycine as the amino acid used for conjugation is unknown. Regardless of the bile acid amino acid conjugation, the physiological consequence of conjugation is decreased passive diffusion across cell membranes, increased water-solubility at acidic pH, and increased resistance to precipitation in the presence of high concentrations of calcium as compared to unconjugated bile acid species. These properties are critical for maintaining the high concentration of bile acids required to facilitate lipid digestion and absorption.

Although humans typically synthesize approximately 0.5 g of bile acids per day to maintain the bile acid pool, the maximal rate of bile acid synthesis can reach 4–6 g per day. With regard to the source of these bile acids, the classical (CYP7A1) pathway accounts for the bulk of the bile acids made by the liver in rodents and humans. These estimates are derived from in vivo biochemical tracer studies using labelled precursors selective for the individual biosynthetic pathways and are strongly supported by evidence from human subjects with inborn errors in bile acid biosynthesis and from genetically modified mouse models. In mice, the classical pathway accounts for ~70% of total bile acid synthesis in adults and is the predominant pathway in neonates. In humans, biochemical tracer studies suggested that the classical pathway accounts for more than 90% of bile acid synthesis. That estimate is in good agreement with the finding that fecal levels of bile acids were reduced more than 90% in an adult human subject with an inherited *CYP7A1* deficiency. In contrast to mice, the alternative pathway appears to be the

predominant biosynthetic pathway in human neonates (35). Indeed, *CYP7A1* activity is low or absent in newborns. As such, infants with inherited *CYP7B1* defects are unable to synthesize mature bile acids and present with severe life-threatening liver disease.

Inherited Defects in Bile Acid Synthesis

Although inherited defects in bile acid biosynthesis are rare, the study of these disorders has played an important role in advancing our understanding of bile acid metabolism. The findings have also been key for determining the human relevance of experimental observations from mice engineered to knock out bile acid biosynthesis genes. The severe phenotype that is often associated with these inborn errors, which includes liver failure and death in early childhood, illustrates the importance of bile acids for hepatic and intestinal function. The pathophysiological effects include reduction of bile acid pool size, loss of bile acid-dependent bile flow, decreased biliary excretion of cholesterol and xenobiotics, reduced intestinal absorption of cholesterol and fat-soluble vitamins, and accumulation of cytotoxic bile acid biosynthetic intermediates. Disease-associated mutations in humans have been identified in ten of the 18 enzymes involved in bile acid biosynthesis (Table 1). Many of these genes have also been knocked out in mice. The list of genes with inborn errors includes; cholesterol 7α-hydroxylase (*CYP7A1*), sterol 27-hydroxylase (*CYP27A1*), oxysterol 7α-hydroxylase (*CYP7B1*), 3β-hydroxy-Δ5-C27-steroid oxidoreductase (*HSD3B7*), Δ4-3-oxosteroid 5β-reductase (*AKR1D1*), α-methylacyl-coenzyme A racemase (*AMACR*), D-bifunctional protein (*HSD17B4*), branched-chain acyl CoA oxidase (ACOX2), bile acid-CoA ligase (*SLC27A5*), and *BAAT* (24). In addition, disorders that disrupt peroxisome biogenesis such as Zellweger syndrome, neonatal adrenoleucodystropy and infantile Refsum disease also affect bile acid synthesis. These defects in genes required for peroxisome formation

indirectly affect the expression and activity of peroxisomal enzymes, including those involved in the final enzymatic side chain cleavage steps of bile acid biosynthesis. As such, patients with peroxisome biogenesis disorders accumulate atypical mono-, di- and tri-hydroxy C-27 bile acids.

A single enzyme defect is not generally sufficient to eliminate production of all bile acids, because multiple biosynthetic pathways exist and the intermediates are often substrates for more than one enzyme. However, the result is often a severe reduction in the levels of normal primary bile acids and the appearance of bile acid biosynthetic intermediates and abnormal bile acid species, which can be detected in serum or urine by methods such as fast atom bombardment ionisation-mass spectrometry and gas chromatography-mass spectrometry. Depending on the step in the biosynthetic pathway and the nature of the mutation (i.e. missense vs nonsense mutation or deletion), the clinical consequences of enzyme defects are varied, with the most severe producing neonatal cholestatic liver disease or neurological disease later in life. The effects of inherited defects in *CYP7A1* and *CYP7B1* on bile acid synthesis were introduced earlier. Only a few human subjects homozygous for a *CYP7A1* deficiency have been reported and the natural course of that disorder has not been described. Adult *CYP7A1*-deficient patients presented with an HMG-CoA reductase inhibitor (statin)-resistant hyperlipidaemia but were otherwise asymptomatic. Despite the absence of detectable *CYP7A1* protein, a low level of cholesterol 7α-hydroxylase activity could still be detected in the liver biopsy from an affected subject, suggesting additional enzyme(s) may be partially compensating in humans. Inactivation of CYP7A1 in mice has a more significant effect on bile acid biosynthesis. However, loss of both CYP7A1 and CYP27A1, even in mice, is not sufficient to block the formation of primary bile acids, albeit at a significantly diminished level (Rizzolo et al., 2019). *CYP7B1* deficiency is associated with a serious and often fatal neonatal liver disease. It should be noted that mutations

in *CYP7B1* are also a rare cause of spastic paraplegia (spastic paraplegia-5A, SPG5A), a recessive neurological disorder. The pathogenesis of this progressive motor-neuron degenerative disease is likely due to loss of *CYP7B1*-dependent metabolism of cholesterol and neurosteroids in the central nervous system rather than alterations in bile acid synthesis.

The most commonly reported inherited defect in bile acid synthesis is *HSD3B7*-deficiency, which affects both the classical and alternative pathways. *HSD3B7*-deficiency is characterized by progressive intrahepatic cholestasis, and the clinical manifestations include unconjugated bilirubinemia, jaundice, elevated serum aminotransferase levels, steatorrhea, fat-soluble vitamin deficiency, pruritus, and poor growth. For inherited defects in *AKR1D1*, patients present with neonatal cholestasis, low or absent primary bile acids, and elevated levels of bile acid biosynthetic intermediates. Cerebrotendinous xanthomatosis (CTX) is a rare, inherited disease caused by mutations in the mitochondrial enzyme *CYP27A1*. In CTX, bile acid synthesis via the alternative pathway is greatly reduced, and synthesis via the classical pathway is rerouted such that primary bile acid production is diminished but not eliminated. Although CTX is associated with a period of neonatal cholestasis, its pathophysiology is mainly related to deposition of cholesterol and oxysterols, such as cholestanol, in tendons and brain. As a result, the major clinical manifestations typically do not present until the second or third decade of life and are characterized by a slow progressive neurological dysfunction, cerebellar ataxia, premature atherosclerosis, cataracts and tendinous xanthomas. Finally, defects in the enzymes responsible for bile acid conjugation, bile acid CoA: amino acid *N*-acyltransferase (BAAT) and bile acid CoA synthetase (BACS, also called BACL; SLC27A5), have been identified and characterized. Patients with these BAAT defects present with high serum levels of unconjugated bile acids and malabsorption of dietary fat and fat-soluble vitamins, illustrating the importance of

conjugation to maintain the high intraluminal concentrations of bile acids required for efficient lipid digestion and absorption. Early bile acid replacement therapy with cholic acid, chenodeoxycholic acid or their conjugates in the case of bile acid conjugation defects can suppress or even reverse the biochemical abnormalities associated with many of the inherited bile acid biosynthetic defects and may be lifesaving. The basis for this therapeutic approach is two-fold. First, administration of exogenous primary bile acids partially restores the endogenous bile acid pool to drive hepatic bile flow and facilitate intestinal lipid absorption. Second, administration of exogenous cholic acid or chenodeoxycholic acid inhibits endogenous bile acid synthesis through feedback mechanisms described earlier. This blocks production and accumulation of the cytotoxic biosynthetic intermediates and abnormal bile acid species that are involved in the disease pathogenesis or progression.

Regulation of Bile Acid Biosynthesis

The biosynthesis of bile acids is tightly controlled and regulated by bile acids, oxysterols, cytokines, nutrients, growth factors, diurnal rhythm and hormones such as thyroid hormone, glucocorticoids and insulin (36). These various factors operate primarily by controlling expression of *CYP7A1*, the rate-limiting step in bile acid biosynthesis. This section will focus on the negative feedback regulation of *CYP7A1* by bile acids, a major physiological pathway for maintaining bile acid homoeostasis. Studies dating from the 1960s showed that *CYP7A1* activity and hepatic bile acid biosynthesis increased when bile acid return to the liver was blocked by administration of bile acid sequestrants or by biliary diversion. Conversely, feeding bile acids would suppress *CYP7A1* activity and endogenous bile acid biosynthesis. This negative feedback regulation of *CYP7A1* was later shown to be transcriptional and involve the bile acid-activated

nuclear receptor, farnesoid X-receptor (FXR, gene symbol: *NR1H4*). Initially, it was thought that the end-product regulation of *CYP7A1* expression involved a pathway by which activation of FXR in hepatocytes increased transcription of the atypical orphan nuclear receptor, small heterodimer partner (SHP, gene symbol: *NR0B2*). SHP then antagonized the actions of positive-acting transcription factors important for *CYP7A1* gene expression, such as liver receptor homologue-1 (LRH-1, gene symbol: *NR5A2*) and hepatocyte nuclear factor-4α (HNF4α, gene symbol: *NR2A1*) (37, 38). However, this model could not explain a series of puzzling experimental findings, including the observations that intravenous infusion of bile acids into bile-fistula rats was ineffective at downregulating hepatic *CYP7A1* expression compared to intraduodenal infusion of bile acids, and that bile acids only weakly suppressed CYP7A1 expression when added directly to isolated hepatocytes in culture (39).

Further investigation determined that the major pathway for feedback regulation of bile acid synthesis under normal physiological conditions involves intestinal FXR and gut-liver signaling via the polypeptide hormone fibroblast growth factor-19 (FGF19; mouse ortholog: FGF15) (40). In that pathway, summarized in Figure 5, bile acids activate FXR in ileal enterocytes to induce synthesis of FGF15/19. After its release by the enterocyte, FGF15/19 is carried in the portal circulation to the hepatocyte, where it signals through its cell surface receptor, a complex of the βKlotho protein and fibroblast growth factor receptor-4 (FGFR4), to repress *CYP7A1* expression and bile acid synthesis. The dominant role of this pathway as the major physiological mechanism responsible for feedback repression of *CYP7A1* expression is strongly supported by results obtained using knockout mouse models, including FGFR4, βKlotho, FGF15, and tissue-specific FXR and βklotho knockout mice. There is also compelling

evidence that this pathway is operative in humans, where circulating FGF19 levels inversely correlate with markers of hepatic bile acid synthesis.

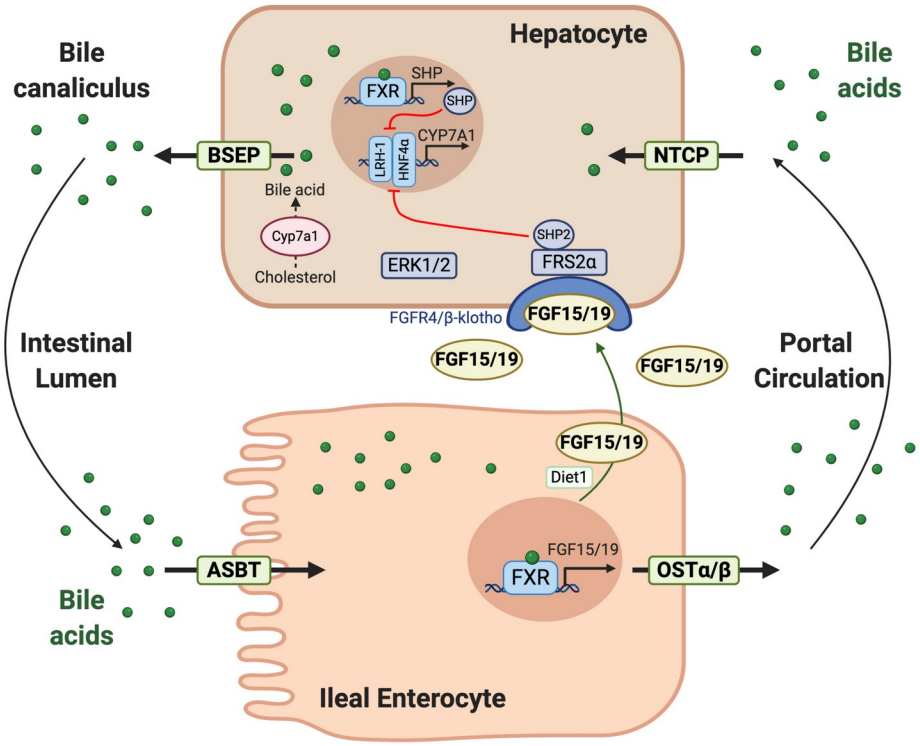

Figure 5. Mechanisms for feedback negative regulation of hepatic bile acid synthesis.

In the major physiological pathway, intestinal bile acids are taken up by the ASBT and activate the nuclear receptor FXR to induce FGF15/19 expression in ileal enterocytes. The basolateral secretion of FGF15/19 protein may be facilitated by the endosomal membrane glycoprotein, Diet1. FGF15/19 is then carried in the portal circulation to the liver, where it binds to its cell-surface receptor, a complex of the receptor tyrosine kinase, FGFR4, and the associated protein βklotho. FGFR4/βKlotho then signals through the docking protein FRS2α and the tyrosine phosphatase Shp2 to stimulate ERK1/2 phosphorylation and block activation of CYP7A1 gene expression by the nuclear factors HNF4α and LRH1. In a direct pathway that may be more significant under pathophysiological conditions, bile acids can activate FXR in hepatocytes to induce expression of SHP, an atypical orphan nuclear receptor. SHP interacts with LRH-1 and HNF4α to block their activation of CYP7A1 transcription.

After binding FGF15/19, the FGFR4/βKlotho complex signals through the docking protein fibroblast growth factor substrate 2 (FRS2α) and the tyrosine phosphatase known as tyrosine-protein phosphatase non-receptor type 11 (Shp2; gene symbol: *PTPN11*) to stimulate extracellular-signal-regulated kinase (ERK1/2) activity and block the activation of *CYP7A1* gene expression by HNF4α, LRH-1, and transcription factor EB (TFEB). The transcriptional repression also involves SHP, because FGF15/19-mediated regulation of *CYP7A1* is blunted in SHP knockout mice. However, details of exactly how these factors and phosphorylation pathways are integrated to repress CYP7A1 transcription are still being clarified. CYP7A1 expression is also regulated by bile acids at the post-transcriptional level. In this pathway, bile acids act via FXR to increase expression of the RNA binding protein ZFP36L1, which binds to the CYP7A1 mRNA and promotes its rapid turnover.

While *CYP7A1* is the rate-limiting enzyme for bile acid synthesis, *CYP8B1* activity determines the amount of cholic acid versus chenodeoxycholic acid (or muricholic acid) synthesized. Thus, it is not surprising that hepatic *CYP8B1* expression is also regulated by bile acids, cholesterol, diurnal rhythm and hormones such as insulin and thyroid hormone. With regard to bile acids, genetic evidence in mice suggests that both the hepatic FXR and gut FXR-FGF15/19 - liver FGFR4/βKlotho signaling pathways contribute to regulation of *CYP8B1* expression by bile acids under normal physiological conditions. In this fashion, the machinery controlling bile acid synthesis and bile acid pool composition responds to changes in intestinal and hepatic bile acid levels.

In contrast to the classical (CYP7A1) pathway, the alternative pathway appears to be primarily regulated by cholesterol delivery to the mitochondrial inner membrane, the site of sterol 27-hydroxylation. The mechanism may be similar to that controlling adrenal steroid

hormone biosynthesis, in which transfer of cholesterol to the mitochondria inner membrane by steroidogenic acute regulatory protein (StAR; STARD1) is rate limiting. The liver expresses several members of the StAR-related lipid transfer (START) domain family of proteins (Chapter 14), and one or more of these proteins could be involved in cholesterol delivery for bile acid synthesis. However, the molecular details of hepatocyte intracellular cholesterol trafficking and mitochondrial delivery for bile acid biosynthesis are not well understood. As such, the mechanisms regulating cholesterol flux through the alternative pathway for bile acid biosynthesis under physiological and pathophysiological states remain undefined. In addition to being regulated by cholesterol delivery, the alternative pathway can also be regulated transcriptionally by bile acids. In that pathway, bile acids act via FXR to induce expression of v-maf avian musculoaponeurotic fibrosarcoma oncogene family protein G (MAFG), which represses transcription of genes important for the alternative bile acid biosynthetic pathway such as *CYP27A1* and *CYP7B1*. MAFG does not affect expression of CYP7A1 but can act to repress a number of genes common to both the classical and alternative pathways for bile acid biosynthesis, thereby acting in a complimentary fashion to the FXR-SHP and FXR-FGF15/19-FGFR4 pathways to control bile acid synthesis and composition (41).

Secondary Metabolism of Bile Acids

After synthesis in the liver, primary bile acids are secreted into bile and pass into the intestine where they encounter the gut microbiota. In the small intestine, most of the conjugated bile acids are efficiently absorbed intact. However, a fraction of the luminal bile acids in the distal small intestine undergo bacterial deconjugation (cleavage of the amide bond linking the bile acid to glycine or taurine) by bile salt hydrolases, a process that continues to near completion in the

colon. Bile salt hydrolase-encoding genes are generally constitutively expressed and are widely distributed among the major bacterial phyla (*Bacteroidetes, Firmicutes, Actinobacteria,* and *Proteobacteria*). After deconjugation, the bile acids can be reabsorbed or undergo additional bacterial transformation for conversion to secondary bile acids. If reabsorbed, unconjugated bile acids are carried back to the liver in the enterohepatic circulation and efficiently reconjugated to taurine or glycine, a cycle originally termed 'damage and repair' by Hofmann (42). The newly 'repaired' (reconjugated) bile acids are secreted into bile along with conjugated bile acids that have returned from the intestine in the enterohepatic circulation and newly synthesized conjugated bile acids.

In the gut, primary bile acids are converted to secondary bile acids by the microbiota through reactions that include dehydroxylation at the C-7 position and oxidation/epimerization of the 3-, 6-, 7- or 12-hydroxyl groups to form oxo or iso epimers (43). The common bacterial modifications of bile acids that occur in humans and mice are summarized in Figure 6. The most significant of these changes is 7-dehydroxylation, which generates the major secondary bile acid species. Bile acid 7α/β-dehydroxylation requires a series of microbial enzymes encoded by a polycistonic bile acid-inducible (bai) regulon. In contrast to the bile salt hydrolases, the bai genes responsible for 7α/β-dehydroxylation are restricted to limited number of bacteria in the genus *Clostridia*. In humans, bile acid 7-dehydroxylation converts cholic acid to deoxycholic acid, a dihydroxy bile acid with hydroxyl groups at the C-3 and C-12 position, and converts chenodeoxycholic acid or ursodeoxycholic acid to lithocholic acid, a mono-hydroxy bile acid with a hydroxyl group at the C-3 position. In rats and mice, the 3,6,7-trihydroxy bile acids (α, β, ω-muricholic acid; hyocholic acid) are converted to the 3,6-dihydroxy bile acids, hyodeoxycholic acid (3α,6α-dihydroxy-5β-cholanoic acid) and murideoxycholic acid (3α,6β-

dihydroxy-5β-cholanoic acid). There is an absolute requirement for bile acids to be deconjugated prior to 7-dehydroxylation. For that reason, deconjugation-resistant synthetic bile acids such as cholylsarcosine, where cholic acid is conjugated to sarcosine (*N*-methylglycine) instead of glycine or taurine, are also resistant to dehydroxylation.

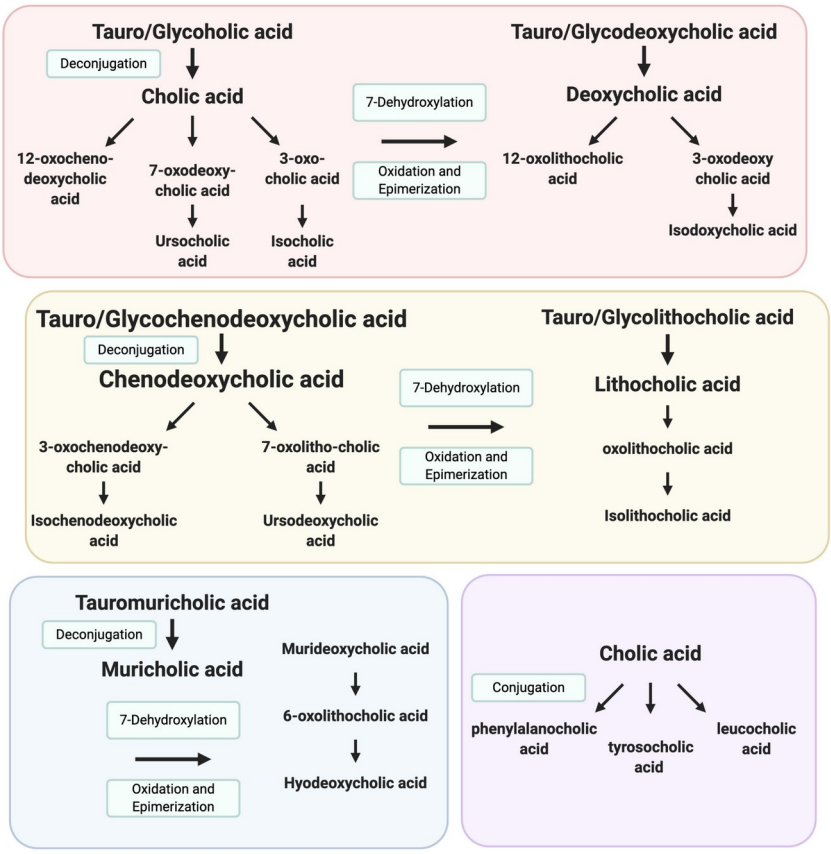

Figure 6. Scheme for bacterial metabolism of bile acids.

Bile acids are biotransformed by the gut microbiota by reactions that deconjugate, 7α/β-dehydroxylate oxidize and epimerize. The major pathways and products are indicated in bold. Oxidation yields the respective oxo-bile acid species, which can be epimerized, converting the 7α-hydroxy bile acids to their 7β-hydroxy epimers (ursocholic acid, ursodeoxycholic acid), and 3α-hydroxy bile acids to their 3β-hydroxy epimers (isocholic acid, isodeoxycholic acid, isochenodeoxycholic acid and isolithocholic acid). In the human caecum, a significant fraction of the bile acids present have been converted to their respective 3β-epimers. In rats and mice, muricholic acid species (α, β, ω-muricholic acid) are converted to the 3,6-dihydroxy bile acids, murideoxycholic acid (3α,6β-dihydroxy-5β-cholanoic acid) and hyodeoxycholic acid (3α,6α-dihydroxy-5β-cholanoic acid).

Another important microbial reaction is the oxidation and epimerization of bile acids, yielding so-called oxo and iso bile acids. This includes epimerization of the 7α-hydroxy group of chenodeoxycholic acid to form the 3α,7β-dihydroxy bile acid, ursodeoxycholic acid, and epimerization of the 3α hydroxy group of cholic acid, ursodeoxychlic acid, deoxycholic acid and lithocholic acid to form their 3β (iso) derivatives. The iso-bile acid derivatives of deoxycholic acid and lithocholic acid constitute a significant of the gut microbial bile acid metabolites.

Bile acid metabolism by the gut microbiota is not restricted to deconjugation, dehydroxylation, oxidation and epimerization reactions. Other reactions include desulfation (removal of the bile acid sulfonate group at the C-3 or C-7 positions) and formation of long chain fatty acid ethyl esters of lithocholic acid, polyesters of deoxycholic acid, and additional side chain amidation products. Recent metabolomics analyses identified three novel microbiota-dependent bile acid amidates, phenylalanocholic acid, tyrosocholic acid and leucocholic acid, in the fecal contents of mice and humans. The novel bile acid amidates were not detected in portal blood, peripheral blood or bile, suggesting that they are rapidly metabolized by the gut and/or do not undergo enterohepatic cycling. The microbial enzymes responsible for this conjugation reaction conjugation have not yet been identified and the physiological or pathophysiological roles of the novel bile acid amidates remains to be determined (44).

The secondary bile acids generated by the gut microbiota can be absorbed and undergo ‘repair’ by the hepatocyte. In addition to reconjugation with taurine/glycine, the hepatic repair reactions include re-epimerization of iso (3β-hydroxy) bile acids to their 3α-hydroxy form, reduction of oxo to hydroxyl groups, and rehydroxylation at the C-7 position to generate the original primary bile acid. Cytochrome P450 Cyp2a12 was recently identified as the enzyme responsible for rehydroxylation at the C-7 position in mice (45). Hepatic bile acid 7α-

rehydroxylation is carried out to varying degrees in many species, but does not occur in humans, in agreement with the absence of a human CYP2A gene orthologous to Cyp2a12. These interspecies differences in hepatic bile acid 7α-rehydroxylation activity are reflected in the amount of conjugated deoxycholic acid present in bile, which can range from 0% to 10% of the bile acids in rats, mice, guinea pigs, prairie dogs and hamsters, to 15–30% in dogs and humans, and greater than 90% in rabbits. The bile acid 7-dehydroxylation activity in the gut is also an important determinant of the amount of deoxycholic acid in the bile acid pool, because the abundance of 7-dehydroxylating bacteria can vary many-fold between individuals and under different dietary or pathophysiological conditions.

The bacterial biotransformation of bile acids carried out in the gut is important for several reasons. First, these modifications decrease the aqueous solubility of bile acids and increase their hydrophobicity, resulting in a marked lowering of their monomeric concentration in the aqueous phase of the luminal contents. This in turn reduces intestinal bile acid absorption and increases bile acid loss in the feces. Second, the input of secondary bile acids from the intestine influences the composition of the circulating pool of bile acids. This in turn affects the physiological and pathophysiological actions of the bile acid pool because secondary bile acids have distinct detergent properties, signaling activities and toxicities compared to their primary bile acid precursors. Third, bile acids affect the composition of the gut microbiota, with complex downstream effects on whole body metabolism and disease pathogenesis.

Enterohepatic Circulation of Bile Acids

The concept of an enterohepatic circulation by which constituents secreted by the liver into the intestine are returned via the portal circulation was postulated more than 300 years ago

by Mauritius van Reverhorst and the seventeenth century Neapolitan physician and mathematician Giovanni Alfonso Borelli (42). Anatomically, the gut–liver circulation can be subdivided into a portal and extraportal pathway. The extraportal pathway consists primarily of the lymphatic drainage from the intestine into the superior vena cava. This process is important for chylomicron lipoprotein particle-mediated transport of cholesterol, triglycerides, fat-soluble vitamins and phospholipids, but plays little role in bile acid absorption. In contrast, bile acids undergo a portal enterohepatic circulation. In that process, bile acids are secreted by the liver with other biliary constituents into the biliary tract and stored in the gallbladder (in most, but not all species). In response to a meal, the gallbladder contracts and empties its contents into the lumen of the small intestine, where bile acids function to facilitate lipid digestion and absorption. Unlike dietary lipids, there is limited absorption of bile acids in the proximal small intestine. Most bile acids travel to the distal small intestine (ileum), where they are almost quantitatively reabsorbed and exported into the portal circulation (45, 46). In the bloodstream, bile acids are bound to albumin and carried back to the liver for uptake and resecretion into bile. In adult humans, the enterohepatic circulation maintains a whole-body bile acid pool size of approximately 2–4 g. The bile acid pool cycles several times per meal, or about six times per day. Almost 95% of the bile acids that pass into the intestine are reabsorbed, such that only about 0.2–0.6 g of bile acids escape reabsorption and are eliminated in the feces each day (47). Viewed as its individual components, the bile acid enterohepatic circulation consists of a series of storage chambers (the gallbladder and small intestine), valves (the sphincter of Oddi and ileocaecal valve), mechanical pumps (the hepatic canaliculi, the biliary tract, and the small intestine) and chemical pumps (primarily the hepatocyte and ileal enterocyte, with their respective transporters). The major transporter proteins responsible for the enterohepatic of bile acids are

listed in Table 2 and are shown schematically in Figure 7. In Chapter 4, we investigate the mechanism of *nor*Ursodeoxycholic acid (*nor*UDCA), a synthetic C-23 side chain-shortened analog of the hydrophilic native bile acid ursodeoxycholic acid (UDCA), to induce a bicarbonate-rich hypercholeresis. *nor*UDCA's resistance to side-chain conjugation with glycine or taurine (48) allows its ability to bypass the enterohepatic circulation and undergo the cholehepatic shunt pathway proposed by Hofmann (48, 49); its importance in a therapeutic context is further discussed in more detail in Chapter 3.

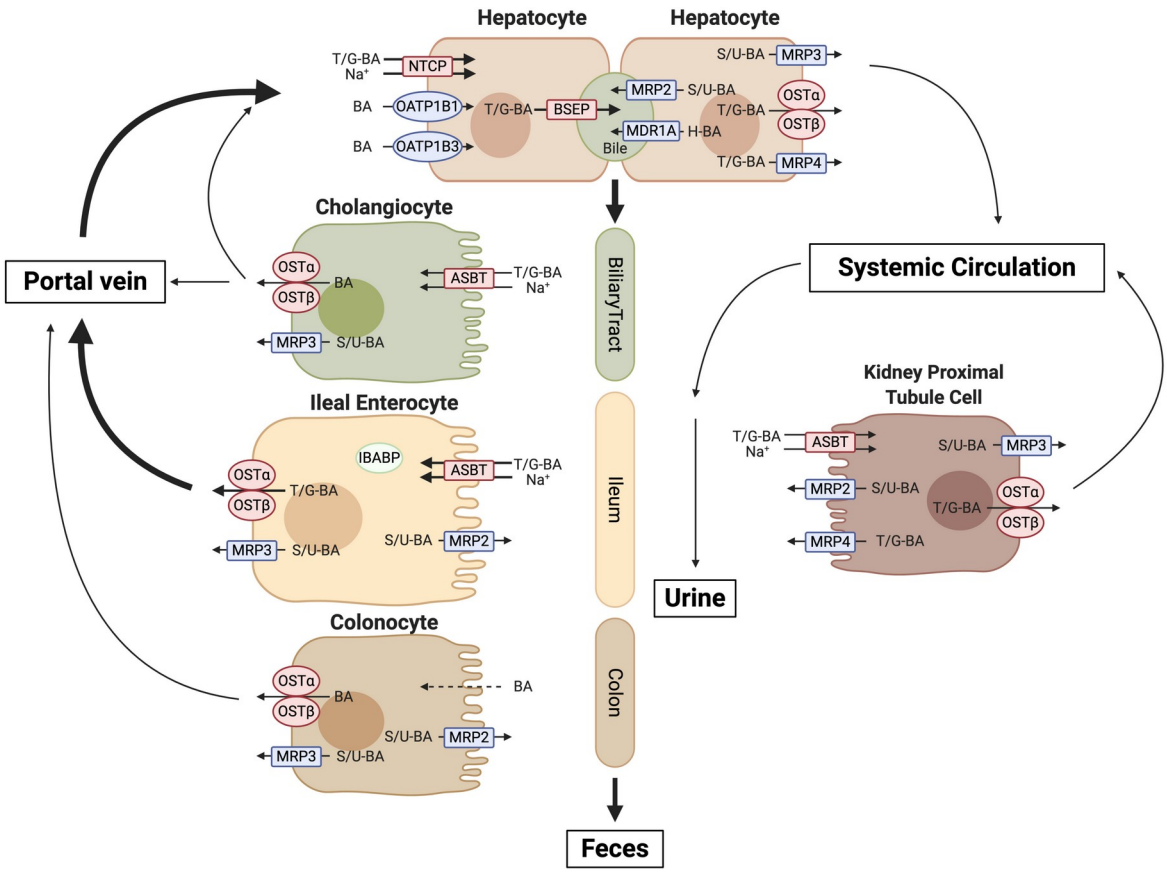

Figure 7. Enterohepatic circulation of bile acids showing the major tissues and transport proteins.

After their synthesis or reconjugation, taurine and glycine-conjugated bile acids (T/G-BA) are secreted into bile by the canalicular bile salt export pump (BSEP). Bile acids modified by sulfation (S-BA) or glucuronidation (U-BA) are secreted into bile by the multidrug resistance-associated protein-2 (MRP2) or multidrug resistance protein-1 (MDR1A). A fraction of the bile acids secreted into bile acids undergo cholehepatic shunting. In this pathway, conjugated bile acids are taken up by cholangiocytes via the apical sodium-dependent bile acid transporter (ASBT), and exported across the basolateral membrane via the heteromeric transporter OSTα-

OSTβ, and possibly MRP3, for return to the hepatocyte via the periductular capillary plexus. Ultimately, bile acids pass through the biliary tree and empty into the intestinal lumen. Bile acids are poorly absorbed in the proximal small intestine, but efficiently taken up by the ileal enterocytes via the ASBT. The bile acids bind to the ileal bile acid binding protein (IBABP) in the cytosol and are efficiently exported across the basolateral membrane into the portal circulation by OSTα-OSTβ. MRP3 is a minor contributor to basolateral export of native bile acids from the enterocyte, but may have a more significant role in export of modified bile acids. Although most bile acids are absorbed in the small intestine, colonocytes express appreciable levels of MRP3 and OSTα-OSTβ. These carriers may serve to export unconjugated bile acids (BA) that were taken up by passive diffusion from the lumen of the colon. After their absorption from the intestine, bile acids travel back to the liver, where they are cleared by the Na^+-taurocholate cotransporting polypeptide (NTCP) and members of the organic anion transport protein family, such as OATP1B1 and OATP1B3 in humans. Under cholestatic conditions, unconjugated, conjugated, or modified bile acids can be effluxed across the basolateral (sinusoidal) membrane of the hepatocyte by OSTα-OSTβ, MRP3 or MRP4 into the systemic circulation. Under normal physiological conditions, a fraction of the bile acid escapes first pass hepatic clearance and enters the systemic circulation. The free bile acids are filtered by the renal glomerulus, efficiently reclaimed by the ASBT in the proximal tubules, and exported back into the systemic circulation, thereby minimizing their excretion in the urine. A fraction of the glucuronidated or sulphated bile acids can also be exported across the apical membrane by MRP2.

Table 2. Major Transport Proteins of the Enterohepatic Circulation of Bile Acids.

Transport Protein (Gene)	Location	Function	Human Disorder	Mouse KO
Hepatocyte				
NTCP (*SLC10A1*)	BLM	Na^+-dependent uptake of conjugated BAs	Hypercholanemia	Yes
OATP1B1, 1B3 (*SLCO1B1, 1B3*) Oatp1b2 (rodents)	BLM	Na^+-independent uptake of OAs and unconjugated BAs	Rotor syndrome	Yes
MRP3 (*ABCC3*)	BLM	ATP-dependent export of OAs and modified BAs	None	Yes
MRP4 (*ABCC4*)	BLM	ATP-dependent export of OAs and modified BAs	PEL-negative blood group	Yes
OSTα-OSTβ (*SLC51A*; *SLC51B*)	BLM	Na^+-independent export of BAs	Congenital diarrhea	Yes
FIC1 (*ATP8B1*)	CM	ATP-dependent PS flipping	Progressive familial cholestasis type 1	Yes
BSEP (*ABCB11*)	CM	ATP-dependent export of BAs	Progressive familial cholestasis	Yes

			type 2	
MDR3 (*ABCB4*)	CM	ATP-dependent export of PC	Progressive familial cholestasis type 3	Yes
MRP2 (*ABCC2*)	CM	ATP-dependent export of OAs and modified BAs	Dubin–Johnson syndrome	Yes
Cholangiocyte, Ileal Enterocyte, Kidney Proximal Tubule Cell				
ASBT (*SLC10A2*)	ApM	Na^+-dependent uptake of BAs	Primary bile acid malabsorption	Yes
IBABP (*FABP6*)	Cytosol	Cytosolic BA transport	None	Yes
OSTα-OSTβ (*SLC51A*; *SLC51B*)	BLM	Na^+-independent export of BAs	Congenital diarrhea	Yes
MRP3 (*ABCC3*)	BLM	ATP-dependent export of OAs and modified BAs	None	Yes

ApM, apical membrane; BA, bile acid; BLM, basolateral membrane; CM canalicular membrane; KO, knockout; OA, organic anion.

Hepatic Bile Acid Transport

Bile acids are taken up from the bloodstream across the hepatocyte sinusoidal (basolateral) membrane by both sodium-dependent and sodium-independent mechanisms. The Na^+-taurocholate co-transporting polypeptide (NTCP; gene symbol: *SLC10A1*) is the primarily sodium-dependent transporter responsible for the uptake of conjugated bile acids, which constitute more than 80% of bile acid uptake in the liver. In contrast, members of the organic anion transporting polypeptide (OATP) family are primarily responsible for hepatic uptake of unconjugated bile acids and also contribute to clearance of conjugated bile acids in some species such as mouse. Human NTCP is a 349-amino acid (approximately 45-kDa) polytopic membrane glycoprotein and founding member of the SLC10 family of solute carriers (SLC, solute carrier) which also includes the ileal apical sodium-dependent bile acid transporter (ASBT, gene symbol: *SLC10A2*).

Cloned and characterized in 1991 (50), the transporter is expressed almost exclusively by hepatocytes and functions as an electrogenic sodium-solute cotransporter. Its transport properties have been characterized extensively *in vitro*, and NTCP efficiently transports all the major glycine and taurine-conjugated bile acids, but only weakly transports unconjugated bile acids (46, 51). A primary role for NTCP in the clearance of conjugated bile acids is strongly supported by genetic evidence in humans and mice. In humans, inherited defects in the NTCP gene (*SLC10A1*) are associated with elevated (5 to more than 100-fold) plasma levels of conjugated bile acids ("hypercholanemia"), in the absence of pruritus or evidence of liver disease (52). Similarly, administration of an NTCP inhibitor (myrcludex B) also significantly increases plasma bile acid levels in healthy humans. NTCP-deficient mice exhibited a complex bimodal bile acid phenotype where approximately 60 to 70% of the mice remained normocholanemic (serum bile

acid levels in the normal range; less than 20 μM) as a result of a compensatory increase in hepatic OATP-mediated bile acid clearance. The remaining ~30 to 40% of the NTCP-deficient mice did not induced hepatic OATP expression and were markedly hypercholanemic (serum bile acid levels increased more than 20-fold) (53). In addition to being the major hepatic bile acid uptake transporter, NTCP was identified as a cell surface receptor for the binding and entry of Hepatitis B (HBV) and Hepatitis Delta (HDV) viruses (54).

Members of the OATP family mediate sodium-independent bile acid transport across the hepatocyte sinusoidal membrane and are primarily responsible for uptake of unconjugated bile acids. The bile acid-transporting OATPs are polytopic membrane glycoproteins that share no sequence identity with the sodium-dependent bile acid transporters. The OATPs were originally assigned to the *SLC21* transporter gene family. However, a revised species-independent nomenclature system was adopted in 2004, in which OATP refers to protein isoforms (OATP1B1, OATP1B3, etc.) and *SLCO* ('O', referring to members of the OATP family; *SLCO1B1*, *SLCO1B3*, etc.) refers to the individual genes. The OATP-type transporters constitute a large family with 11 human genes and 16 murine genes that fall within six subgroups. In humans, OATP1B1 (gene symbol: *SLCO1B1*; original protein name: OATP-C) and OATP1B3 (gene symbol: *SLCO1B3*; original protein name: OATP8) account for most hepatic sodium-independent bile acid clearance. The mouse genome encodes only a single gene in the OATP1B subfamily (Oatp1b2; gene symbol: *Slco1b2*), and *SLCO1B1* and *SLCO1B3* arose in primates by gene duplication after divergence from rodents. A primary role for OATP1B1/OATP1B3 in the hepatic clearance of unconjugated bile acids is strongly supported by genetic evidence. In humans, the combined loss of *SLCO1B1* and *SLCO1B3* on chromosome 12 causes Rotor syndrome, a rare benign disorder characterised by elevated plasma levels of conjugated bilirubin

and unconjugated bile acids (55). In mice, genetic deletion of the entire orthologous *Slco1a/1b* locus (*Slco1a1, 1a3, 1a4, 1a5, 1a6, 1b2*) or *Slco1b2* alone results in defective hepatic clearance of unconjugated bile acids. OATPs do not appear to significantly contribute to hepatic clearance of conjugated bile acids in mice under normal physiological conditions with a functional NTCP. However, serum conjugated bile acids are significantly increased following pharmacological inhibition of NTCP in *Slco1a/1b* knockout versus wildtype mice.

After their uptake across the hepatocyte sinusoidal membrane, bile acids travel to the canalicular membrane for secretion into bile. Because bile acids are potent detergents, their cellular uptake and export must be carefully balanced to avoid excess intracellular accumulation. It is likely that bile acids are protein-bound or sequestered in some fashion during their hepatocellular transit. Existing evidence argues against a role for vesicular intracellular transport of bile acids. In plasma, bile acids are carried bound to albumin. In hepatocytes, cytosolic proteins such as liver fatty acid binding protein (L-FABP; gene symbol *FABP1*; identified as the "hepatic Z protein" that binds bile acids), and the aldo-keto reductase (AKR) family member AKR1C2 (3α-hydroxysteroid dehydrogenase type III; identified as "hepatic Y' protein" that binds bile acids) may serve a similar role for intracellular transport. However, the molecular mechanisms remain poorly defined, and it is unclear whether bile acids returning in the enterohepatic circulation and newly synthesized bile acids share common transport pathways through the hepatocyte. Regardless of the mechanisms, conjugated bile acids are shuttled to the canalicular membrane for secretion into bile by the ATP-dependent bile salt export pump (BSEP; gene symbol: *ABCB11*). This 160-kDa polytopic membrane glycoprotein is a member of the ATP binding cassette (ABC) transporter family and closely related to the multidrug resistance protein-1 (MDR1)/P-glycoprotein. When analyzed in transfected mammalian cells, BSEP

efficiently transports conjugated and unconjugated bile acids. However, in vivo, bile acids are first conjugated to glycine or taurine prior to secretion, as evidenced by the low proportions of unconjugated bile acids typically found in bile (less than 5%). A primary role for BSEP in the canalicular secretion of bile acids is strongly supported by genetic evidence in humans and mice. In humans, mutations in *ABCB11* are the cause of progressive familial intrahepatic cholestasis type 2 (PFIC-2), which is characterized by biliary bile acid concentrations less than 1% of normal (46). Mutations in *ABCB11* that impair synthesis, cellular trafficking, or stability of the BSEP protein lead to severe disease, including neonatal progressive cholestasis, jaundice, and hepatobiliary cancers (56). *Abcb11* deficiency also leads to progressive liver disease in mice that have been backcrossed onto a C57BL/6J background, although only a mild phenotype is observed in other background mouse strains. In hepatocytes, a small amount of the bile acid undergoes phase 2 metabolism by the addition of sulphate or glucuronide and is secreted into bile by other ABC transporters, primarily the multidrug resistance protein-2 (MRP2; gene symbol *ABCC2*). However, the compensatory protective mechanisms in mice versus humans is likely due to species differences in the bile acid pool composition and phase I metabolism of bile acids. In murine species and to a much lesser extent in humans, bile acids undergo hepatic phase I metabolism and are modified by hydroxylation at additional sites on the steroid nucleus. These polyhydroxylated bile acid species are less injurious and can be secreted into bile by MRP2 and possibly the breast cancer-related protein (BCRP; gene symbol: *ABCG2*) or MDR1/P-glycoprotein (gene symbol: *ABCB1*) (57). Sinusoidal membrane bile acid transport proceeds in the direction of uptake under normal physiological conditions. However, bile acids can also be exported from the hepatocyte by efflux back across the sinusoidal membrane into blood to protect the cell from bile acid overload under pathophysiological conditions in which canalicular

secretion is impaired. This sinusoidal membrane efflux may also play a role under physiological conditions in the liver, analogous to the 'hepatocyte-hopping' that was demonstrated for conjugated bilirubin and drugs (58). Under conditions of an increased bile acid load returning in the portal circulation, such as after a meal, a fraction of the bile acids absorbed by hepatocytes closest to the portal vein can be rerouted to blood by sinusoidal membrane efflux transporters and taken up by hepatocytes closer to the central vein for secretion into bile. This dynamic mechanism recruits additional hepatocytes within the liver lobule for bile acid clearance and could serve as an additional safeguard to protect the periportal hepatocytes from bile acid overload. The major transporters involved in hepatocyte sinusoidal membrane bile acid efflux are the ABC transporter, multidrug resistance protein-4 (MRP4; gene symbol *ABCC4*), and the heteromeric organic solute transporter (OST) OSTα-OSTβ (gene symbols: *SLC51A*, *SLC51B*). The ABC transporter multidrug resistance protein-3 (MRP3; gene symbol: *ABCC3*) may also be involved, but preferentially transports phase 2 metabolites such as glucuronidated or sulphated bile acids rather than taurine/glycine conjugated bile acids.

Intestinal Transport of Bile Acids

Bile acids are taken up by passive mechanisms in the proximal small intestine and colon and active transport in distal ileum (Figure 7). As a result of bacterial metabolism and species differences in bile acid conjugation or host bile acid metabolism, the bile acid pool may include taurine or glycine conjugates, unconjugated bile acids, and more hydrophobic bile acid species such as sulfated or polyhydroxylated bile acid species. A portion of the more hydrophobic bile acid species are protonated in the intestinal lumen and will passively diffuse across the apical membrane of enterocytes or colonocytes. However, most bile acids in the intestinal lumen are

conjugated and ionised. As such, their uptake requires a specific transporter. This active transport across the enterocyte apical brush border membrane is present only in the distal part of the small intestine (terminal ileum) (59). Physiologically, this is important because it ensures that luminal bile acid concentrations remain sufficiently high down the length of the small intestine to aid in fat absorption and reduce bacterial growth. In the terminal ileum, bile acids are almost quantitatively reabsorbed by the ASBT, a 348-amino acid (approximately 45-kDa) polytopic membrane glycoprotein that shares sequence identity with NTCP. However, unlike NTCP, it's only reported physiological substrate is conjugated and unconjugated bile acids (45). ASBT also functions as an electrogenic sodium-solute co-transporter and is remarkably specific for bile acids. First cloned in 1994 (60), ASBT was discovered to transport all the major species of bile acids, including unconjugated hydrophilic species, but is primarily responsible for uptake of conjugated bile acids and unconjugated trihydroxy bile acids that are membrane impermeant. In the intestine, there is a gradient of expression along the cephalocaudal axis restricting the majority of bile acid reabsorption to the terminal ileum (61-63). Given that enterocytes, and specifically ileocytes, are the main absorptive cells of the intestine, ASBT's expression is observed on the villus tip and not the crypts (45, 60, 64).

ASBT has proven to play a major role in the pathogenesis of various metabolic and gastrointestinal diseases. A central role for the ASBT in intestinal absorption of bile acids is strongly supported by genetic evidence in humans and mice, mutations in ASBT cause primary bile acid malabsorption due to a disruption of ileal bile acid uptake and EHC (65). In humans, inherited mutations in ASBT (*SLC10A2*) causes primary bile acid malabsorption, an idiopathic intestinal disorder associated with congenital diarrhea, fat-malabsorption, and interruption of the

enterohepatic circulation of bile acids. In mice, inactivation of the ASBT largely abolished intestinal bile acid absorption (37) and increased fecal bile acid and lipid excretion (66).

After their internalization by ileal enterocytes, bile acids are likely transported bound to cytosolic proteins to prevent their interaction with membranes and to reduce cytotoxicity. The best-characterized enterocyte bile acid carrier protein is the ileal bile acid binding protein (IBABP; also called the ileal lipid binding protein; gene symbol: *FABP6*), a member of the fatty acid binding protein family (Chapter 5). IBABP is an abundant small soluble 14-kDa protein that constitutes almost two percent of cytosolic protein in ileal enterocytes. IBABP expression parallels that of the ASBT and is induced by bile acids acting through FXR. Although capable of binding fatty acids, IBABP preferentially binds bile acids, with a stoichiometry of two or three bile acids per molecule of IBABP. In terms of binding specificity, IBABP has higher affinity for conjugated versus unconjugated bile acids and this difference is greater for the mouse versus human IBABP orthologue. A role for IBABP in intestinal bile acid transport is supported by genetic evidence in mice (67). In the IBABP null mouse, apical to basolateral transport of taurocholate is reduced when analysed using the inverted gut sac method of Wilson and Wiseman. Bile acid metabolism is also altered, suggesting that IBABP may also be involved in enterocyte bile acid sensing. However, no inherited defects or polymorphisms that affect bile acid metabolism have yet been described for human IBABP.

Bile acids are exported across the enterocyte basolateral membrane into the portal circulation by a heteromeric transporter, OSTα-OSTβ (gene symbols: *SLC51A* and *SLC51B*) (68). In addition to its localization to the intestinal ileum (61), it is also highly expressed by cholangiocytes and the epithelial cells of renal proximal tubule, and expressed at lower levels by hepatocyte, colonocytes, chromaffin cells of the adrenal gland, and the enterocytes of the

duodenum and jejunum. This unusual facilitative carrier shares no sequence identity with the other bile acid transport proteins, and requires expression of two distinct protein subunits encoded on separate chromosomes. The larger OSTα subunit is a 340-amino acid membrane protein with seven predicted transmembrane domains, whereas the smaller OSTβ subunit is a 128-amino acid predicted type I membrane protein. OSTα-OSTβ has been characterized using in vitro cell-based models. Co-expression of both subunits and their association is required for trafficking of the protein complex to the plasma membrane and solute transport. OSTα-OSTβ operates as a facilitative bidirectional carrier with a broad substrate specificity that includes all the major species of bile acids, as well as solutes such as prostaglandins, steroids, and steroid sulphates.

Cholestasis is the major pathophysiologic condition in which OSTαβ expression and regulation is altered. Under cholestatic conditions, specifically in human primary biliary cirrhosis, OSTαβ is upregulated to counteract increased bile acids and toxins, and minimize bile acid induced injury (69, 70). In mice, inactivation of the OSTα or OSTβ gene significantly impairs ileal bile acid transport and alters bile acid signaling through the FXR-FGF15/19-FGFR4 signaling pathway. In humans, inherited dysfunctional mutations in OSTα (*SLC51A*) or OSTβ (*SLC51B*) are associated with congenital diarrhea, steatorrhea, and fat-soluble vitamin malabsorption. The patients also exhibited features of liver disease, potentially due to the loss of OSTα-OSTβ function in hepatocytes and biliary epithelial cells. Although best characterized in the ileal enterocyte, the ASBT and OSTα-OSTβ are also expressed in other epithelia, including the cholangiocytes lining the biliary tract, the gallbladder epithelium and the kidney proximal tubules cells. As in the ileum, ASBT and OSTα-OSTβ function in the kidney to reabsorb most of the bile acids in the adjacent lumen of the proximal tubules for transport in plasma back to the

liver. However, in the biliary tract and gallbladder, ASBT and OSTα-OSTβ are thought to function in cholehepatic or cholecystohepatic shunting of bile acids. In those shunt pathways, a fraction of the biliary or gallbladder bile acids are reabsorbed and emptied into the portal circulation for reuptake by hepatocytes liver. The physiological significance of this pathway is still unclear, but may be acting to stimulate hepatic bile flow.

Our lab has previously characterized OSTα null mice which have been reported to have alterations in bile acid homeostasis which is characterized by reduced bile acid pool size due to decreased hepatic bile acid synthesis and downregulation of CYP7α1 (71, 72). Accompanying changes in bile acid homeostasis, the ileal morphology present with blunted, fused villi and dysplasic crypts (73). While the ileal phenotype appears to be similar to an irritable bowel disease such as Ulcerative Colitis or Crohn's Disease, there is only a mild increase in inflammatory cells and no change in pro-inflammatory genes like TNFα or IL1β (73), however we predict that the morphology is consistent with repeated damage and healing. In Chapter 4, I describe the OSTα null mouse as a model of intestinal bile acid stasis to understand the molecular mechanisms of bile acid induced injury and restitution response in ileal enterocytes.

Bile acids as Signaling Molecules

In addition to their role as detergents to solubilize biliary and dietary lipids, bile acids function as signaling molecules. Bile acids act as endogenous ligands to activate nuclear and G-protein-coupled receptors (36, 74). The best-characterized bile acid receptors are the nuclear receptor FXR and the G-protein-coupled receptor TGR5. However, bile acids can also act through other nuclear receptors (pregnane X receptor, PXR; vitamin D receptor, VDR; constitutive androstane receptor, CAR), other G protein coupled receptors (muscarinic receptors; sphingosine-1-

phosphate receptor-2), and through signal transduction pathways such as those mediated by the α5β1 integrin, protein kinase C, Jun N-terminal kinase, and MAPK/ERK (75).

Although bile acids were shown to activate isoforms of protein kinase C and modulate cell growth, the concept of bile acids as hormones or signaling molecules was not firmly established until the discovery in 1999 that bile acids activate FXR (38, 76). Both conjugated and unconjugated bile acids are natural agonists for FXR, with the following rank order of potency: chenodeoxycholic acid > lithocholic acid ≈ deoxycholic acid > cholic acid. However, it should be noted that some natural bile acids such as ursodeoxycholic acid and muricholic acid are unable to activate FXR and may even be competitive inhibitors or antagonists. As such, FXR activity is affected by changes in the composition of the bile acid pool. FXR is mainly expressed in liver, intestine, kidney and adrenal, with only low levels of expression reported in tissues such as adipose, heart, pancreas, artery and circulating macrophage. Consistent with its gastrointestinal expression and bile acid ligand specificity, FXR controls a network of genes to regulate hepatic bile acid synthesis, enterohepatic cycling of bile acids, and the protective mechanisms to prevent bile acid overload and cytotoxicity (Figure 5). In the liver, FXR suppresses expression of NTCP, increases bile acid conjugation and induces expression of efflux transporters such as BSEP and OSTα-OSTβ. Thus, activation of FXR in hepatocytes reduces bile acid synthesis and increases bile acid export across the canalicular membrane into bile or across the sinusoidal membrane back into blood. In the small intestine, FXR reduces ASBT expression, and induces expression of IBABP, OSTα-OSTβ and the polypeptide hormone FGF15/19 to protect the ileal enterocyte from bile acid accumulation (Figure 5). FXR also plays important protective roles in the gastrointestinal tract beyond its effects on bile acid homoeostasis. These

functions of FXR in the gut include inducing expression of genes important for intestinal barrier function, antimicrobial defense, and inhibiting inflammation and cell proliferation (77, 78).

In 2002, two groups independently demonstrated that the G-protein coupled receptor TGR5 (also called membrane-type bile acid receptor, M-BAR; GPR131; G protein-coupled bile acid receptor 1, GPBAR1; gene symbol: *GPBAR1*) was activated by low concentrations of bile acids. TGR5 is a $G\alpha_s$-coupled membrane receptor that stimulates adenylate cyclase, increases intracellular cAMP levels, and signals through downstream pathways such as those mediated by protein kinase A and the transcription factor CREB (cAMP response element-binding protein). However, unlike classical G-protein coupled receptors such as the β-adrenergic receptor, TGR5 does not appear to undergo desensitization when exposed to high concentrations of bile acids for extended periods. Both conjugated and unconjugated bile acids bind and activate TGR5, with a preference for hydrophobic bile acids in the following rank order of potency: lithocholic acid > deoxycholic acid > chenodeoxycholic acid > cholic acid. As a result of differences in their bile acid specificity for activation and their cellular localization (intracellular vs cell surface), changes in the bile acid pool composition will differentially affect signaling via FXR and TGR5. Furthermore, these ligand specificity differences have been exploited to identify synthetic agonists that selectively activate the two receptors, greatly facilitating the study of their in vivo roles.

TGR5 is widely expressed, with highest levels in gallbladder and low to moderate levels in liver and the intestinal tract. In liver, TGR5 is not expressed by hepatocytes, but is moderately expressed by the nonparenchymal cells, including cholangiocytes, sinusoidal endothelial cells, Kupffer cells and resident immune cells. In these cells, TGR5 plays a role in modulating the immune system and hepatic microcirculation. In the biliary tract, TGR5 functions to stimulate

gallbladder filling and to couple biliary bile acid concentrations to bile acid reabsorption and fluid secretion. In the small intestine and colon, TGR5 is not expressed by mature enterocytes or colonocytes. However intestinal stem cells express TGR5 to couple bile acid levels to regeneration of the intestinal epithelium. TGR5 is highly expressed by intestinal enteroendocrine cells, where it signals to stimulate incretin hormone glucagon-like peptide-1 (GLP-1) release in response to bile acids. TGR5 is also expressed in the gut enteric nervous system, where it mediates the effects of bile acids on intestinal motility. Beyond the liver and the gastrointestinal tract, TGR5 functions in other tissues and cell types, including brown adipose, muscle, brain and macrophages. Recent evidence has implicated TGR5 in modulation of the immune system and the inflammatory response, in energy and glucose metabolism, and in the central nervous system pathways for pain and itch.

Scope of the Dissertation

It is increasingly evident that beyond their classical role as detergents in the digestive process and end products of cholesterol catabolism, bile acids are important regulators of liver and gastrointestinal function, lipid and glucose metabolism, and energy homoeostasis. In this dissertation we used cell-based and knockout mouse models to investigate the relationship of bile acid hydrophobicity and bile acid-associated injury, and to elucidate the therapeutic mechanism of actions of the cholehepatic drug *nor*Ursodeoxycholic acid (*nor*UDCA) and bile acid enterohepatic circulation blockers.

In Chapter 2, we introduce the *Cyp2c70* KO mouse which has allowed us and others in the field to overcome the challenge of modeling hydrophobic bile acid-associated injury and human cholestatic liver disease. The *Cyp2c70* KO model successfully shifts the murine bile acid

composition towards a more injurious, human-like bile acid pool and spontaneously develops hallmarks of cholestasis. We utilize this *in vivo* tool to evaluate the therapeutic benefit of reducing hepatic bile acid burden by pharmacologically inhibiting the ASBT and blocking bile acid return to the liver in the enterohepatic circulation. In addition, we explore the relationship between bile acid hydrophobicity, detergent properties, and their cytotoxic effects.

In Chapter 3, we interrogate the mechanism of action of the therapeutic bile acid analog, *nor*Ursodeoxycholic acid, currently in Phase III clinical trials for the cholestatic liver disease, primary sclerosing cholangitis. This chapter highlights our findings which support *nor*UDCA's proposed ability to evade the enterohepatic circulation and undergo cholehepatic shunting. Consequently, we also confirm that the choleretic actions of *nor*UDCA are not dependent on active transport by any of the major BA transporters evaluated (Ostα, ASBT or Oatp1a/1b family members). Most notably, our findings suggest TMEM16A activation as a mechanism of action for the therapeutic effects of induced by *nor*UDCA.

In Chapter 4, we describe our model of intestinal bile acid stasis, the *Ostα*$^{-/-}$ mouse, which presents with a bile acid accumulation-dependent ileal phenotype, resemblant of an ongoing injury and restitution response. We explore the protective role of pharmacologically inhibiting bile acid uptake using an ASBT inhibitor and several other BA-based therapeutic approaches. While ASBT inhibition reversed ileal phenotype, other anti-cholestatic approaches such as the hydrophilic bile acid (UDCA) and bile acid sequestrant (colesevelam) had little effect. Additionally, approaches to reduce the antioxidant response pathway induced in *Ostα*$^{-/-}$ mice such as Nox1 ablation and reactive oxygen species (ROS) quenching by the antioxidant N-acetyl-cysteine (NAC) did not result in histological improvement.

Finally, Chapter 5 summarizes of our novel findings and their overall significance. Additionally, it highlights other remaining unanswered questions related to bile acid induced injury and proposes future directions for bile acid-based therapeutics. Together, these studies contribute to the mechanistic understanding of the role that bile acids and bile acid transporters plays in the pathogenesis and treatment of hepatobiliary and gastrointestinal disease.

References

1. Hofmann AF. Bile acids: trying to understand their chemistry and biology with the hope of helping patients. *Hepatology* 49: 1403-1418, 2009.
2. Thomas C, Pellicciari R, Pruzanski M, Auwerx J, and Schoonjans K. Targeting bile-acid signalling for metabolic diseases. *Nature Reviews Drug Discovery* 7: 678-693, 2008.
3. Wang DQ, Tazuma S, Cohen DE, and Carey MC. Feeding natural hydrophilic bile acids inhibits intestinal cholesterol absorption: studies in the gallstone-susceptible mouse. *Am J Physiol Gastrointest Liver Physiol* 285: G494-502, 2003.
4. Hofmann AF, Hagey LR, and Krasowski MD. Bile salts of vertebrates: structural variation and possible evolutionary significance. *J Lipid Res* 51: 226-246, 2010.
5. Hofmann AF. Chemistry and enterohepatic circulation of bile acids. *Hepatology* 4: 4S-14S, 1984.
6. Hofmann AF, and Hagey LR. Bile acids: chemistry, pathochemistry, biology, pathobiology, and therapeutics. *Cell Mol Life Sci* 65: 2461-2483, 2008.
7. Hofmann AF, and Hagey LR. Key discoveries in bile acid chemistry and biology and their clinical applications: history of the last eight decades. *J Lipid Res* 55: 1553-1595, 2014.
8. Bonde Y, Eggertsen G, and Rudling M. Mice Abundant in Muricholic Bile Acids Show Resistance to Dietary Induced Steatosis, Weight Gain, and to Impaired Glucose Metabolism. *PLoS One* 11: e0147772, 2016.
9. Barrasa JI, Olmo N, Lizarbe MA, and Turnay J. Bile acids in the colon, from healthy to cytotoxic molecules. *Toxicol In Vitro* 27: 964-977, 2013.

10. Bernstein H, Holubec H, Bernstein C, Ignatenko NA, Gerner E, Dvorak K, Besselsen D, Blohm-Mangone KA, Padilla-Torres J, Dvorakova B, Garewal H, and Payne CM. Deoxycholate-induced colitis is markedly attenuated in Nos2 knockout mice in association with modulation of gene expression profiles. *Dig Dis Sci* 52: 628-642, 2007.

11. Payne CM, Weber C, Crowley-Skillicorn C, Dvorak K, Bernstein H, Bernstein C, Holubec H, Dvorakova B, and Garewal H. Deoxycholate induces mitochondrial oxidative stress and activates NF-kappaB through multiple mechanisms in HCT-116 colon epithelial cells. *Carcinogenesis* 28: 215-222, 2007.

12. Araki Y, Andoh A, Bamba H, Yoshikawa K, Doi H, Komai Y, Higuchi A, and Fujiyama Y. The cytotoxicity of hydrophobic bile acids is ameliorated by more hydrophilic bile acids in intestinal cell lines IEC-6 and Caco-2. *Oncol Rep* 10: 1931-1936, 2003.

13. Barrasa JI, Olmo N, Perez-Ramos P, Santiago-Gomez A, Lecona E, Turnay J, and Lizarbe MA. Deoxycholic and chenodeoxycholic bile acids induce apoptosis via oxidative stress in human colon adenocarcinoma cells. *Apoptosis* 16: 1054-1067, 2011.

14. Li D, and Cao WB. Bile acid receptor TGR5, NADPH Oxidase NOX5-S and CREB Mediate Bile Acid-Induced DNA Damage In Barrett's Esophageal Adenocarcinoma Cells. *Sci Rep-Uk* 6: 2016.

15. Palmeira CM, and Rolo AP. Mitochondrially-mediated toxicity of bile acids. *Toxicology* 203: 1-15, 2004.

16. de Aguiar Vallim TQ, Tarling EJ, and Edwards PA. Pleiotropic roles of bile acids in metabolism. *Cell Metab* 17: 657-669, 2013.

17. Hofmann AF, and Eckmann L. How bile acids confer gut mucosal protection against bacteria. *Proc Natl Acad Sci U S A* 103: 4333-4334, 2006.

18. Cipriani S, Mencarelli A, Chini MG, Distrutti E, Renga B, Bifulco G, Baldelli F, Donini A, and Fiorucci S. The bile acid receptor GPBAR-1 (TGR5) modulates integrity of intestinal barrier and immune response to experimental colitis. *PLoS One* 6: e25637, 2011.

19. Schwarz M, Lund EG, Setchell KD, Kayden HJ, Zerwekh JE, Bjorkhem I, Herz J, and Russell DW. Disruption of cholesterol 7alpha-hydroxylase gene in mice. II. Bile acid deficiency is overcome by induction of oxysterol 7alpha-hydroxylase. *J Biol Chem* 271: 18024-18031, 1996.

20. Erickson SK, Lear SR, Deane S, Dubrac S, Huling SL, Nguyen L, Bollineni JS, Shefer S, Hyogo H, Cohen DE, Shneider B, Sehayek E, Ananthanarayanan M, Balasubramaniyan N, Suchy FJ, Batta AK, and Salen G. Hypercholesterolemia and changes in lipid and bile acid metabolism in male and female cyp7A1-deficient mice. *J Lipid Res* 44: 1001-1009, 2003.

21. Lan T, Haywood J, and Dawson PA. Inhibition of ileal apical but not basolateral bile acid transport reduces atherosclerosis in apoE(-)/(-) mice. *Atherosclerosis* 229: 374-380, 2013.

22. Dietschy JM, and Turley SD. Control of cholesterol turnover in the mouse. *J Biol Chem* 277: 3801-3804, 2002.

23. Russell DW. The enzymes, regulation, and genetics of bile acid synthesis. *Annu Rev Biochem* 72: 137-174, 2003.

24. Vaz FM, and Ferdinandusse S. Bile acid analysis in human disorders of bile acid biosynthesis. *Mol Aspects Med* 56: 10-24, 2017.

25. Russell DW, Halford RW, Ramirez DMO, Shah R, and Kotti T. Cholesterol 24-hydroxylase: an enzyme of cholesterol turnover in the brain. *Annu Rev Biochem* 78: 1017-1040, 2009.

26. Tempel W, Grabovec I, MacKenzie F, Dichenko YV, Usanov SA, Gilep AA, Park H-W, and Strushkevich N. Structural characterization of human cholesterol 7α-hydroxylase. *J Lipid Res* 55: 1925-1932, 2014.

27. Takahashi S, Fukami T, Masuo Y, Brocker CN, Xie C, Krausz KW, Wolf CR, Henderson CJ, and Gonzalez FJ. Cyp2c70 is responsible for the species difference in bile acid metabolism between mice and humans. *J Lipid Res* 57: 2130-2137, 2016.

28. Honda A, Miyazaki T, Iwamoto J, Hirayama T, Morishita Y, Monma T, Ueda H, Mizuno S, Sugiyama F, Takahashi S, and Ikegami T. Regulation of bile acid metabolism in mouse models with hydrophobic bile acid composition. *J Lipid Res* 61: 54-69, 2020.

29. Straniero S, Laskar A, Savva C, Hardfeldt J, Angelin B, and Rudling M. Of mice and men: murine bile acids explain species differences in the regulation of bile acid and cholesterol metabolism. *J Lipid Res* 61: 480-491, 2020.

30. Oteng AB, Higuchi S, Banks AS, and Haeusler RA. Cyp2c-deficiency depletes muricholic acids and protects against high-fat diet-induced obesity in male mice but promotes liver damage. *Mol Metab* 53: 101326, 2021.

31. de Boer JF, Verkade E, Mulder NL, de Vries HD, Huijkman N, Koehorst M, Boer T, Wolters JC, Bloks VW, van de Sluis B, and Kuipers F. A human-like bile acid pool induced by deletion of hepatic Cyp2c70 modulates effects of FXR activation in mice. *J Lipid Res* 61: 291-305, 2020.

32. Hubbard B, Doege H, Punreddy S, Wu H, Huang X, Kaushik VK, Mozell RL, Byrnes JJ, Stricker-Krongrad A, Chou CJ, Tartaglia LA, Lodish HF, Stahl A, and Gimeno RE. Mice deleted for fatty acid transport protein 5 have defective bile acid conjugation and are protected from obesity. *Gastroenterology* 130: 1259-1269, 2006.

33. Kirilenko BM, Hagey LR, Barnes S, Falany CN, and Hiller M. Evolutionary analysis of bile acid-conjugating enzymes reveals a complex duplication and reciprocal loss history. *Genome Biol Evol* 11: 3256-3268, 2019.

34. Moschetta A, Xu F, Hagey LR, van Berge-Henegouwen GP, van Erpecum KJ, Brouwers JF, Cohen JC, Bierman M, Hobbs HH, Steinbach JH, and Hofmann AF. A phylogenetic survey of biliary lipids in vertebrates. *J Lipid Res* 46: 2221-2232, 2005.

35. Schwarz M, Lund EG, Lathe R, Björkhem I, and Russell DW. Identification and characterization of a mouse oxysterol 7alpha-hydroxylase cDNA. *J Biol Chem* 272: 23995-24001, 1997.

36. Chiang JYL. Bile acid metabolism and signaling. *Compr Physiol* 3: 1191-1212, 2013.

37. Dawson PA, Haywood J, Craddock AL, Wilson M, Tietjen M, Kluckman K, Maeda N, and Parks JS. Targeted deletion of the ileal bile acid transporter eliminates enterohepatic cycling of bile acids in mice. *J Biol Chem* 278: 33920-33927, 2003.

38. Makishima M, Okamoto AY, Repa JJ, Tu H, Learned RM, Luk A, Hull MV, Lustig KD, Mangelsdorf DJ, and Shan B. Identification of a nuclear receptor for bile acids. *Science* 284: 1362-1365, 1999.

39. Pandak WM, Heuman DM, Hylemon PB, Chiang JY, and Vlahcevic ZR. Failure of intravenous infusion of taurocholate to down-regulate cholesterol 7 alpha-hydroxylase in rats with biliary fistulas. *Gastroenterology* 108: 533-544, 1995.

40. Inagaki T, Choi M, Moschetta A, Peng L, Cummins CL, McDonald JG, Luo G, Jones SA, Goodwin B, Richardson JA, Gerard RD, Repa JJ, Mangelsdorf DJ, and Kliewer SA. Fibroblast growth factor 15 functions as an enterohepatic signal to regulate bile acid homeostasis. *Cell Metab* 2: 217-225, 2005.

41. de Aguiar Vallim TQ, Tarling EJ, Ahn H, Hagey LR, Romanoski CE, Lee RG, Graham MJ, Motohashi H, Yamamoto M, and Edwards PA. MAFG is a transcriptional repressor of bile acid synthesis and metabolism. *Cell Metab* 21: 298-311, 2015.

42. Hofmann AF, and Hagey LR. Key discoveries in bile acid chemistry and biology and their clinical applications: history of the last eight decades. *J Lipid Res* 55: 1553-1595, 2014.

43. Dawson PA, and Karpen SJ. Intestinal transport and metabolism of bile acids. *J Lipid Res* 56: 1085-1099, 2015.

44. Quinn RA, Melnik AV, Vrbanac A, Fu T, Patras KA, Christy MP, Bodai Z, Belda-Ferre P, Tripathi A, Chung LK, Downes M, Welch RD, Quinn M, Humphrey G, Panitchpakdi M, Weldon KC, Aksenov A, da Silva R, Avila-Pacheco J, Clish C, Bae S, Mallick H, Franzosa EA, Lloyd-Price J, Bussell R, Thron T, Nelson AT, Wang M, Leszczynski E, Vargas F, Gauglitz JM, Meehan MJ, Gentry E, Arthur TD, Komor AC, Poulsen O, Boland BS, Chang JT, Sandborn WJ, Lim M, Garg N, Lumeng JC, Xavier RJ, Kazmierczak BI, Jain R, Egan M, Rhee KE, Ferguson D, Raffatellu M, Vlamakis H, Haddad GG, Siegel D, Huttenhower C, Mazmanian SK, Evans RM, Nizet V, Knight R, and Dorrestein PC. Global chemical effects of the microbiome include new bile-acid conjugations. *Nature* 579: 123-129, 2020.

45. Dawson PA. Role of the intestinal bile acid transporters in bile acid and drug disposition. *Handb Exp Pharmacol* 169-203, 2011.

46. Dawson PA, Lan T, and Rao A. Bile acid transporters. *J Lipid Res* 50: 2340-2357, 2009.

47. Voronova V, Sokolov V, Al-Khaifi A, Straniero S, Kumar C, Peskov K, Helmlinger G, Rudling M, and Angelin B. A physiology-based model of bile acid distribution and metabolism under healthy and pathologic conditions in human beings. *Cell Mol Gastroenterol Hepatol* 10: 149-170, 2020.

48. Yoon YB, Hagey LR, Hofmann AF, Gurantz D, Michelotti EL, and Steinbach JH. Effect of side-chain shortening on the physiologic properties of bile acids: hepatic transport and effect on biliary secretion of 23-nor-ursodeoxycholate in rodents. *Gastroenterology* 90: 837-852, 1986.

49. Gurantz D, and Hofmann AF. Influence of bile acid structure on bile flow and biliary lipid secretion in the hamster. *Am J Physiol* 247: G736-748, 1984.

50. Hagenbuch B, Stieger B, Foguet M, Lubbert H, and Meier PJ. Functional expression cloning and characterization of the hepatocyte Na+/bile acid cotransport system. *Proc Natl Acad Sci U S A* 88: 10629-10633, 1991.

51. Alrefai WA, and Gill RK. Bile acid transporters: structure, function, regulation and pathophysiological implications. *Pharm Res* 24: 1803-1823, 2007.

52. Liu R, Chen C, Xia X, Liao Q, Wang Q, Newcombe PJ, Xu S, Chen M, Ding Y, Li X, Liao Z, Li F, Du M, Huang H, Dong R, Deng W, Wang Y, Zeng B, Pan Q, Jiang D, Zeng H, Sham P, Cao Y, Maxwell PH, Gao Z-L, Peng L, and Wang Y. Homozygous p.Ser267Phe in SLC10A1 is associated with a new type of hypercholanemia and implications for personalized medicine. *Sci Rep* 7: 9214, 2017.

53. Slijepcevic D, Kaufman C, Wichers CGK, Gilglioni EH, Lempp FA, Duijst S, de Waart DR, Elferink RPJO, Mier W, Stieger B, Beuers U, Urban S, and van de Graaf SFJ. Impaired uptake of conjugated bile acids and hepatitis b virus pres1-binding in na(+) - taurocholate cotransporting polypeptide knockout mice: Liver Biology/Pathobiology. *Hepatology* 62: 207-219, 2015.

54. Yan H, Zhong G, Xu G, He W, Jing Z, Gao Z, Huang Y, Qi Y, Peng B, Wang H, Fu L, Song M, Chen P, Gao W, Ren B, Sun Y, Cai T, Feng X, Sui J, and Li W. Sodium taurocholate cotransporting polypeptide is a functional receptor for human hepatitis B and D virus. *Elife* 3: 2012.

55. van de Steeg E, Stránecký V, Hartmannová H, Nosková L, Hřebíček M, Wagenaar E, van Esch A, de Waart DR, Oude Elferink RPJ, Kenworthy KE, Sticová E, al-Edreesi M, Knisely AS, Kmoch S, Jirsa M, and Schinkel AH. Complete OATP1B1 and OATP1B3 deficiency causes human Rotor syndrome by interrupting conjugated bilirubin reuptake into the liver. *J Clin Invest* 122: 519-528, 2012.

56. Strautnieks SS, Byrne JA, Pawlikowska L, Cebecauerova D, Rayner A, Dutton L, Meier Y, Antoniou A, Stieger B, Arnell H, Ozcay F, Al-Hussaini HF, Bassas AF, Verkade HJ, Fischler B, Nemeth A, Kotalova R, Shneider BL, Cielecka-Kuszyk J, McClean P, Whitington PF, Sokal E, Jirsa M, Wali SH, Jankowska I, Pawlowska J, Mieli-Vergani G, Knisely AS, Bull LN, and Thompson RJ. Severe bile salt export pump deficiency: 82 different ABCB11 mutations in 109 families. *Gastroenterology* 134: 1203-1214, 2008.

57. Li J, and Dawson PA. Animal models to study bile acid metabolism. *Biochim Biophys Acta Mol Basis Dis* 1865: 895-911, 2019.

58. van de Steeg E, Wagenaar E, van der Kruijssen CMM, Burggraaff JEC, de Waart DR, Elferink RPJO, Kenworthy KE, and Schinkel AH. Organic anion transporting polypeptide 1a/1b-knockout mice provide insights into hepatic handling of bilirubin, bile acids, and drugs. *J Clin Invest* 120: 2942-2952, 2010.

59. Beuling E, Kerkhof IM, Nicksa GA, Giuffrida MJ, Haywood J, aan de Kerk DJ, Piaseckyj CM, Pu WT, Buchmiller TL, Dawson PA, and Krasinski SD. Conditional Gata4 deletion in mice induces bile acid absorption in the proximal small intestine. *Gut* 59: 888-895, 2010.

60. Shneider BL, Dawson PA, Christie DM, Hardikar W, Wong MH, and Suchy FJ. Cloning and molecular characterization of the ontogeny of a rat ileal sodium-dependent bile acid transporter. *J Clin Invest* 95: 745-754, 1995.

61. Dawson PA, Hubbert M, Haywood J, Craddock AL, Zerangue N, Christian WV, and Ballatori N. The heteromeric organic solute transporter alpha-beta, Ostalpha-Ostbeta, is an ileal basolateral bile acid transporter. *J Biol Chem* 280: 6960-6968, 2005.

62. Hruz P, Zimmermann C, Gutmann H, Degen L, Beuers U, Terracciano L, Drewe J, and Beglinger C. Adaptive regulation of the ileal apical sodium dependent bile acid transporter (ASBT) in patients with obstructive cholestasis. *Gut* 55: 395-402, 2006.

63. Meier Y, Eloranta JJ, Darimont J, Ismair MG, Hiller C, Fried M, Kullak-Ublick GA, and Vavricka SR. Regional distribution of solute carrier mRNA expression along the human intestinal tract. *Drug Metab Dispos* 35: 590-594, 2007.

64. Kolhatkar V, Diao L, Acharya C, Mackerell AD, Jr., and Polli JE. Identification of novel nonsteroidal compounds as substrates or inhibitors of hASBT. *J Pharm Sci* 101: 116-126, 2012.

65. Oelkers P, Kirby LC, Heubi JE, and Dawson PA. Primary bile acid malabsorption caused by mutations in the ileal sodium-dependent bile acid transporter gene (SLC10A2). *J Clin Invest* 99: 1880-1887, 1997.

66. Dawson PA, Haywood J, Craddock AL, Wilson M, Tietjen M, Kluckman K, Maeda N, and Parks JS. Targeted deletion of the ileal bile acid transporter eliminates enterohepatic cycling of bile acids in mice. *J Biol Chem* 278: 33920-33927, 2003.

67. Praslickova D, Torchia EC, Sugiyama MG, Magrane EJ, Zwicker BL, Kolodzieyski L, and Agellon LB. The ileal lipid binding protein is required for efficient absorption and transport of bile acids in the distal portion of the murine small intestine. *PLoS One* 7: e50810, 2012.

68. Dawson PA, Hubbert ML, and Rao A. Getting the mOST from OST: Role of organic solute transporter, OSTalpha-OSTbeta, in bile acid and steroid metabolism. *Biochim Biophys Acta* 1801: 994-1004, 2010.

69. Soroka CJ, Mennone A, Hagey LR, Ballatori N, and Boyer JL. Mouse organic solute transporter alpha deficiency enhances renal excretion of bile acids and attenuates cholestasis. *Hepatology* 51: 181-190, 2010.

70. Boyer JL, Trauner M, Mennone A, Soroka CJ, Cai SY, Moustafa T, Zollner G, Lee JY, and Ballatori N. Upregulation of a basolateral FXR-dependent bile acid efflux transporter OSTalpha-OSTbeta in cholestasis in humans and rodents. *Am J Physiol Gastrointest Liver Physiol* 290: G1124-1130, 2006.

71. Rao A, Haywood J, Craddock AL, Belinsky MG, Kruh GD, and Dawson PA. The organic solute transporter alpha-beta, Ostalpha-Ostbeta, is essential for intestinal bile acid transport and homeostasis. *Proc Natl Acad Sci U S A* 105: 3891-3896, 2008.

72. Ferrebee CB, Li J, Haywood J, Pachura K, Robinson BS, Hinrichs BH, Jones RM, Rao A, and Dawson PA. Organic Solute Transporter alpha-beta Protects Ileal Enterocytes From Bile Acid-Induced Injury. *Cell Mol Gastroenterol Hepatol* 5: 499-522, 2018.

73. Lan T, Rao A, Haywood J, Kock ND, and Dawson PA. Mouse organic solute transporter alpha deficiency alters FGF15 expression and bile acid metabolism. *J Hepatol* 57: 359-365, 2012.

74. de Aguiar Vallim TQ, Tarling EJ, and Edwards PA. Pleiotropic roles of bile acids in metabolism. *Cell Metab* 17: 657-669, 2013.

75. Copple BL, and Li T. Pharmacology of bile acid receptors: Evolution of bile acids from simple detergents to complex signaling molecules. *Pharmacol Res* 104: 9-21, 2016.

76. Parks DJ, Blanchard SG, Bledsoe RK, Chandra G, Consler TG, Kliewer SA, Stimmel JB, Willson TM, Zavacki AM, Moore DD, and Lehmann JM. Bile acids: natural ligands for an orphan nuclear receptor. *Science* 284: 1365-1368, 1999.

77. Inagaki T, Moschetta A, Lee Y-K, Peng L, Zhao G, Downes M, Yu RT, Shelton JM, Richardson JA, Repa JJ, Mangelsdorf DJ, and Kliewer SA. Regulation of antibacterial defense in the small intestine by the nuclear bile acid receptor. *Proc Natl Acad Sci U S A* 103: 3920-3925, 2006.

78. Gadaleta RM, van Erpecum KJ, Oldenburg B, Willemsen ECL, Renooij W, Murzilli S, Klomp LWJ, Siersema PD, Schipper MEI, Danese S, Penna G, Laverny G, Adorini L, Moschetta A, and van Mil SWC. Farnesoid X receptor activation inhibits inflammation and preserves the intestinal barrier in inflammatory bowel disease. *Gut* 60: 463-472, 2011.

Chapter 2: Ileal bile acid transporter inhibition in *Cyp2c70* KO mice ameliorates cholestatic liver injury

This chapter is adapted from the following published open-source article:

Jennifer K. Truong[1], Ashley L. Bennett[1], Caroline Klindt[1], Ajay C. Donepudi[1], Sudarshan R. Malla[1], Kimberly J. Pachura[1], Alex Zaufel[2], Tarek Moustafa[2], Paul A. Dawson[1], Saul J. Karpen[1].
Ileal bile acid transporter inhibition in Cyp2c70 KO mice ameliorates cholestatic liver injury. *Journal of Lipid Research* 63(9): 100261.

[1]Department of Pediatrics, Division of Pediatric Gastroenterology, Hepatology and Nutrition, Emory University School of Medicine, Children's Healthcare of Atlanta, Atlanta, Georgia, United States

[2]Division of Gastroenterology and Hepatology, Department of Internal Medicine, Medical University of Graz, Austria

Denotes corresponding authors

Graphical Abstract:

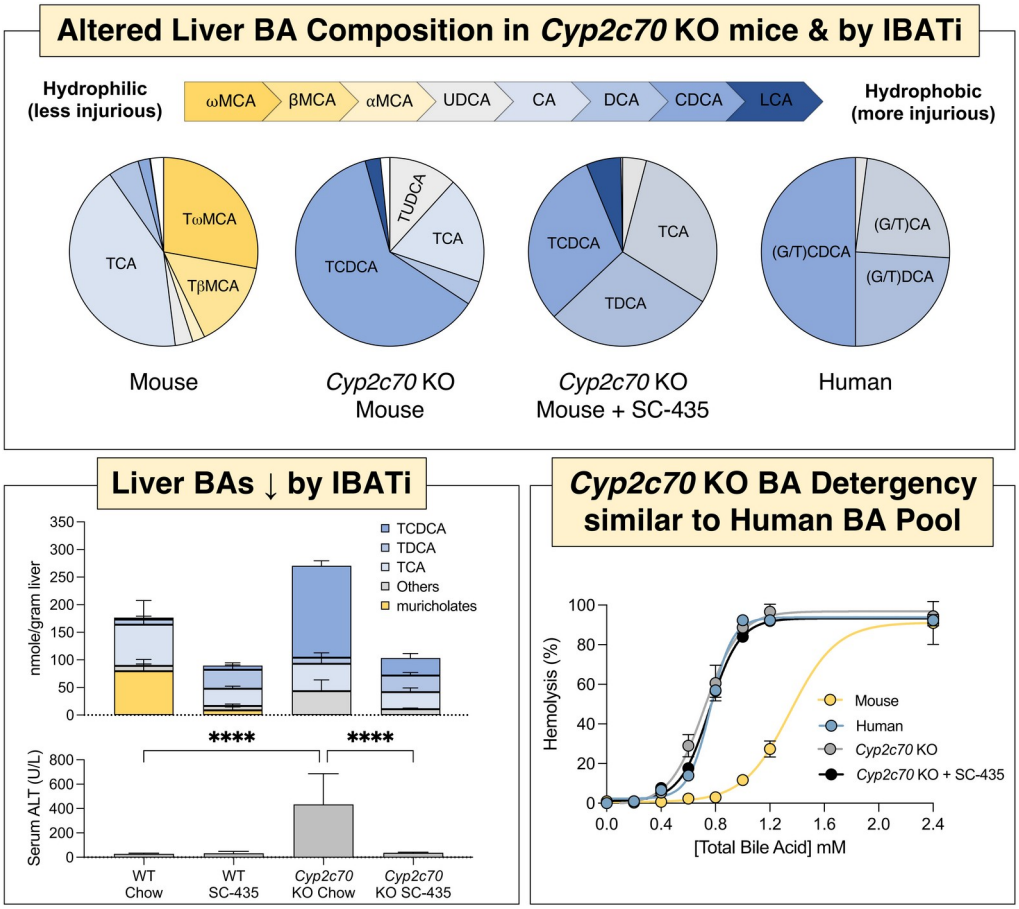

Abbreviations: ALP, alkaline phosphatase; ALT, alanine aminotransferase; ASBT, apical sodium-dependent bile acid transporter; AST, aspartate aminotransferase; BA, bile acid; BSEP, bile salt export pump; CA, cholic acid; CDCA, chenodeoxycholic acid; Ck-19, cytokeratin-19; DCA, deoxycholic acid; FXR, farnesoid X-receptor; HI, hydrophobicity index; IBAT, ileal bile acid transporter; IBATi, ileal bile acid transporter inhibitor; LCA, lithocholic acid; LDH, lactate dehydrogenase; MCA, muricholic acid; Ntcp, Na+-taurocholate cotranporting polypeptide; Oatp, organic anion cotransporting polypeptide; PFIC, progressive familial intrahepatic cholestasis; RBC, red blood cell; TCA, taurocholic acid; TCDCA, taurochenodeoxycholic acid; TDCA, taurodeoxycholic acid; TLCA, taurolithocholic acid; TMCA, tauromuricholic acid; TUDCA, tauroursodeoxycholic acid; UDCA, ursodeoxycholic acid.

Abstract

Cyp2c70 is the liver enzyme in rodents responsible for synthesis of the primary 6-hydroxylated muricholate bile acid (BA) species. *Cyp2c70* KO mice are devoid of protective, hydrophilic muricholic acids (MCAs), leading to a more human-like BA composition and subsequent cholestatic liver injury. Pharmacological inhibition of the ileal BA transporter (IBAT) has been shown to be therapeutic in cholestatic models. Here, we aimed to determine if IBAT inhibition with SC-435 is protective in *Cyp2c70* KO mice. As compared to WT mice, we found male and female *Cyp2c70* KO mice exhibited increased levels of serum liver injury markers, and our evaluation of liver histology revealed increased hepatic inflammation, macrophage infiltration and biliary cell proliferation. We demonstrate serum and histologic markers of liver damage were markedly reduced with SC-435 treatment. Additionally, we show hepatic gene expression in pathways related to immune cell activation and inflammation were significantly up regulated in *Cyp2c70* KO mice and reduced to levels indistinguishable from WT with IBAT inhibition. In *Cyp2c70* KO mice, the liver BA content was significantly increased, enriched in chenodeoxycholic acid (CDCA), and more hydrophobic, exhibiting a hydrophobicity index value and red blood cell lysis properties similar to human liver BAs. Furthermore, we determined IBAT inhibition reduced the total hepatic BA levels but did not affect overall hydrophobicity of the liver BAs. These findings suggest that there may be a threshold in the liver for pathological accretion of hydrophobic BAs and reducing hepatic BA accumulation can be sufficient to alleviate liver injury, independent of BA pool hydrophobicity.

Introduction

Bile acids (BAs) are synthesized from cholesterol in all vertebrate species, secreted into bile and empty into the intestine, where they play an important role in the digestion and absorption of lipids and fat-soluble vitamins (1). Beyond their role as detergents, BAs also function as signaling molecules and regulate cellular and whole-body metabolism (2). The amphipathic properties of BAs that enable effective micellization and transport of lipids in aqueous environments such as the biliary tract and gut lumen, also confer the potential for cytotoxicity when the normal secretion and compartmentalization of BAs in the enterohepatic circulation is impaired (3, 4). Despite being the subject of considerable study (3, 5-7), the role of BAs and toxic bile in the pathogenesis of human cholestatic liver disease remains a fundamental unresolved question (8-10). The use of laboratory animal models, particularly the mouse, has played a significant role in developing our understanding of BA homeostasis and mechanisms of BA mediated injury (8-10). Importantly, species-specific differences in BA compositions need to be considered when attempting to use mouse models to understand mechanisms of BA-related disease and injuries in humans (11). These differences include a structurally distinct, more hydrophilic BA composition (2) and a ~7-fold higher BA biosynthesis rate in mice (50 mg/kg/day) compared to humans (7 mg/kg/day) (12). These differences significantly impact the BA's physicochemical and signaling properties, metabolism, interaction with the microbiome, and potential for cytotoxicity, thereby presenting translational challenges when attempting to model the BA-induced injury in human cholestatic liver disease (11). Particularly important for the mouse-human BA composition comparisons is the abundant hepatic synthesis of 6-hydroxylated primary BA species (muricholates) in mice, 7α-rehydroxylation of conjugated deoxycholic acid (DCA) and lithocholic acid (LCA) in mice but not humans, and the amino acid

specificity for N-acyl-amidation (conjugation) of the BA side chain in mice (almost exclusively taurine conjugates) versus humans (~2.5:1 mixture of glycine to taurine conjugates in bile) (11).

The cytochrome P450, *Cyp2c70*, was recently identified as the enzyme responsible for muricholate synthesis in mice (13-16), converting chenodeoxycholic acid (CDCA) (3α,7α-hydroxy) and ursodeoxycholic acid (UDCA) (3α,7β-hydroxy) to α-muricholic acid (MCA) (3α,6β,7α-hydroxy) and β-MCA (3α,6β,7β-hydroxy) (17). As a result of the step catalyzed by *Cyp2c70* during primary BA synthesis, hydrophilic and less injurious 6-hydroxylated MCAs constitute almost half of the circulating BA pool in mice. In contrast, MCAs are not present in the BA pool of humans, who lack *Cyp2c70* or a gene that performs a similar enzymatic function. To better model the role of the more hydrophobic and injurious human BA pool in the pathogenesis of disease, several groups have begun characterizing *Cyp2c* locus and *Cyp2c70* KO mice, models with a more human-like BA composition (13, 16-18). *Cyp2c70* KO mice spontaneously develop neonatal cholestasis, as evidenced by significant increases in serum biomarkers, and changes in histology and gene expression characteristic of cholestatic liver injury (14, 17). The liver injury phenotype was quantitatively more severe in female mice, however male mice also exhibited significant liver damage. The absence of protective MCAs and increased production of CDCA contributes to the increased hydrophobicity and cytotoxicity of the BA pool, resulting in hepatic injury and BA retention. Indeed, treatment of *Cyp2c70* KO mice with the hydrophilic BA UDCA reduced the hydrophobicity of the BA pool and normalized liver histology and hepatic injury markers (18). In the present study, we explored the concept that the BA contribution to liver injury extends beyond their hydrophobicity. Common to the reported *Cyp2c70* KO mouse models generated is an increase in the liver total BA content (13, 17, 18). In the *Mdr2* KO (*Abcb4* KO) model of cholestatic liver injury and sclerosing cholangitis,

pharmacological inhibition of the ileal BA transporter (IBAT/ASBT; *Slc10a2*) increases fecal BA elimination, leading to reductions in liver BA concentrations and improvement in biomarkers of hepatocellular and cholestatic damage (8, 19). IBAT inhibitors are being evaluated in clinical trials as an anticholestatic therapy (20) and have demonstrated clinical benefit in children and been approved for the treatment of progressive familial intrahepatic cholestasis (PFIC) and Alagille syndrome (21, 22). In the following study, we tested whether blocking IBAT-mediated return of BAs to the liver in the enterohepatic circulation would be protective in *Cyp2c70* KO mice and investigated the predicted cytotoxicity of the humanized BA pool composition in this model. IBAT inhibition did not change the overall hydrophobicity of the liver-associated BAs, but significantly reduced the liver accretion of BAs in *Cyp2c70* KO mice leading to normalization of liver histology, gene expression, and serum biomarkers of liver injury to WT levels.

Materials and Methods

Materials

The IBAT inhibitor (IBATi) SC-435; (4R,5R)-5-[4-[4-(1-aza-4-azoniabicyclo[2.2.2]octan-4-yl)butoxy] phenyl]-3,3-dibutyl-7,8-dimethoxy-1,1-dioxo-4,5-dihydro-2H-1λ6-benzothiepin-4-ol) was received as a research gift from Shire Pharmaceuticals.

Animals

All animal experiments were approved by the Institutional Animal Care and Use Committees at Emory University. *Cyp2c70* KO mice (C57BL/6 background) were generated by Gene Edit Biolabs (Atlanta, GA) using CRISPR-Cas9 technology by microinjecting Cas9/gRNA into single-cell stage mouse embryos to produce founder (F0) mice. A strategy targeting exon 2 of *Cypc270* was used and followed the approach described by Honda *et. al* (14). The plasmid DNA J1-3 encoding the gRNA and Cas9 was used for microinjection. The *Cyp2c70* gRNA right target sequence was AGATGATTATTAGTGTA and the left target sequence was CTCTTGTCACTGTTCCA. The resulting F0 mouse encoded a deletion of 1,277 bp that included the entire targeted region encompassing exon 2 (supplemental Fig. S1A). The mice were genotyped by real-time quantitative PCR (RT-qPCR) and DNA sequencing. The primers used to detect the WT *Cyp2c70* allele were forward primer 5'-TCTTCTTGCCTTCAACAGCA-3' and reverse primer 5'-AACCATTGCACAGAGCACAG-3’ and yielded a product size of 662 bp. To detect the mutant *Cyp2c70* allele encoding the exon 2 deletion, the same forward primer was used with reverse primer 5'-GAAAGCCCATGAGAGAGGAA-3’ and yielded a product size of 350 bp (supplemental Fig. S1B). The F0 mouse was bred to the next generation (F1) and subsequent offspring from F4-F5 were confirmed by genotyping. The male and female WT and

Cyp2c70 KO mice were born at expected Mendelian ratios and used for our *in vivo* studies. The female breeding mice were fed ad libitum rodent breeder chow (21% of calories as fat; PicoLab Diet 20 No. 5058; PicoLab Cat. No. 0007689) and maintained in cages with standard bedding (1/8" Bed-O-Cobbs; Andersons Lab Bedding Products) and pulp cotton fiber nesting material (Nestlets; Anacare). The offspring were weaned at 4 weeks instead of 3 weeks of age since this appeared to improve viability, in agreement with the reported findings for an independent line of *Cyp2c70* KO mice (18). Absence of *Cyp2c70* protein in livers of *Cyp2c70* KO mice was confirmed by Western Blot analysis using an antibody raised against amino acids 366–390 (24 amino acids, PRKTTQDVEFRGYHIPKGTSVMAC) (23) (supplemental Fig. S1C). The WT and *Cyp2c70* KO mice were maintained on a C57BL/6 background. The adult mice were maintained on ad libitum rodent chow (13% of calories as fat; PicoLab Rodent Diet 20; LabDiet) and group-housed in ventilated cages (Super Mouse 750 Microisolator System; Lab Products) containing standard bedding at 22ºC in the same 12:12h light/dark cycle-controlled room of animal facility to minimize environmental differences. For the study, male and female WT and *Cyp2c70* KO mice were fed chow or chow plus 0.006% (w/w) SC-435, which provided approximately 11 mg/kg/day of the IBATi (24).

Mouse sample collection and analysis

The mice were fed ad libitum and not fasted prior to blood collection and euthanasia to collect tissues. Mouse blood was collected into MiniCollect Z Serum Separation tubes (Greiner Bio-One #450472) from the submandibular vein. The serum was isolated by centrifugation at 1500 g for 20 minutes at room temperature. Serum chemistries including alkaline phosphatase (ALP), alanine aminotransferase (ALT), aspartate aminotransferase (AST), and BAs were measured at

the Emory University Department of Animal Resources Quality Assurance and Diagnostic Laboratory using an Alfa Wassermann Vet Axcel chemistry analyzer. Tissue collection: Following euthanasia under isoflurane anesthesia, the mouse livers were perfused with 3 mL of PBS and harvested. After weighing, the liver tissue was subdivided as previously described (25). Lobes 2 and 5 were flash frozen in liquid nitrogen for Western Blot and RNA analysis. Lobe 4 was embedded in OCT for frozen section preparation. The remainder of the liver lobes (1, 3, 6 and 7) were used for histological analysis. Mouse spleens were also harvested and weighed.

Histological analysis and immunohistochemistry

The liver samples were fixed in 10% neutral formalin (Sigma-Aldrich) for 24 h, transferred to 70% ethanol, embedded in paraffin, and processed for sectioning by Children's Healthcare of Atlanta Pathology Services. Histological sections (5 μm) were cut. Consecutive sections were used for staining with H&E and Sirius Red. For immunohistochemistry, liver section slides were deparaffinized and subjected to antigen retrieval using Rodent Decloaker (Biocare #RD913M). To block endogenous peroxides, the sections were incubated for 15 minutes in BLOXALL Readymade Solution (Vector Labs #SP6000). The sections were washed with MilliQ water, and then incubated in Powerblock solution (Biogenex #HK0855K) for 15 minutes, followed by incubation with 3% donkey serum diluted in phosphate-buffered saline solution (PBS) for 1 h at room temperature. The slides were subsequently incubated with primary antibody overnight at 4ºC (1:500 Ck-19 Abcam #ab52625, 1:100 F4/80 Cell Signaling #70076). The following day, slides were washed 3 times in phosphate-buffered saline solution with 0.1% Tween 20 for 5 minutes, incubated in Signal Stain Boost IHC detection (Cell Signaling #8114) for 45 minutes, and washed. The color was developed using Signal Stain DAB substrate (Cell Signaling #11725)

and counterstained with hematoxylin (Sigma #HHS16) for 30 seconds. The slides were dehydrated with increasing ethanol concentrations (70% - 100%) and placed in xylene. The slides were then mounted using Vectamount Permanent Solution (Vector Labs #H5000).

Image Analysis

Immunohistochemistry slides were scanned with the 40X objective using NanoZoomer (Hamamatsu). Quantification of Sirius Red staining and immunohistochemistry for cytokeratin-19 (Ck-19) and F4/80 was performed using the latest QuPath release (version 0.2.3) (26). Briefly, Ck-19 and F4/80 immunohistochemistry slides were scanned (ndpi files) and imported into QuPath. The entire tissue section was selected as a single annotation using the built-in Magic Wand tool. For Ck-19 and F4/80 slides, cell counts were carried out using the positive cell detection tool to identify hematoxylin-stained nuclei and then thresholding for DAB positive-staining cells to determine the number of DAB-positive cells/mm^2 tissue. Identical settings and thresholds were applied to all slides for a given stain and experiment. Positive Sirius Red staining was quantified using the pixel classification tool with a residual threshold of -0.12. Sirius Red positive tissue was expressed as the percent of pixels above the threshold for the total tissue area examined. All slides for a given experiment were set to specific parameter thresholds with minimal adjustments for staining variation.

Gene expression measurements

Total RNA was extracted from frozen liver tissue using TRIzol reagent (Invitrogen, Carlsbad, CA) and a RNeasy Mini Kit (Qiagen), and cDNA was generated using a High Capacity cDNA Reverse Transcription Kit (Applied Biosystems). Real-time PCR (RT-PCR) was performed on a

QuantStudio™ 5 Real-Time PCR System (Applied Biosystems) using a SYBR Green qPCR Master Mix (Bimake.com). Quantification of relative gene expression was conducted by calculating fold change relative to Cyclophilin D as a reference gene using the ΔΔ C(t) method. The mouse primer sets used are listed in the supplemental methods. For RNA-Seq and gene set enrichment analysis**,** total RNA was extracted from frozen liver tissue using TRIzol reagent (Invitrogen, Carlsbad, CA). RNA-Seq libraries were prepared by Novogene Co., Ltd and sequenced on an Illumina HiSeq1000 system. Differential expression analysis was performed using the DESeq2 R package of Bioconductor (27). The resulting *P* values were adjusted using the Benjamini-Hochberg procedure to control for the false discovery rate (28). Differentially expressed genes with a log2 fold change > 1.0 and adjusted $P < 0.05$ (multiple testing false discovery rate 5%) were selected for functional annotation (GEO series accession number: GSE183251). Pathway analysis of the RNA-Seq data was performed using MetaCore (GeneGo Inc, Saint Joseph, MI) and the Kyoto Encyclopedia of Genes and Genomes (KEGG) and Database for Annotation, Visualization, and Integrated Discovery (DAVID) (29, 30).

Protein expression measurements

For Western blot analysis, total protein extracts were prepared from flash frozen liver tissue by homogenization in RIPA buffer (30 mM Hepes pH 7.4, 150 mM NaCl, 1% Nonident P-40, 0.5% sodium deoxycholate, 0.1% sodium dodecyl sulfate, 5 mM EDTA) supplemented with a combined protease and phosphatase inhibitor cocktail. Proteins were reduced and denatured in Laemmli sample buffer containing fresh DTT, resolved on 4-12% Bis-Tris gels, transferred to nitrocellulose membranes, immunodetected with antibodies, and imaged using a ChemiDoc

system (BioRad). The source of the primary and secondary antibodies used in the study are provided in the Supplemental Information, Table S2.

Liver BA determination

The liver BA content was measured using previously described methods (31). Briefly, frozen liver tissue samples (40–60 mg each) were extracted using Folch's extraction procedure to remove apolar lipids (lower phase) and precipitated proteins (interphase) before the addition of deuterated internal standards (32). Analytes were separated by high-performance liquid chromatography (HPLC) using a C18 reversed phase column prior to quantification by mass spectrometry using a combination of deuterium-labelled internal standards and unlabeled standards. The following BAs were measured: cholic acid (CA), ursodeoxycholic acid (UDCA), CDCA, deoxycholic acid (DCA), lithocholic acid (LCA), and their glycine and taurine conjugates; as well as αMCA, βMCA, γMCA (hyocholic), ωMCA, and their taurine conjugates.

Red blood cell (RBC) lysis assay

Whole blood is harvested from an anesthetized adult C57BL/6 mouse by cardiac puncture and collected into a tube with EDTA at a final concentration of 1.8 mg/mL (5 mM). Whole blood is centrifuged at 2500 rpm for 5 minutes at room temperature. The plasma and buffy coat are aspirated off, and the RBC pellet is resuspended in Buffer A (10 mM $CaCl_2$, 150 mM NaCl, 25 mM glucose, 10 mM Tris-HCl, pH 7.4) at a ratio of 10 mL of Buffer A per 1 mL of packed RBCs. Calcium at a final concentration of 10 mM was included to enhance the hemolytic activity of the BAs (33). The cells were washed 3 times in Buffer A by centrifuging at 2500 g for 5 minutes. After the final wash, RBCs were resuspended in Buffer A (1 mL of packed RBCs is

diluted up to a final volume of 40 mL) and kept on ice until ready to use. Taurine and glycine conjugated BA sodium salts were dissolved in Buffer A and diluted to the desired final BA concentration in a 150 µL total volume and added to round bottom 96-well plates prior to the addition of 142 µL of washed RBC suspension. The mixture was then incubated at 37º C for 30 minutes. After incubation, the plate is centrifuged at 4500 g for 5 minutes at room temperature to pellet unlysed cells. A 100 µL aliquot of the supernatant containing the free hemoglobin released from lysed RBCs is transferred to a clear, flat bottom 96-well plate and absorbance is read at 515 nm. Hemolysis for the individual BAs or BA mixtures is reported as percent of the RBC lysis induced by the positive control (0.1% Triton-X 100).

Cell culture, MTT, and lactate dehydrogenase assays

Alpha mouse liver 12 cells (AML12, ATCC) were used to measure BA toxicity. AML12 cells were cultured at 37°C in 5% CO_2 and maintained in DMEM (4.5 g/L glucose) supplemented with 10% fetal bovine serum (FBS), 1% penicillin/streptomycin and 20 mM L-glutamine. For the cell viability assays, AML12 cells were plated on collagen I coated 96-well plates at a density of 10,000 cells/well. The next day, the cells were preincubated in complete medium containing the indicated BAs for 1 h and then treated for 2 h with a final concentration of 1 mg/mL of the MTT reagent (3-(4, 5-dimethylthiazol-2-yl)-2, 5-diphenyltetrazolium-bromide) (Molecular Probes™ M6494). Absorbance of each well was read using a BioTek™ Synergy™ HTX Multi-Mode Microplate (Molecular Devices, Sunnyvale, CA, USA) at a wavelength of 570 nm and the percent cell viability reported was normalized to vehicle control. To measure lactate dehydrogenase release (LDH), parallel 96-well plates of AML12 cells were preincubated for 4 h in complete media containing the indicated BAs, and then for 30 minutes with reagent as

according to manufacturer's protocol (BioLegend, catalog #42640). Following the addition of stop solution, absorbance was measured at 490 nm and cytotoxicity was reported relative to internal high and low controls.

Statistical analyses

For the box and whisker plots, median values (line), interquartile range (boxes), and min to max values (whiskers are shown). For the liver BA composition analysis and BA toxicity assays, mean value ± standard deviation is shown. The data were evaluated for statistically significant differences using the Mann-Whitney test, the two-tailed Student's t test, ANOVA and Tukey-Kramer honestly significant difference post-hoc test or Sidak's multiple comparisons test (GraphPad Prism; Mountain View, CA). Differences were considered statistically significant at $P < 0.05$.

Results

IBAT inhibition protects against *Cyp2c70* deficiency-associated liver disease

To determine whether interrupting the enterohepatic circulation of BAs with an IBATi is protective against development of the liver injury associated with *Cyp2c70* deficiency, male and female WT and *Cyp2c70* KO mice were fed chow or chow supplemented with 0.006% SC-435 (~11 mg/kg/day) for 8 weeks as outlined in Fig. 1A and supplemental Fig. S2A. In agreement with previously reported studies (14, 18), the liver injury phenotype is more pronounced in female *Cyp2c70* KO mice. For clarity, figures in the main text show the results for female mice and findings for male mice are presented in the Supplemental Materials. The body weights of *Cyp2c70* KO mice fed chow or chow plus IBATi were lower than WT mice at 4 weeks of age (supplemental Fig. S1D), becoming similar to WT mice by 12 weeks for both female (Fig. 1B) and male (supplemental Fig. S2B) mice. As previously reported, the liver to body weight ratio (Fig. 1C and supplemental Fig. S2C) is significantly elevated in *Cyp2c70* KO mice. In addition, *Cyp2c70* KO mice had a significantly higher spleen to body weight ratio, which suggests the presence of liver injury-associated portal hypertension in these animals (Fig. 1D and supplemental Fig. S2D) (34). Treatment with IBATi reduced the increase in liver and spleen weights in *Cyp2c70* KO mice.

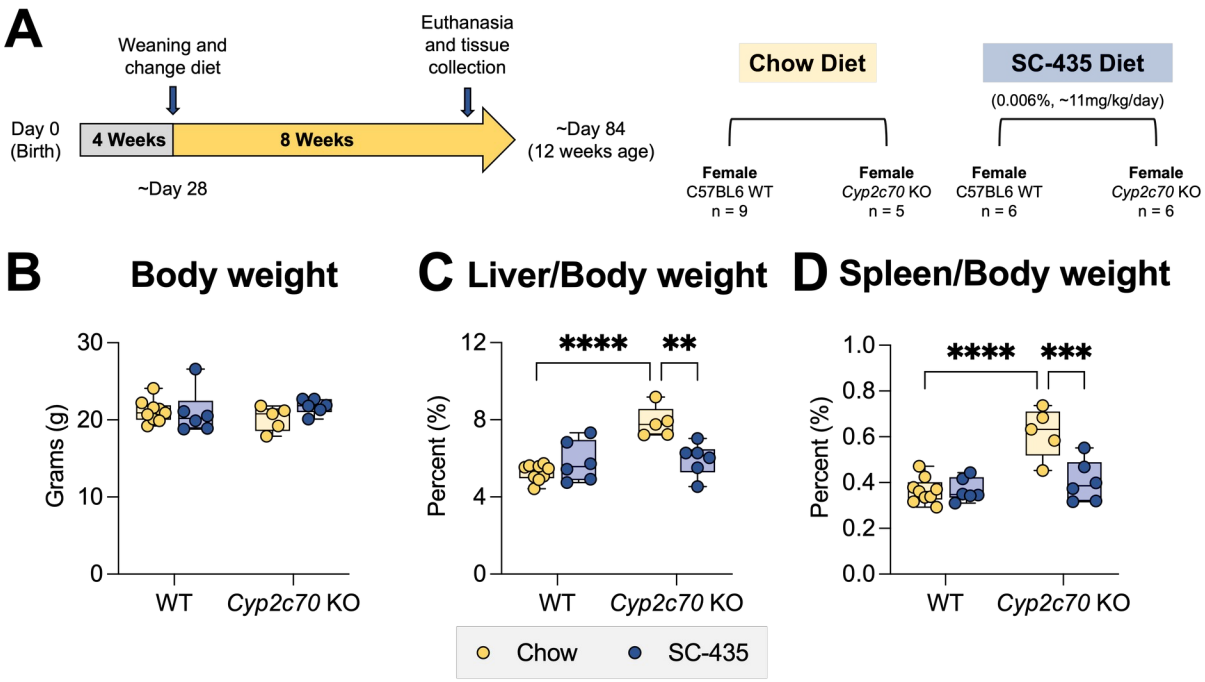

Figure 1. Liver and spleen weights are elevated in female *Cyp2c70* KO mice.

A: Experimental scheme. Mice are weaned at 4 weeks and maintained on chow or switched to SC-435 diet until sacrifice and tissue was collected at 12 weeks of age. B: Body weights. C: Liver/Body weights. D: Spleen/Body weights. Asterisks indicate significant differences between groups. Median values (line), interquartile range (boxes) and min to max values are shown ($^{**}P < 0.01$, $^{***}P < 0.001$, $^{****}P < 0.0001$); n = 5 – 9 mice per group.

Female and male *Cyp2c70* KO mice maintained on chow diet exhibited strongly elevated serum levels of liver injury markers as compared to WT mice. This included levels of ALP, an indicator of cholestatic liver injury, which were significantly elevated in female (Fig. 2A) and male (supplemental Fig. S3A) *Cyp2c70* KO compared to WT mice of the same age. The same trend was observed for serum levels of the liver cytosolic enzymes ALT (Fig. 2B and supplemental Fig. S3B) and AST (Fig. 2C and supplemental Fig. S3C) and for BAs in female and male *Cyp2c70* KO mice. This robust increase of these liver injury markers (Fig. 2 and supplemental Fig. S3) was successfully blocked with IBAT inhibition.

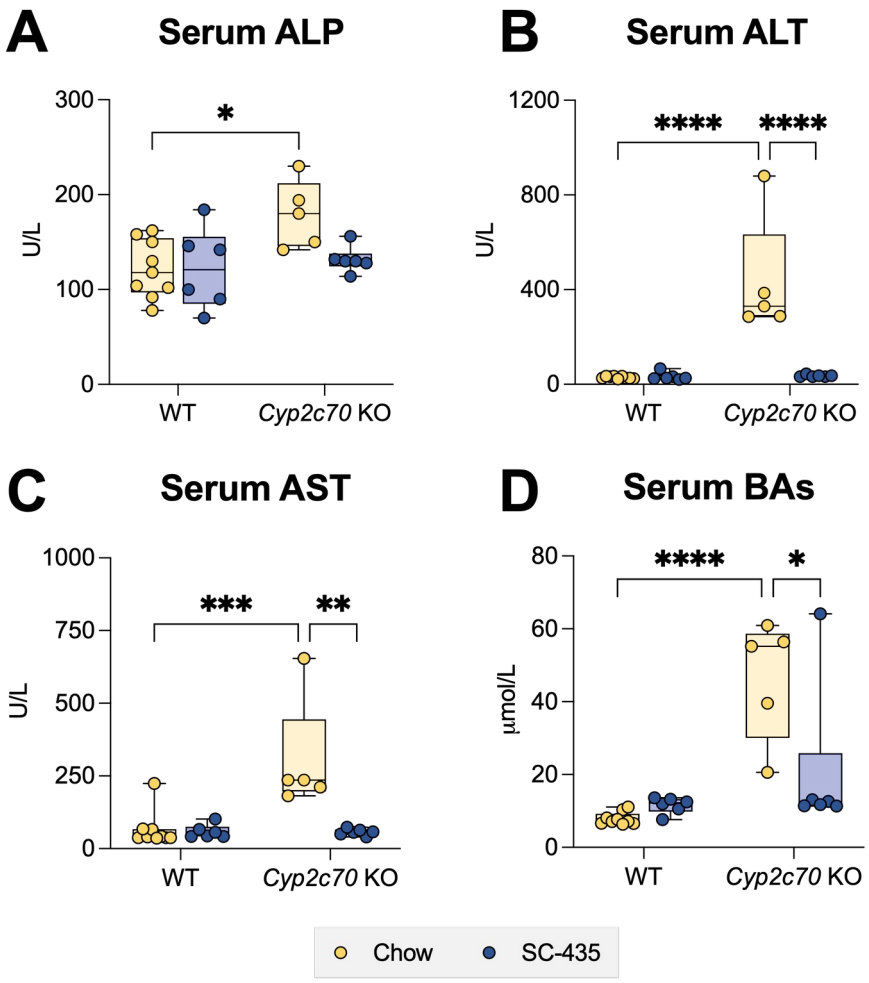

Figure 2. Female *Cyp2c70* KO mice have elevated serum liver injury markers and are protected from cholestatic injury by the IBAT inhibitor SC-435.

A: Serum alkaline phosphatase (ALP). B: Serum alanine aminotransferase (ALT). C: Serum aspartate aminotransferase (AST). D: Serum bile acids (BAs). Asterisks indicate significant differences between groups. Median values (*line*), interquartile range (*boxes*) and min to max values are shown (*whiskers*) (*$P < 0.05$, **$P < 0.01$, ***$P < 0.001$, ****$P < 0.0001$); n = 5 – 9 mice per group.

At 12 weeks of age, female *Cyp2c70* KO mice exhibited many characteristic histological features of cholestatic liver injury, as measured by immunohistochemistry for Ck-19 delineating

ductular reaction and F4/80 for macrophage infiltration, and Sirius Red staining for collagen deposition (Fig. 3). QuPath-mediated analysis of the liver images revealed that IBAT inhibition attenuated the increase in biliary cell proliferation (Ck-19, Fig. 3B), macrophage infiltration (F4/80, Fig. 3C), and fibrosis (Sirius Red, Fig. 3D) observed in *Cyp2c70* KO mice to levels indistinguishable from WT mice. Findings for the male cohort of *Cyp2c70* KO mice were similar, however the magnitude of the histological changes was less pronounced than that observed for female *Cyp2c70* KO mice (Supplemental Fig. S4A-S4D).

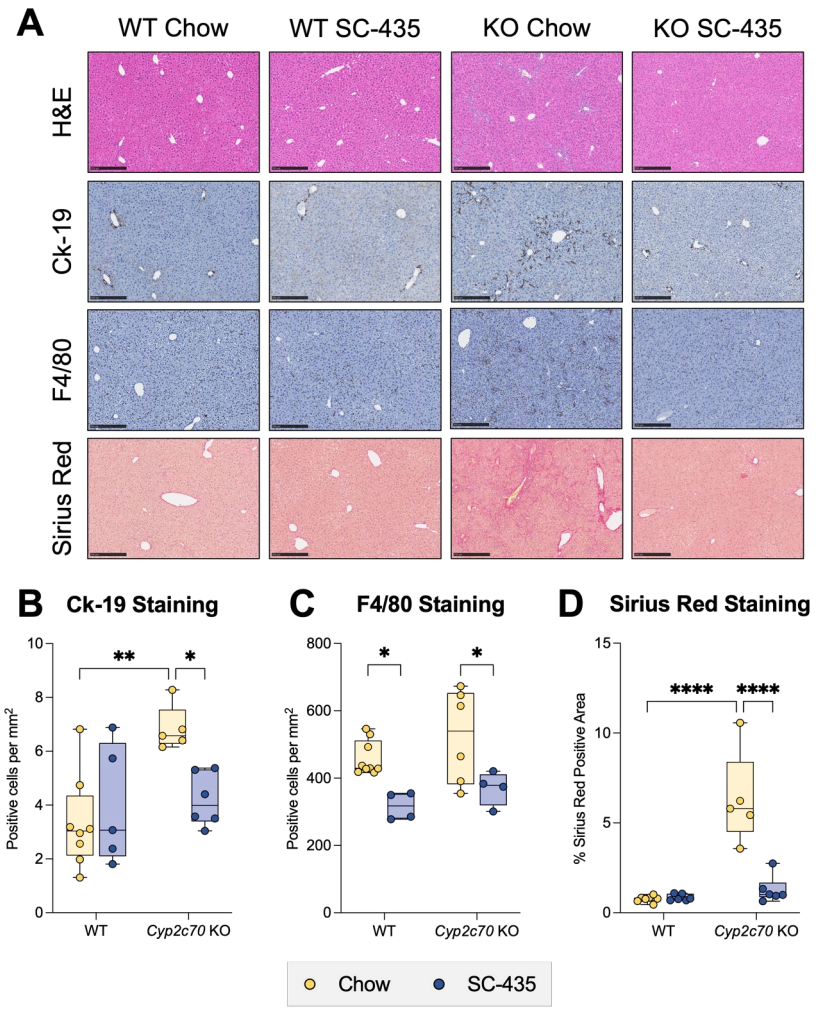

Figure 3. Immune and fibrotic responses in female *Cyp2c70* KO mice are alleviated with SC-435 treatment.

A: Morphological response to SC-435 treatment in WT and *Cyp2c70 KO* mice. From top to bottom panel: Hematoxylin and eosin (H&E), Cytokeratin-19 (Ck-19), F4/80, and Sirius Red stained liver sections (original magnification 10X) from the indicated genotypes and treatments groups. *Scale bar*, 250 μm. Quantification of positive B: Ck-19, C: F4/80 cells per mm^2, and D: Percent Sirius Red positive area of the entire liver section. Asterisks indicate significant differences between groups. Median values (*line*), interquartile range (*boxes*) and min to max values are shown (*whiskers*) (*$P < 0.05$, **$P < 0.01$, ****$P < 0.0001$); n = 5 – 9 mice per group.

To complement the histological findings, expression of marker genes for hepatic inflammation, fibrosis and biliary proliferation were measured. Quantitative real time PCR measurements revealed that liver mRNA levels of interleukin 1 beta (Il-1β, Fig. 4A), transforming growth factor beta (Tgf-β, Fig. 4B), type I collagen (Col1a1, Fig. 4C), tissue inhibitor matrix metalloproteinase-1 (Timp-1, Fig. 4D), and Ck-19 (Fig. 4F) were significantly elevated in female *Cyp2c70* KO mice, and restored to WT levels with IBAT inhibition. In contrast, no significant change was observed in mRNA levels of α smooth muscle alpha-actin (α-Sma, Fig. 4E). In the male cohort of *Cyp2c70* KO mice, liver mRNA levels for Tgf-β, Timp-1, and Ck-19 were significantly increased, with a trend towards increased *Col1al* mRNA, and no significant changes observed in the mRNA levels of Il-1β and α-Sma. As in the female cohort, IBAT inhibition blocked the increase in expression of these liver injury markers in the male *Cyp2c70* KO mice (Supplemental Figs. S5A-S5F).

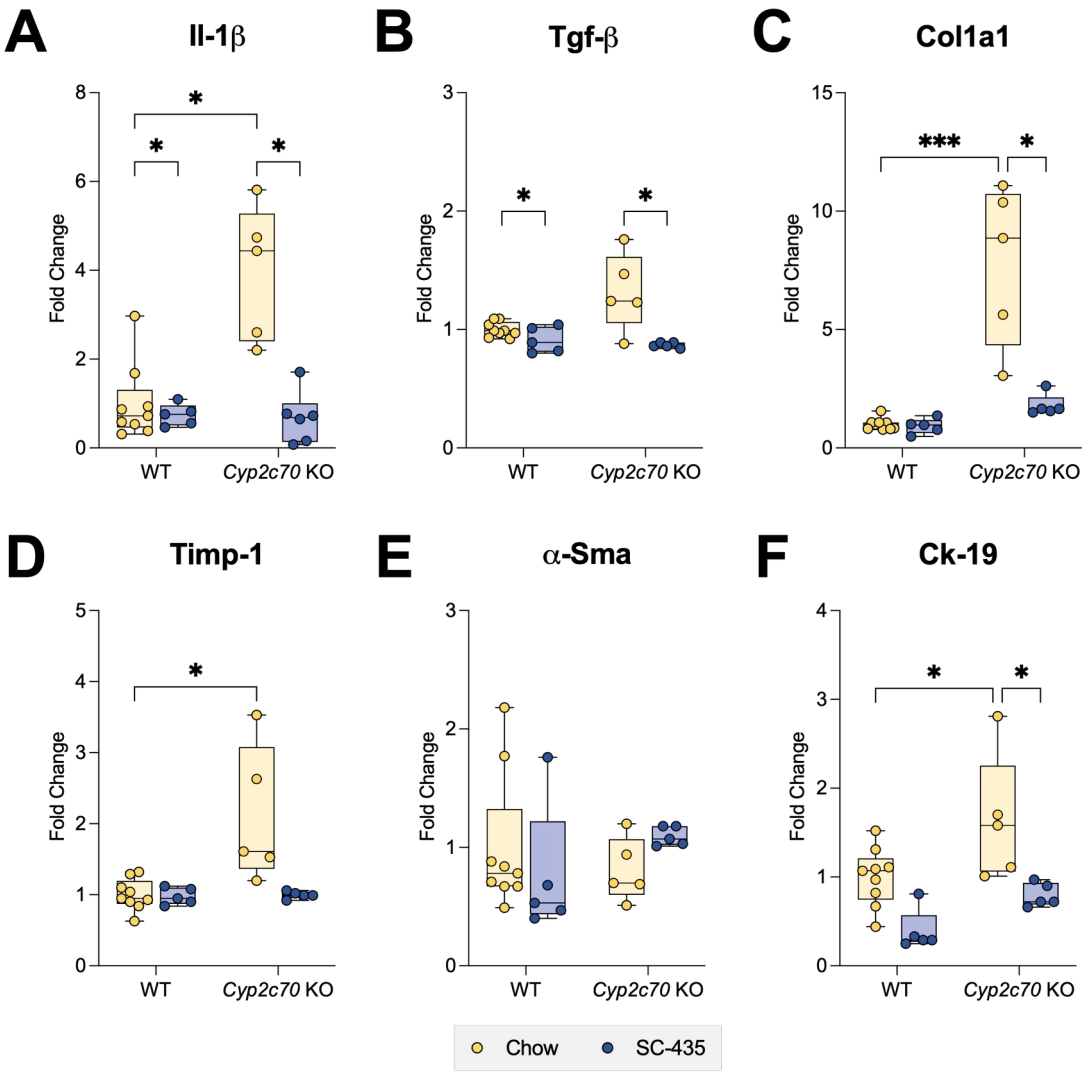

Figure 4. Increased hepatic expression of inflammation and fibrosis-related genes in female *Cyp2c70* KO mice is alleviated with SC-435 treatment.

A: Il-1β, B: Tgf-β, C: Col1a1, D: Timp-1, E: α-Sma, and F: Ck-19 gene expression. RNA was isolated from livers of individual mice and used for real-time PCR analysis. The mRNA expression was normalized using cyclophilin and the results for each gene are expressed relative to chow-fed WT mice for each gene. Asterisks indicate significant differences between groups. Median values (*line*), interquartile range (*boxes*) and min to max values are shown (*whiskers*) (*$P < 0.05$, ***$P < 0.001$); n = 5 – 9 mice per group.

IBAT Inhibition reduces expression of inflammatory pathway genes

To identify pathways that may underlie the IBATi's therapeutic benefit, RNA-Seq analysis was performed using livers from female and male WT and *Cyp2c70* KO mice fed chow or SC-435-containing chow diet (Fig. 5). Identification of differentially expressed genes with a log2 (fold-change) > 1 and adjusted $P < 0.05$ in female chow-fed *Cyp2c70* KO versus chow-fed WT mice revealed 216 genes were down regulated and 1138 genes were up regulated in *Cyp2c70* KO versus WT mice (total of 1354 differentially expressed genes). Using the same approach, female *Cyp2c70* KO mice fed chow versus SC-435 were also compared. In that analysis, 721 genes were down regulated, and 414 genes were up regulated in *Cyp2c70* KO mice by the SC-435 treatment (1135 total differentially expressed genes).

Gene set enrichment analysis was used to identify potential pathways that mediate hepatoprotective actions of the IBATi. We used Kyoto Encyclopedia of Genes and Genomes (KEGG) analysis and the Database for Annotation, Visualization, and Integrated Discovery (DAVID) to annotate the genes to the pathway level. The absence of *Cyp2c70* significantly upregulated 48 pathways and downregulated 13 pathways when compared to WT by KEGG analysis (Fig. S6). IBAT inhibition in *Cyp2c70* KO mice downregulated 37 pathways and upregulated 6 pathways when compared to chow fed *Cyp2c70* KO mice. To further understand the gene expression changes associated with reversal of *Cyp2c70* KO-associated liver injury, the genes upregulated in *Cyp2c70* KO versus WT mice (1138 genes) and downregulated in *Cyp2c70* KO mice fed SC-435 versus chow (721 genes) were identified and compared. This analysis identified 488 genes whose expression decreased toward WT levels with SC-435 treatment and were largely related to pathways associated with inflammatory and immune response (Fig. 5). Expression of genes for inflammatory cytokines commonly found elevated in cholestasis such as

Ccl2, *Cxcl1*, *Cxcl2* and *Cxcl10* (35) was ameliorated by SC-435 treatment. The same approach was taken to narrow the list of genes down-regulated in *Cyp2c70* KO versus WT mice (216 genes) and those upregulated in *Cyp2c70* KO mice fed SC-435 versus chow (414 genes). This identified 85 genes whose expression increased toward WT levels with SC-435 treatment and were largely related to lipid and xenobiotic metabolic processes. In addition to BA biosynthetic genes, cholesterol 7α-hydroxylase (*Cyp7a1*) and sterol 12α-hydroxylase (*Cyp8b1*), genes encoding enzymes that contribute to sulfation and metabolism of steroids and BAs in the liver such as *Hsd17b7*, *Sult2a1,* and *Sult2a2* were significantly elevated in IBATi treated animals. Because of the observed sex differences in the hepatic injury phenotype in this model, analysis of the liver gene expression changes in male mice was performed separately (Supplemental Fig. S7). In the male mice, examination of genes upregulated in *Cyp2c70* KO versus WT mice (778 genes) and those downregulated in *Cyp2c70* KO mice in response to SC-435 feeding (1188 genes) revealed 563 common genes, which were largely related to pathways associated with inflammatory and immune response. Examination of genes down-regulated in *Cyp2c70* KO versus WT mice (172 genes) and those upregulated in *Cyp2c70* KO mice in response to SC-435 feeding (391 genes) revealed 90 common genes, which were largely related to pathways related to lipid and xenobiotic metabolic processes. Common pathways pointing towards alleviating inflammation were found and changes in hepatic gene expression in the male group are shown in Supplemental Fig. S8.

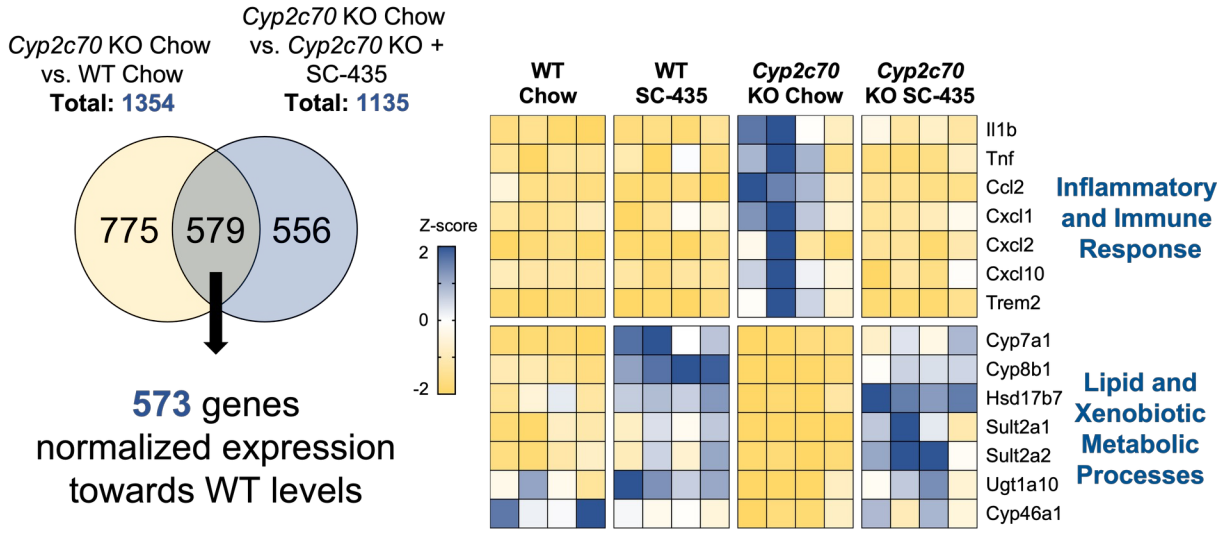

Figure 5. Female mouse liver RNA-Seq analysis.

Venn diagram showing the number of differentially expressed genes identified in *Cyp2c70 KO* mice versus WT, and *Cyp2c70* KO mice fed chow versus chow plus SC-435. Intersection represents the subset of genes (488 down regulated plus 85 up regulated) whose expression is normalized towards WT levels. Change in expression are displayed as change in Z-score on heatmap for representative genes from the indicated pathways that were normalized with SC-435 treatment. Each column in the heatmap represents an individual animal.

IBAT inhibition alters BA metabolism and reduces hepatic BA content in *Cyp2c70* KO mice

To investigate the mechanisms underlying the hepatoprotective effects of IBAT inhibition in *Cyp2c70* KO mice, quantitative real-time PCR and immunoblotting were used to measure mRNA and protein expression of selected liver genes important for BA homeostasis and liver BA composition. Hepatic mRNA and protein expression of *Cyp7a1* and particularly *Cyp8b1* are decreased in female *Cyp2c70* KO versus WT mice (Fig. 6A, 6B). Treatment with the IBATi significantly increased hepatic *Cyp7a1* and *Cyp8b1* expression in all groups. This was particularly pronounced in *Cyp2c70* KO mice, where *Cyp8b1* mRNA and protein expression increased more than 10-fold with IBAT inhibition (Fig. 6E). In hepatocytes, BAs are taken up across the sinusoidal membrane by sodium-dependent and independent mechanisms involving the Na^+-taurocholate co-transporting polypeptide (Ntcp; *Slc10a1*) and members of the Organic Anion Transport Protein (Oatp) family, respectively, whereas the bile salt export pump (Bsep; *Abcb11*) mediates hepatocyte BA secretion across the canalicular membrane. Expression of Ntcp mRNA was reduced in *Cyp2c70* KO mice and restored to WT levels with IBAT inhibition (Fig. 6C). In contrast, Bsep mRNA and protein expression were not significantly altered in *Cyp2c70* KO mice or in response to IBATi treatment (Fig. 6D, 6E). Qualitatively similar changes were observed in the male cohort of *Cyp2c70* KO mice, although the decrease in hepatic *Cyp8b1* expression is significantly attenuated in male versus female *Cyp2c70* KO mice. However, there were no sex-specific differences in the response to IBATi treatment at the mRNA (Fig. 6A-6D; supplemental Fig. S9A-S9D) or protein expression (Fig 6E, supplemental Fig. S9E) levels for these genes.

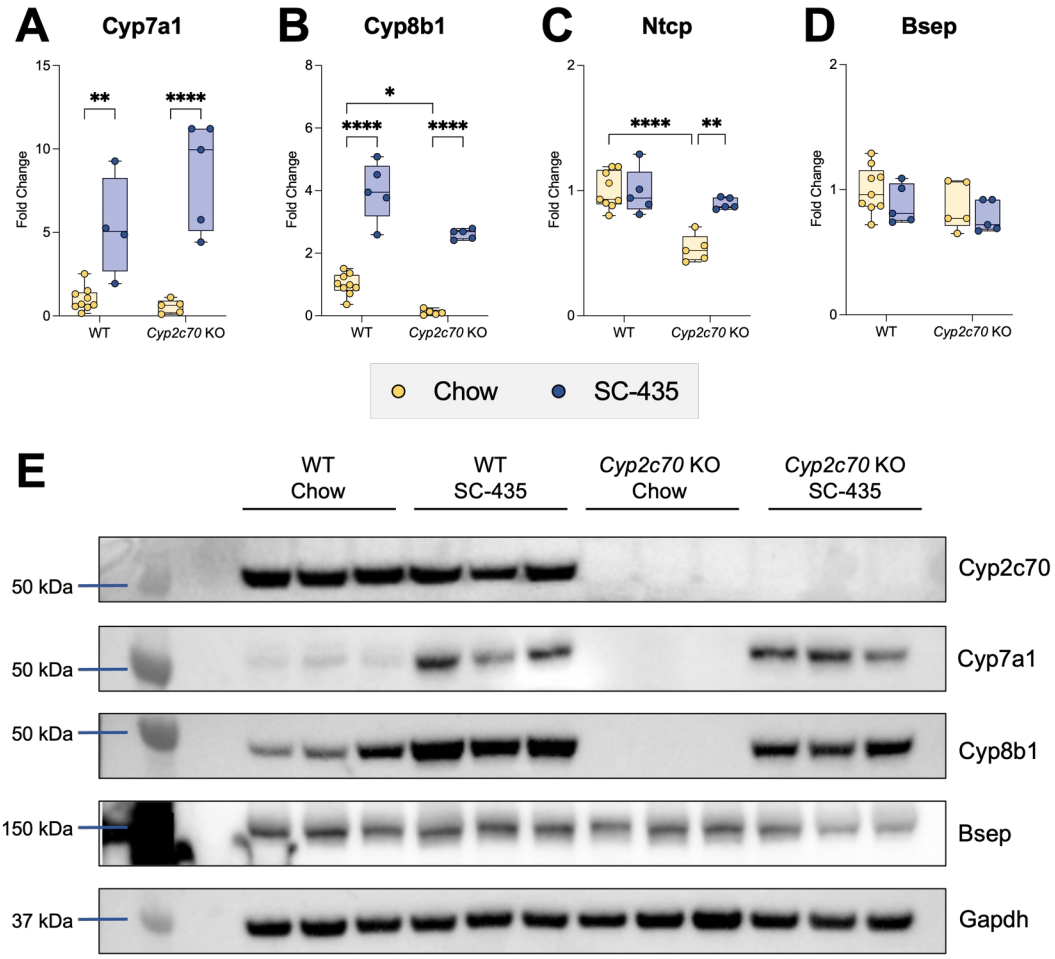

Figure 6. IBAT inhibition increases hepatic expression of BA metabolism genes in female WT and *Cyp2c70* KO mice.

RNA was isolated from livers of individual mice and used for real-time PCR analysis. The mRNA expression was normalized using cyclophilin and the results for each gene are expressed relative to chow-fed WT mice for each gene. A: Cyp7a1; B: Cyp8b1; C: Ntcp; D: Bsep. Asterisks indicate significant differences between groups. Median values (*line*), interquartile range (*boxes*) and min to max values are shown (*whiskers*) (*$P < 0.05$, **$P < 0.01$, ****$P < 0.0001$); n = 5 – 9 mice per group. E: Protein was isolated from livers of individual mice and used for Western Blot analysis, n = 3 mice per group.

To determine how IBAT inhibition affected liver BA composition and content in the *Cyp2c70* KO mice, liver extracts were prepared and analyzed by HPLC-electrospray ionization mass spectrometry (36). The pool of liver-associated BAs included primarily taurine conjugates, with unconjugated BAs constituting less than ~2% of the total in all groups. The total and contribution of individual BAs to the liver content for female mice are shown in Fig. 7 and individual BA species are shown in supplemental Table S3. In addition to being devoid of MCAs, *Cyp2c70* KO mouse livers are enriched in taurochenodeoxycholic acid (TCDCA) and have an increased amount of tauroursodeoxycholic acid (TUDCA). This increase in TUDCA is likely due to several mechanism including: 1) the increased production of CDCA, which can be converted to 7-keto-lithocholic acid by gut bacterial 7αhydroxysteroid dehydrogenases and then reduced to UDCA or CDCA by the hepatocyte enzyme 11β-hydroxysteroid dehydrogenase1 (37, 38), and 2) the loss of Cyp2c70-mediated conversion of UDCA to βMCA (13, 14, 17, 39). The levels of taurolithocholic acid (TLCA) were also significantly increased in female *Cyp2c70* KO mouse livers but constituted less than 3% of the total BAs.

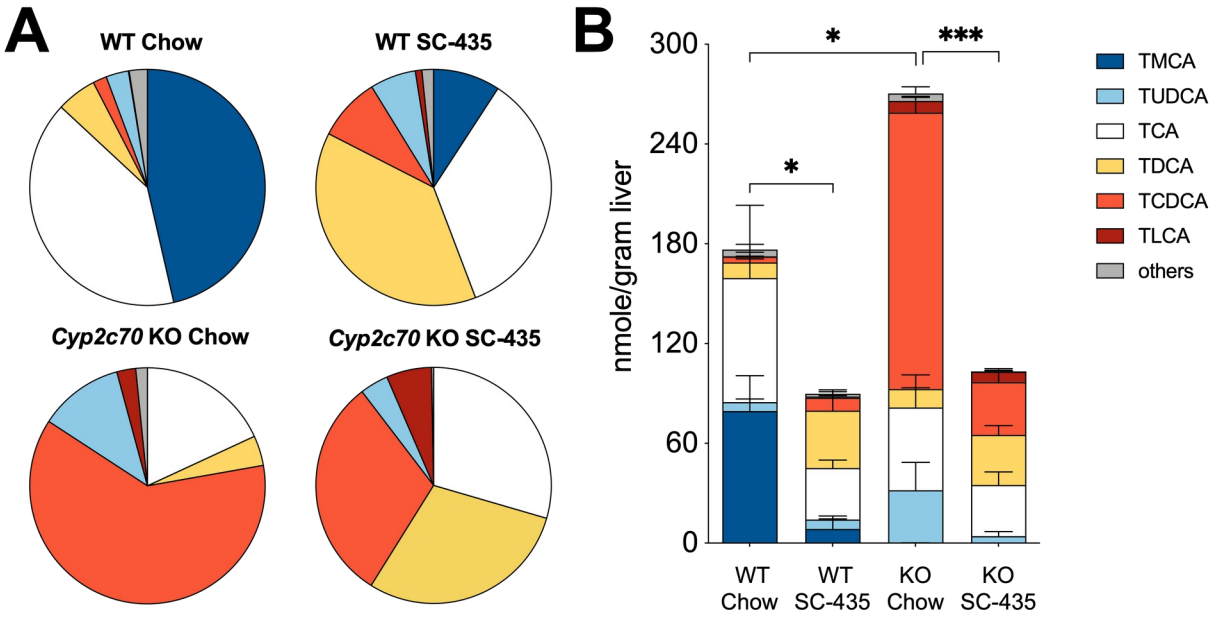

Figure 7. IBAT inhibition prevents the increase in liver BA retention in female *Cyp7c70* KO mice.

A: Muricholates are absent in *Cyp2c70* KO mice. Pie charts for the liver BA profiles. B: Absence of *Cyp2c70* increased the total amount of liver-associated BAs and the amount of taurochenodeoxycholic acid (TCDCA) in *Cyp2c70* KO mice. Mean values ± SD are shown (*$P < 0.05$, ***$P < 0.001$); n = 4 mice per group.

The overall effect is to significantly increase the hydrophobicity of the liver BAs, with the calculated hydrophobicity index (HI) (40) value increasing from -0.28 in WT mice to +0.28 in *Cyp2c70* KO mice (Fig. 8A). In agreement with previous reports (24), IBAT inhibition reduced the proportion of hydrophilic TMCAs and increased TDCA and TCDCA in livers of WT mice, thereby elevating the calculated HI from -0.28 to +0.18. In *Cyp2c70* KO mice, IBAT inhibition reduced the proportion of TCDCA plus TUDCA, increased the proportion of TCA plus TDCA, and further increased the calculated HI of the liver-associated BAs to +0.36. To reconcile how IBAT inhibition can both increase hydrophobicity of the hepatic BA content and reduce liver injury in *Cyp2c70* KO mice, the total liver BA content was compared between groups. Hepatic BA content in chow fed female *Cyp2c70* KO was significantly increased by 53% versus WT mice (Fig. 7B). Despite increases in hepatic Cyp7a1 expression and a predicted increase in hepatic BA synthesis, treatment with the IBATi to interrupt the BA enterohepatic circulation significantly reduced the total liver BA content by 49% and 62% in female WT and *Cyp2c70* KO mice, respectively. The IBATi-associated improvement in liver histology and serum markers of injury and decrease in liver BA content in *Cyp2c70* KO mice in the absence of a reduction in the overall hydrophobicity of the liver BAs, suggests that reducing the hepatic BA accumulation may be sufficient to alleviate the injury. The hepatic toxicity of CDCA has been well documented in animal models, and levels of liver associated TCDCA were reduced along with the serum transaminases in the IBATi treated *Cyp2c70* KO mice (Figs. 8B, 8C). The liver BAs in male mice showed the same trends with inactivation of *Cyp2c70* and the response to IBAT inhibition as the female mice (supplemental Fig. S10 and Table S4). The hepatic BA content in chow fed male *Cyp2c70* KO was increased by 65% versus WT mice and reduced with IBATi treatment by 56% and 54% in the WT and *Cyp2c70* KO mice, respectively. Total liver

BA levels were lower in male versus female *Cyp2c70* KO mice, in agreement with the milder liver injury phenotype. However, hydrophobicity of the liver BAs was similarly elevated in male and female *Cyp2c70* KO versus WT mice and in male and female IBATi-treated versus untreated mice (supplemental Fig. S11). The calculated hydrophobicity values were -0.31 and +0.23 in chow and IBATi-treated WT male mice, respectively and +0.25 and +0.34 in chow and IBATi-treated male *Cyp2c70* KO mice. As in the female mice, the amount of liver associated TCDCA and the serum levels of ALT and AST were reduced in the IBATi-treated male *Cyp2c70* KO mice (supplemental Fig. S11).

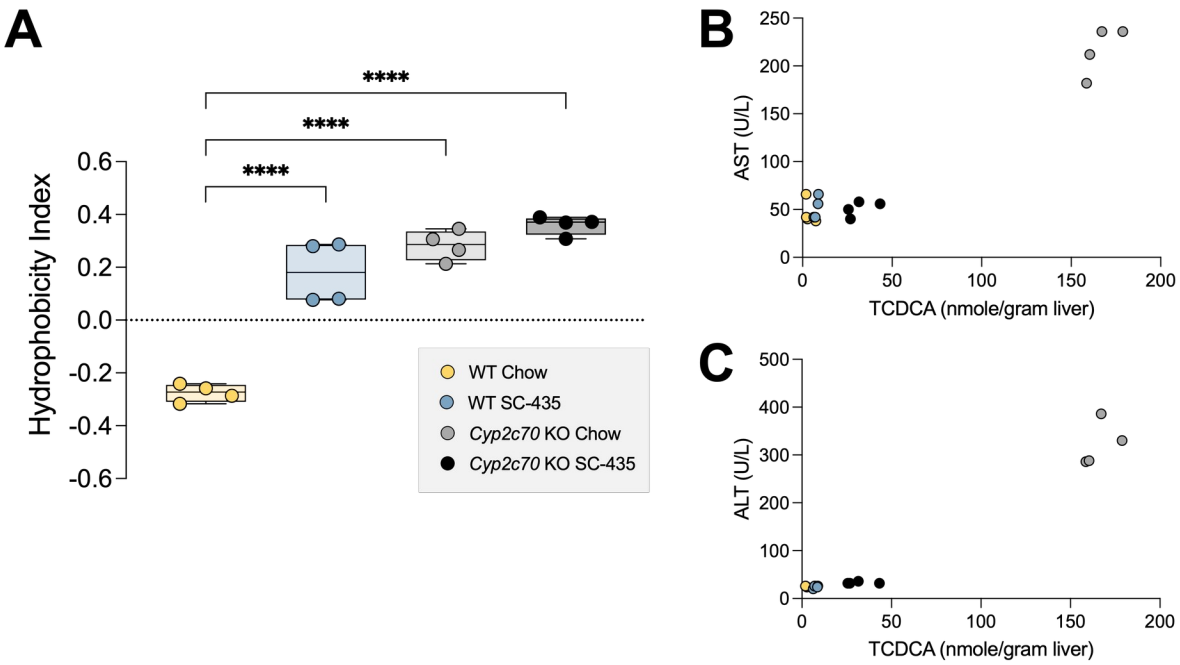

Figure 8. IBAT inhibition does not reduce liver BA hydrophobicity in female *Cyp7c70* KO mice.

A: Liver BA composition was used to calculate the hydrophobicity index. IBAT inhibition and inactivation of *Cyp2c70* increases the hydrophobicity of the liver BA pool. Asterisks indicate significant differences between groups. Median values (*line*), interquartile range (*boxes*) and min to max values are shown (*whiskers*) (***$P < 0.001$); n = 4 mice per group. B and C: Liver amount of taurochenodeoxycholic acid (TCDCA) and serum levels of alanine aminotransferase (ALT) and aspartate aminotransferase (AST) are reduced in IBAT inhibitor treated *Cyp2c70* KO mice.

Detergency of the hepatic BA pool in *Cyp2c70* KO mice

To complement the *in vivo* findings, the ability of individual BAs and BA mixtures to induce membrane damage and toxicity was assessed. The *in vitro* toxicity of BAs generally correlate with their detergency, which is concentration dependent and reflects their ability to self-aggregate (41). As a measurement of detergency and the potential for membrane lipid bilayer damage, the ability of individual conjugated BAs to lyse red blood cells (RBC) was evaluated. Whereas this model system has been used previously to study individual BAs from a variety of species (42), cytolytic properties of the individual taurine-conjugated muricholate species, TαMCA, TβMCA and TωMCA have not been reported. The detergency of individual taurine conjugated BAs partially followed their hydrophobicity estimated from their reported relative retention time by HPLC using a C18 octadecylsilane stationary phase (40, 43) (Fig. 9A), with TCDCA ≥ TDCA >> TCA > TαMCA>> TβMCA >> TωMCA = TUDCA. Despite having a 1-octanol-water partition coefficient that is identical to TCDCA (44), TUDCA shows no hemolytic activity over the concentration range examined. Interestingly, TαMCA and TβMCA showed cytolytic activity that was intermediate between TUDCA and TCA whereas TωMCA, microbial-derived 6β-epimer of TαMCA, exhibited an RBC lytic activity similar to TUDCA and failed to induce hemolysis in this assay. For comparison, the RBC lytic activity of a limited number of individual glycine-conjugated BAs are shown (Fig. 9A) with GDCA > GCDCA >> GCA = GUDCA. To examine the detergency and toxicity properties of the BA compositions in the WT and *Cyp2c70* KO mice fed chow and IBATi, the RBC assay was performed using mixtures of BAs approximating the measured hepatic BA compositions shown in Fig. 7. As expected, the WT mouse liver BA composition, which contains almost 50% hydrophilic muricholates, exhibits weak cytolytic activity. Mixtures modeling the hepatic BA composition of female *Cyp2c70* KO

mice fed chow or chow containing IBATi were approximately twice as potent in the RBC lysis assay and exhibit activity similar to a model human liver BA composition (45) (Fig. 9B). To complement these findings, two additional measurements of cellular toxicity were assessed. Similar results were obtained using the BA mixtures approximating the hepatic BA compositions for WT and *Cyp2c70* KO mice when measuring cellular viability and metabolic activity using a MTT assay (Fig. 9C), and cellular cytotoxicity using lactate dehydrogenase (LDH) release (Fig. 9D).

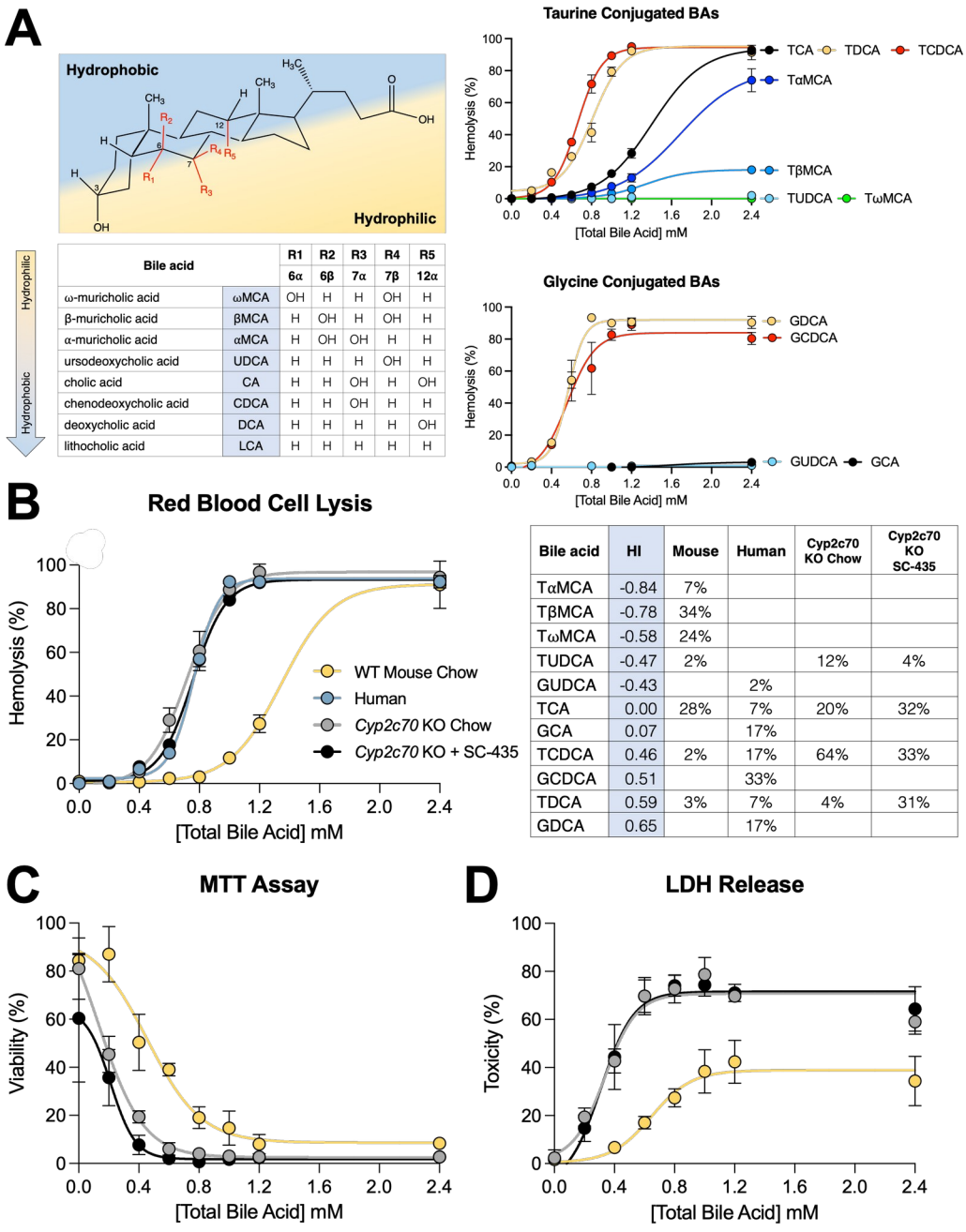

Bile acid		R1 6α	R2 6β	R3 7α	R4 7β	R5 12α
ω-muricholic acid	ωMCA	OH	H	H	OH	H
β-muricholic acid	βMCA	H	OH	H	OH	H
α-muricholic acid	αMCA	H	OH	OH	H	H
ursodeoxycholic acid	UDCA	H	H	H	OH	H
cholic acid	CA	H	H	OH	H	OH
chenodeoxycholic acid	CDCA	H	H	OH	H	H
deoxycholic acid	DCA	H	H	H	H	OH
lithocholic acid	LCA	H	H	H	H	H

Bile acid	HI	Mouse	Human	Cyp2c70 KO Chow	Cyp2c70 KO SC-435
TαMCA	-0.84	7%			
TβMCA	-0.78	34%			
TωMCA	-0.58	24%			
TUDCA	-0.47	2%		12%	4%
GUDCA	-0.43		2%		
TCA	0.00	28%	7%	20%	32%
GCA	0.07		17%		
TCDCA	0.46	2%	17%	64%	33%
GCDCA	0.51		33%		
TDCA	0.59	3%	7%	4%	31%
GDCA	0.65		17%		

Figure 9. The liver BAs of *Cyp2c70* KO mice are more cytotoxic and resemble a human-like composition.

A: The structure, common name, position of the hydroxyl groups, relative hydrophobicity and hemolysis potential of the individual major BAs commonly found in mammals. Red blood cells isolated from mouse whole blood were incubated with the indicated concentrations of BAs for 30

min at 37°C and the amount of hemolysis was measured. B: Composition and hemolysis profile of liver BAs in female WT and *Cyp2c70* KO mice fed chow or chow plus SC-435 as compared to human. The calculated hydrophobicity index (HI) and compositions of the BA mixtures used for the incubations are shown. C: AML12 (alpha mouse liver 12) cells were incubated with the indicated concentration of BA mixtures modeling the liver BA composition of WT or *Cyp2c70* KO mice and cell viability was quantified by MTT assay. D: AML12 cells were incubated with the indicated concentration of BA mixtures and BA toxicity measured by lactate dehydrogenase (LDH) release. Mean values $\pm$ SD are shown.

Discussion

The major finding of this study is that reduction of hepatic BA accumulation with IBAT inhibition protects *Cyp2c70* KO mice from hepatic injury, independent of the hydrophobicity of the BA pool. Although BAs have previously been implicated as a factor in cholestatic liver disease (3, 5-7), the precise mechanisms by which BAs and toxic bile contribute to the pathogenesis of human cholestatic liver disease remains a fundamental unresolved question (8-10). Identification of *Cyp2c70* as the hepatic cytochrome P450 enzyme responsible for the synthesis of muricholates by the Myomorpha suborder of rodents (mice, rats, voles, jerboas) (2) was a significant breakthrough in the field (13), and has enabled the generation and study of *Cyp2c70* KO mice as a laboratory model with a more human-like hydrophobic BA composition (14, 15, 17, 18). As previously reported by others, the *Cyp2c70* KO mice in this study lack hydrophilic 6-hydroxylated MCAs and possess a hepatic BA composition dominated by CDCA. This change in primary BA synthesis by *Cyp2c70* KO mice was associated with increases in liver and spleen weight, elevation of serum markers of liver damage, and histological evidence of liver injury including ductular reaction, immune cell infiltration, and fibrosis. The liver injury phenotype was more pronounced in female versus male *Cyp2c70* KO mice. This observation has been previously reported and was attributed in part to a greater reduction in hepatic *Cyp8b1* expression and reduced synthesis of CA, a more hydrophilic BA, in the female versus male *Cyp2c70* KO mice (18).

In addition to a more hydrophobic CDCA-enriched BA composition, liver BA content has been reported to be elevated in *Cyp2c70* KO versus WT mice (14, 15). This is despite a reduction in hepatic BA synthesis and the whole-body BA pool size (14, 18). The mechanisms responsible for the increased hepatic BA retention in *Cyp2c70* KO mice have not been identified

but may include the lower bile secretory capacity for hydrophobic versus hydrophilic BAs (46, 47), or hydrophobic BA-induced damage to cytoplasmic organelles (3, 48), the canalicular membrane (49-51), intrahepatic ductules (Canals of Hering) or bile ducts (52, 53). Whereas the increased hydrophobicity of the BA pool in *Cyp2c70* KO mice likely has a significant role in initiating the hepatocellular damage, persistent elevated intrahepatic BA levels may play a role in driving the progression of hepatocellular injury. To further understand the mechanisms underlying the liver injury in *Cyp2c70* KO mice, we studied the effects of pharmacological inhibition of the ileal BA transporter, an intervention that has previously been shown to reduce liver BA concentrations and yield benefit in the *Mdr2* KO mouse model of cholestatic and bile duct injury (8, 19).

IBAT inhibition significantly increases the hepatic expression of *Cyp7a1* and *Cyp8b1* in WT and *Cyp2c70* KO mice. This was particularly evident for *Cyp8b1* in female *Cyp2c70* KO mice, resulting in a predicted shift in hepatic BA synthesis towards CA and away from CDCA. However, IBAT inhibition also significantly increases BA flux into the colon, where the BAs undergo bacterial deconjugation and 7a-dehydroxylation, thereby increasing the conversion of CA to DCA (54). Unconjugated dihydroxy BAs such as CDCA and DCA are sufficiently hydrophobic to undergo passive absorption in the colon (55, 56) and are transported back to the liver in the portal circulation for uptake, reconjugation, and resecretion into bile. Interestingly, *Cyp2a12* has recently been identified as the mouse liver enzyme responsible for the 7α-rehydroxylation of TDCA to TCA (14). However, as observed for previous studies of IBAT inhibition in mice (24), the increased return of DCA to the liver appears to overwhelm the ability of *Cyp2a12* to efficiently convert TDCA to TCA. As a result, there is an increase in the hepatic proportion of TDCA, a hydrophobic dihydroxy BA with detergency properties similar to

TCDCA (57). In agreement with previous findings (14, 18), examination of the liver BA composition of *Cyp2c70* KO mice in this study revealed a significant increase in hydrophobic BA species and calculated hydrophobicity index. Hydrophobic BAs such as CDCA are known to induce liver toxicity, whereas hydrophilic bile acids like UDCA are rarely associated with liver damage (9, 58). In support of the hypothesis that the altered BA composition plays an important role in the liver injury phenotype, administration of UDCA to *Cyp2c70* KO mice has been shown to increase the hydrophilicity of biliary BAs, improve liver histology, reduce plasma BA and transaminases levels, and normalize the hepatic and intestinal function towards that of WT mice (18). This was also evident in *Cyp2c70-Cyp2a12* double KO mice, where UDCA feeding improved neonatal viability and was protective in the male and female double KO mice at 6 weeks of age and in mael double KO mice at 20 weeks of age. (59). In contrast, UDCA-treated female *Cyp2c70-Cyp2a12* double KO mice still exhibited significant liver injury, with a a greatly elevated hepatic BA content and TLCA-enriched hydrophobic BA composition (59). When the steroidal FXR agonist obeticholic acid was recently evaluated in *Cyp2c70* KO mice, short-term 4-week treatment did not improve the hepatic fibrosis or development of cholangiopathy, despite suppressing BA synthesis (60). The lack of a beneficial effect was attributed to an increase in the hydrophobicity of biliary BAs in the obeticholic acid treated *Cyp2c70* KO mice. Paradoxically, administration of an IBAT inhibitor to *Cyp2c70* KO mice in this study prevented the development of cholangiopathy and liver fibrosis, despite increasing the hydrophobicity of the liver BAs to HI values similar to those of serum and bile BA samples analyzed in the obeticholic acid-treated *Cyp2c70* KO mice (60). This is likely due to the significant reduction in the retention of liver-associated BAs, which are decreased more than 50% in the IBAT inhibitor-treated *Cyp2c70* KO mice. In our study, the markers of liver injury AST and ALT were elevated

in *Cyp2c70* KO mice when hepatic levels of the hydrophobic BA TCDCA exceeded ~50 nmol/g of liver. As a result of an efficient BA enterohepatic circulation, previously synthesized BAs that have been secreted into bile and reabsorbed from the intestine are thought to account for approximately 95% of the liver BA flux, with newly synthesized BAs constituting the remaining ~5% (54, 61). Although hepatic BA synthesis is induced by interruption of the enterohepatic circulation, new synthesis is insufficient to account for a block in ileal active reabsorption (62). This may help explain the differences between our study and the reported findings for obeticholic acid treated *Cyp2c70* KO mice (60). Hepatic BA content was not measured in that study however we hypothesize that obeticholic acid suppression of hepatic BA synthesis was not adequate to yield similar decreases in the hepatic BA content. Interestingly, IBAT inhibition has been shown to reduce hepatic BA retention and improve biomarkers of hepatocellular and cholestatic injury in *Mdr2* KO mice (8, 19), whereas a 4 or 6-week treatment of this model with obeticholic acid showed only limited therapeutic benefit (63, 64).

The development of cholangiopathy and liver fibrosis in *Cyp2c70* KO mice has been attributed to the lack of the 6-hydroxylated MCAs, which normally comprise upwards of 40-50% of the murine BA pool. Whereas the physicochemical properties of CA, DCA, CDCA, LCA and their taurine and glycine conjugates have been the subject of considerable study (41, 44, 57) and the bactericidal activity of individual unconjugated MCAs have been reported (65), the detergency properties of taurine conjugated MCAs or mixtures of conjugated MCAs and non-trihydroxylated BAs have not been described. Using the RBC lysis model as measure of detergency, TαMCA and TβMCA demonstrated membrane lysis properties intermediate between TUDCA and the more hydrophobic BA species TCA, TDCA, and TCDCA. Whereas bacteria-mediated reactions such as 7α-dehydroxylation that convert primary to secondary BAs typically

increases detergency, microbial epimerization of the 6-hydroxy group of βMCA to yield the murine major secondary BA ωMCA dramatically reduces its detergent properties. This may be due to the alpha-orientation of the 6-hydroxy group in ωMCA, which like the 7β-hydroxy group in UDCA is equatorial to the plane of the steroid nucleus and favors interaction with water (43, 66). Mixtures of BAs approximating the measured hepatic BA composition in *Cyp2c70* KO mice were remarkably similar to that reported for human liver in the RBC lysis assay, supporting the concept that while still imperfect, the *Cyp2c70* KO mice may more closely model BA effects in the pathogenesis of liver disease in humans.

In summary, IBAT inhibition improved cholangiopathy and the hepatic injury in *Cyp2c70* KO mice despite increasing hepatic BA synthesis and hydrophobicity of the hepatic BA pool. The improvement was associated with a reduction in the total hepatic BA accumulation. The findings suggest that in addition to the important role of hydrophobicity, there may be a therapeutically addressable threshold for hepatic BA-induced injury by targeting the return of BAs to the liver by inhibiting the function of the intestinal bile acid transporter. Further studies will be required to determine if similar mechanisms are responsible in part for the clinical benefit of IBAT inhibitors that was recently demonstrated in children with PFIC and Alagille syndrome (21, 22).

Acknowledgements

We thank Shire Pharmaceutical for the research gift of the SC-435, Drs. Eddy Morgan and Choon-Myung Lee (Emory University) for the research gift of anti-rodent Cyp2c22/2c70 antibody, and Dr. Aldo Roda (University of Bologna) for helpful discussion regarding BA hydrophobicity and detergency. We acknowledge the Emory University Department of Animal Resources Quality Assurance and Diagnostic Laboratory for serum chemistry analyses and Children's Healthcare of Atlanta Pathology Services for liver histology services. Portions of this work were presented at the Annual Meeting of the American Association for the Study of Liver Disease (12-15 November 2021), the Experimental Biology Meeting (2-5 April 2022) and the XXVI International Bile Acid Meeting (9-10 July 2022).

Funding

This research was supported by the National Institute of Diabetes and Digestive and Kidney Diseases grants DK047987 (P.A.D.) and DK056239 (S.J.K.), the Meredith Brown Fund at Emory, and Mason Trust Fund (S.J.K.). T.M. is recipient of the Andrew K. Burroughs Fellowship from the European Association for the Study of the Liver and supported by the Doctoral College "Metabolic and Cardiovascular Disease" (AZ) of the Austrian Science Fund (FWF, DK-MCD W1226). J.K.T. was supported by T32-GM008367 and an NIH diversity supplement (DK047987-28S1). C.K. was supported by the Deutsche Forschungsgemeinschaft (KL 3389/1-1).

Data availability statement

The liver RNA-Seq dataset is available from the GEO repository with the following accession number: GSE145020.

Supplementary Material

Supplemental Table S1: Mouse primer sets used for RT-PCR analysis

Gene name	Forward primer 5'-3'	Reverse primer 5'-3'
Col1a1	TAGGCCATTGTGTATGCAGC	ACATGTTCAGCTTTGTGGACC
Tgf-β	CACCGGAGAGCCCTGGATA	TGTACAGCTGCCGCACACA
IL-1β	CAACCAACAAGTGATATTCTCCATG	GATCCACACTCTC CAGCTGCA
Timp1	AGGTGGTCTCGTTGATTTCT	GTAAGGCCTGTAGCTGTGCC
α-SMA	GTTCAGTGGTGCCTCTGTCA	ACTGGGACGACATGGAAAAG
Cyp8b1	TTCGACTTCAAGCTGGTCGA	CAAAGCCCCAGCGCCT
Bsep	CTGCCAAGGATGCTAATGCA	CGATGGCTACCCTTTGCTTC
Ntcp	ATGACCACCTGCTCCAGCTT	GCCTTTGTAGGGCACCTTGT
Cyp7a1	CAGGGAGATGCTCTGTGTTCA	AGGCATACATGCAAAACCTCC
Ck-19	CCGGACCCTCCCGAGATTA	CTCCACGCTCAGACGCAAG
Cyclophilin	GGCCGATGACGAGCCC	TGTCTTTGGAACTTTGTCTGCA

Supplemental Table S2: Source of the primary and secondary antibodies used in the study

Antibody	**Catalog #**	**Dilutions**	**Vendor**
Bsep	PA5-78690	1:1000	Invitrogen
Cyp7a1	PA5-100892	1:1000	Invitrogen
Cyp8b1	PA5-37088	1:1000	Invitrogen
Cyp2c22/70		1:3000	Gift (23)
Gapdh	MA5-15738	1:5000	Invitrogen
Goat anti-mouse IgG-HRP	sc-2005	1:5000	Santa Cruz
Goat anti-rabbit IgG-HRP	sc-2064	1:5000	Santa Cruz
Ck-19	ab52625	1:500	Abcam
F4/80	70076	1:100	Cell Signaling

	WT Chow	WT SC-435	*Cyp2c70* KO Chow	*Cyp2c70* KO SC-435
TαMCA	3.76 ± 3.11[a]	2.13 ± 1[a]	BLD	BLD
TβMCA	26.52 ± 11.49[a]	2.51 ± 1.62[a]	BLD	BLD
TωMCA	49.13 ± 9[a]	3.91 ± 3.55[b]	BLD	BLD
TCA	74.71 ± 43.73[a]	30.96 ± 4.68[a]	49.73 ± 19.68[a]	30.75 ± 7.84[a]
TDCA	9.33 ± 2.09[a]	34.49 ± 12.51[b]	11.15 ± 0.77[a]	30.11 ± 5.63[b]
TCDCA	3.54 ± 2.62[a]	7.72 ± 1.22[a]	166.27 ± 9.13[b]	31.79 ± 8.1[c]
TUDCA	5.37 ± 1.94[a]	5.68 ± 2.13[a]	31.71 ± 16.79[b]	4.21 ± 2.69[a]
TLCA	0.18 ± 0.07[a]	0.82 ± 0.48[a]	7.05 ± 2.68[b]	6.15 ± 0.98[b]
GCA	0.11 ± 0.05[a]	BLD	0.13 ± 0.04[a]	BLD
GCDCA	BLD	BLD	0.25 ± 0.03[a]	BLD
αMCA	0.18 ± 0.13[a]	0.15 ± 0.14[a]	BLD	BLD
βMCA	0.87 ± 0.43[a]	0.21 ± 0.19[b]	BLD	BLD
ωMCA	0.84 ± 0.61[a]	0.43 ± 0.49[a]	0.08 ± 0.04[a]	BLD
CA	1.98 ± 2.01[a]	0.52 ± 0.41[a]	2.39 ± 2.77[a]	0.26 ± 0.12[a]
DCA	BLD	0.12 ± 0.03[a]	BLD	0.08 ± 0.03[a]
CDCA	BLD	BLD	0.96 ± 0.72[a]	0.08 ± 0.03[a]
UDCA	BLD	0.1 ± 0.07[a]	0.57 ± 0.5[a]	BLD

Supplemental Table S3. Female mouse liver BA composition.

BAs were extracted from liver homogenate and analyzed using electrospray ionization mass spectrometry. BA concentrations (nmol/g liver) are reported as mean ± SD; n = 4 mice per group. Values with different superscript letters are significantly different ($P < 0.05$) according to ordinary two-way ANOVA and Sidak's multiple comparisons test or T-test when appropriate. BLD = below level of detection.

	WT Chow	WT SC-435	*Cyp2c70* KO Chow	*Cyp2c70* KO SC-435
TαMCA	5.99 ± 5.95[a]	0.11 ± 0.13[a]	0.58 ± 0.16[a]	0.15 ± 0.19[a]
TβMCA	24.48 ± 24.95[a]	1.15 ± 0.52[a]	0.35 ± 0.18[a]	0.25 ± 0.15[a]
TωMCA	0.06 ± 0.05[a]	0.02 ± 0.03[a]	0.8 ± 0.62[b]	BLD
TCA	26.24 ± 21.48[a]	10.17 ± 4.36[a]	23.5 ± 2.98[a]	10.96 ± 5.09[a]
TDCA	4.37 ± 2.91[a]	13.3 ± 8.9[a]	0.18 ± 0.03[b]	6.14 ± 3.06[a,b]
TCDCA	0.42 ± 0.25[a]	1.09 ± 0.34[a]	68.37 ± 38.09[b]	26.54 ± 16.86[a,b]
TUDCA	1.47 ± 1.37[a]	1.71 ± 1.37[a]	9.29 ± 6.57[b]	1.23 ± 0.85[a]
TLCA	0.03 ± 0.02[a]	0.13 ± 0.15[a]	1.77 ± 1.11[a]	2.07 ± 1.93[a]
GCA	BLD	BLD	BLD	BLD
GCDCA	BLD	BLD	BLD	BLD
αMCA	BLD	BLD	BLD	BLD
βMCA	0.23 ± 0.45	BLD	BLD	BLD
ωMCA	BLD	BLD	BLD	BLD
CA	0.19 ± 0.38	BLD	BLD	BLD
DCA	BLD	BLD	BLD	BLD
CDCA	BLD	BLD	BLD	BLD
UDCA	BLD	BLD	BLD	BLD
LCA	BLD	0.18 ± 0.21[a]	BLD	0.42 ± 0.11[b]

Supplemental Table S4. Male mouse liver BA composition.

BAs were extracted from liver homogenate and analyzed using electrospray ionization mass spectrometry. BA concentrations (nmol/g liver) are reported as mean ± SD; n = 4 mice per group. Values with different superscript letters are significantly different ($P < 0.05$) according to ordinary two-way ANOVA and Sidak's multiple comparisons test or T-test when appropriate. BLD = below level of detection.

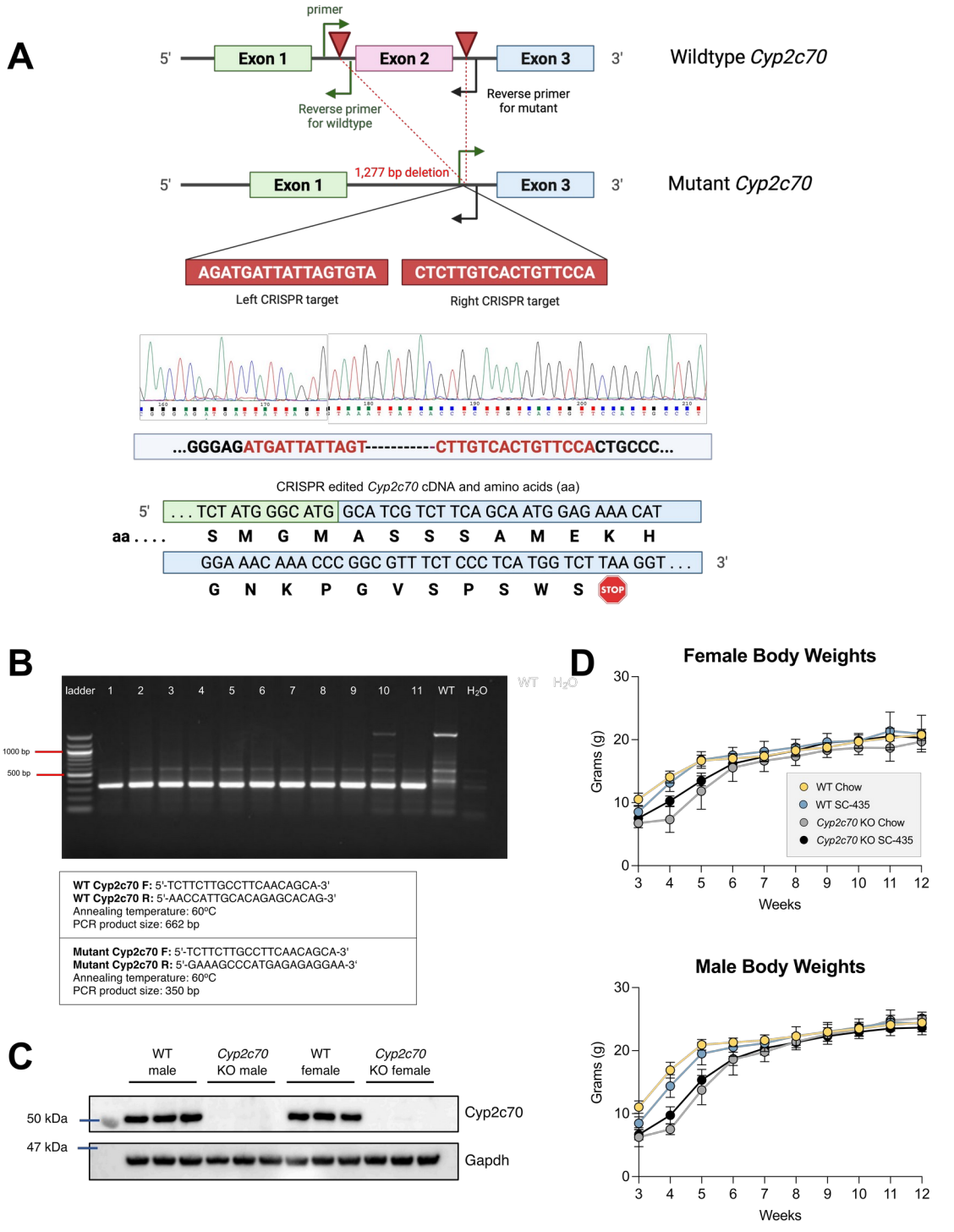

Supplemental Figure S1. Generation of *Cyp2c70* KO mouse.

A: CRISPR target site in WT *Cyp2c70* and predicted cDNA and amino acid sequences of mutant *Cyp2c70*. Primers were designed for genotyping mice to detect the 1,277 bp deletion in *Cyp2c70* induced by Cas9. The indicated forward and reverse primers amplify the WT allele (662 bp) or mutant allele (350 bp). The predicted mutant *Cyp2c70* cDNA and protein, which arise from splicing of exon 1 to exon 3, are shown. The mutant allele encodes a predicted transcript with a frameshift at amino acid position 57 and premature stop at codon 78. The WT *Cyp2c70* encodes a 489 amino acid polypeptide whereas the predicted mutant *Cyp2c70* allele encodes a predicted 77 amino acid polypeptide with a unique 19 amino acid C-terminus. B: PCR genotyping of *Cyp2c70*$^{-/-}$, *Cyp2c70*$^{+/-}$, and WT mice (lanes 1 to 11). C: Immunoblotting of liver extracts from adult male and female WT and *Cyp2c70 KO* mice. Protein (0.25 μg) of liver detergent extract from individual mice were subjected to SDS-PAGE and immunoblotting using a rabbit anti-murine Cyp2c70 antibody. Predicted size of the Cyp2c70 protein is 56 kDa. D: Body weight of female and male WT and *Cyp2c70 KO* mice fed chow or chow plus SC-435 starting at 4 weeks of age. Body weight was monitored weekly. N = 5 – 9 mice per group.

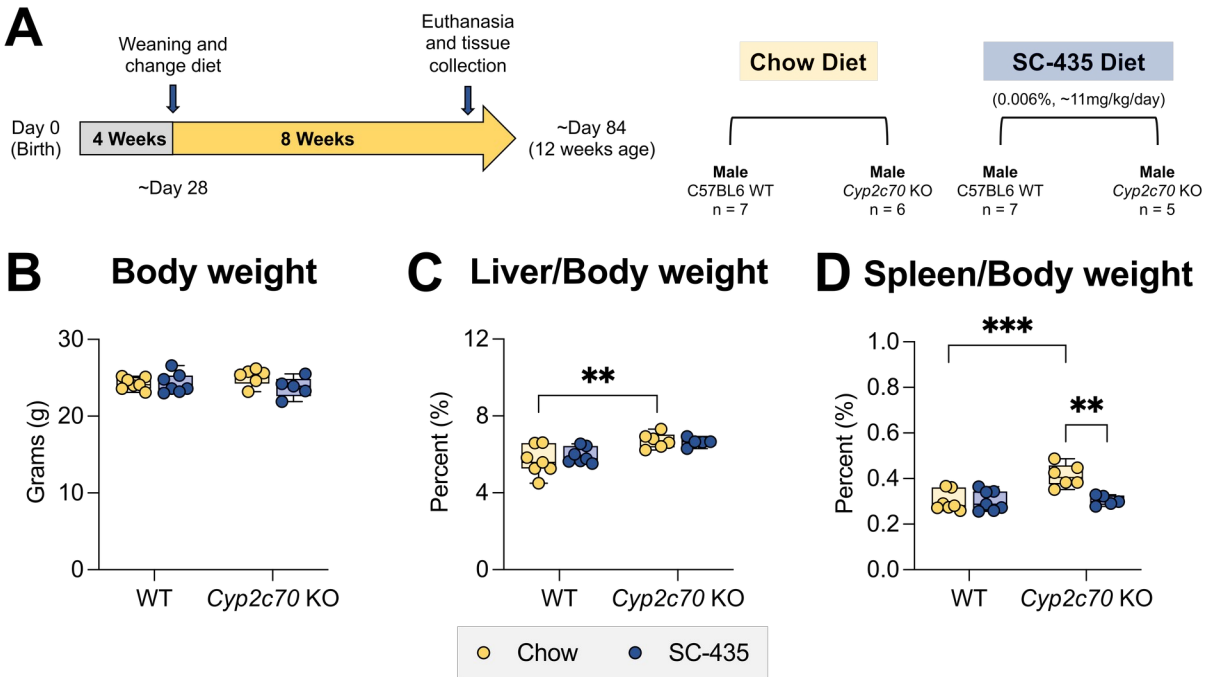

Supplemental Figure S2. Liver and spleen weights are elevated in male Cyp2c70 KO mice. A: Experimental scheme. Mice are weaned at 4 weeks and maintained on chow or switched to SC-435 diet until sacrifice and tissue was collected at 12 weeks of age. B: Body weights. C: Liver/Body weights. D: Spleen/Body weights. Asterisks indicate significant differences between groups. Median values (line), interquartile range (boxes) and min to max values are shown (*P < 0.05, **P < 0.01); n = 5 – 9 mice per group.

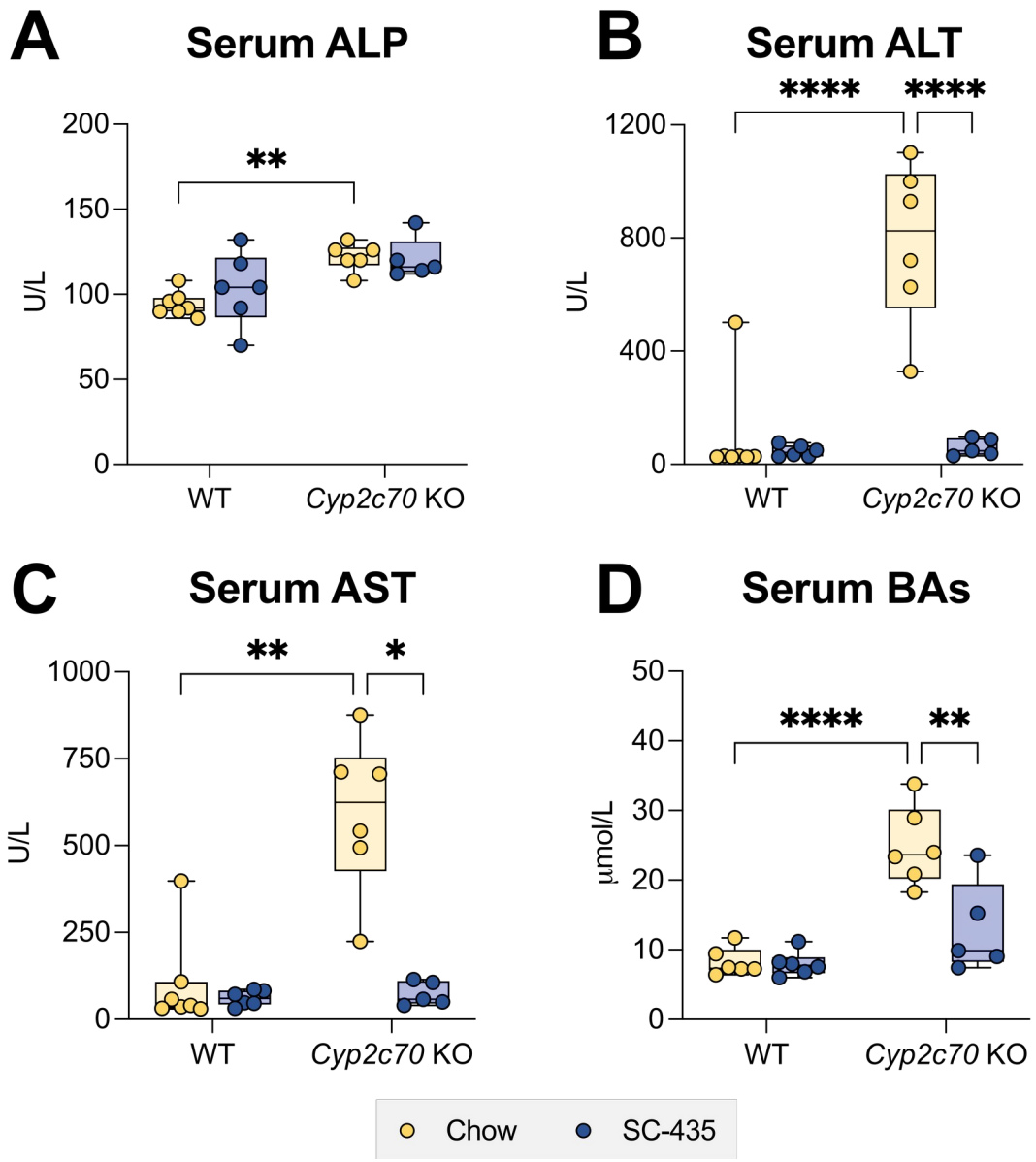

Supplemental Figure S3. Male *Cyp2c70* KO mice have elevated serum liver injury markers and are protected from cholestatic injury by the IBAT inhibitor SC-435.

A: Serum alkaline phosphatase (ALP). B: Serum alanine aminotransferase (ALT). C: Serum aspartate aminotransferase (AST). D: Serum bile acids (BAs). Asterisks indicate significant differences between groups. Median values (*line*), interquartile range (*boxes*) and min to max values are shown (*whiskers*) (*$P < 0.05$, **$P < 0.01$, ****$P < 0.0001$); n = 5 – 9 mice per group.

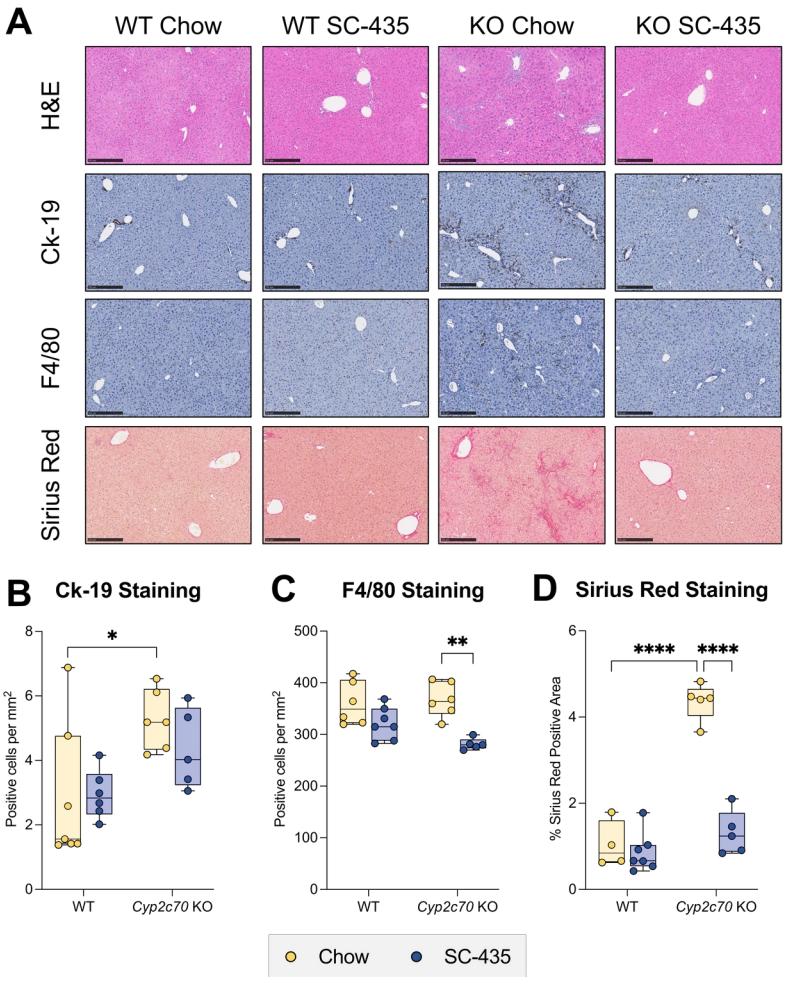

Supplemental Figure S4. Immune and fibrotic responses in male *Cyp2c70* KO mice are alleviated with SC-435 treatment.

A: Morphological response to SC-435 treatment in WT and *Cyp2c70* KO mice. From top to bottom panel: Hematoxylin and eosin (H&E), Cytokeratin-19 (Ck-19), F4/80, and Sirius Red stained liver sections (original magnification 10X) from the indicated genotypes and treatments groups. *Scale bar*, 250 µm. Quantification of positive B: Ck-19, C: F4/80 cells per mm^2, and D: Percent Sirius Red positive area of the entire liver section. Asterisks indicate significant differences between groups. Median values (*line*), interquartile range (*boxes*) and min to max values are shown (*whiskers*) (*$P < 0.05$, ****$P < 0.0001$); n = 5 – 9 mice per group.

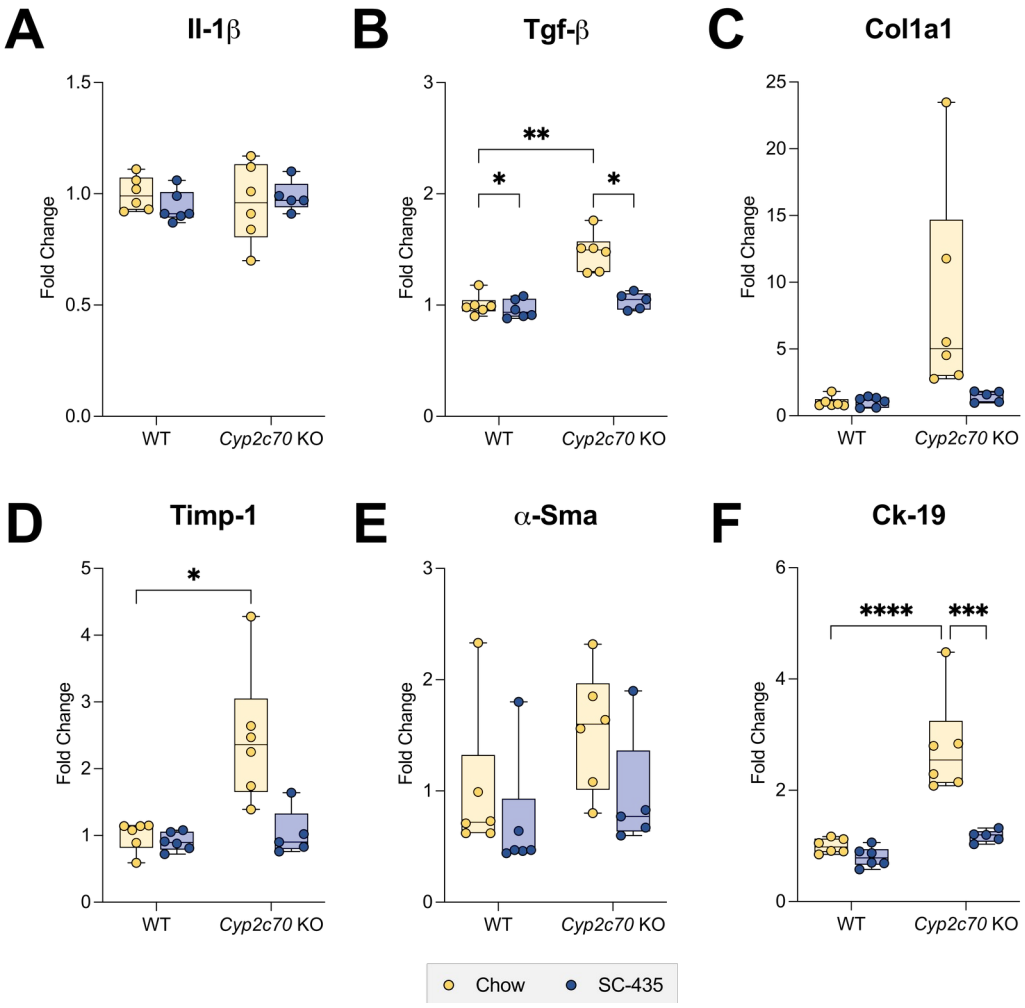

Supplemental Figure S5. Increased hepatic expression of inflammation and fibrosis-related genes in male *Cyp2c70* KO mice is alleviated with SC-435 treatment.

A: Il-1β, B: Tgf-β, C: Col1a1, D: Timp-1, E: α-Sma, and F: Ck-19 gene expression. RNA was isolated from livers of individual mice and used for real-time PCR analysis. The mRNA expression was normalized using cyclophilin and the results for each gene are expressed relative to chow-fed WT mice for each gene. Asterisks indicate significant differences between groups. Median values (*line*), interquartile range (*boxes*) and min to max values are shown (*whiskers*) (*$P < 0.05$, ***$P < 0.001$; ****$P < 0.0001$); n = 5 – 9 mice per group.

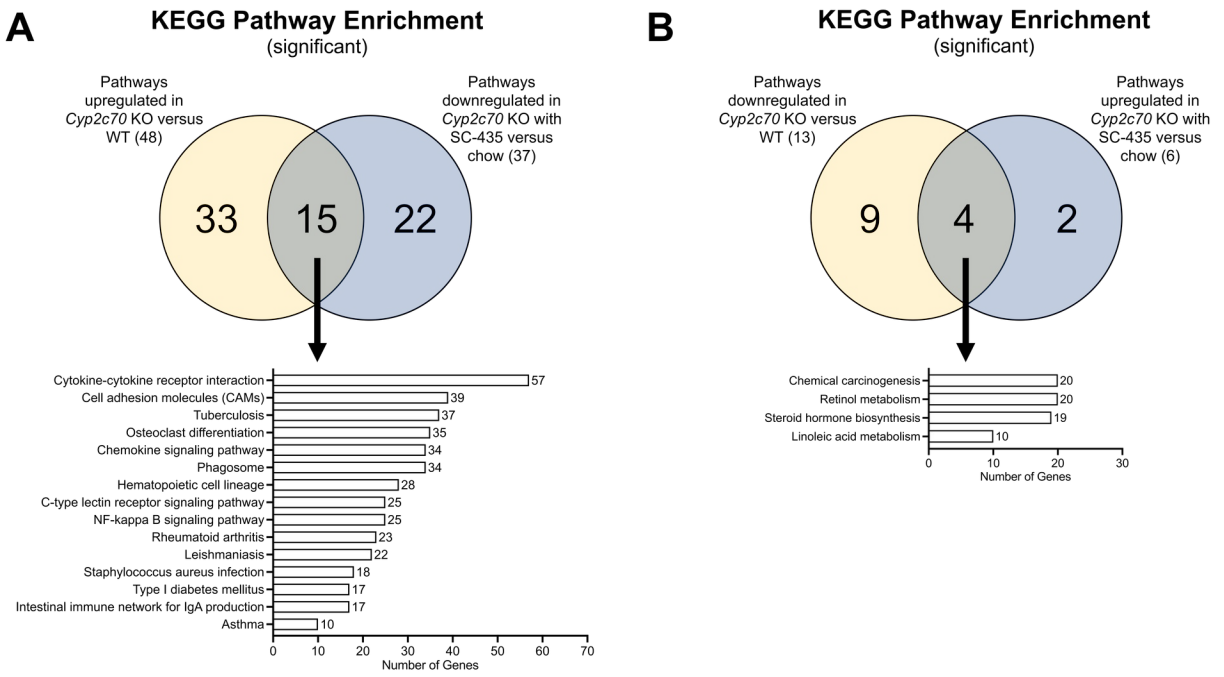

Supplemental Figure S6. KEGG enrichment analysis of significant pathways modified by IBAT inhibition in female *Cyp2c70* KO mice.

(A) Common KEGG pathways repressed by IBAT inhibition that are elevated in absence of *Cyp2c70*. (A) Common KEGG pathways activated by IBAT inhibition that are suppressed in absence of *Cyp2c70*.

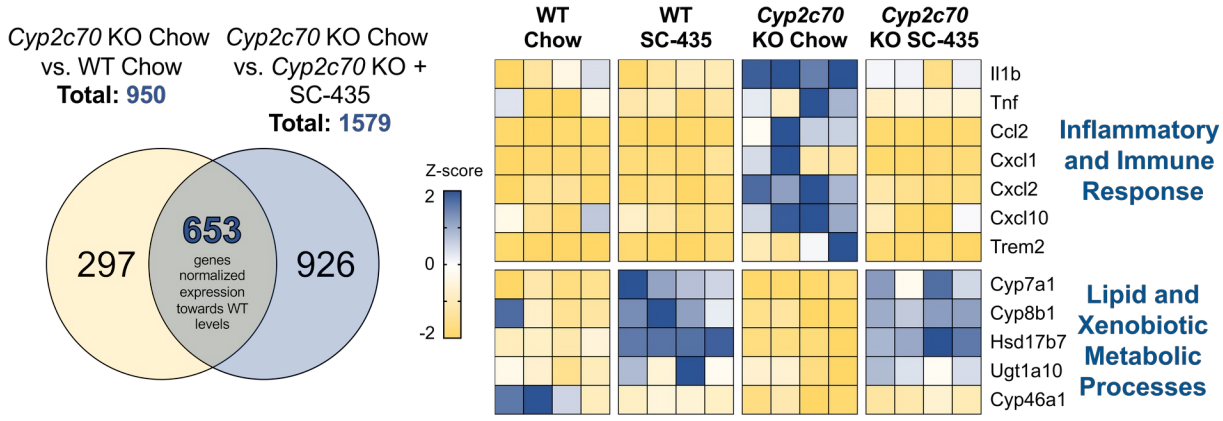

Supplemental Figure S7. Male mouse liver RNA-Seq analysis.

Venn diagram showing the number of differentially expressed genes identified in *Cyp2c70 KO* mice versus WT, and *Cyp2c70* KO mice fed chow versus chow plus SC-435. Intersection represents the subset of genes whose expression is normalized towards WT levels. Change in expression are displayed as change in Z-score on heatmap for selected representative genes from indicated the pathways. Each column represents an individual animal.

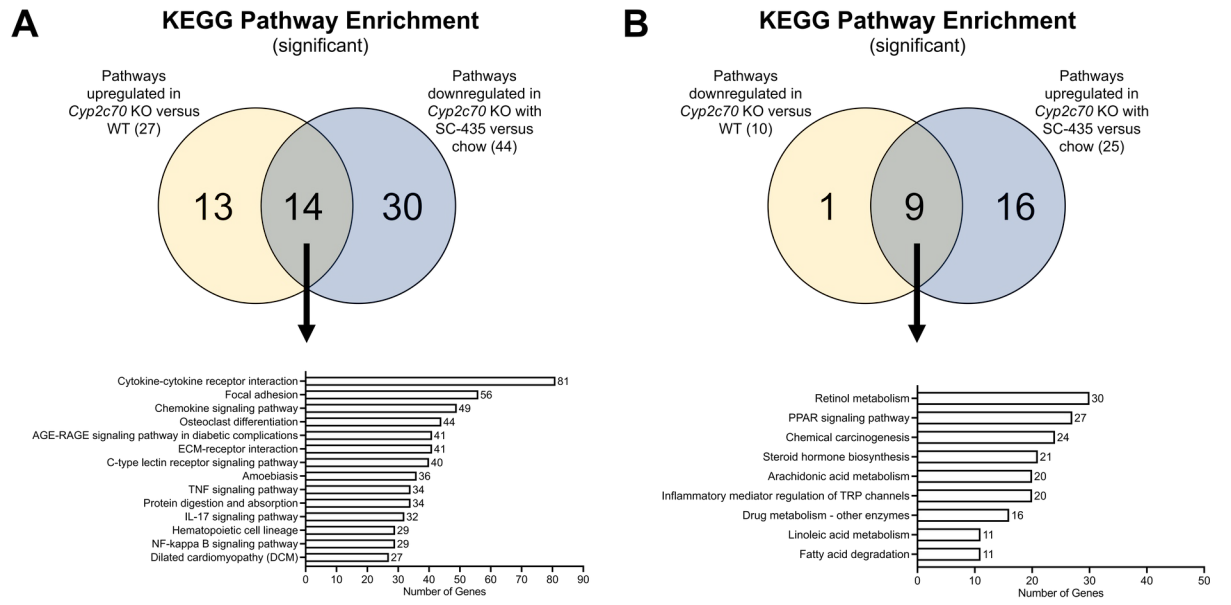

Supplemental Figure S8. KEGG enrichment analysis of significant pathways modified by IBAT inhibition in male *Cyp2c70* KO mice.

(A) Common KEGG pathways repressed by IBAT inhibition that are elevated in absence of *Cyp2c70*. (A) Common KEGG pathways activated by IBAT inhibition that are suppressed in absence of *Cyp2c70*.

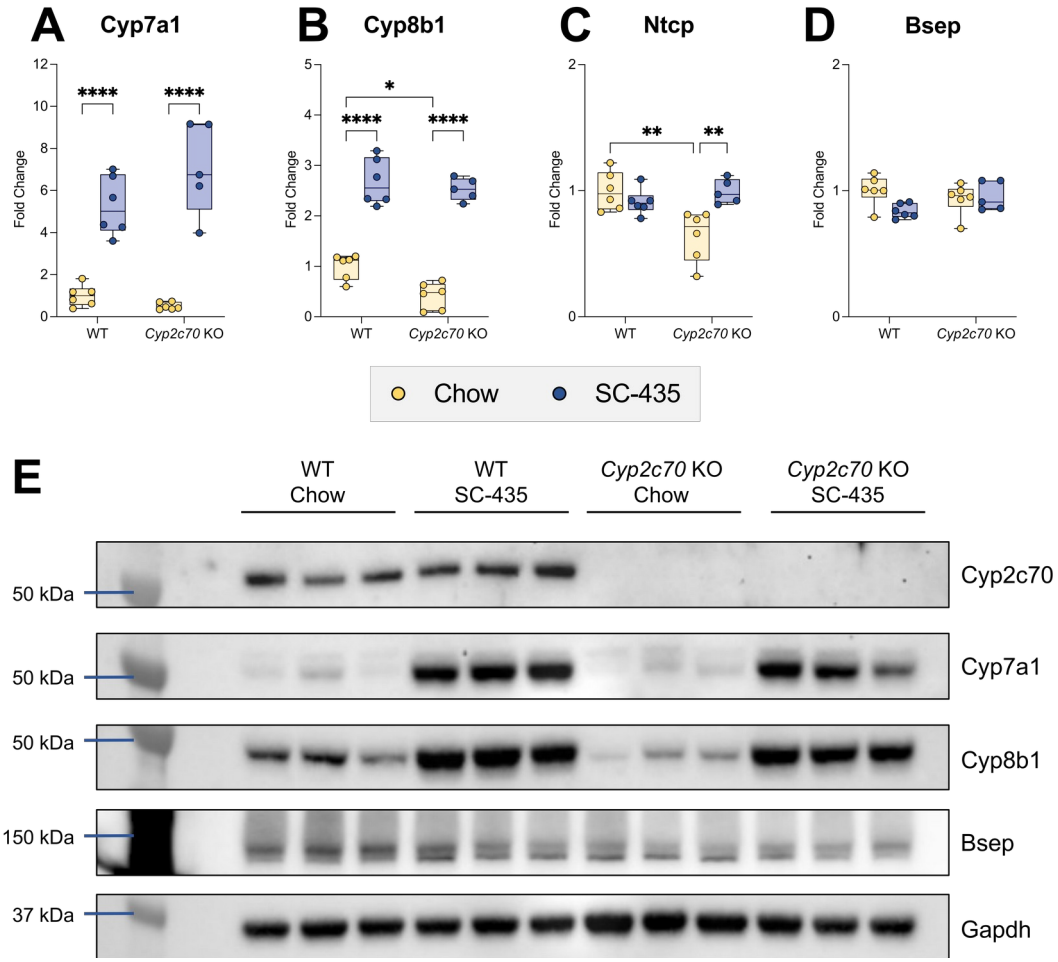

Supplemental Figure S9. IBAT inhibition increases hepatic expression of BA metabolism genes in male WT and *Cyp2c70* KO mice.

RNA was isolated from livers of individual mice and used for real-time PCR analysis. The mRNA expression was normalized using cyclophilin and the results for each gene are expressed relative to chow-fed WT mice for each gene. A: Cyp7a1; B: Cyp8b1; C: Ntcp; D: Bsep. Asterisks indicate significant differences between groups. Median values (*line*), interquartile range (*boxes*) and min to max values are shown (*whiskers*) (*$P < 0.05$, **$P < 0.01$, ****$P < 0.0001$); n = 5 – 9 mice per group. E: Protein was isolated from livers of individual mice and used for Western Blot analysis, n = 3 mice per group.

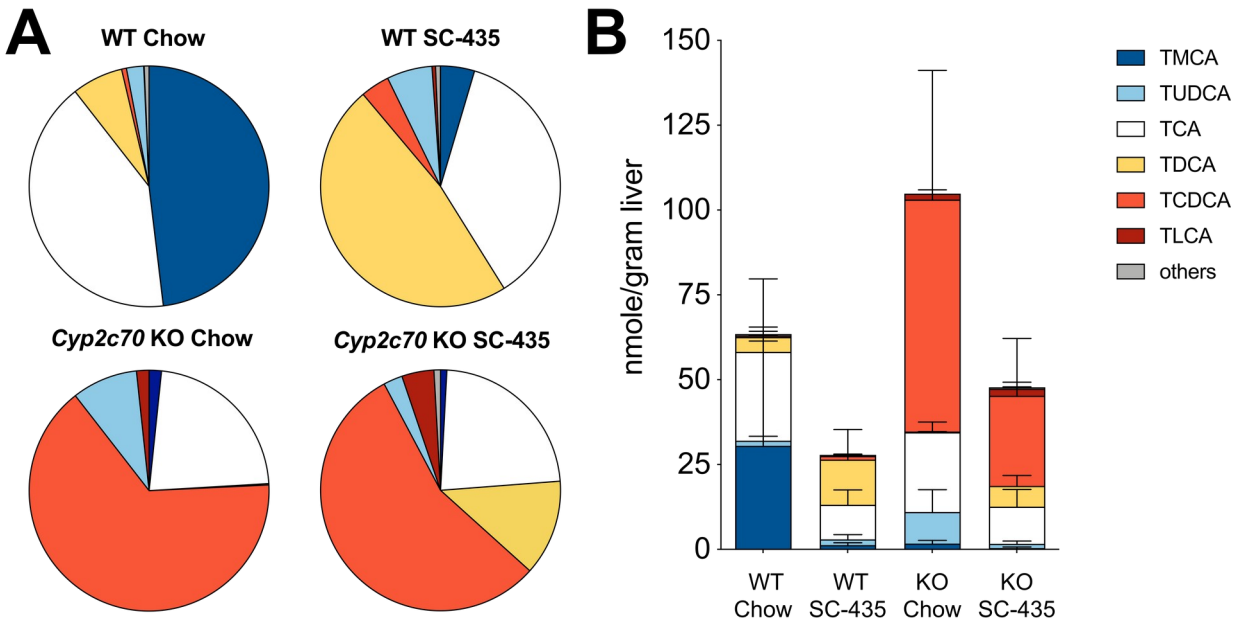

Supplemental Figure S10. IBAT inhibition prevents the increase in liver BA retention in male *Cyp7c70* KO mice.

A: Muricholates are absent in *Cyp2c70* KO mice. Pie charts for the liver BA profiles. B: Absence of *Cyp2c70* increased the total amount of liver BAs and the amount of taurochenodeoxycholic acid (TCDCA) in *Cyp2c70* KO mice. Mean values ± SD are shown; n = 4 mice per group.

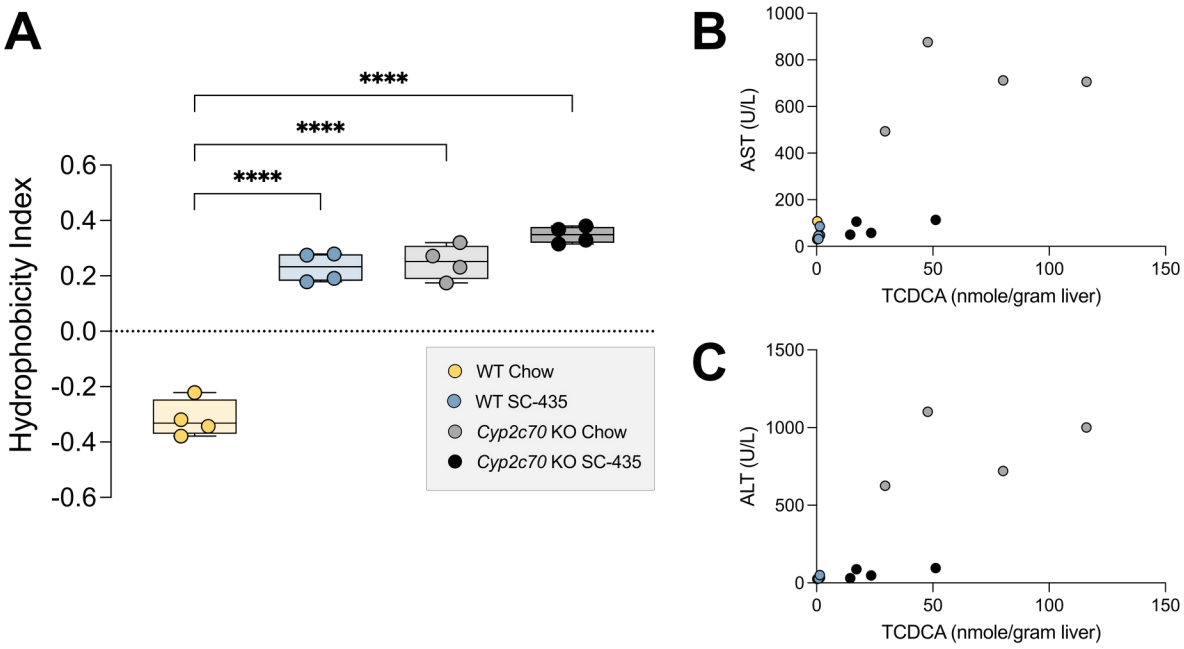

Supplemental Figure S11. IBAT inhibition does not reduce liver BA hydrophobicity in male *Cyp7c70* KO mice.

A: Liver BA composition was used to calculate the hydrophobicity index. IBAT inhibition and inactivation of *Cyp2c70* increases the hydrophobicity of the liver BA pool. Asterisks indicate significant differences between groups. Median values (*line*), interquartile range (*boxes*) and min to max values are shown (*whiskers*) (***$P < 0.001$); n = 4 mice per group. B and C: Total liver taurochenodeoxycholic acid (TCDCA) and serum levels of alanine aminotransferase (ALT) and aspartate aminotransferase (AST) are reduced in IBAT inhibitor treated *Cyp2c70* KO mice.

References

1. Hofmann AF. Bile acids: trying to understand their chemistry and biology with the hope of helping patients. *Hepatology* 49: 1403-1418, 2009.
2. Hofmann AF, Hagey LR, and Krasowski MD. Bile salts of vertebrates: structural variation and possible evolutionary significance. *J Lipid Res* 51: 226-246, 2010.
3. Perez MJ, and Briz O. Bile-acid-induced cell injury and protection. *World J Gastroenterol* 15: 1677-1689, 2009.
4. Hofmann AF, and Hagey LR. Bile acids: chemistry, pathochemistry, biology, pathobiology, and therapeutics. *Cell Mol Life Sci* 65: 2461-2483, 2008.
5. Malhi H, Guicciardi ME, and Gores GJ. Hepatocyte death: a clear and present danger. *Physiol Rev* 90: 1165-1194, 2010.
6. Barrasa JI, Olmo N, Lizarbe MA, and Turnay J. Bile acids in the colon, from healthy to cytotoxic molecules. *Toxicol In Vitro* 27: 964-977, 2013.
7. Copple BL, and Li T. Pharmacology of bile acid receptors: Evolution of bile acids from simple detergents to complex signaling molecules. *Pharmacol Res* 104: 9-21, 2016.
8. Baghdasaryan A, Fuchs CD, Osterreicher CH, Lemberger UJ, Halilbasic E, Pahlman I, Graffner H, Krones E, Fickert P, Wahlstrom A, Stahlman M, Paumgartner G, Marschall HU, and Trauner M. Inhibition of intestinal bile acid absorption improves cholestatic liver and bile duct injury in a mouse model of sclerosing cholangitis. *J Hepatol* 64: 674-681, 2016.
9. Woolbright BL, and Jaeschke H. Novel insight into mechanisms of cholestatic liver injury. *World J Gastroenterol* 18: 4985-4993, 2012.

10. Jansen PL, Ghallab A, Vartak N, Reif R, Schaap FG, Hampe J, and Hengstler JG. The ascending pathophysiology of cholestatic liver disease. *Hepatology* 65: 722-738, 2017.

11. Li J, and Dawson PA. Animal models to study bile acid metabolism. *Biochim Biophys Acta Mol Basis Dis* 1865: 895-911, 2019.

12. Dietschy JM, and Turley SD. Control of cholesterol turnover in the mouse. *J Biol Chem* 277: 3801-3804, 2002.

13. Takahashi S, Fukami T, Masuo Y, Brocker CN, Xie C, Krausz KW, Wolf CR, Henderson CJ, and Gonzalez FJ. Cyp2c70 is responsible for the species difference in bile acid metabolism between mice and humans. *J Lipid Res* 57: 2130-2137, 2016.

14. Honda A, Miyazaki T, Iwamoto J, Hirayama T, Morishita Y, Monma T, Ueda H, Mizuno S, Sugiyama F, Takahashi S, and Ikegami T. Regulation of bile acid metabolism in mouse models with hydrophobic bile acid composition. *J Lipid Res* 61: 54-69, 2020.

15. Straniero S, Laskar A, Savva C, Hardfeldt J, Angelin B, and Rudling M. Of mice and men: murine bile acids explain species differences in the regulation of bile acid and cholesterol metabolism. *J Lipid Res* 61: 480-491, 2020.

16. Oteng AB, Higuchi S, Banks AS, and Haeusler RA. Cyp2c-deficiency depletes muricholic acids and protects against high-fat diet-induced obesity in male mice but promotes liver damage. *Mol Metab* 53: 101326, 2021.

17. de Boer JF, Verkade E, Mulder NL, de Vries HD, Huijkman N, Koehorst M, Boer T, Wolters JC, Bloks VW, van de Sluis B, and Kuipers F. A human-like bile acid pool induced by deletion of hepatic Cyp2c70 modulates effects of FXR activation in mice. *J Lipid Res* 61: 291-305, 2020.

18. de Boer JF, de Vries HD, Palmiotti A, Li R, Doestzada M, Hoogerland JA, Fu J, La Rose AM, Westerterp M, Mulder NL, Hovingh MV, Koehorst M, Kloosterhuis NJ, Wolters JC, Bloks VW, Haas JT, Dombrowicz D, Staels B, van de Sluis B, and Kuipers F. Cholangiopathy and Biliary Fibrosis in Cyp2c70-Deficient Mice Are Fully Reversed by Ursodeoxycholic Acid. *Cell Mol Gastroenterol Hepatol* 11: 1045-1069, 2021.

19. Miethke AG, Zhang W, Simmons J, Taylor AE, Shi T, Shanmukhappa SK, Karns R, White S, Jegga AG, Lages CS, Nkinin S, Keller BT, and Setchell KD. Pharmacological inhibition of apical sodium-dependent bile acid transporter changes bile composition and blocks progression of sclerosing cholangitis in multidrug resistance 2 knockout mice. *Hepatology* 63: 512-523, 2016.

20. Karpen SJ, Kelly D, Mack C, and Stein P. Ileal bile acid transporter inhibition as an anticholestatic therapeutic target in biliary atresia and other cholestatic disorders. *Hepatol Int* 14: 677-689, 2020.

21. Gonzales E, Hardikar W, Stormon M, Baker A, Hierro L, Gliwicz D, Lacaille F, Lachaux A, Sturm E, Setchell KDR, Kennedy C, Dorenbaum A, Steinmetz J, Desai NK, Wardle AJ, Garner W, Vig P, Jaecklin T, Sokal EM, and Jacquemin E. Efficacy and safety of maralixibat treatment in patients with Alagille syndrome and cholestatic pruritus (ICONIC): a randomised phase 2 study. *Lancet* 398: 1581-1592, 2021.

22. Thompson RJ, Arnell H, Artan R, Baumann U, Calvo PL, Czubkowski P, Dalgic B, D'Antiga L, Durmaz O, Fischler B, Gonzales E, Grammatikopoulos T, Gupte G, Hardikar W, Houwen RHJ, Kamath BM, Karpen SJ, Kjems L, Lacaille F, Lachaux A, Lainka E, Mack CL, Mattsson JP, McKiernan P, Ozen H, Rajwal SR, Roquelaure B, Shagrani M, Shteyer E, Soufi N, Sturm E, Tessier ME, Verkade HJ, and Horn P. Odevixibat treatment

in progressive familial intrahepatic cholestasis: a randomised, placebo-controlled, phase 3 trial. *Lancet Gastroenterol Hepatol* 2022.

23. Lee CM, Lee BS, Arnold SL, Isoherranen N, and Morgan ET. Nitric oxide and interleukin-1beta stimulate the proteasome-independent degradation of the retinoic acid hydroxylase CYP2C22 in primary rat hepatocytes. *J Pharmacol Exp Ther* 348: 141-152, 2014.

24. Rao A, Kosters A, Mells JE, Zhang W, Setchell KD, Amanso AM, Wynn GM, Xu T, Keller BT, Yin H, Banton S, Jones DP, Wu H, Dawson PA, and Karpen SJ. Inhibition of ileal bile acid uptake protects against nonalcoholic fatty liver disease in high-fat diet-fed mice. *Science translational medicine* 8: 357ra122, 2016.

25. Fickert P, Pollheimer MJ, Beuers U, Lackner C, Hirschfield G, Housset C, Keitel V, Schramm C, Marschall HU, Karlsen TH, Melum E, Kaser A, Eksteen B, Strazzabosco M, Manns M, Trauner M, and International PSCSG. Characterization of animal models for primary sclerosing cholangitis (PSC). *J Hepatol* 60: 1290-1303, 2014.

26. Bankhead P, Loughrey MB, Fernandez JA, Dombrowski Y, McArt DG, Dunne PD, McQuaid S, Gray RT, Murray LJ, Coleman HG, James JA, Salto-Tellez M, and Hamilton PW. QuPath: Open source software for digital pathology image analysis. *Sci Rep* 7: 16878, 2017.

27. Love MI, Huber W, and Anders S. Moderated estimation of fold change and dispersion for RNA-seq data with DESeq2. *Genome Biol* 15: 550, 2014.

28. Li J, Witten DM, Johnstone IM, and Tibshirani R. Normalization, testing, and false discovery rate estimation for RNA-sequencing data. *Biostatistics* 13: 523-538, 2012.

29. Huang da W, Sherman BT, and Lempicki RA. Systematic and integrative analysis of large gene lists using DAVID bioinformatics resources. *Nat Protoc* 4: 44-57, 2009.

30. Huang DW, Sherman BT, Tan Q, Kir J, Liu D, Bryant D, Guo Y, Stephens R, Baseler MW, Lane HC, and Lempicki RA. DAVID Bioinformatics Resources: expanded annotation database and novel algorithms to better extract biology from large gene lists. *Nucleic Acids Res* 35: W169-175, 2007.

31. Amplatz B, Zohrer E, Haas C, Schaffer M, Stojakovic T, Jahnel J, and Fauler G. Bile acid preparation and comprehensive analysis by high performance liquid chromatography-high-resolution mass spectrometry. *Clin Chim Acta* 464: 85-92, 2017.

32. Folch J, Lees M, and Sloane Stanley GH. A simple method for the isolation and purification of total lipides from animal tissues. *J Biol Chem* 226: 497-509, 1957.

33. Child P, and Rafter J. Calcium enhances the hemolytic action of bile salts. *Biochim Biophys Acta* 855: 357-364, 1986.

34. Das M, Boerma M, Goree JR, Lavoie EG, Fausther M, Gubrij IB, Pangle AK, Johnson LG, and Dranoff JA. Pathological changes in pulmonary circulation in carbon tetrachloride (CCl4)-induced cirrhotic mice. *PLoS One* 9: e96043, 2014.

35. Cai SY, Ouyang X, Chen Y, Soroka CJ, Wang J, Mennone A, Wang Y, Mehal WZ, Jain D, and Boyer JL. Bile acids initiate cholestatic liver injury by triggering a hepatocyte-specific inflammatory response. *JCI Insight* 2: e90780, 2017.

36. Wagner M, Fickert P, Zollner G, Fuchsbichler A, Silbert D, Tsybrovskyy O, Zatloukal K, Guo GL, Schuetz JD, Gonzalez FJ, Marschall HU, Denk H, and Trauner M. Role of farnesoid X receptor in determining hepatic ABC transporter expression and liver injury in bile duct-ligated mice. *Gastroenterology* 125: 825-838, 2003.

37. Hirano S, and Masuda N. Epimerization of the 7-hydroxy group of bile acids by the combination of two kinds of microorganisms with 7 alpha- and 7 beta-hydroxysteroid dehydrogenase activity, respectively. *J Lipid Res* 22: 1060-1068, 1981.

38. Penno CA, Morgan SA, Vuorinen A, Schuster D, Lavery GG, and Odermatt A. Impaired oxidoreduction by 11beta-hydroxysteroid dehydrogenase 1 results in the accumulation of 7-oxolithocholic acid. *J Lipid Res* 54: 2874-2883, 2013.

39. Wahlström A, Al-Dury S, Ståhlman M, Bäckhed F, and Marschall H-U. Cyp3a11 is not essential for the formation of murine bile acids. *Biochemistry and Biophysics Reports* 10: 70-75, 2017.

40. Heuman DM. Quantitative estimation of the hydrophilic-hydrophobic balance of mixed bile salt solutions. *J Lipid Res* 30: 719-730, 1989.

41. Roda A, Hofmann AF, and Mysels KJ. The influence of bile salt structure on self-association in aqueous solutions. *J Biol Chem* 258: 6362-6370, 1983.

42. Coleman R, Iqbal S, Godfrey PP, and Billington D. Membranes and bile formation. Composition of several mammalian biles and their membrane-damaging properties. *Biochem J* 178: 201-208, 1979.

43. Armstrong MJ, and Carey MC. The hydrophobic-hydrophilic balance of bile salts. Inverse correlation between reverse-phase high performance liquid chromatographic mobilities and micellar cholesterol-solubilizing capacities. *J Lipid Res* 23: 70-80, 1982.

44. Roda A, Minutello A, Angellotti MA, and Fini A. Bile acid structure-activity relationship: evaluation of bile acid lipophilicity using 1-octanol/water partition coefficient and reverse phase HPLC. *J Lipid Res* 31: 1433-1443, 1990.

45. Garcia-Canaveras JC, Donato MT, Castell JV, and Lahoz A. Targeted profiling of circulating and hepatic bile acids in human, mouse, and rat using a UPLC-MRM-MS-validated method. *Journal of lipid research* 53: 2231-2241, 2012.

46. Zhao XM, and Montet JC. Effects of bile salt supplementation on biliary secretion in estrogen-treated rats. *J Nutr Biochem* 1: 420-425, 1990.

47. Arrese M, Pizarro M, Solis N, and Accatino L. Adaptive regulation of hepatic bile salt transport: role of bile salt hydrophobicity and microtubule-dependent vesicular pathway. *J Hepatol* 26: 694-702, 1997.

48. Palmeira CM, and Rolo AP. Mitochondrially-mediated toxicity of bile acids. *Toxicology* 203: 1-15, 2004.

49. Heuman DM, and Bajaj R. Ursodeoxycholate conjugates protect against disruption of cholesterol-rich membranes by bile salts. *Gastroenterology* 106: 1333-1341, 1994.

50. Miyake H, Tazuma S, Miura H, Yamashita G, and Kajiyama G. Partial characterization of mechanisms of cytoprotective action of hydrophilic bile salts against hydrophobic bile salts in rats: relation to canalicular membrane fluidity and packing density. *Dig Dis Sci* 44: 197-202, 1999.

51. Ghallab A, Hofmann U, Sezgin S, Vartak N, Hassan R, Zaza A, Godoy P, Schneider KM, Guenther G, Ahmed YA, Abbas AA, Keitel V, Kuepfer L, Dooley S, Lammert F, Trautwein C, Spiteller M, Drasdo D, Hofmann AF, Jansen PLM, Hengstler JG, and Reif R. Bile Microinfarcts in Cholestasis Are Initiated by Rupture of the Apical Hepatocyte Membrane and Cause Shunting of Bile to Sinusoidal Blood. *Hepatology* 69: 666-683, 2019.

52. Khan FM, Komarla AR, Mendoza PG, Bodenheimer HC, Jr., and Theise ND. Keratin 19 demonstration of canal of Hering loss in primary biliary cirrhosis: "minimal change PBC"? *Hepatology* 57: 700-707, 2013.

53. Hohenester S, Wenniger LM, Paulusma CC, van Vliet SJ, Jefferson DM, Elferink RP, and Beuers U. A biliary HCO3- umbrella constitutes a protective mechanism against bile acid-induced injury in human cholangiocytes. *Hepatology* 55: 173-183, 2012.

54. Dawson PA, and Karpen SJ. Intestinal transport and metabolism of bile acids. *J Lipid Res* 56: 1085-1099, 2015.

55. Mekhjian HS, Phillips SF, and Hofmann AF. Colonic absorption of unconjugated bile acids: perfusion studies in man. *Dig Dis Sci* 24: 545-550, 1979.

56. Schiff ER, Small NC, and Dietschy JM. Characterization of the kinetics of the passive and active transport mechanisms for bile acid absorption in the small intestine and colon of the rat. *J Clin Invest* 51: 1351-1362, 1972.

57. Hofmann AF, and Roda A. Physicochemical properties of bile acids and their relationship to biological properties: an overview of the problem. *J Lipid Res* 25: 1477-1489, 1984.

58. Ashby K, Navarro Almario EE, Tong W, Borlak J, Mehta R, and Chen M. Review article: therapeutic bile acids and the risks for hepatotoxicity. *Aliment Pharmacol Ther* 47: 1623-1638, 2018.

59. Ueda H, Honda A, Miyazaki T, Morishita Y, Hirayama T, Iwamoto J, Nakamoto N, and Ikegami T. Sex-, age-, and organ-dependent improvement of bile acid hydrophobicity by ursodeoxycholic acid treatment: A study using a mouse model with human-like bile acid composition. *PLoS One* 17: e0271308, 2022.

60. Li R, Hovingh MV, Koehorst M, de Blaauw P, Verkade HJ, de Boer JF, and Kuipers F. Short-term obeticholic acid treatment does not impact cholangiopathy in Cyp2c70-deficient mice with a human-like bile acid composition. *Biochim Biophys Acta Mol Cell Biol Lipids* 1867: 159163, 2022.

61. Hofmann AF, Schteingart CD, and Lillienau J. Biological and medical aspects of active ileal transport of bile acids. *Ann Med* 23: 169-175, 1991.

62. Dawson PA, Haywood J, Craddock AL, Wilson M, Tietjen M, Kluckman K, Maeda N, and Parks JS. Targeted deletion of the ileal bile acid transporter eliminates enterohepatic cycling of bile acids in mice. *J Biol Chem* 278: 33920-33927, 2003.

63. Baghdasaryan A, Claudel T, Gumhold J, Silbert D, Adorini L, Roda A, Vecchiotti S, Gonzalez FJ, Schoonjans K, Strazzabosco M, Fickert P, and Trauner M. Dual farnesoid X receptor/TGR5 agonist INT-767 reduces liver injury in the Mdr2-/- (Abcb4-/-) mouse cholangiopathy model by promoting biliary HCO(-)(3) output. *Hepatology* 54: 1303-1312, 2011.

64. An P, Wei G, Huang P, Li W, Qi X, Lin Y, Vaid KA, Wang J, Zhang S, Li Y, Or YS, Jiang LJ, and Popov YV. A novel non-bile acid FXR agonist EDP-305 potently suppresses liver injury and fibrosis without worsening of ductular reaction. *Liver Int* 40: 1655-1669, 2020.

65. Watanabe M, Fukiya S, and Yokota A. Comprehensive evaluation of the bactericidal activities of free bile acids in the large intestine of humans and rodents. *J Lipid Res* 58: 1143-1152, 2017.

66. Hall SR, Maslen EN, and Cooper A. The crystal and molecular structure of 3[alpha],6[alpha]-dihydroxy-5[beta]-cholan-24-oic acid, C24O4H40. *Acta Crystallographica Section B %@ 0567-7408* 30: 1441-1447, 1974.

Chapter 3: Active Enterohepatic Cycling is Not Required for the Choleretic Actions of 24-norUrsodeoxycholic Acid in Mice

This chapter is adapted from the following manuscript currently in revisions for *JCI Insights*:

Jennifer K. Truong[1]*, Jianing Li[1]*, Qin Li[2], Kimberly Pachura[1], Anuradha Rao[1], Sanjeev Gumber[3], Claudia Daniela Fuchs[4], Michael Trauner[4], Andrew P. Feranchak[2], Saul J. Karpen[1], Paul A. Dawson[1]

[1]Department of Pediatrics, Division of Pediatric Gastroenterology, Hepatology and Nutrition, Emory University School of Medicine, Children's Healthcare of Atlanta, Atlanta, Georgia; [2]Department of Pediatrics, University of Pittsburgh Medical Center Children's Hospital of Pittsburgh, Pittsburgh, Pennsylvania; [3]Division of Pathology and Laboratory Medicine, Yerkes National Research Center, Emory University School of Medicine, Atlanta, Georgia; [4]Hans Popper Laboratory of Molecular Hepatology, Division of Gastroenterology and Hepatology, Department of Internal Medicine III, Medical University of Vienna, Austria

Denotes equal contribution*

Denotes corresponding author

Graphical Abstract:

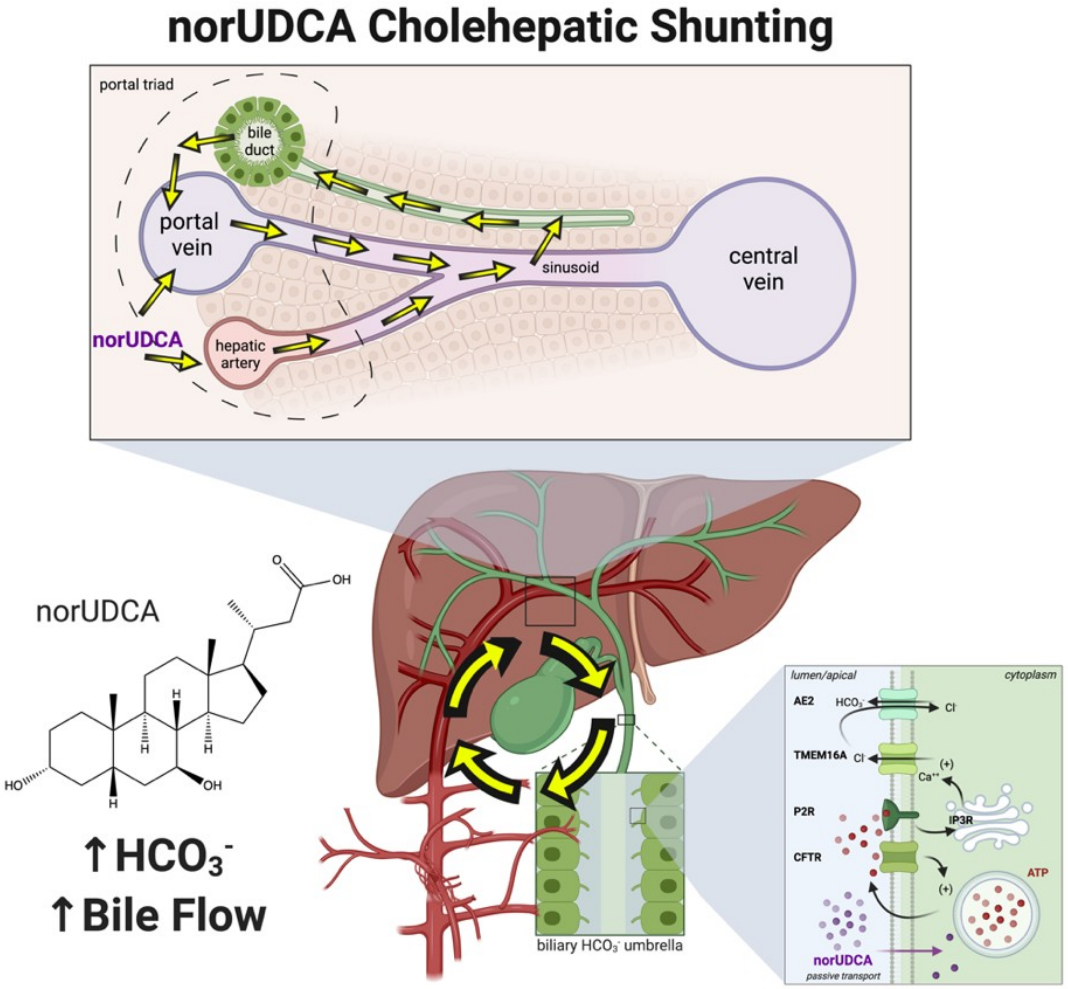

Abbreviations: ABC, ATP-binding cassette; ALP, alkaline phosphatase; ALT, alanine aminotransferase; ANO1, anoctamin-1; ASBT, apical sodium-dependent bile acid transporter; ASBTi, ASBT inhibitor; AST, aspartate aminotransferase; ATP, P-type ATPase; BSEP, bile salt export pump; CA, cholic acid; CAR, constitutive androstane receptor; CFTR, cystic fibrosis transmembrane conductance regulator; CHOL, cholesterol; DCA, deoxycholic acid; FGF15, fibroblast growth factor 15; FXR, farnesoid X-receptor; IBABP, ileal bile acid binding protein; LCA, lithocholic acid; LRRC8A, leucine-rich repeat-containing protein 8; Mdr2, multidrug resistance protein 2; MLC, mouse large cholangiocyte; OST, organic solute transporter; Ntcp, Na-taurocholate co-transporting polypeptide; OATP, organic anion transporting polypeptide; PCN, pregnenolone 16a-carbonitrile; PSC, Primary Sclerosing Cholangitis; PXR, pregnane X-receptor; siRNA, small interfering RNA; TBILI, total bilirubin; TCA, taurocholic acid; TCDCA, taurochenodeoxycholic acid; TDCA, taurodeoxycholic acid; TMEM16A, transmembrane member 16A; THDCA, taurohyodeoxycholic acid; TαMCA, tauro-α-muricholic acid; TβMCA, tauro-β-muricholic acid; TωMCA, tauro-ω-muricholic acid; TUDCA, tauroursodeoxycholic acid; TP, total protein; VDR, vitamin D receptor; WT, wild type.

Abstract

The superior ability of *nor*ursodeoxycholic acid (*nor*UDCA) to induce bicarbonate-rich bile secretion has been attributed to its ability to undergo cholehepatic shunting. The goal of this study was to investigate the mechanisms underlying the choleretic actions of *nor*UDCA and role of the bile acid transporters using mouse and cell-based models. Here, we show that the apical sodium-dependent bile acid transporter (ASBT), Organic solute transporter-alpha (OSTα), and Organic anion transporting polypeptide 1a/1b (Oatp1a/1b) transporters are dispensable for *nor*UDCA-stimulation of bile flow and biliary bicarbonate secretion. Chloride channels in biliary epithelial cells provide the driving force for biliary secretion. *nor*UDCA potently stimulated chloride currents in mouse large cholangiocytes, which was blocked by siRNA silencing and pharmacological inhibition of the calcium-activated chloride channel transmembrane member 16A (TMEM16A), while unaffected by ASBT inhibition. In agreement, blocking intestinal bile acid reabsorption by co-administration of an ASBT inhibitor or bile acid sequestrant did not impact *nor*UDCA stimulation of bile flow in wildtype mice. The results indicate that these major bile acid transporters are not directly involved in the absorption, cholehepatic shunting, or choleretic actions of *nor*UDCA. Additionally, the findings support further investigation of the therapeutic synergy between *nor*UDCA and ASBT inhibitors or bile acid sequestrants for cholestatic liver disease.

Introduction

*nor*Ursodeoxycholic acid (*nor*UDCA) (drug name: norucholic acid) is a synthetic C-23 side chain-shortened analog of the hydrophilic native bile acid ursodeoxycholic acid (UDCA) and is resistant to side-chain conjugation with glycine or taurine (1). The pharmacological properties and physiological actions of *nor*UDCA make it a therapeutic candidate for a variety of cholestatic liver diseases (1, 2). In preclinical studies, oral administration of *nor*UDCA reduced liver injury and biliary fibrosis in bile duct ligated mice and in *Abcb4/Mdr2*$^{-/-}$ mice, whereas administration of UDCA aggravated liver and bile duct injury (3, 4). In those models, *nor*UDCA induced detoxification and renal elimination of bile acids and exhibited anti-proliferative, anti-fibrotic, and anti-inflammatory properties (3-7). In Phase 2 clinical trials, administration of *nor*UDCA for 12 weeks reduced serum alkaline phosphatase (ALP) and other liver enzyme markers of cholestasis in patients with Primary Sclerosing Cholangitis (PSC) (8), and reduced serum alanine aminotransferase (ALT) in patients with non-alcoholic fatty liver disease (9).

The therapeutic mechanisms of action that mediate the beneficial effects of *nor*UDCA remain the subject of ongoing study (10, 11), but most likely involves stimulation of bicarbonate secretion to maintain the protective biliary 'bicarbonate umbrella' (12). Administration of side chain-shortened dihydroxy bile acids such as *nor*UDCA produce bicarbonate-rich bile flow that far exceeds that reported for any natural bile acid and in excess of what can be explained by their osmotic effects (1, 13). The superior ability of *nor*UDCA versus UDCA to induce a hypercholeresis has been attributed to *nor*UDCA's ability to evade side chain conjugation (amidation) to glycine or taurine and undergo cholehepatic shunting. In the original pathway proposed over 30 years ago by Hofmann (1, 14), unconjugated *nor*UDCA is secreted by hepatocytes into bile and absorbed in protonated form by cholangiocytes lining the biliary tract,

thereby generating a bicarbonate ion from biliary CO_2. *nor*UDCA then crosses the biliary epithelium and enters the periductular capillary plexus, which drains into the portal vein (or directly into the hepatic sinusoids), delivering *nor*UDCA for uptake by hepatocytes, resecretion into bile, and additional rounds of cholehepatic shunting. We know now that apical membrane cyclic AMP (cAMP) and Ca^{2+}-activated Cl^- channels in cholangiocytes play a critical role in promoting bicarbonate-secretion by the biliary epithelium via the chloride/bicarbonate anion exchanger (AE2; *SLC4A2*) (15, 16). For example, secretin acting via its basolateral membrane receptor increases intracellular cAMP and stimulates cystic fibrosis transmembrane conductance regulator (CFTR)-mediated Cl^- secretion. In addition to CFTR, the Ca^{2+}-activated Cl^- channel transmembrane member 16A (TMEM16A; also called anoctamin-1, ANO1) is expressed by cholangiocytes and plays a particularly important role in regulating biliary anion efflux under basal conditions and in response to stimuli such as bile acids (17, 18). In those studies, activation of TMEM16A by the conjugated therapeutic bile acid tauroursodeoxycholic acid (TUDCA) was dependent upon its ASBT-mediated uptake into the cell (17). However, in contrast to native C-24 bile acids, the interaction of side chain shortened C-23 bile acids such as *nor*UDCA with these mechanisms of biliary secretion remains largely unexplored.

Unmodified *nor*UDCA that escapes absorption in the biliary tract travels along with other biliary constituents into the small intestine where it is reabsorbed and carried in the enterohepatic circulation back to the liver for uptake and resecretion into bile. In this fashion, *nor*UDCA can undergo multiple rounds of cholehepatic shunting, or a combination of enterohepatic cycling and cholehepatic shunting, before it is excreted in the urine or feces following the conversion to a more polar metabolite by hepatic phase 1 or phase 2 metabolism (primarily phase 2 glucuronidation) (1, 14, 19, 20). The physicochemical and permeability properties of *nor*UDCA

(Supplemental Table 1) are generally consistent with a role for passive diffusion in the absorption of *nor*UDCA (21). However, carrier-mediated cellular uptake and export mechanisms also play prominent roles in the absorption and disposition of many drugs and endobiotics (22-24), and the contribution of bile acid and organic anion transporters to the absorption and cholehepatic shunting of *nor*UDCA has not been fully explored (25). In this study, we used knockout mouse and cell-based models to investigate the mechanisms by which *nor*UDCA stimulates biliary secretion to determine if an active enterohepatic circulation and the major bile acid transporters ASBT and OSTα-OSTβ are required for *nor*UDCA's hypercholeretic effects.

Materials and Methods

Materials. *nor*UDCA (24-nor-5β-cholan-23-oic acid) was received as a research gift from Dr. Falk Pharma to Dr. Michael Trauner. SC-435; (4R,5R)-5-[4-[4-(1-aza-4-azoniabicyclo[2.2.2]octan-4-yl)butoxy] phenyl]-3,3-dibutyl-7,8-dimethoxy-1,1-dioxo-4,5-dihydro-2H-1λ6-benzothiepin-4-ol) was received as a research gift from Shire Pharmaceuticals. Colesevelam was provided by Dr. Alan Hofmann (University of California at San Diego). TMEM16A inhibitor (TMEM16Ainh-A01) 2-(5-ethyl-4-hydroxy-6-methylpyrimidin-2-ylthio)-N-(4-(4-methoxyphenyl) thiazol-2-yl) acetamide was purchased from Millipore Sigma.

Animals. The *Asbt*$^{-/-}$ mice (*C57BL/6NJ-Slc10a2*$^{tm1a(KOMP)Mbp}$; Asbt knockout-first, reporter-tagged insertion with conditional potential; Targeting Project CSD76540; https://www.komp.org/ProductSheet.php?cloneID=617849) were obtained from the Knockout Mouse Project (KOMP) Baylor College of Medicine Repository and colonies of *Asbt*$^{-/-}$ and matched WT mice are maintained at the Emory University School of Medicine. Characterization of the ileal and liver Asbt mRNA expression, fecal bile acid excretion, and bile acid pool size and composition in male and female WT and Asbt knockout-first mice is shown in Supplemental Figure 1. The matched background strain WT and *Ostα*$^{-/-}$*Asbt*$^{-/-}$ mice were generated as described previously (26). Male Oatp1a/1b gene cluster knockout mice (*Oatp1a/1b*$^{-/-}$) (FVB.129P2-Del(Slco1b2-Slco1a5)1Ahs) and background-matched WT FVB mice were purchased from Taconic Biosciences. For the ASBTi and colesevelam studies, WT male mice (C57BL/6J) mice were obtained from Jackson Labs.

Animal treatments and bile flow measurements. All experiments were performed using male mice, 3 months of age (25-30 g body weight). The indicated genotypes were fed rodent chow (Envigo; Teklad custom Diet No. TD.160819; global 18% protein rodent diet) for 7 days. For the next 7 days, the mice were fed TD.160819 rodent chow or TD.160819 rodent chow containing the indicated combinations of 0.5% (w/w) *nor*UDCA, 0.006% ASBTi (SC-435; dose ~11 mg/kg/day), or 2% (w/w) colesevelam. The amount of *nor*UDCA, ASBTi, and colesevelam administered was selected based on published studies demonstrating sufficient doses to induce bile flow (*nor*UDCA) or disrupt the enterohepatic circulation of bile acids (ASBTi, colesevelam) (5, 27, 28). Based on an estimate of 3 g of diet consumed per day per 25 g body weight, the dose of *nor*UDCA was approximately 600 mg/kg/day. Bile flow was measured in mice as previously described (3). At the end of the bile collection period, blood was obtained by cardiac puncture to measure plasma chemistries. Portions of the liver were taken for histology and measurements of gene expression.

Plasma biochemistries and biliary solute measurements. Plasma chemistries were measured at the Emory University Department of Animal Resources Quality Assurance and Diagnostic Laboratory. The bile samples were used immediately after isolation to measure HCO_3^-, pH, total CO_2, Na, K, Cl, and glucose using a blood gas analyzer (i-STAT; Abbott Point of Care Inc) in the Clinical Pathology Laboratory, Emory University-Yerkes National Primate Research Center. Biliary glutathione concentrations were measured in the Emory University Pediatric Biomarkers Core Facility. Biliary bile acid, cholesterol and phospholipid concentrations were measured enzymatically as previously described (29, 30).

Histological analysis. The liver segments were fixed in 10% neutral formalin (Sigma-Aldrich), embedded in paraffin and processed by Children's Healthcare of Atlanta Pathology Services. Histological sections (5 μm) were cut and stained with H&E. The liver histology was assessed in a blinded fashion by a certified veterinary pathologist (S.G.).

*Bile acid measurements***.** To characterize the *Asbt*$^{-/-}$ mice, feces were collected from single-housed adult male and female mice over a 72-hour period. The total fecal bile acid content was measured by enzymatic assay (29, 31). Pool size was determined as the bile acid content of the small intestine, liver, and gallbladder removed from non-fasted mice (32, 33). Quantitative analysis of the biliary bile acids from chow or *nor*UDCA-fed mice was carried out at the Clinical Mass Spectrometry Laboratory at Cincinnati Children's Hospital Medical Center as described (34). For the *nor*UDCA feeding studies, fecal samples were collected from the cages of group-housed mice with standard bedding at the end of the 7-day chow or *nor*UDCA feeding period. Fecal bile acid composition was determined using a Hewlett-Packard Agilent gas chromatography/mass spectrometer in the Pediatric Biomarkers Core Facility at Emory University as described (35).

RNA-Seq analysis. Total RNA was extracted from frozen liver tissue using TRIzol reagent (Invitrogen, Carlsbad, CA). RNA-Seq libraries were prepared by Novogene Co., Ltd and sequenced on an Illumina HiSeq1000 system. Differential expression analysis was performed using the DESeq2 R package of Bioconductor (36). The resulting *P* values were adjusted using the Benjamini-Hochberg procedure to control for the false discovery rate (37). Differentially expressed genes with a fold change > 1.0 and adjusted $P < 0.05$ were selected for functional

annotation (GEO series accession number: GSE145020). Pathway analysis of the RNA-Seq data was performed using MetaCore (GeneGo Inc, Saint Joseph, MI).

Luciferase assays. Human liver cells (Huh7) were transfected with expression plasmids for a chimeric nuclear receptor encoding the ligand binding domain of mouse PXR fused to the DNA binding domain of GAL4 along with a 5x Upstream Activation Sequence (UAS)-luciferase reporter, or expression plasmids for human FXR or VDR along with FXR or VDR-responsive luciferase reporter plasmids. Ligand additions and measurements of luciferase activity were performed as described (27).

Measurement of Cl^- Currents. Studies were performed in mouse large cholangiocytes (MLC) isolated from normal mice (BALB/c) and immortalized by transfection with the SV40 large-T antigen gene as previously described (38). Membrane currents were measured by whole−cell patch−clamp techniques with a standard extracellular and intracellular (pipette) solution. Recordings were made with an Axopatch 200B amplifier (Axon Instruments, Foster City, CA) and digitized and analyzed using pCLAMP version 11.0.3 as described (39). Two voltage protocols were utilized: (1) holding potential of –40 mV, with ramp protocol from –100mV to +100mV for duration 450ms at 2 second intervals; (2) holding potential –40 mV, with 450−ms steps from –100 mV to +100 mV in 20−mV increments. Protocol 1 was utilized for real−time tracings and protocol 2 for generation of current−voltage (I−V) plots. Results are reported as current density (pA/pF) to normalize for differences in cell size. Details of the buffer solutions, voltage protocols, and data acquisition are described in further detail in the Supplemental Materials.

In vitro *Colesevelam bile acid binding assay*. Bile acid binding to colesevelam was carried out as described (40).

Data availability. The liver RNA-Seq dataset is available from the GEO repository with the following accession number: GSE145020.

Statistical analyses. For the box and whisker plots, median values (line), interquartile range (boxes), and min to max values (whiskers) are shown. For the liver BA composition analysis and gene expression, mean value ± SD is shown. The data were evaluated for statistically significant differences using the Mann-Whitney test, the two-tailed Student's t test, ANOVA (with a Tukey-Kramer honestly significant difference post-hoc test) or Sidak's multiple comparisons test (GraphPad Prism; Mountain View, CA). Values with different superscript letters are significantly different ($P < 0.05$).

Study approval. All animal experiments were approved by the Emory University Institutional Animal Care and Use Committee in accordance with NIH guidelines for the ethical treatment of animals.

Results

To determine if the major bile acid transporter ASBT and an active enterohepatic circulation of bile acids are required for the bicarbonate-rich choleresis induced by *nor*UDCA, we examined bile flow and biliary bicarbonate output in background strain-matched WT and *Asbt*$^{-/-}$ mice fed chow or chow plus 0.5% *nor*UDCA for 7 days. The experimental scheme and morphological response to *nor*UDCA administration are shown in Supplemental Figure 2. Administration of *nor*UDCA to WT and *Asbt*$^{-/-}$ mice for 7 days tended to reduce body weight (Supplemental Figure 2B, C), but did not affect small intestinal length or weight, colon length or weight, or kidney weight (data not shown). The liver weight and liver to body weight ratio were increased in both genotypes with *nor*UDCA treatment (Supplemental Figure 2D, E). However, analysis of H&E-stained liver sections revealed no apparent histological differences between the genotypes or treatment groups (Supplemental Figure 2F), and plasma chemistries were not significantly different between the chow and *nor*UDCA-fed groups for both genotypes (Supplemental Table 2).

The effect of *nor*UDCA-administration on bile flow and biliary solute output is shown in Figure 1 and summarized in Table 1. On the rodent chow diet, bile flow, bicarbonate concentration, biliary bicarbonate output, and bile pH were similar in WT and *Asbt*$^{-/-}$ mice. In agreement with a block in ileal active reabsorption of bile acids, the concentration and biliary output of bile acids were reduced by more than 50% in chow-fed *Asbt*$^{-/-}$ versus WT mice (Figure 1D, E). As compared to chow-fed mice, administration of *nor*UDCA increased the bile flow rate by 5 to 6-fold, biliary bicarbonate concentration by 2-fold, and bicarbonate output more than 10-fold in both WT and *Asbt*$^{-/-}$ mice (Figure 1A, B, C; Table 1). *nor*UDCA-feeding also increased bile acid output by approximately 4-fold and 8-fold in WT and *Asbt*$^{-/-}$ mice, respectively (Figure

1D, E). Since the ability of *nor*UDCA to stimulate a bicarbonate-rich choleresis is thought to be secondary to its potential for cholehepatic shunting and enrichment in bile, biliary bile acid composition was determined for chow and *nor*UDCA-treated WT and *Asbt*$^{-/-}$ mice. The output and relative proportion of each bile acid species are shown (Figure 1E, F). As compared to chow-fed WT mice, *Asbt*$^{-/-}$ mice had a more hydrophobic bile acid composition, with reduced relative amounts of 6-hydroxylated bile acid species such as tauro-β-muricholic acid (TβMCA), and increased amounts of taurocholic acid (TCA) and its gut microbiota-derived product taurodeoxycholic acid (TDCA). Following administration of *nor*UDCA, the biliary bile acid composition became more hydrophilic in *Asbt*$^{-/-}$ mice and remarkably similar to WT mice, with *nor*UDCA accounting for approximately 60% of the total biliary bile acids in both genotypes. There was also a large reduction in the proportion of TCA and TDCA in *Asbt*$^{-/-}$ mice following *nor*UDCA treatment. The biliary bile acid hydrophobicity changes are reflected in the calculated Hydrophobicity Index, which decreased from +0.166 to -0.483 in *Asbt*$^{-/-}$ mice with *nor*UDCA feeding, but was largely unchanged in WT mice (calculated Hydrophobicity Index value of -0.453 versus -0.489 in chow and *nor*UDCA-fed mice, respectively). For comparison, the amounts of different bile acid species excreted into the feces are shown (Supplemental Figure 3). Under chow-fed conditions, the fecal bile acid content was approximately 5-fold greater in *Asbt*$^{-/-}$ versus WT mice and included a higher proportion of cholic acid and deoxycholic acid. Administration of *nor*UDCA in the diet increased the fecal bile acid content in both WT and *Asbt*$^{-/-}$ mice and shifted the endogenous bile acid composition toward the 6-hydroxylated muricholate species. The increase in fecal bile acid levels was driven primarily by the exogenous *nor*UDCA, however the amount of endogenous bile acid in feces was also increased in both WT mice and *Asbt*$^{-/-}$ mice after administration of *nor*UDCA.

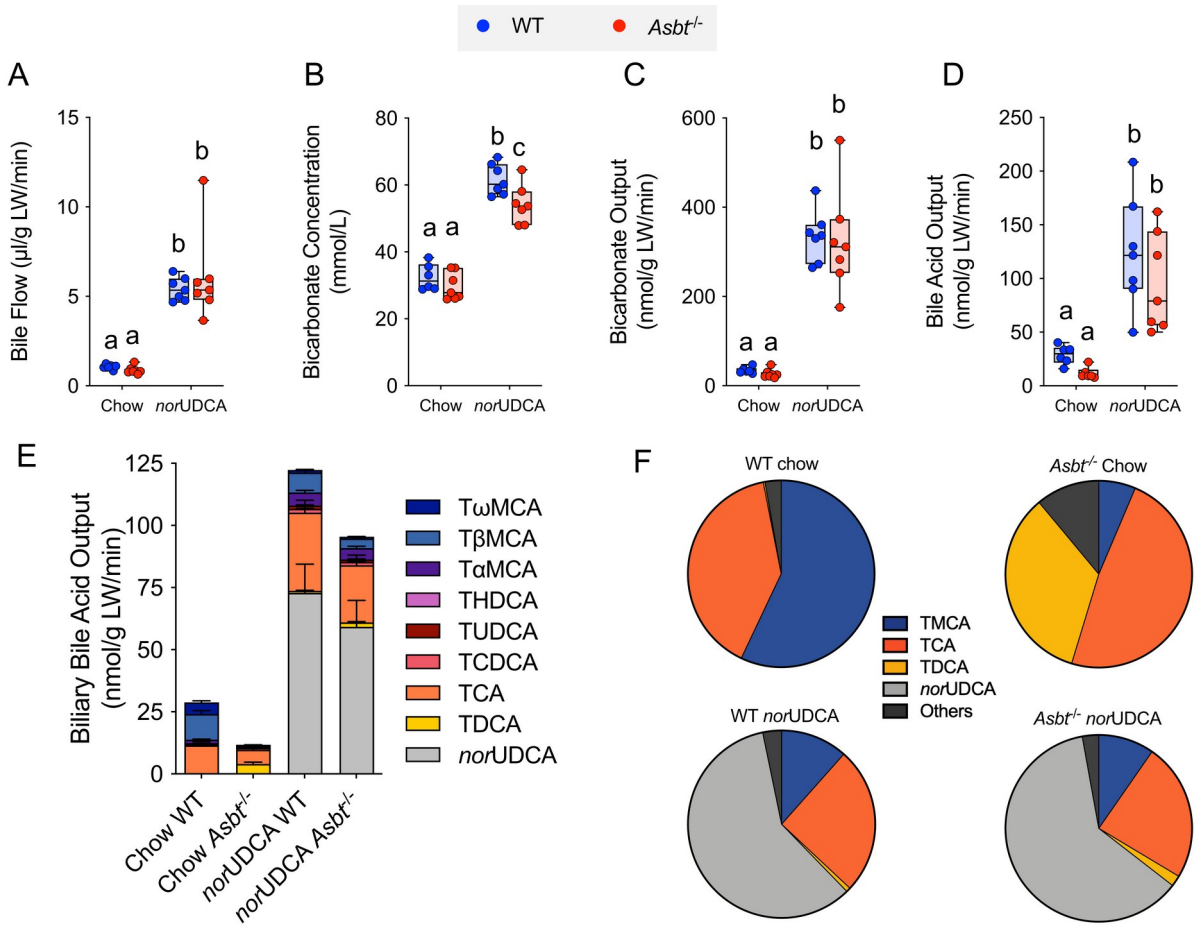

Figure 1. *nor*UDCA treatment increases bile flow and biliary bicarbonate and solute output in WT and *Asbt*$^{-/-}$ mice.

(**A**) Bile flow. (**B**) Biliary bicarbonate concentration. (**C**) Bicarbonate output. (**D**) Biliary bile acid output. (**E**) Biliary bile acid species output (mean + SEM). (**F**) Biliary bile acid composition expressed as pie charts. Unless indicated, mean + SD are shown; n = 6-7 mice per group. Distinct lowercase letters indicate significant differences between groups ($P < 0.05$).

The effect of *nor*UDCA-feeding on the output of other biliary solutes in WT and *Asbt*$^{-/-}$ mice are shown in Table 1. The total glutathione concentration and output tended to be higher in chow-fed *Asbt*$^{-/-}$ versus WT mice. This may be a mechanism to increase bile acid-independent bile flow to compensate for interruption of the bile acid enterohepatic circulation and reductions in bile acid-dependent bile flow. Administration of *nor*UDCA to WT and *Asbt*$^{-/-}$ mice did not change the biliary glutathione concentration but increased biliary glutathione output by 3 to 4-fold in both genotypes. Biliary cholesterol levels were slightly decreased in WT and *Asbt*$^{-/-}$ mice fed the *nor*UDCA diet, but total cholesterol output was elevated versus chow-fed mice due to increases in bile flow. In contrast to biliary cholesterol, administration of *nor*UDCA dramatically reduced biliary phospholipid secretion in both WT and *Asbt*$^{-/-}$ mice, in agreement with previous studies (1, 3, 4). This ineffective coupling of *nor*UDCA and phospholipid secretion has been attributed to *nor*UDCA's lower surface activity and a reduced ability to extract phospholipid from the canalicular membrane (19). The reduced phospholipid secretion is unlikely due to direct inhibition of Mdr2 (*ABCB4*), the ABC transporter in the canalicular membrane that translocates phosphatidylcholine into bile, since recent in vitro studies using purified ABCB4 demonstrated that *nor*UDCA potently stimulates ABCB4 ATPase activity (41). Overall, these findings argue that the ASBT is not required for the absorption of *nor*UDCA or its ability to stimulate a bicarbonate-rich hypercholeresis in mice.

Table 1. Bile Flow and Composition in WT and *Asbt*$^{-/-}$ Mice Fed Chow or *nor*UDCA Diet

Variable	Chow		*nor*UDCA	
	WT (6)	*Asbt*$^{-/-}$ (7)	WT (7)	*Asbt*$^{-/-}$ (7)
Bile Flow (µl/g LW/min)	1.1 ± 0.1^{a}	0.9 ± 0.2^{a}	5.4 ± 0.6^{b}	6.0 ± 2.5^{b}
Bicarbonate (mM)	32 ± 4^{a}	30 ± 4^{a}	62 ± 5^{b}	54 ± 6^{c}
Bicarbonate Output (nmol/g LW/min)	34 ± 7^{a}	27 ± 10^{a}	335 ± 58^{b}	324 ± 117^{b}
Bile pH	7.6 ± 0.1^{a}	7.7 ± 0.1^{a}	7.9 ± 0.1^{b}	7.7 ± 0.1^{a}
Bile Acid (mM)	26.8 ± 5.8^{a}	12.8 ± 2.5^{b}	22.5 ± 8.4^{a,b}	16.5 ± 7.2^{a,b}
Bile Acid Output (nmol/g LW/min)	28.9 ± 8.8^{a}	11.8 ± 5.4^{a}	123.6 ± 52.2^{b}	96.2 ± 45.8^{b}
Glutathione (mM)	0.65 ± 0.81^{a}	1.41 ± 0.82^{a}	0.74 ± 0.37^{a}	0.80 ± 0.42^{a}
Glutathione Output (nmol/g LW/min)	0.7 ± 1.0^{a}	1.3 ± 0.9^{a}	4.0 ± 2.1^{b}	4.5 ± 2.5^{b}
Cholesterol (µg/µl)	0.17 ± 0.07^{a,b}	0.2 ± 0.06^{a}	0.1 ± 0.04^{b}	0.1± 0.07^{a,b}
Cholesterol Output (µg/g LW/min)	0.2 ± 0.1^{a}	0.2 ± 0.1^{a}	0.4 ± 0.2^{a,b}	0.6 ± 0.4^{b}
Phospholipid (mM)	2.4 ± 1.3	3.0 ± 1.4	BLD	BLD
Phospholipid Output (nmol/g LW/min)	2.7 ± 1.8	2.9 ± 1.9	BLD	BLD

Values are expressed as the mean ± SD. The number of mice per group are indicted (n). Values with different superscript letters are significantly different ($P < 0.05$) according to ordinary two-way ANOVA and Sidak's multiple comparisons test. BLD, below level of detection; LW, liver weight.

OSTα-OSTβ is a heteromeric bi-directional facilitative transporter and is responsible for bile acid export across the basolateral membrane of various epithelium. Similar to the ASBT, OSTα-OSTβ is expressed by ileal enterocytes and cholangiocytes. However, OSTα-OSTβ is also expressed at lower levels in proximal small intestine and in colon, where it may be involved in the export of bile acids that were taken up across the apical membrane of the epithelium by passive diffusion (42, 43). Due to their higher pKa, a fraction of unconjugated and glycine-conjugated bile acids are protonated in the lumen and gain entry to the epithelium by nonionic diffusion (44). Once inside the cytoplasmic compartment, weak acids ionize at this neutral pH, potentially impeding their exit from the cell by passive diffusion and necessitating the requirement for an efflux carrier such as OSTα-OSTβ. To determine if OSTα-OSTβ may be contributing to the absorption and bicarbonate-rich choleresis induced by *nor*UDCA, we examined bile flow and biliary bicarbonate output in background strain-matched WT and *Ostα*$^{-/-}$ *Asbt*$^{-/-}$ mice fed chow or chow plus 0.5% *nor*UDCA for 7 days. *Ostα*$^{-/-}$*Asbt*$^{-/-}$ mice were selected for these studies in place of *Ostα*$^{-/-}$ mice because inactivation of the Asbt protects *Ostα*$^{-/-}$ mice from ileal injury and attenuates the associated adaptive changes such as lengthening of the small intestine, and ileal histological alterations such as villous blunting, increased numbers of mucin-producing cells, and increased cell proliferation (26). These changes were predicted to complicate interpretation of the findings with regards to the role of OSTα-OSTβ transport activity in the intestinal absorption and choleretic actions of *nor*UDCA. The experimental scheme and morphological response to *nor*UDCA administration is shown in Supplemental Figure 4. As with the WT and *Asbt*$^{-/-}$ mice, liver to body weight ratio was increased in *Ostα*$^{-/-}$ *Asbt*$^{-/-}$ and matched WT mice with *nor*UDCA treatment (Supplemental Figure 4E). Compared to chow-fed mice, administration of *nor*UDCA increased bile flow rate by 5 to 6-fold, biliary

bicarbonate concentration by 2-fold, bicarbonate output by more than 10-fold, and glutathione output by 5 to 6-fold in WT mice and background strain-matched mice lacking both Asbt and Ostα (Figure 2).

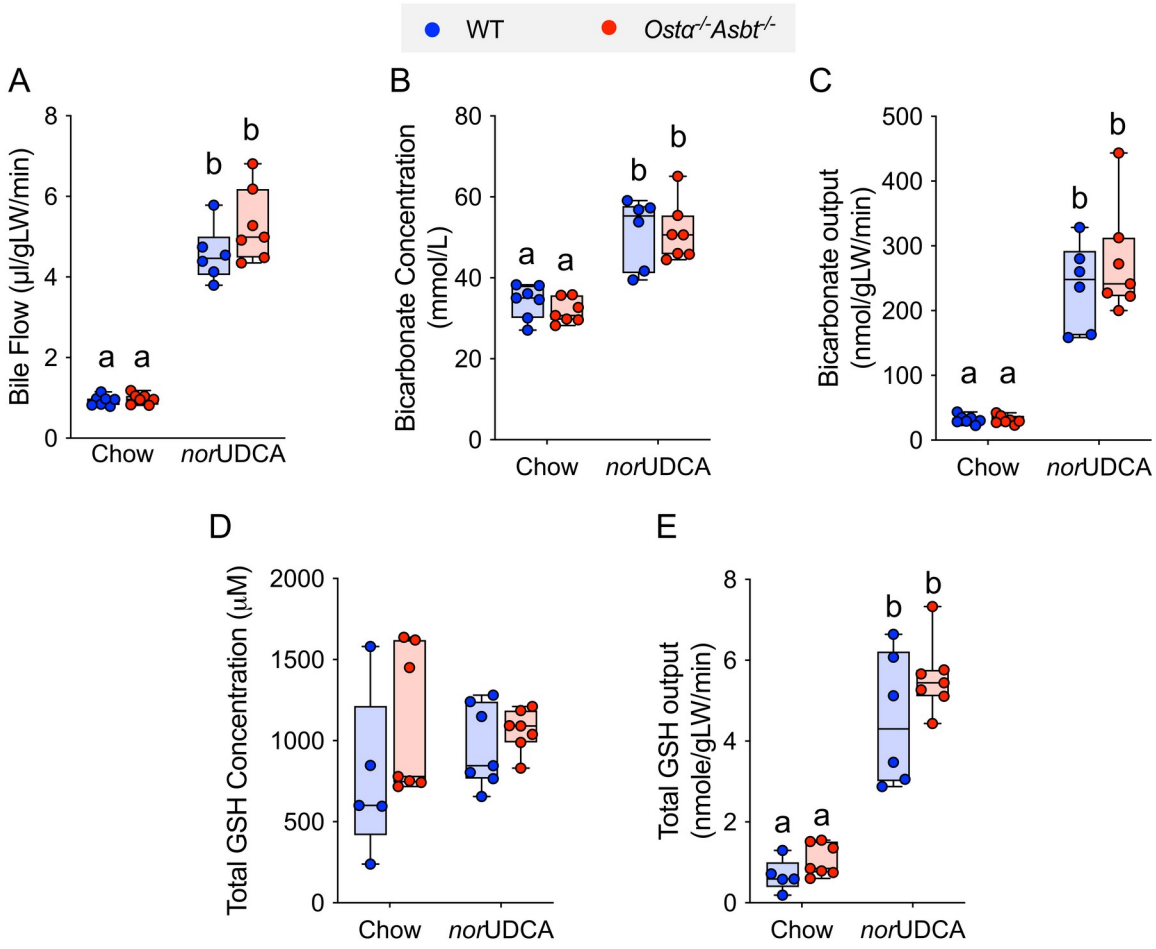

Figure 2. *nor*UDCA treatment increases bile flow and biliary bicarbonate and solute output in WT and *Ostα*$^{-/-}$*Asbt*$^{-/-}$ mice.

(**A**) Bile flow. (**B**) Biliary bicarbonate concentration. (**C**) Bicarbonate output. (**D**) Glutathione concentration. (**E**) Glutathione output. Mean + SD, n = 5-7 mice per group. Distinct lowercase letters indicate significant differences between groups ($P < 0.05$).

The negative findings for Asbt and Ostα-Asbt null mice do not exclude the potential involvement of other membrane transporters. We hypothesized that *nor*UDCA may act in a feed-forward fashion to induce hepatocyte or cholangiocyte expression of transporters involved in *nor*UDCA's disposition, cholehepatic shunting, or mechanism of action. To identify potential candidates, RNA-Seq analysis was performed using livers from WT mice fed chow or *nor*UDCA-containing diets. Using a log2(fold-change) > 1 and multiple testing (FDR 5%), 1232 downregulated and 1087 upregulated genes were identified in *nor*UDCA-treated versus chow-fed WT mice. Narrowing our focus to the liver membrane transporter gene transcriptome revealed 80 Solute Carrier (*SLC*) family members, 16 ATP-binding cassette (*ABC*) family members, and 15 transporting P-type ATPases (*ATP*) family members (Figure 3A, 3B; Supplemental Figure 5A) that are differentially expressed in *nor*UDCA versus chow-fed control WT mice. Of these hepatic genes, expression of 30 *SLC*, 10 *ABC*, and 3 *ATP*-type transporters were significantly induced. Among the most highly induced transporter genes in *nor*UDCA-treated mice was *Slco1a4* (Oatp1a4; originally called Oatp2). Members of the Oatp1a/1b family such as Oatp1a4 are sodium-independent facilitative uptake carriers that mediate hepatocellular clearance of a variety of organic anions, steroids, sulfated, and glucuronidated metabolites (45). Notably, Oatp1a4 has a substrate specificity that includes bile acids and is expressed on the sinusoidal membrane of perivenous hepatocytes (46).

To further pursue the RNA-Seq findings, real-time PCR was used to measure mRNA expression of select transporters and genes critical for bile acid homeostasis (Figure 3C). Administration of *nor*UDCA induced Oatp1a4 mRNA expression by more than 6-fold in WT and *Asbt*$^{-/-}$ mice, whereas other hepatic OATP family genes, Oatp1a1, Oatp1b2 and Oatp2b1 were largely unaffected. Regarding other transporters involved in bile acid or cholesterol

metabolism, hepatic expression of Asbt was decreased, whereas Ntcp (*Slc10a1*), Bsep (*Abcb11*), Mrp2 (*Abcc2*), and Abcg5/8 expression were modestly increased, and Mrp3 (*Abcc3*) RNA levels were increased by 3-to-4 fold (Figure 3C). In liver, expression of the bile acid biosynthetic genes *Cyp7a1* and *Cyp8b1* were significantly increased in *Asbt*$^{-/-}$ mice fed *nor*UDCA versus WT mice (Figure 3C). In ileum, administration of *nor*UDCA tended to reduce mRNA expression of the bile acid-related genes Asbt, Fgf15, and Ostα-Ostβ, but had little effect on Ibabp (*Fabp6*) expression (Supplemental Figure 5B). Notably, administration of *nor*UDCA significantly induced expression of PXR-target genes, including *Slco1a4*, *Abcc3*, and *Cyp3a11*. These findings are in agreement with pathway analysis of the RNA-Seq data, which identified pregnane X-receptor (PXR)-mediated direct regulation of xenobiotic metabolizing enzymes as one of the top-regulated pathways (Supplemental Figure 6A). To directly test the hypothesis that *nor*UDCA may be acting directly via PXR or other bile acid-activated nuclear receptors, the ability of *nor*UDCA to activate mouse PXR, human farnesoid X-receptor (FXR) and human vitamin D receptor (VDR) was examined in transfected human Huh7 cells. Whereas the positive control compounds pregnenolone 16α-carbonitrile (PCN), GW4064 and 25-hydroxy vitamin D activated their cognate receptors in this assay, *nor*UDCA failed to increase the activity of the PXR, FXR or VDR reporter plasmids (Supplemental Figure 6B).

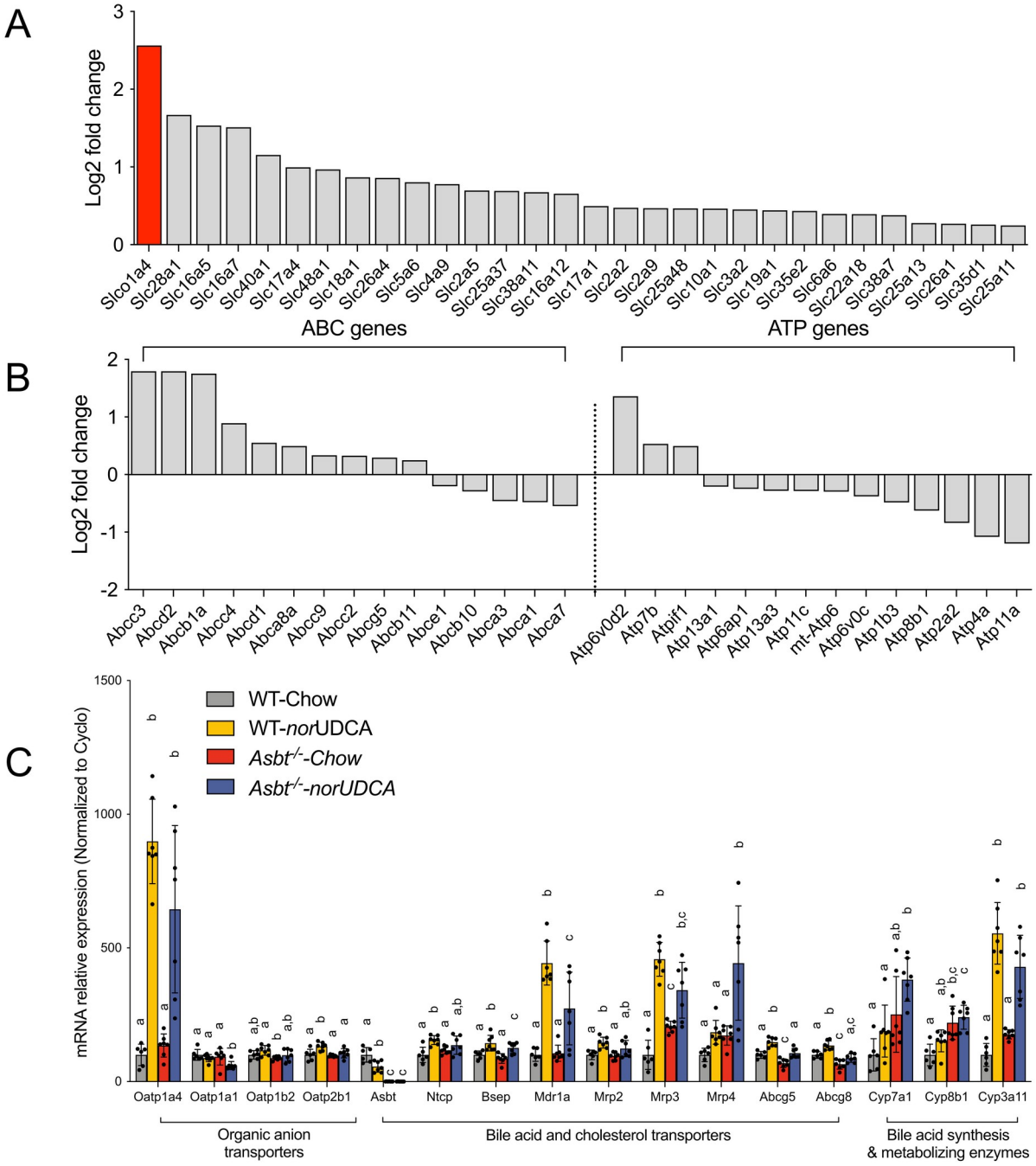

Figure 3. *nor*UDCA treatment alters expression of a limited number of hepatic transporter genes. RNA-Seq analysis of livers from WT mice fed chow or the *nor*UDCA-diet.

(**A**) Differentially expressed *SLC* membrane transporter genes whose expression was significantly induced ($P < 0.05$; n = 6 per group) in *nor*UDCA-treated versus chow mice. (**B**)

Differentially expressed *ABC* transporter and *ATP* P-type ATPase genes ($P < 0.05$; n = 6 per group) in the *nor*UDCA-treated versus chow mice. (**C**) Hepatic expression of the indicated transporters and bile acid-related biosynthesis or metabolizing enzymes in WT and *Asbt*$^{-/-}$ mice fed chow or the *nor*UDCA-containing diet for 7 days. RNA was isolated from livers of individual mice and used for real time PCR analysis. The mRNA expression was normalized using cyclophilin and the results for each gene are expressed relative to chow-fed WT mice (set at 100%). Mean + SD, n = 6-7 mice per group. Distinct lowercase letters indicate significant differences between groups ($P < 0.05$).

The significant increase observed for hepatic Oatp1a4 expression raised the prospect that this transporter may be induced in a feed-forward fashion to facilitate hepatic clearance and cholehepatic shunting of *nor*UDCA. To directly test that hypothesis, the ability of *nor*UDCA to induce bile secretion and biliary bicarbonate output was examined in background (FVB) strain-matched WT and *Oatp1a/1b*$^{-/-}$ mice, in which *Slco1a1*, *Slco1a4*, *Slco1a5*, *Slco1a6* and *Slco1b2* have been excised by cre-mediated deletion of the *Slco1a/1b* gene cluster (47). The well-characterized *Oatp1a/1b*$^{-/-}$ mouse model was selected for these studies since the various Oatp1a and Oatp1b transporters display considerable overlap in their tissue expression and substrate specificity, and other members of the murine Oatp1a/1b subfamily could partially compensate for loss of Oatp1a4 alone. The experimental scheme and morphological response to *nor*UDCA feeding in *Oatp1a/1b*$^{-/-}$ mice are shown in Supplemental Figure 7. Administration of *nor*UDCA to the FVB background WT and *Oatp1a/1b*$^{-/-}$ mice for 7 days decreased body weight for both genotypes and increased the liver weight and liver to body weight ratio in the WT mice. Bile flow and biliary solute output are shown in Figure 4. Bile flow and biliary bicarbonate concentration, bicarbonate output, and pH were similar in the chow-fed WT and *Oatp1a/1b*$^{-/-}$ mice. Similar to WT C57BL/6J mice, administration of *nor*UDCA to WT FVB mice significantly increased bile flow by 4.7-fold, biliary bicarbonate concentration by 1.6-fold, and bicarbonate output by 7.5-fold as compared to chow-fed mice. In the *Oatp1a/1b*$^{-/-}$ mice, administration of *nor*UDCA induced a 5-fold increase in bile flow rate, 2-fold increase in biliary bicarbonate concentration, and 11-fold increase in bicarbonate output.

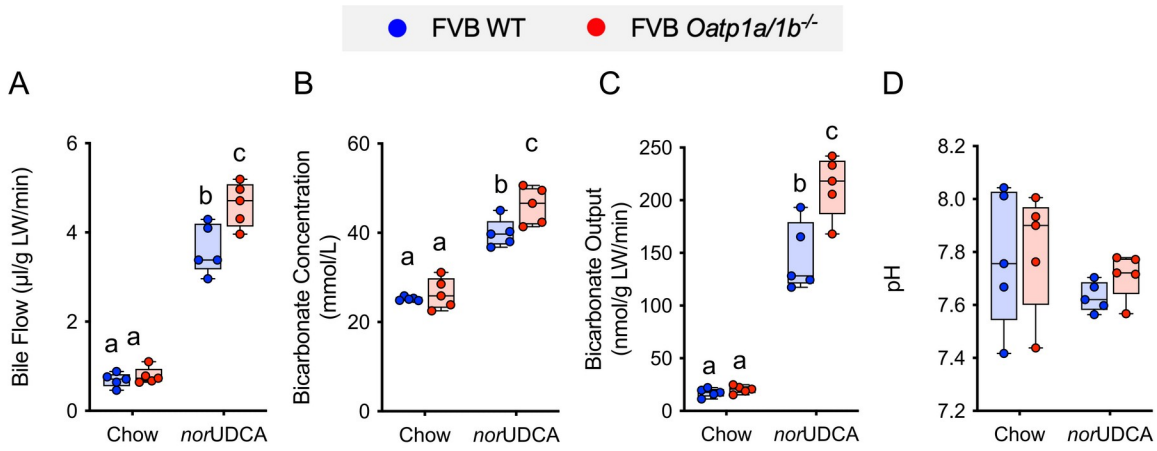

Figure 4. *nor*UDCA treatment increases bile flow and biliary bicarbonate and solute output in WT and *Oatp1a/1b*$^{-/-}$ mice.

(**A**) Bile flow. (**B**) Biliary bicarbonate concentration. (**C**) Bicarbonate output. (**D**) Biliary pH. Mean + SD, n = 5 mice per group. Distinct lowercase letters indicate significant differences between groups ($P < 0.05$).

Our findings indicate that the major bile acid transporters Asbt, Ostα-Ostβ, and Oatp1a/1b family members are not required for the choleretic activity of *nor*UDCA. However, the question remains as to how *nor*UDCA induces such a potent bicarbonate-rich hypercholeresis. Opening of the cholangiocyte apical membrane Cl^- channels provides the critical driving force for biliary bicarbonate and fluid secretion (15). In addition to the cAMP-activated Cl^- channel CFTR (48), the Ca^{2+}-activated Cl^- channel TMEM16A (ANO1) and the volume-regulated Cl^- channel LRRC8A have been identified to play important roles in cholangiocyte secretion (17, 49). We focused our studies on TMEM16A for the following reasons: 1) In *Cftr*$^{-/-}$ mice administration of *nor*UDCA was still able to induce bile flow and biliary bicarbonate secretion, although to a lower extent than in WT mice (5), and 2) UDCA and TUDCA has been shown to stimulate cholangiocyte fluid secretion by activation of TMEM16A Cl^- channels (17). As shown in Figure 5A, *nor*UDCA potently stimulated Cl^- channel activity in mouse large cholangiocytes (MLC) with the properties previously described for TMEM16A (17, 50). To confirm TMEM16A-dependent chloride secretion, siRNA targeted to TMEM16A was able to successfully reduce TMEM16A protein levels in MLCs (Supplemental Figure 8) and resulted in the subsequent loss of Cl^- secretion during *nor*UDCA treatment, strongly suggesting *nor*UDCA was directly stimulating Cl^- secretion by TMEM16A activation. In Figure 5B, TMEM16A-dependent chloride secretion was further confirmed by pre-incubation with the TMEM16A-inhibitor A01, which also abolished the *nor*UDCA stimulation of chloride currents in these cells. Previous studies have shown that inhibition of the ASBT blocks TUDCA stimulation of Cl^- currents in cholangiocytes (17). In agreement with our *in vivo* studies showing that loss of the ASBT did not affect the bicarbonate-rich hypercholeresis induced by *nor*UDCA,

pre-incubation of MLC with the ASBT inhibitor SC-435 did not impact the *nor*UDCA-stimulation of Cl^- channels.

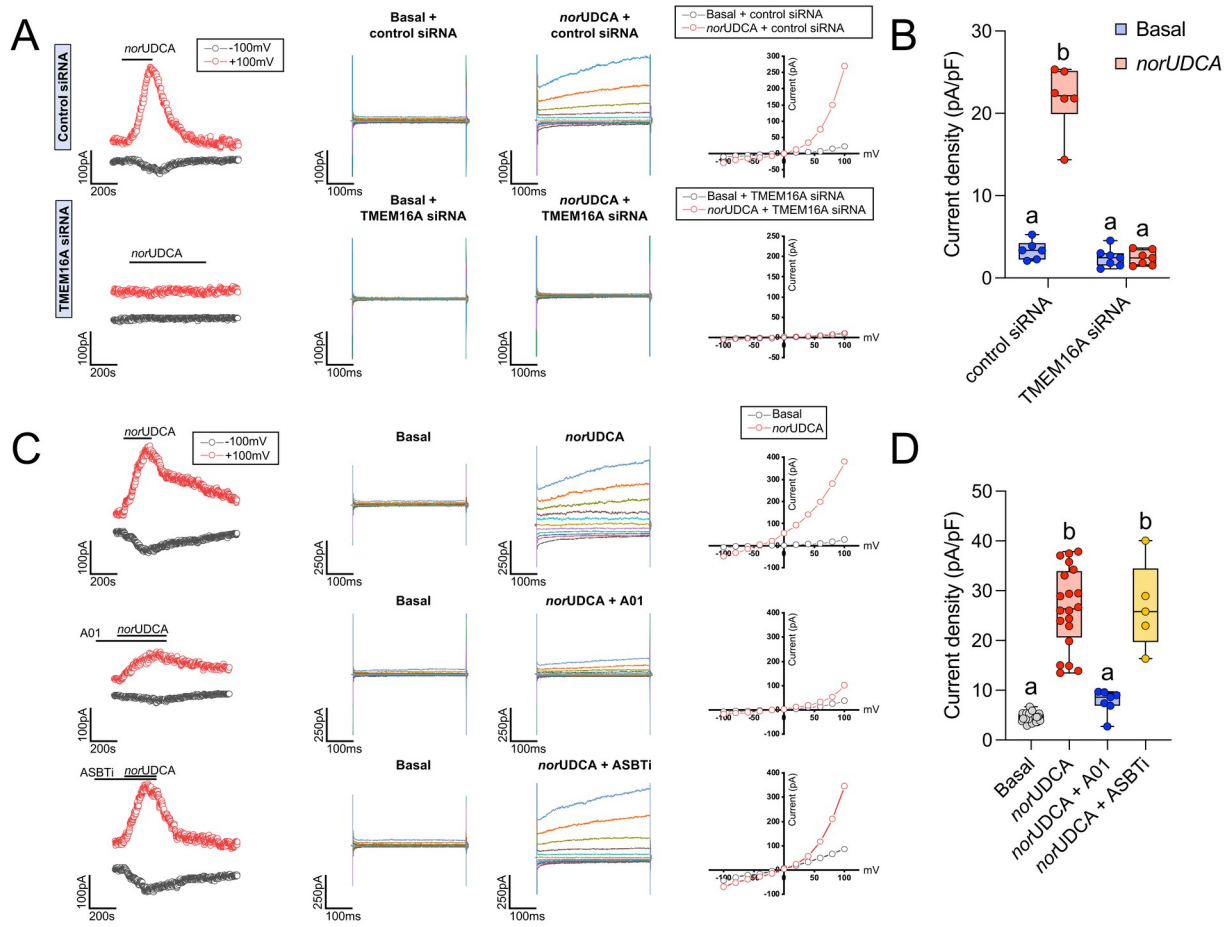

Figure 5. *nor*UDCA stimulates TMEM16A Cl^- currents independent of ASBT transport.

(A) Representative whole−cell currents in MLC cells transfected with nontargeting or TMEM16A siRNA measured under basal conditions or exposure to *nor*UDCA (250 μM). Currents measured at -100 mV (black) or +100 mV (red), representing I_{Cl^-} are shown. Compound exposure is indicated by the black bar. A voltage−step protocol from a holding potential of -40 mV, with 450−ms steps from –100 to +100 mV in 20−mV increments. Currents demonstrated time−dependent activation at membrane potentials +100 mV. The I−V plot was generated from these protocols during basal (black) and *nor*UDCA−stimulated (red) conditions. **(B)** Cumulative data demonstrating maximum increase in current density (pA/pF) in response to *nor*UDCA in the

absence or presence of TMEM16A siRNA silencing, n = 5 – 6 cells per group. **(C)** Representative whole−cell currents in MLC cells measured under basal conditions and during exposure to *nor*UDCA (250 μM) following pre-incubation with vehicle (top), TMEM16A inhibitor (10 μM A01; middle) or ASBTi (100 nM SC-435; bottom). Currents measured at -100 mV (black) or +100 mV (red), representing I_{Cl^-} are shown. Compound exposure is indicated by the black bar. A voltage−step protocol from a holding potential of -40 mV, with 450−ms steps from –100 to +100 mV in 20−mV increments. Currents demonstrated time−dependent activation at membrane potentials +100 mV. The I−V plot was generated from these protocols during basal (black) and *nor*UDCA−stimulated (red) conditions. Cumulative data demonstrating maximum increase in current density (pA/pF) in response to *nor*UDCA in the absence or presence of TMEM16A inhibitor or ASBTi, n = 5 – 35 cells per group. Values with distinct superscript lowercase letters are significantly different ($P < 0.05$) according to ordinary two-way ANOVA and Sidak's multiple comparisons test, mean ± SD.

Administration of *nor*UDCA (3), ASBT inhibitors (51, 52), and a bile acid sequestrant (28) have previously shown benefit in the *Abcb4/Mdr2*$^{-/-}$ mouse model of cholestasis and appear to involve overlapping and complementary therapeutic mechanisms of action. Prompted by our observations of the *nor*UDCA-fed *Asbt*$^{-/-}$ mice and SC-435-treated MLC, we examined the effect of pharmacological interruption of the enterohepatic circulation of bile acids on the choleretic actions of *nor*UDCA by co-administering an ASBTi (SC-435) or bile acid sequestrant (Colesevelam). Colesevelam is a second-generation bile acid sequestrant and non-absorbable polymer that binds bile acids through a combination of hydrophobic and ionic interactions and with a higher affinity than first generation sequestrants such as cholestyramine (53). Male WT mice were fed chow, chow supplemented with 0.006% (w/w) ASBTi (SC-435), chow supplemented with 2% (w/w) colesevelam, or those diets plus 0.5% (w/w) *nor*UDCA for 7 days. The experimental scheme and morphological response to *nor*UDCA feeding is shown in Supplemental Figure 9. Administration of *nor*UDCA to mice for 7 days tended to reduce body weight, particularly when co-administered with an ASBTi (Supplemental Figure 9B, C), and increase the liver to body weight ratio (Supplemental Figure 9E). However, analysis of H&E-stained liver sections revealed no apparent histological differences between the treatment groups (Supplemental Figure 9F), and the plasma chemistries were not significantly different between the groups (Supplemental Table 3). The levels of bile acids excreted into the feces for each of the treatment groups are shown in Supplemental Figure 9G. Administration of the ASBTi versus colesevelam resulted in a greater increase in the fecal bile acid content, however both treatments induced similar changes in fecal bile acid composition versus chow control mice (Supplemental Figure 9H). Administration of *nor*UDCA in the diet increased the fecal bile acid content in all

treatment groups, due to increased excretion of the exogenous *nor*UDCA, as well as an increase in endogenous bile acids.

Similar to the findings for *Asbt*$^{-/-}$ mice, *nor*UDCA significantly increased bile flow by 3 to 4-fold, bicarbonate concentration by ~2-fold, and bicarbonate output by ~8-fold in WT mice when co-administered with an ASBTi (Figure 6A, B, C). Remarkably, *nor*UDCA also stimulated a similar bicarbonate-rich choleresis when co-administered with colesevelam. In agreement with the block in intestinal absorption of bile acids, biliary bile acid concentrations were reduced in ASBTi and colesevelam-treated versus control chow mice, however, administration of *nor*UDCA significantly increased biliary bile acid output in all the treatment groups (Figure 6F). The observation that co-administration of colesevelam did not attenuate the *nor*UDCA-induced hypercholeresis prompted an examination of the ability of colesevelam to bind *nor*UDCA versus endogenous bile acids in simulated small intestinal fluid. In accord with previous findings, colesevelam efficiently bound glycodeoxycholic acid (GCDCA) and taurodeoxycholic acid (TDCA) *in vitro* (40). However, under the same conditions, there was minimal binding of *nor*UDCA to colesevelam (Supplemental Figure 10) providing a potential explanation for the inefficacy of co-administered colesevelam to antagonize the actions of *nor*UDCA. In summary, pharmacological inhibition of intestinal bile acid absorption does not impede *nor*UDCA's ability to induce a bicarbonate-rich hypercholeresis in mice.

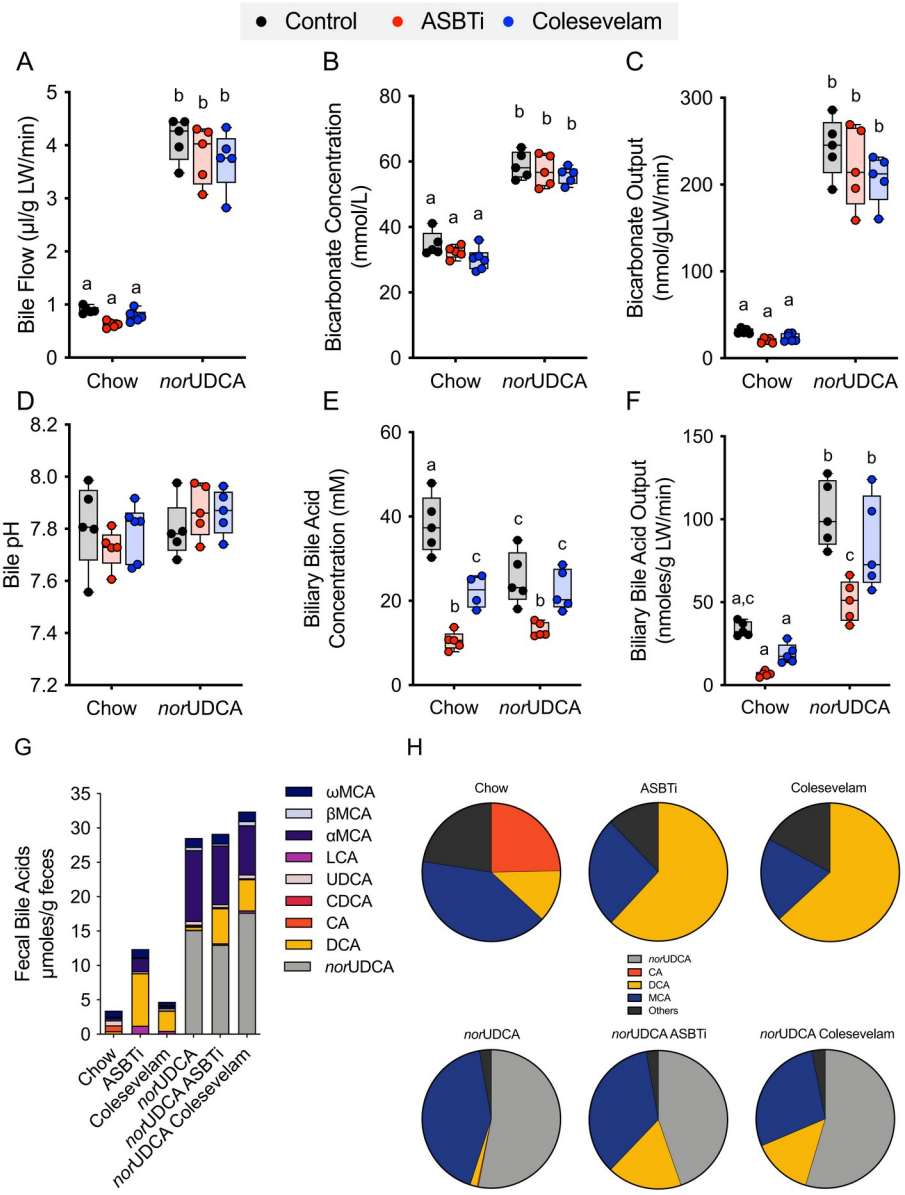

Figure 6. Pharmacological inhibition of intestinal bile acid absorption does not alter *nor*UDCA-induction of a bicarbonate-rich hypercholeresis in mice.

(**A**) Bile flow. (**B**) Biliary bicarbonate concentration. (**C**) Bicarbonate output. (**D**) Biliary pH. (**E**) Biliary bile acid concentration. (**F**) Biliary bile acid output. (**G**) Fecal bile acids (mean values). (**H**) Fecal bile acid composition expressed as pie charts. Unless indicated, mean + SD are shown; n = 5 mice per group. Distinct lowercase letters indicate significant differences between groups ($P < 0.05$).

Discussion

When first characterized by Hofmann and colleagues, side chain shortened dihydroxy bile acids such as *nor*CDCA, norDCA and *nor*UDCA were shown to induce a bicarbonate-rich bile flow exceeding that of which could be accounted for by existing theories for bile formation and led the authors to propose a model involving cholehepatic shunting of unconjugated *nor* bile acids (1, 13, 20). Although currently in therapeutic development for the treatment of liver disease (8, 9, 54), important questions remain regarding the molecular mechanisms underlying the biliary bicarbonate secretion induced by *nor*UDCA and its hypothesized cholehepatic shunting. The major findings of this study are 1) *nor*UDCA directly stimulates the Ca^{2+}-activated Cl^- channel TMEM16A in mouse cholangiocytes and 2) the major bile acid carriers ASBT, OSTα-OSTβ, and OATP transporters are not required for orally administered *nor*UDCA to stimulate a bicarbonate-rich hypercholeresis.

In our studies, *nor*UDCA activated TMEM16A chloride channels, which are thought to be the final common pathway responsible for bile acid-stimulated ductal secretion. In that paradigm, *nor*UDCA is proposed to stimulate ATP-release and P2 purinergic receptor signaling through the IP3 receptor to release Ca^{2+} and activate TMEM16A Cl^- secretion (15, 17, 55). Interestingly, the UDCA-stimulation of cholangiocyte ATP release is thought to require CFTR and may act by stimulating the trafficking and fusion of ATP-containing vesicles with the apical membrane (39, 56, 57). However, *nor*UDCA-induced stimulation of biliary bile flow and bicarbonate secretion is at least partly CFTR-independent (5), raising the prospect that *nor*UDCA may be stimulating ATP release or bicarbonate secretion by additional mechanisms.

The physiologic properties and metabolism of side chain-shortened C-23 *nor*-bile acids such as *nor*UDCA have been the subject of considerable study (1, 19, 20). Due to a higher

critical micelle concentration (CMC) (17 mM) than many natural bile acids, *nor*UDCA is more likely present in monomeric rather than micellar form in bile (58). Based on their findings, Hofmann and coworkers proposed that C-23 *nor*-dihydroxy bile acids are sufficiently hydrophobic to be absorbed by passive diffusion (14). However, membrane transporters participate in the intestinal absorption and hepatic clearance of various hydrophobic drugs and endobiotics, including unconjugated C-24 bile acids (47, 59). Yet to date, study of the contribution of individual bile acid and organic anion carriers to the transport of *nor*UDCA has been largely restricted to transfected cell-based models (25). The ASBT and OSTα-OSTβ play a central role in the intestinal reabsorption of bile acids and are expressed by the biliary epithelium (31-33). As such, it was possible that these major bile acid transporters could play a direct or indirect role in the absorption, cholehepatic shunting, and choleretic actions of *nor*UDCA.

In agreement with previous studies, administration of *nor*UDCA significantly increased bile flow and bicarbonate concentration in WT mice, and similar results were observed for *Asbt*$^{-/-}$ and *Ostα*$^{-/-}$*Asbt*$^{-/-}$ mice. Biliary bile acid output, typically lower in *Asbt*$^{-/-}$ versus WT mice, was significantly increased by administration of *nor*UDCA. This was driven primarily by the increase in bile flow since the biliary total bile acid concentration was not significantly changed. However, *nor*UDCA administration significantly altered the biliary bile acid composition, with *nor*UDCA accounting for more than half the biliary bile acid species and a concomitant reduction in endogenous bile acid species. In *Asbt*$^{-/-}$ mice and mice treated with ASBT inhibitors, the biliary bile acid composition becomes more hydrophobic and enriched in TCA and TDCA. This is most likely due to increased hepatic TCA synthesis and an increased flux of TCA into the colon, where it is metabolized to deoxycholic acid (DCA), passively reabsorbed, and carried back to the liver for uptake and reconjugation in hepatocytes (29, 52, 60). Following

administration of *nor*UDCA, the biliary endogenous bile acid composition in WT and *Asbt*$^{-/-}$ mice become remarkably similar. Interestingly, there was an increase in fecal endogenous bile acids observed in WT mice treated with *nor*UDCA, which may be secondary to decreased ileal Asbt expression or weak inhibition of ileal Asbt activity. Using cell-based models, hydrophobic unconjugated bile acids, such as CDCA, DCA, UDCA, LCA, exhibited little apparent ASBT-mediated uptake over background, but are still able to compete for conjugated bile acid uptake (61).

We hypothesized that *nor*UDCA may induce hepatic expression of its own transporter(s) in a feed-forward fashion to facilitate cholehepatic shunting. RNA-Seq analysis revealed that *nor*UDCA induced expression of only a small subset of hepatic transporter genes, including several transporters involved in bile acid homeostasis, Oatp1a4, Mrp3, Mrp4, and Mdr1a. Interestingly, many of the genes induced by *nor*UDCA are PXR targets, raising the prospect that *nor*UDCA may be acting directly or indirectly via PXR. When investigated, *nor*UDCA did not directly activate mouse PXR or the bile acid sensing nuclear receptors, FXR or VDR as measured using nuclear receptor-luciferase reporter assays in transfected human hepatoma Huh7 cells. These results agree with recent results showing that *nor*UDCA did not activate or inhibit FXR in HepG2 cells transfected with a FXR reporter plasmid (62). Other hepatic gene expression pathways that were significantly induced by administration of *nor*UDCA included those regulated by the nuclear receptor Constitutive Androstane Receptor (CAR; *NR1L3*). Unlike PXR, FXR, or VDR, bile acids do not directly bind and activate CAR (63), but may act indirectly through a ligand-independent mechanism to stimulate CAR nuclear translocation and activate of CAR target genes (64). However, the role of CAR in the actions of *nor*UDCA remain to be investigated.

We focused our attention on Oatp1a4, since its expression was most highly induced in the hepatic transporter transcriptome in *nor*UDCA-fed WT mice. Oatp1a4 (originally called Oatp2) is expressed on the hepatocyte sinusoidal membrane, transports a variety of organic anions, and contributes to the hepatic clearance of steroid sulfates, bile acids, and drugs (65-67). However, the three most abundant hepatic Oatp isoforms in rodents, Oatp1a1, Oatp1b2 and Oatp1a4, exhibit overlapping substrate specificity (45), prompting us to use the *Oatp1a/1b*$^{-/-}$ mouse model lacking all 3 transporters for our studies (47). Similar to *Asbt*$^{-/-}$ and *Ostα*$^{-/-}$*Asbt*$^{-/-}$ mice, loss of the Oatp1a/1b transporters did not impair the ability of *nor*UDCA to stimulate a bicarbonate-rich hypercholeresis. This is in line with data obtained using cells stably expressing human liver OATPs, which failed to detect appreciable *nor*UDCA transport by human NTCP, OATP1B1, OATP1B3 or OATP2B1 (25). The finding that biliary bicarbonate concentration and bile flow increases in the *nor*UDCA-fed WT and various transporter knockout models is strongly consistent with the mechanism for cholehepatic shunting of *nor*UDCA proposed by Hofmann (1), however the study had several limitations. This included the use of a high pharmacological dose of *nor*UDCA administered in the diet. Although widely used for previous studies in mice (3-5), the higher dose may obscure the contribution of saturable carrier-mediated mechanisms to the absorption, disposition and actions of *nor*UDCA. Another limitation of the study is that only the unmodified *nor*UDCA was quantified and *nor*UDCA metabolites such as the *nor*UDCA glucuronides were not measured (3, 19). However, it should be noted that whereas transport of *nor*UDCA glucuronides into bile are likely mediated by the canalicular ABC transporter MRP2 (*ABCC2*), studies in TR- rats, which encode a mutant Mrp2 gene, maintain normal levels of secretion of the side chain shorted dihydroxy bile acid *nor*-deoxycholic acid (*nor*DCA) (68). Together with our findings, these studies support the concept that much of the enterohepatic

cycling and cholecholic shunting of *nor*UDCA is passive and does not require the ASBT, OSTα-OSTβ, NTCP, OATPs or MRP2. It is still possible that canalicular transporters such as the bile salt export pump (*ABCB11*), MDR1 (*ABCB1*) or other ABC transporters are involved in the hepatocyte secretion of unmodified *nor*UDCA into bile. In that regard, the mRNA expression of Mdr1 (*Abcb1a*) and Bsep (*Abcb11*) are increased in *nor*UDCA-treated mice. In cholangiocytes, basolateral membrane export of *nor*UDCA may be facilitated by Mrp3 (*Abcc3*), whose mRNA expression is induced in *nor*UDCA-treated mice. Although Mrp3 prefers glucuronidated substrates and is not essential for ileal enterocyte absorption of conjugated bile acids (69, 70), Mrp3 is also expressed by cholangiocytes and there is evidence that unconjugated bile acids may be substrates (71).

One of the most translational findings in this study is the ability of *nor*UDCA to increase bile flow and biliary bicarbonate when co-administered with an ASBTi or bile acid sequestrant. Based on our findings with the *Asbt*$^{-/-}$ mice, it was not surprising that the choleretic actions of *nor*UDCA was unaffected by an ASBTi. However, co-administration of *nor*UDCA with a bile acid sequestrant had not been previously examined. This contrasts with UDCA, whose interactions with bile acid sequestrants has been studied *in vitro*, in animal models, and in human subjects (72-74). In those studies, cholestyramine and colestimide efficiently bound and reduced the intestinal absorption of co-administered UDCA. As such, it was surprising that co-administration of colesevelam did not attenuate the choleretic actions of *nor*UDCA. Using *in vitro* assays, colesevelam bound *nor*UDCA poorly versus conjugated bile acids, however additional studies will be required to determine if this is a general property of all bile acid sequestrants. Although both ASBT inhibition and administration of bile acid sequestrants interrupt the enterohepatic circulation of bile acids, there are important differences regarding the

mechanism of action by which they improve features of cholestasis (28, 51, 52, 75). In the present study, ASBT inhibition reduces total biliary bile acid concentrations, yet in the presence of *nor*UDCA, bile flow was still induced. These findings indicate that pharmacological ileal ASBT inhibition does not antagonize *nor*UDCA's positive effects on bile flow, and that in certain settings the two therapeutic approaches may have beneficial synergistic effects in cholestatic models. This includes the reduced biliary bile acid concentration, more hydrophilic biliary bile acid composition, and elevated biliary bicarbonate concentration observed with *nor*UDCA plus ASBT inhibition versus ASBT inhibition alone.

Collectively, our findings demonstrate that *nor*UDCA does not require the major bile acid transporters, ASBT, OSTα-OSTβ or members of the OATP1a/1b family for absorption, cholehepatic shunting to induce a bicarbonate-rich hypercholeresis. The superior hypercholeretic activity of *nor*UDCA is likely dependent upon its ability to evade hepatic amidation with taurine or glycine, and its ability to activate TMEM16A-stimulated bicarbonate-rich fluid secretion over multiple rounds of cholehepatic shunting in a transporter-independent fashion. Importantly, these results also provide support for further investigation of the therapeutic potential of a combination of *nor*UDCA and blockers of the enterohepatic circulation of bile acids in cholestatic liver disease.

Acknowledgements

We thank Shire Pharmaceutical for the research gift of the SC-435, Dr. Alan Hofmann (University of California, San Diego) for the research gift of the colesevelam, Drs. Kenneth Setchell and Wujuan Zhang (Cincinnati Children's Clinical Mass Spectrometry Laboratory) for analysis of the mouse biliary bile acid samples, Dr. Steve Kliewer (University of Texas Southwestern Medical Center) for the PXR expression and reporter plasmids, and Dr. James Fleet (Purdue University) for the VDR expression plasmids. We also thank Ashley Bennet for assistance with the bile collections and Dr. Ivo P. van de Peppel for assistance with the nuclear receptor assays. We acknowledge the Emory Pediatrics Biomarkers Core for assistance with the bile acid and glutathione measurements, Children's Healthcare of Atlanta Pathology Services for assistance processing tissues, and the Yerkes Nonhuman Primate Molecular Pathology Core for assistance with the histological analysis. Portions of this work were presented at the Annual Meeting of the American Association for the Study of Liver Disease in San Francisco, CA, 8-13 November 2018 and the XXVI International Bile Acid Meeting in Amsterdam, 9-10 July 2022, and have appeared in abstract form, Hepatology 2018; 68: 46A. This research was supported by the National Institutes of Health, National Institute of Diabetes and Digestive and Kidney Diseases grants DK047987 (P.A.D.) and DK056239 (S.J.K.), the Meredith Brown Fund at Emory (S.J.K.), and Children’s Healthcare of Atlanta and Emory University’s Pediatric Biomarkers Core. JKT was supported by T32-GM008367 and an NIH diversity supplement (DK047987-28S1). MT was supported by the Austrian Science Foundation (FWF) through projects F3517, F7310, and I2755.

Supplementary Material

Materials

*nor*UDCA (24-*nor*-5β-cholan-23-oic acid) was received as a research gift from Dr. Falk Pharma to Dr. Michael Trauner. The purity of the *nor*UDCA was confirmed by HPLC analysis. The ASBT inhibitor SC-435; (4R,5R)-5-[4-[4-(1-aza-4-azoniabicyclo[2.2.2]octan-4-yl)butoxy] phenyl]-3,3-dibutyl-7,8-dimethoxy-1,1-dioxo-4,5-dihydro-2H-1λ6-benzothiepin-4-ol) was received as a research gift from Shire Pharmaceuticals, and the ASBT inhibitory activity was confirmed using MDCK cells stably transfected with the human ASBT (IC_{50} ~18 nM). Colesevelam was provided by Dr. Alan Hofmann (University of California at San Diego) and was received as a research gift from GelTex Pharmaceuticals/Genzyme. TMEM16A inhibitor (TMEM16Ainh-A01) 2-(5-ethyl-4-hydroxy-6-methylpyrimidin-2-ylthio)-N-(4-(4-methoxyphenyl) thiazol-2-yl) acetamide was purchased from Millipore Sigma (Cat #613551).

Animals and Tissue Collection

All animal experiments were approved by the Institutional Animal Care and Use Committees at Emory University. The *Asbt*$^{-/-}$ mice (*C57BL/6NJ-Slc10a2*$^{tm1a(KOMP)Mbp}$; Asbt knockout-first, reporter-tagged insertion with conditional potential; Targeting Project CSD76540; https://www.komp.org/ProductSheet.php?cloneID=617849) were obtained from the Knockout Mouse Project (KOMP) Baylor College of Medicine Repository, and colonies of *Asbt*$^{-/-}$ and matched wild type (WT) mice generated from *Asbt*$^{+/-}$ crosses are maintained at the Emory University School of Medicine. The Asbt knockout-first mice were selected for these studies in place of the *Slc10a2*$^{tm1pda/J}$ whole body knockout mice (29) because they are in a pure C57BL/6NJ background and can be used to generate Asbt-floxed and tissue-specific null mice.

Characterization of the ileal and liver Asbt mRNA expression, fecal bile acid excretion, and bile acid pool size in male and female WT and Asbt knockout-first mice is shown in **Supporting Figure 1.** The *Ostα*$^{-/-}$*Asbt*$^{-/-}$ and background-matched WT mice were generated as described previously (26). *Ostα*$^{-/-}$*Asbt*$^{-/-}$ mice were selected for these studies in place of *Ostα*$^{-/-}$ mice because inactivation of the Asbt protects *Ostα*$^{-/-}$ mice from ileal injury and prevents/attenuates the associated adaptive changes including lengthening of the small intestine, ileal hypertrophy, villous blunting, increased numbers of mucin-producing cells, and increased cell proliferation (26). These adaptive changes were predicted to complicate interpretation of the findings with regards to the role of Ostα-Ostβ transport activity in the intestinal absorption and the choleretic actions of *nor*UDCA. Male Oatp1a/1b gene cluster knockout mice (*Oatp1a/1b*$^{-/-}$) (FVB.129P2-Del(Slco1b2-Slco1a5)1Ahs) and background-matched WT mice were purchased from Taconic Biosciences. For the ASBTi and colesevelam studies, WT male mice (C57BL/6J) were obtained from Jackson Labs. The mice were group-housed in ventilated cages (Super Mouse 750 Microisolator System; Lab Products) containing bedding (1/8" Bed-O-Cobbs; Andersons Lab Bedding Products) at temperature (22ºC) in the same 12h/12h light/dark cycle-controlled room of animal facility to minimize environmental differences and fed ad libitum rodent chow (13% of calories as fat; PicoLab Rodent Diet 20; LabDiet).

Animal Treatment and Bile Flow Measurements

All *nor*UDCA experiments were performed using male mice, 3 months of age (approximately 25-30 g body weight). The indicated genotypes were fed rodent chow (Envigo; Teklad custom Diet No. TD.160819; global 18% protein rodent diet) for 7 days. For the next 7 days, the mice were fed TD.160819 rodent chow or TD.160819 rodent chow containing the indicated

combinations of 0.5% (w/w) *nor*UDCA, 0.006% (w/w) ASBTi (SC-435; dose ~11 mg/kg/day), or 2% (w/w) colesevelam. The amount of *nor*UDCA, ASBTi, and colesevelam administered was selected based on published studies demonstrating these doses are sufficient to induce bile flow (*nor*UDCA) or disrupt the enterohepatic circulation of bile acids (ASBTi, colesevelam) (5, 27, 28). Based on an estimate of 3 g of diet consumed per day per 25 g body weight, the dose of *nor*UDCA administered is approximately 15 mg per 25 g mouse per day (600 mg/kg/day). At the end of the 7-day treatment period, bile flow in the mice was measured as previously described (3). Briefly, non-fasted mice were anesthetized using an isoflurane/O_2 mixture, placed on a 37°C heating pad and maintained under isoflurane anesthesia during the procedure. Following laparotomy, the common bile duct was ligated, and gallbladder was cannulated. Residual gallbladder bile and hepatic bile secreted during the first 10 minutes of the collection period was discarded. Bile was then collected under a layer of mineral oil in pre-weighed tubes on ice for 120 minutes. Bile flow was determined gravimetrically and normalized to liver weight.

At the end of the bile collection period, blood was obtained by cardiac puncture to measure plasma chemistries. Liver wet weight was recorded at the time of necropsy. Portions of the liver were flash-frozen in liquid nitrogen and stored at -80º C for analysis of gene expression or fixed in 10% neutral formalin (Sigma-Aldrich) for embedding in paraffin and histological analysis. Small intestine was divided into 5 equal length segments and flushed with ice-cold phosphate-buffered saline (PBS) to remove luminal contents before weighing and flash-freezing in liquid nitrogen.

Plasma Biochemistries and Biliary Solute Measurements

Plasma chemistries, including total protein, albumin, alkaline phosphatase, alanine aminotransferase, aspartate aminotransferase, gamma-glutamyl transpeptidase, total bilirubin and cholesterol were measured at the Emory University Department of Animal Resources Quality Assurance and Diagnostic Laboratory. Immediately after isolation, the bile samples were used for determination of HCO_3^-, pH, total CO_2, Na^+, K^+, Cl^-, and glucose using a blood gas analyzer (i-STAT; Abbott Point of Care Inc) in the Clinical Pathology Laboratory, Emory University-Yerkes National Primate Research Center. Biliary glutathione concentrations were measured by HPLC in the Emory University Pediatrics Biomarkers Core Facility as described previously (76). Biliary bile acid and cholesterol concentrations were measured enzymatically as previously described (29, 30). In order to quantify biliary phospholipids, bile samples underwent chloroform-methanol extraction, followed by digestion with perchloric acid, and enzymatic assay to measure inorganic phosphate at the Wake Forest School of Medicine Lipid, Lipoprotein and Atherosclerosis Analysis Laboratory.

Histological Analysis

The liver tissue samples were fixed in 10% neutral formalin (Sigma-Aldrich) for 12 h and then stored in 70% (v/v) ethanol until processed for histology. Samples were embedded in paraffin and processed by Children's Healthcare of Atlanta Pathology Services. Histologic sections (5 μm) were cut and stained with H&E. The liver histology was assessed in a blinded fashion by a certified veterinary pathologist (S.G.). Representative micrographs were collected using the Emory University Integrated Cellular Imaging Core.

Bile Acid Measurements

In order to characterize bile acid metabolism in the Asbt knockout-first mice, feces were collected from single-housed adult male and female mice over a 72-hour period. The total fecal bile acid content was measured by enzymatic assay (29, 31). Non-fasted mice were sacrificed, and small intestine plus luminal contents, liver, and gallbladder were removed *en bloc* to measure the bile acid pool size. Total bile acids were extracted in ethanol (32), measured by enzymatic assay, and analyzed by HPLC as described (33). Individual bile acid species were identified using an evaporative light scatter detector (Alltech ELSD 800). Bile acids were quantified by comparison to known amounts of authentic standards purchased from Steraloids (Newport, RI). Quantitative analysis of the biliary bile acids from chow or *nor*UDCA-fed mice was carried out at the Clinical Mass Spectrometry Laboratory at Cincinnati Children's Hospital Medical Center. Briefly, biliary bile acids were extracted on a reverse-phase/solid-phase cartridge and analyzed using a Waters Quattro Premier XE triple quadruple mass spectrometer interfaced with Aquity UPLC system. Quantification of bile acids was based on a validated isotope dilution mass spectrometry method (34). Calibration curves were built with 20 of the mouse bile acids using the single ion recording (SIR) function on the mass spectrometer (LLOQ = 5 ng/ml; ULOQ = 1000 ng/ml). The bile acid Hydrophobic index was calculated according to Heuman using a value of -0.68 for the *nor*UDCA anion (77, 78).

For the *nor*UDCA feeding studies, fecal samples were collected from cages of group-housed mice with standard bedding at the end of the 7-day chow or *nor*UDCA feeding period. The fecal bile acid composition was determined using a Hewlett-Packard Agilent gas chromatography-mass spectrometer (GC/MS) in the Department of Pediatrics Biomarkers Core Facility at Emory University. Briefly, 50 mg of crushed dried feces mixed with 10 nmol of internal standard, 5β-Cholanic acid 7α, 12α-diol (Steraloids), resuspended in 75% methanol plus

250 mM NaOH and heated at 80°C for 2 h. After centrifugation, the bile acids were extracted on a reverse-phase/solid-phase cartridge (C-18 columns; Supelco) and dried down under nitrogen. The bile acids were then methylated by resuspension in acetyl-chloride (Sigma-Aldrich)/methanol (1:20; v:v) and heating at 55ºC for 20 min. For derivatization, the samples were dried under nitrogen, resuspended in N,O-Bis(trimethylsilyl)trifluoroacetamide (Sigma-Aldrich)/ pyridine (Sigma-Aldrich)/ chlorotrimethyl-silane (Sigma-Aldrich) (5:5:0.1; v:v:v), and incubated for 1 h at room temperature. The derivatized bile acids were then dried at room temperature and resuspended in heptane for GC/MS analysis and compared to authentic standards for *nor*UDCA, UDCA, CDCA, LCA, DCA, CA, αMCA, βMCA, and ωMCA (35).

RNA-Seq Analysis

Total RNA was extracted from frozen liver tissue using TRIzol reagent (Invitrogen, Carlsbad, CA). RNA-Seq libraries were prepared by Novogene Co., Ltd and sequenced on an Illumina HiSeq1000 system. The original data obtained from the high throughput sequencing platforms were transformed to sequenced reads by base calling. Raw data are recorded in a FASTQ file which contains sequenced reads and corresponding sequencing quality information. Sequences were aligned to the mouse genome using STAR (79). The number of reads that mapped to each gene was used to quantify RNA expression, which is indicated as fragments per kilobase or transcript sequence per million base pairs sequenced (80). Differential expression analysis was performed using the DESeq2 R package of Bioconductor (36). The resulting *P* values were adjusted using the Benjamini-Hochberg procedure to control for the false discovery rate (37). Differentially expressed genes with a fold change > 1.0 and adjusted $P < 0.05$ were selected for functional annotation (GEO series accession number: GSE145020). Pathway analysis of the

RNA-Seq data was performed using MetaCore (GeneGo Inc, Saint Joseph, MN) with a threshold fold change of 2 and *P*-value of 0.05 to indicate a statistically significant difference.

Measurement of Cl^- currents

Membrane currents were measured by whole-cell patch clamp techniques using mouse large cholangiocytes (MLC) (38, 81), which were obtained from Drs. Gianfranco Alpini and Shannon Glaser. To generate the MLCs, cholangiocytes were isolated from normal mice (BALB/c) and immortalized by transfection with the SV40 large-T antigen gene as described (38). MLC demonstrate properties similar to those of freshly isolated large mouse cholangiocytes and functionally express TMEM16A (18). Coverslips with MLC cells were mounted in the recording chamber and perfused with a standard extracellular solution containing: 140 mM NaCl, 4 mM KCl, 1 mM $CaCl_2$, 2 mM $MgCl_2$, 1 mM KH_2PO4, 10 mM D-glucose, and 10 mM HEPES/NaOH (pH 7.4). The patch clamp studies were conducted in the standard whole-cell configuration at room temperature using an Axopatch 200B amplifier (Axon instruments). The patch pipettes were pulled from Warner instrument glass (Model G120F-3) and had a resistance of 4–5 MΩ after filling with the standard intracellular solution containing: 130 mM KCl, 10 mM NaCl, 2 mM $MgCl_2$, 10 mM HEPES/KOH, 0.5 mM $CaCl_2$, and 1 mM EGTA (pH 7.3), corresponding to a free $[Ca^{2+}]_i$ of ~100 nM. The free $[Ca^{2+}]_i$ was calculated using software kindly provided by Guy Droogmans (KU Leuven). Recordings were filtered at 1 kHz and sampled at 10 kHz for storage on a computer and analyzed using pCLAMP 11.0.3 software (Molecular Devices). Results are compared with control studies measured on the same day to minimize any effects of day-to-day variability and reported as current density (pA/pF) to normalize for differences in cell size (18, 82).

TMEM16A silencing

TMEM16A siRNA (TMEM16A-HSS123904) was used to inhibit TMEM16A expression in whole-cell patch clamp experiments. The following sequences of 25-nucleotide long siRNAs were designed and synthesized by Ambion (ThermoFisher Scientific, Cat# 4390827) and transfected in MLCs using Lipofetamine 3000, antisense: UUCUAUAGAUGAUAACUCCdGdA and sense: GGAGUUAUCAUCUAUAGAAdTdT. Negative control from OriGene (SR 30004) was used in control transfections. Block-it TM Fluorescent Oligo (Catalog #2013, Invitrogen) was used to optimize transfection conditions and select transfected cells for whole-cell patch clamp current recording. Experiments were performed 48-72 hours after transfection and the degree of TMEM16A silencing was evaluated by Western Blot analysis. Briefly, protein was extracted from MLCs with RIPA buffer containing protease inhibitors (Roche). Following protein normalization (ThermoFisher, #23223) 25 μg of protein per lane was separated on a 4%–15% gels (Bio-Rad) and transferred to a PVDF membrane (Bio-Rad) at 70V for 90 minutes. Membranes were blocked in 5% nonfat dry milk before probing with anti-mouse TMEM16A antibody (1:1000, Alomone Laboratories, ACL-011) overnight at 4°C. The following day, the membrane was incubated for 1 hour at room temperature in HRP-conjugated secondary antibody Rabbit IgG (1:10,000, Jackson Immuno Research Laboratories, 111-035-144). Signal was visualized using Amersham ECL Western Blotting Detection Kit (GE Healthcare, #RPN2209).

Luciferase Assay

Human liver cells (Huh7) were seeded in a 24-well plate at 1 X 10^5 cells/well in monolayers and cultured at 37°C and 5% CO_2 in modified Eagle's minimal essential medium (EMEM)

supplemented with 10% fetal bovine serum (FBS) and 1% penicillin-streptomycin. The following day, cells at ~85% confluency were transfected using Lipofectamine3000 (Invitrogen) to introduce a control renilla expression plasmid (0.005 μg), where the renilla luciferase gene is driven by a constitutively active promoter from the HSV thymidine kinase gene to monitor transfection efficiency, along with the following plasmid combinations: 1) a chimeric nuclear receptor encoding the ligand binding domain of mouse PXR fused to the DNA binding domain of GAL4 (pGAL4-mPXR-LBD, 0.25 μg) and a 5x Upstream Activation Sequence (UAS)-luciferase reporter (pFR-Luc, 0.025 μg), 2) expression plasmids for human FXR (0.025 μg), RXRα (0.025 μg), and an FXR-responsive luciferase reporter (pECRE-Luc, 0.25 μg), or 3) expression plasmids for human VDR (0.025 μg), RXRα (0.025 μg), and a VDR-responsive luciferase reporter (hCYP24-luc, 0.25 μg). The next day, triplicate wells were incubated in charcoal stripped 10% FBS-containing medium plus vehicle (DMSO), different concentrations of positive control (pregnenolone 16α-carbonitrile, a mouse PXR ligand; GW4064, a synthetic FXR ligand, or 25-hydroxy-vitamin D, a vitamin D receptor ligand), or different concentrations of *nor*UDCA. After a 24 hour treatment, cells were washed in 1X PBS, harvested and processed using Luciferase assay reagents (Dual-Luciferase Reporter Assay System) from Promega. The bioluminescence was monitored using a luminometer (Synergy HTX, Biotek). The results were normalized to TK-renilla activity and presented as relative fold change over the DMSO vehicle group.

In vitro Colesevelam Bile Acid Binding Assay

Bile acid binding to colesevelam was carried out as described (40). Briefly, bile acids were dissolved in simulated intestinal fluid (50 mM KH_2PO_4, 22.4 mM NaOH, pH 6.8) at a

concentration of 2 mM for TDCA or 6 mM for GCDA and norUDCA, and pre-incubated for 30 min on a rotator at 37°C prior to addition to 7.5 mg of colesevelam hydrochloride. Samples were withdrawn at 0, 0.5, 1, 2, 3, 4 and 5 h, filtered through a 0.2 μm syringe filter, and the filtrate was analyzed by enzymatic assay to determine the free bile acid concentration. The difference between the initial (0 h) and free bile acid concentrations was used to calculate the amount of the bile acid bound per mg of colesevelam hydrochloride.

Statistics

For the box and whisker plots, median values (line), interquartile range (boxes), and min to max values (whiskers) are shown. For the liver BA composition analysis and gene expression, mean value ± SD is shown. The data were evaluated for statistically significant differences using the Mann-Whitney test, the two-tailed Student's t test, ANOVA (with a Tukey-Kramer honestly significant difference post-hoc test) or Sidak's multiple comparisons test (GraphPad Prism; Mountain View, CA). Values with different superscript letters are significantly different ($P < 0.05$).

Study approval.

All animal experiments were approved by the Emory University Institutional Animal Care and Use Committee in accordance with NIH guidelines for the ethical treatment of animals.

Supplemental Table S1. Physical and Permeability Properties of UDCA versus *nor*UDCA

	UDCA	***nor*UDCA**
Formula	C24H40O4	C23H38O4
Molecular Weight	392.56[1]	378.553[1]
xLogP3	4.9[1]	4.6[1]
Hydrogen Bond Donor	3[1]	3[1]
Hydrogen Bond Acceptor	4[1]	4[1]
Critical Micelle Concentration (mM)	7[2]	17[3]
Apparent Permeability (x 10^4) (cm/sec in perfused rat jejunum)	0.67[4]	0.64[4]

1. Values computed by PubChem, XLogP3 3.0, Cactvs 3.4.6.11.

2. Hofmann A and Roda A, Hepatology 1984: 25: 1477-1489.

3. Roda A, Hofmann AF, Mysels KJ. J Biol Chem 1983; 258: 6362-6370.

4. Dupas J-L et al, Lipids 2018; 53: 465-468.

Supplemental Table S2. Plasma Chemistries in Chow and *nor*UDCA Diet-fed Wild Type and *Asbt*$^{-/-}$ Mice

Variable	WT (n)		*Asbt*$^{-/-}$ (n)	
	Chow (6)	***nor*UDCA (7)**	**Chow (7)**	***nor*UDCA (7)**
Albumin (g/dL)	1.8 ± 0.8[a]	3.1 ± 0.5[a,b]	2.6 ± 0.5[b]	2.9 ± 0.4[b]
Alkaline phosphatase (U/L)	38 ± 12	37 ± 14	33 ± 12	45 ± 5
Alanine aminotransferase (U/L)	85 ± 59	61 ± 27	120 ± 49	95 ± 39
Aspartate aminotransferase (U/L)	116 ± 67[a,b]	99 ± 28[a]	199 ± 70[b]	146 ± 48[a,b]
Cholesterol (mg/dL)	95 ± 27[a]	151 ± 30[a,b]	109 ± 18[b]	148 ± 41[b]
Gamma-glutamyl transpeptidase (U/L)	9.6 ± 4.6[a]	15.4 ± 4.9[a,b]	15.4 ± 2.8[a,b]	17.1 ± 3.8[b]
Total bilirubin (mg/dL)	3.0 ± 1.3[a,b]	2.6 ± 0.9[a]	3.6 ± 0.6[b]	2.8 ± 0.7[a,b]
Total protein (g/dL)	3.6 ± 0.6	4.6 ± 0.9	3.6 ± 0.9	4.6 ± 0.5

Values are expressed as the mean ± SD. The number of mice per group are indicated (n). Values with different superscript letters are significantly different ($P < 0.05$) by ordinary two-way ANOVA and Sidak's multiple comparisons test.

Supplemental Table S3. Plasma Chemistries in Wild Type Mice after co-administration of *nor*UDCA with an ASBTi or Colesevelam

Variable	Control	ASBTi	Colesevelam	*nor*UDCA	*nor*UDCA ASBTi	*nor*UDCA Colesevelam
Albumin (g/dL)	3.3 ± 0.2	3.0 ± 0.2	3.1 ± 0.2	3.4 ± 0.2	3.0 ± 0.7	3.5 ± 0.2
ALP (U/L)	6.4 ± 6.1	1.6 ± 2.2	8.8 ± 7.2	6.4 ± 5.4	4.0 ± 2.8	6.4 ± 4.6
ALT (U/L)	96 ± 27	96 ± 27	118 ± 46	74 ± 23	143 ± 96	97 ± 53
AST (U/L)	176 ± 60	170 ± 46	247 ± 145	90 ± 25	193 ± 141	115 ± 33
CHOL (mg/dL)	123 ± 13[a]	125 ± 10[a]	110 ± 9[a]	171 ± 14[b]	130 ± 44[a,b]	148 ± 10[a,b]
GGT (U/L)	19.2 ± 4.4	16.8 ± 3.3	14.4 ± 3.6	18.4 ± 6.1	15.2 ± 3.3	16.8 ± 3.3
TBILI (mg/dL)	2.6 ± 0.3[a]	3.4 ± 0.4[a]	2.6 ± 0.5[a]	2.0 ± 0.4[b]	3.1 ± 1.0[a]	1.9 ± 0.4[b]
TP (g/dL)	4.8 ± 0.3	4.3 ± 0.3	4.7 ± 0.4	5.1 ± 0.4	4.4 ± 1.2	5.4 ± 0.4

Values are expressed as the mean ± SD (n = 5 mice per group). Values with different superscript letters are significantly different ($P < 0.05$) by ordinary two-way ANOVA and Sidak's multiple comparisons test. ALP, alkaline phosphatase; ALT, alanine aminotransferase; AST, aspartate aminotransferase; CHOL, cholesterol; GGT, gamma-glutamyl transpeptidase; TBILI, total bilirubin; TP, total protein.

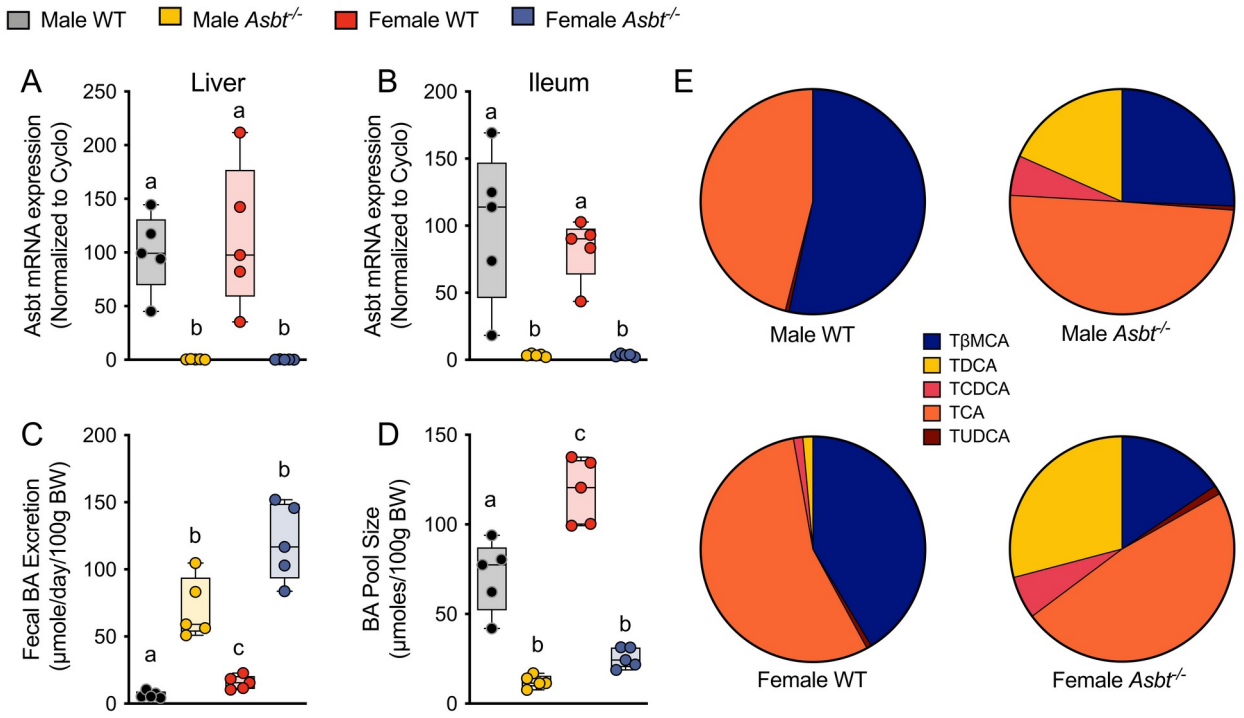

Supplemental Figure S1. Asbt expression, bile acid excretion, bile acid pool size, and pool composition in wild type and Asbt knockout-first (*Asbt*$^{-/-}$) mice.

(**A**) Asbt mRNA levels in liver and (**B**) ileum of male and female WT and *Asbt*$^{-/-}$ mice. RNA was isolated from individual mice and used for real-time PCR analysis. The mRNA expression was normalized to cyclophilin and are shown relative to male WT mice (set at 100%) for each tissue. (**C**) Fecal bile acid excretion in male and female WT and *Asbt*$^{-/-}$ mice. The data are expressed as µmoles/per day per 100 g body weight. (**D**) Bile acid pool size in in male and female WT and *Asbt*$^{-/-}$ mice. The data are expressed as µmoles per 100 g body weight. (A) through (D) Median values (line), interquartile range (boxes), and min to max values (whiskers) are shown (n = 5 mice per group). Values with different superscript letters are significantly different ($P < 0.05$). (**E**) Bile acid pool composition in male and female WT and *Asbt*$^{-/-}$ mice. Pie charts show the mean values (n =5) for the percent compositions of the indicated bile acids. All mice were 3 months of age.

Asbt mRNA expression is reduced to background levels in liver and ileum of *Asbt*$^{-/-}$ mice. Fecal bile acid excretion was increased by approximately 8 to 10-fold in male and female *Asbt*$^{-/-}$ versus WT mice. The increased fecal bile acid excretion was associated with approximately 80 percent reductions in the bile acid pool size of male and female *Asbt*$^{-/-}$ mice. Analysis of the bile acid pool composition by HPLC revealed a large reduction in the proportion of 6-hydroxylated bile acid species and concomitant increase in the proportion of taurocholic acid and its gut microbiota-derived product taurodeoxycholic acid. These changes in fecal bile acid excretion, bile acid pool size and composition in the C57BL/6NJ Asbt knockout-first mice recapitulates the major bile acid phenotype of the previously characterized Asbt knockout mouse model (29). BA, bile acid; BW, body weight; TβMCA, tauro-beta-muricholic acid; TCA, taurocholic acid; TCDCA, taurochenodeoxycholic acid; TDCA, taurodeoxycholic acid; TUDCA, tauroursodeoxycholic acid; WT, wild type.

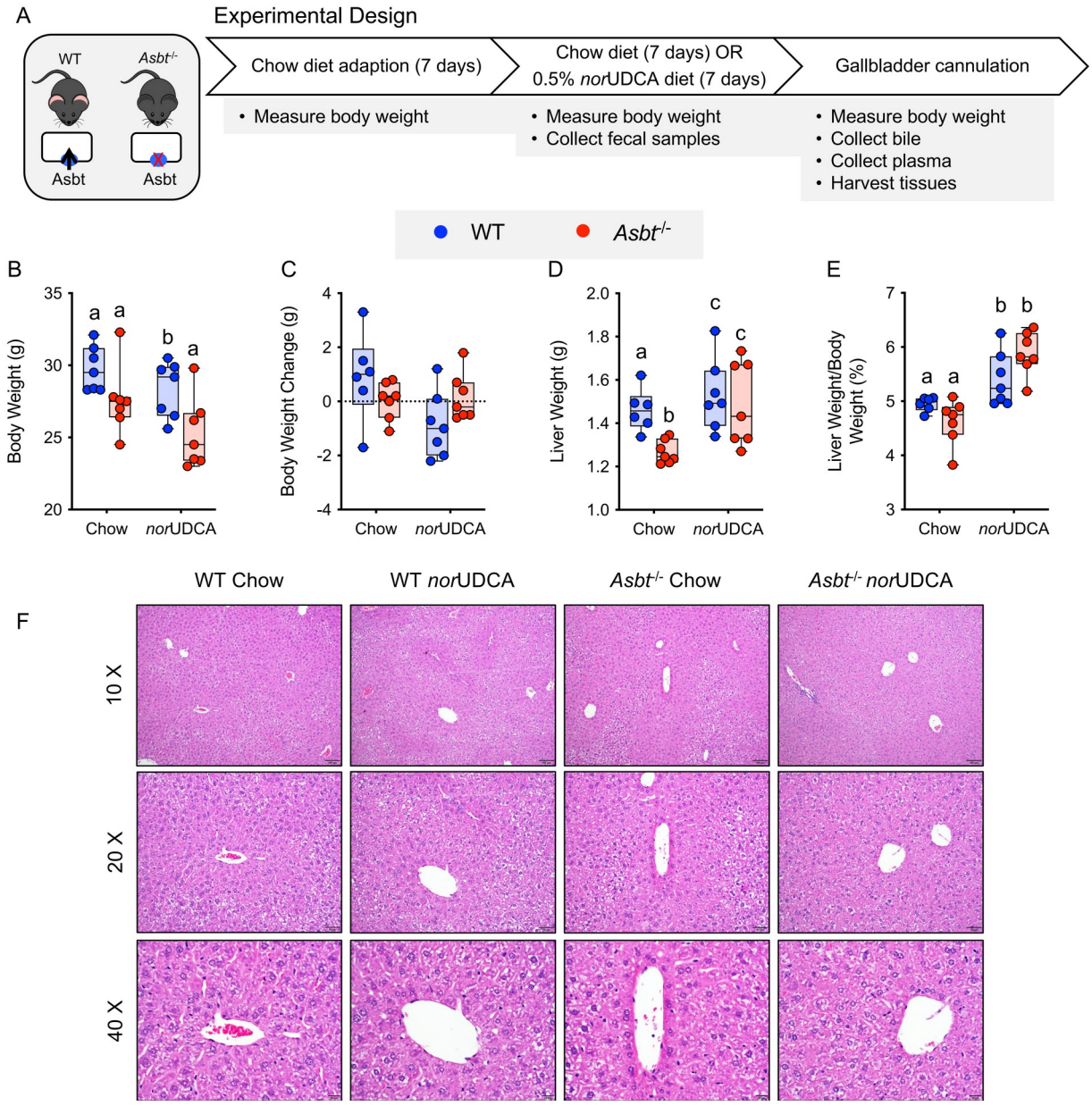

Supplemental Figure S2. Experimental scheme and morphological response to *nor*UDCA treatment in WT and *Asbt*$^{-/-}$ mice.

(**A**) Experimental design. (**B**) Body weight after 7-days of feeding chow or chow plus 0.5% *nor*UDCA. (**C**) Body weight change after 7-days of feeding chow or chow plus 0.5% *nor*UDCA. (**D**) Liver weight. (**E**) Liver to body weight ratio. Median values (line), interquartile range

(boxes), and min to max values (whiskers) are shown, n = 6-7 mice per group. Distinct lowercase letters indicate significant differences between groups ($P < 0.05$). (**F**) Hematoxylin and eosin-stained liver sections (original magnification 10X, 20X, and 40X) from the indicated genotypes and treatments groups. *Scale bars*, 200 μm, 100 μm, 50 μm at 10X, 20X, and 40X, respectively).

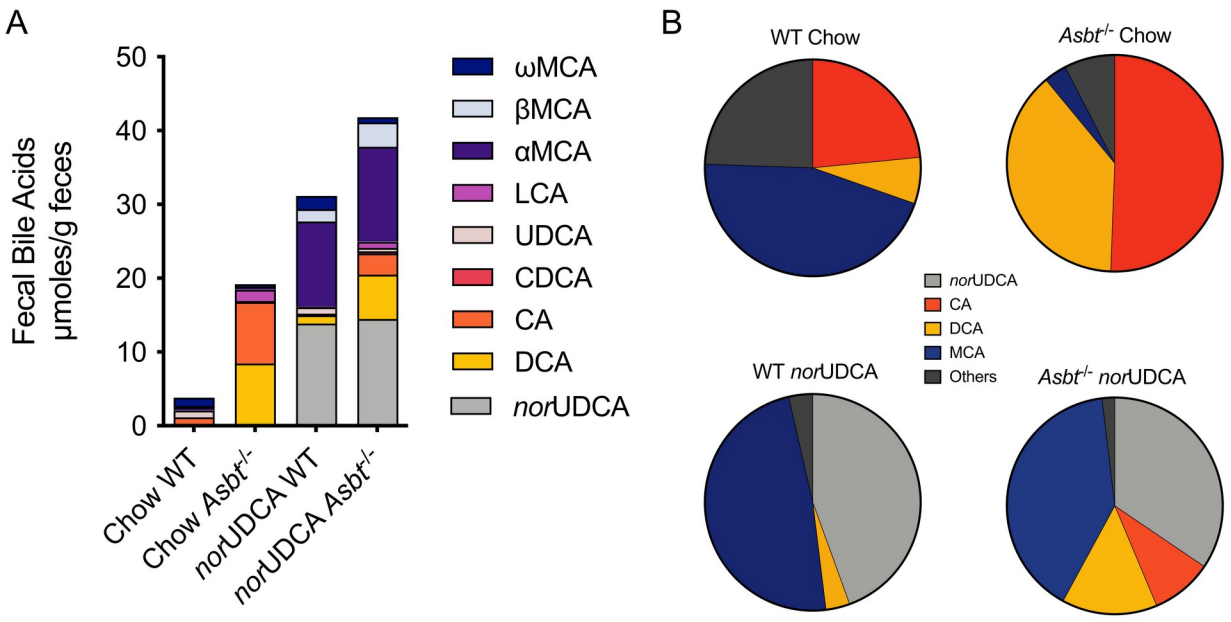

Supplemental Figure S3. Effect of *nor*UDCA treatment on the fecal bile acid profile in WT and *Asbt*$^{-/-}$ mice.

(**A**) *nor*UDCA treatment increased the excretion of endogenous bile acids and the amount of 6-hydroxylated bile acids in feces. (**B**) Pie charts for the fecal bile acid profiles. Mean values are shown for fecal samples collected from cages of group-housed mice (n = 6-7 mice per genotype and treatment condition).

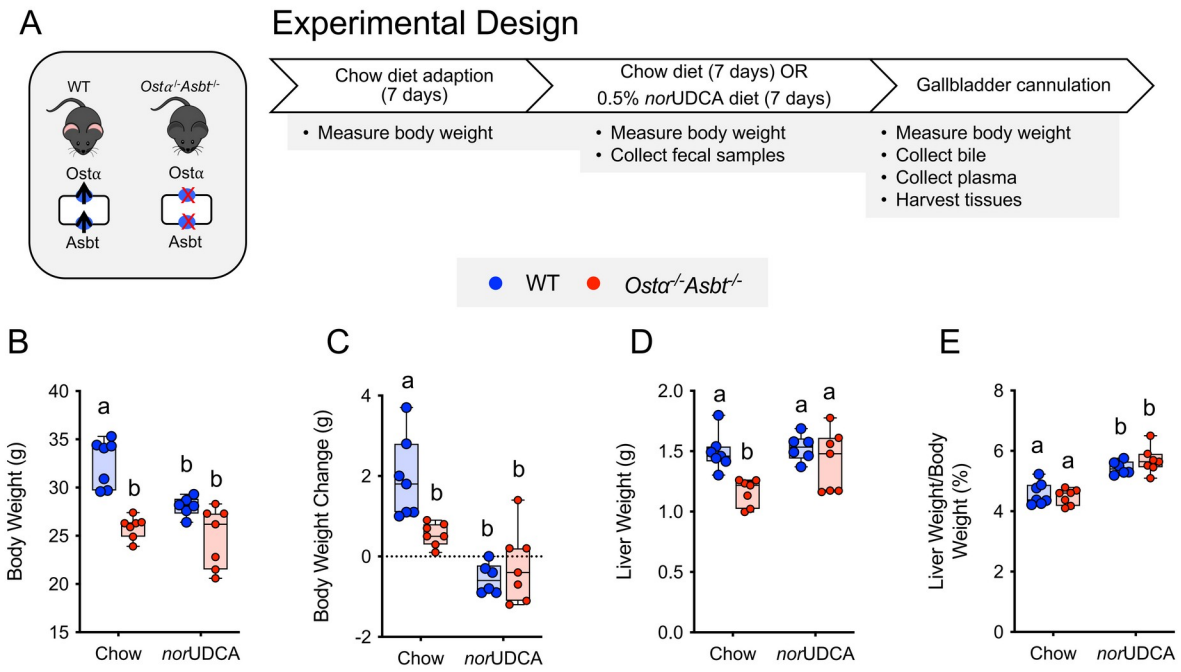

Supplemental Figure S4. Experimental scheme and morphological response to *nor*UDCA treatment in WT and *Ostα*$^{-/-}$*Asbt*$^{-/-}$ mice.

(**A**) Experimental design. (**B**) Body weight after 7-days of feeding chow or chow plus 0.5% *nor*UDCA. (**C**) Body weight change after 7-days of feeding chow or chow plus 0.5% *nor*UDCA. (**D**) Liver weight. (**E**) Liver to body weight ratio. Median values (line), interquartile range (boxes), and min to max values (whiskers) are shown, n = 5-7 mice per group. Distinct lowercase letters indicate significant differences between groups ($P < 0.05$).

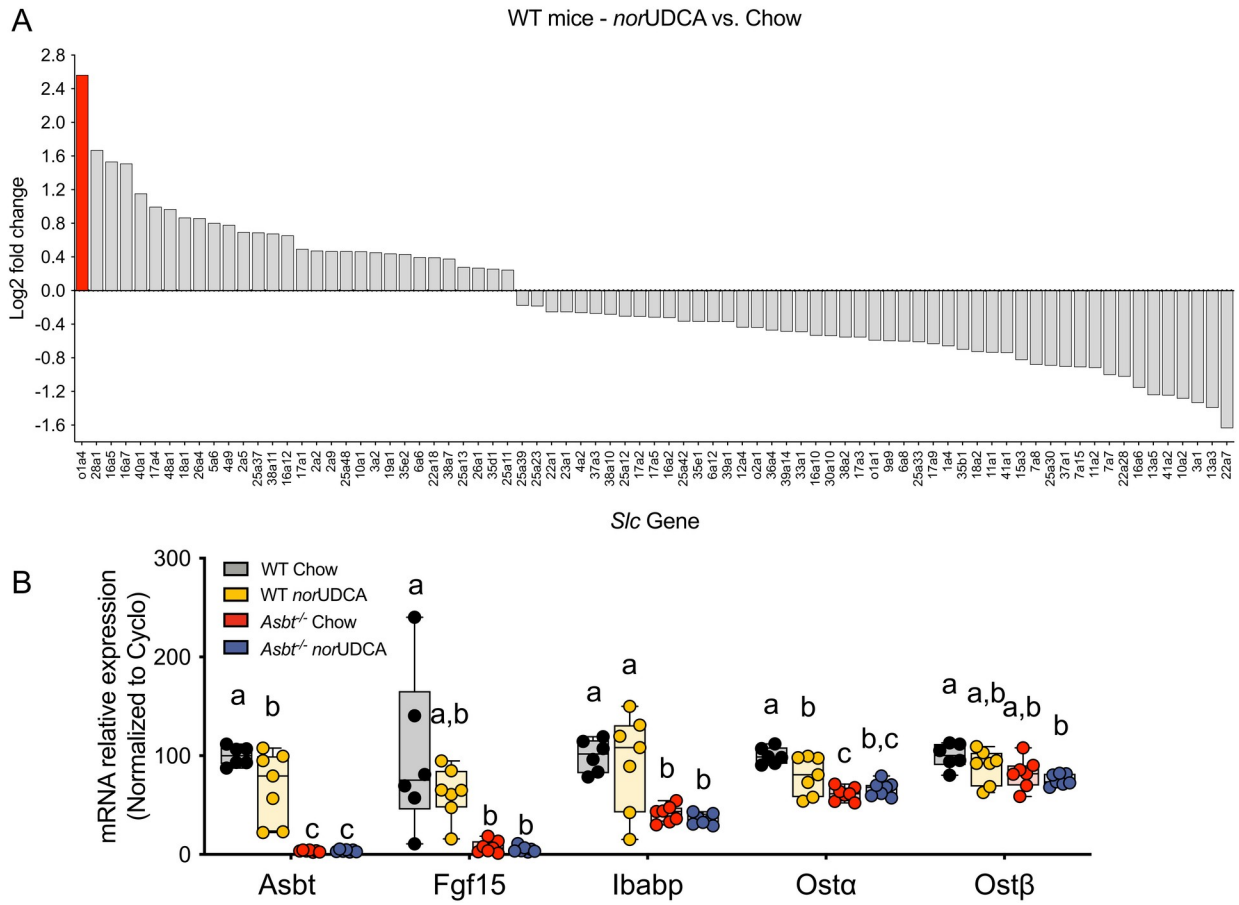

Supplemental Figure S5. Effect of *nor*UDCA treatment on hepatic and ileal gene expression.

(**A**) RNA-Seq analysis of livers from WT mice fed chow or the *nor*UDCA-containing diet. Differentially expressed *SLC* membrane transporter genes ($P < 0.05$; n = 6 per group) in the *nor*UDCA-treated versus chow mice are shown. (**B**) Ileal expression of the indicated bile acid-related genes in WT and *Asbt*$^{-/-}$ mice fed chow or the *nor*UDCA-containing diet for 7 days. RNA was isolated from ileum of individual mice and used for real-time PCR analysis. The mRNA expression was normalized using cyclophilin and the results for each gene are expressed relative to chow-fed WT mice. Median values (line), interquartile range (boxes), and min to max values

(whiskers) are shown, n = 6-7 mice per group. Distinct lowercase letters indicate significant differences between groups ($P < 0.05$).

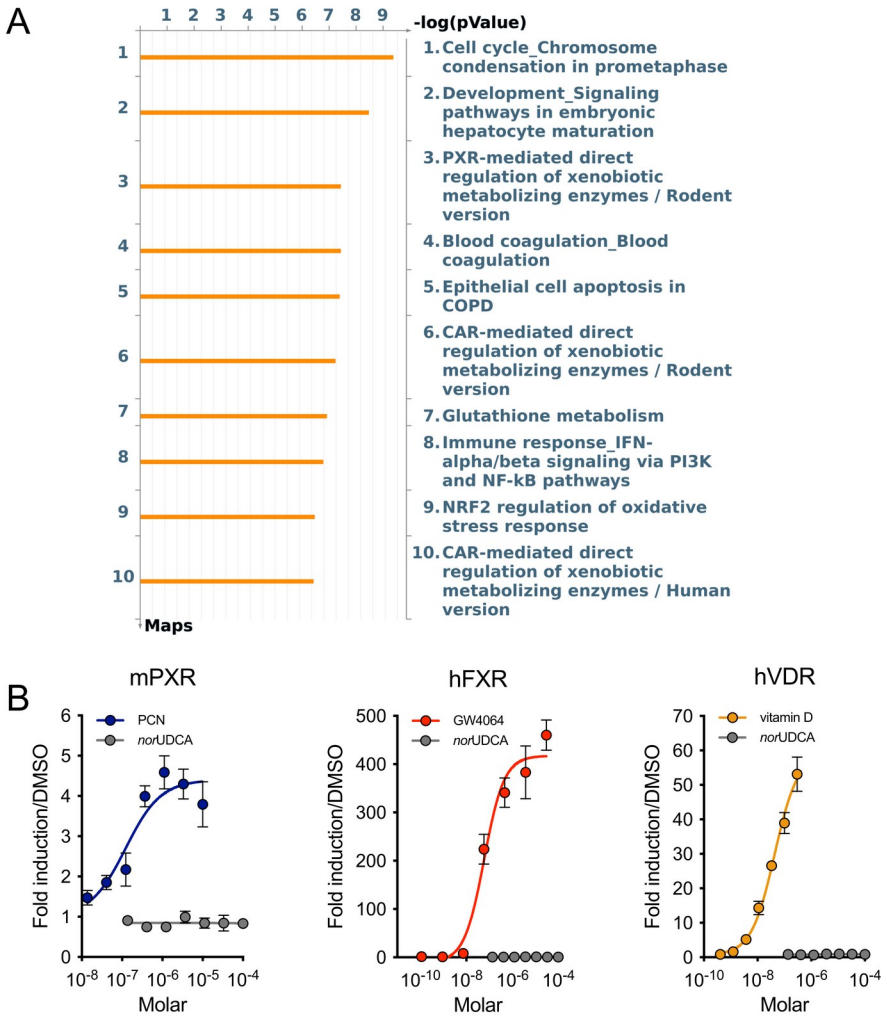

Supplemental Figure S6. Candidate pathways regulated in mouse liver by norUDCA.

(**A**) Pathway analysis of liver gene expression changes in *nor*UDCA treated versus chow-fed mice using a threshold fold change of 2 and *P* value of 0.05. The top 10 pathways and -log(pValue) are shown. (**B**) *nor*UDCA does not directly activate mouse PXR, human FXR or human VDR in transfected Huh7 cells. Huh7 cells were transfected with the indicated nuclear receptor expression and reporter plasmid combinations. One day following transfection, the cells were treated with the indicated concentrations of positive control ligand or *nor*UDCA for 24 h

prior to luciferase activity measurement. The results were normalized to TK-renilla activity and presented as relative fold change versus vehicle (DMSO). Mean values + SD are shown.

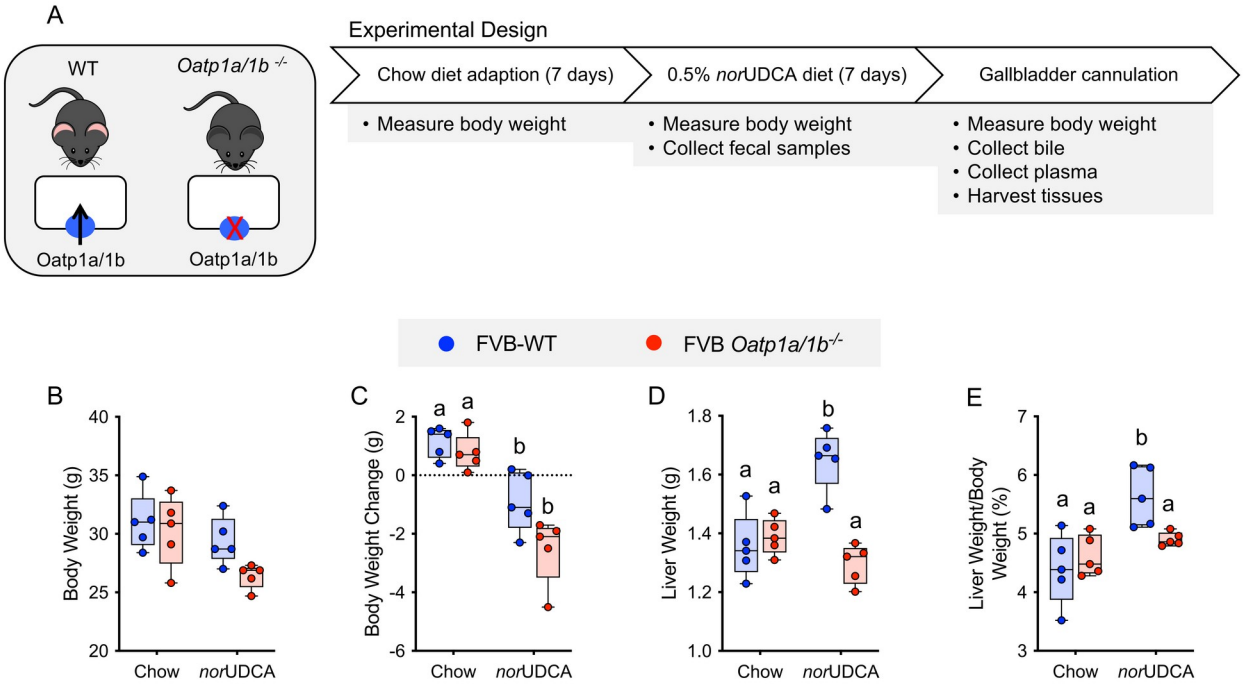

Supplemental Figure S7. Experimental scheme and morphological response to *nor*UDCA treatment in WT and *Oatp1a/1b*$^{-/-}$ mice.

(**A**) Experimental design. (**B**) Body weight. (**C**) Body weight change. (**D**) Liver weight. (**E**) Liver to body weight ratio. Median values (line), interquartile range (boxes), and min to max values (whiskers) are shown, n = 5 mice per group. Distinct lowercase letters indicate significant differences between groups ($P < 0.05$).

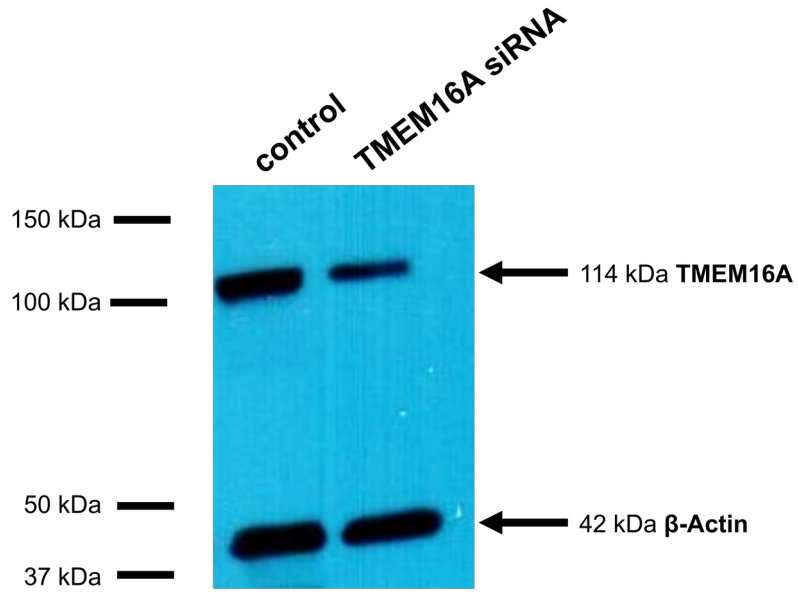

Supplemental Figure S8. Knockdown of TMEM16A expression in Mouse Large Cholangiocytes (MLCs) used for *nor*UDCA treatment and patch clamping studies. Representative western blot demonstrating reduction in TMEM16A protein levels in MLCs following transfection with TMEM16A siRNA as compared to transfection with a nontargeting siRNA (control). Western blotting for β−actin was used as loading control.

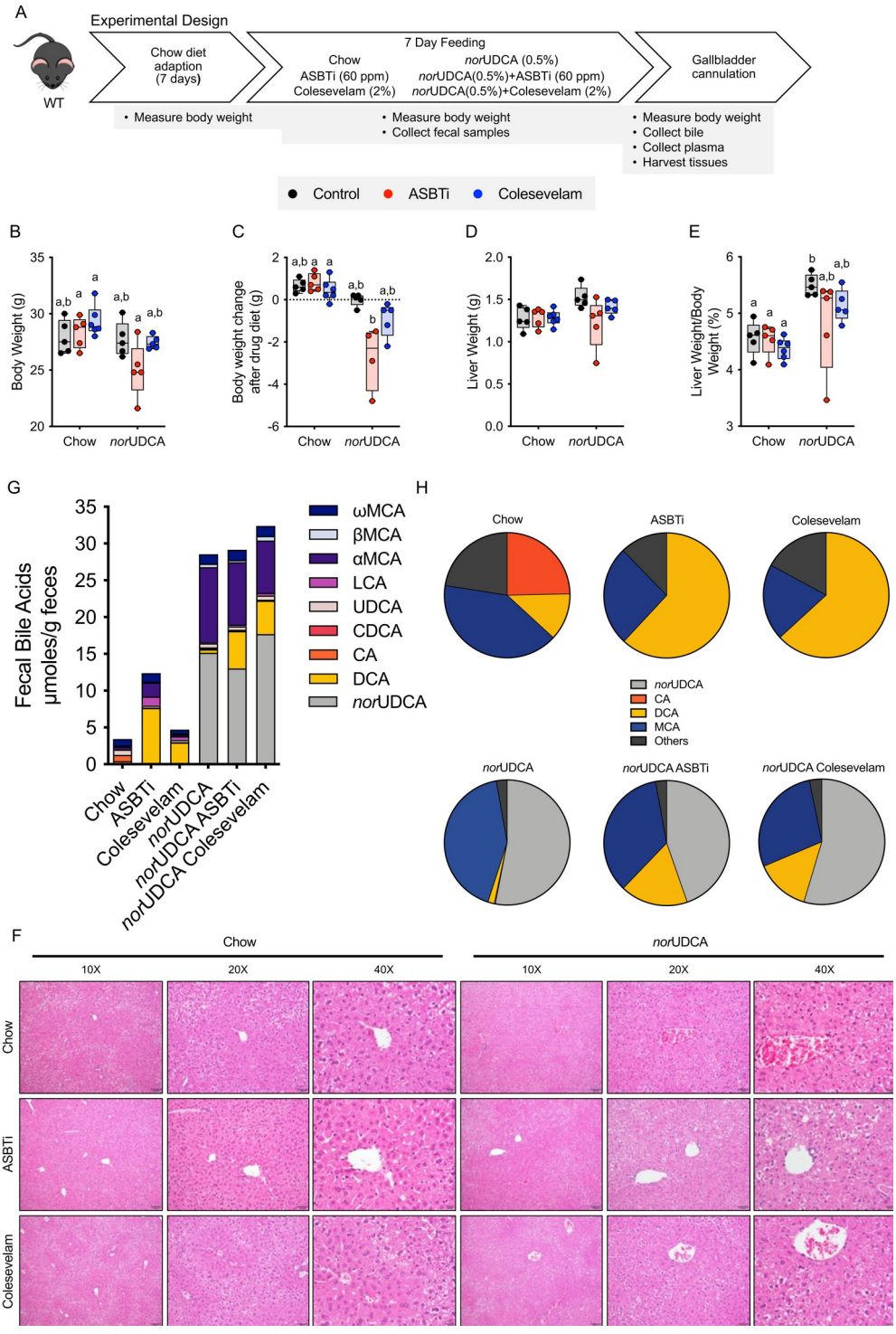

Supplemental Figure S9. Experimental scheme and morphological response of WT mice to co-administration of *nor*UDCA with an ASBT inhibitor or Colesevelam.

(**A**) Experimental design. (**B**) Body weight. (**C**) Body weight change. (**D**) Liver weight. (**E**) Liver to body weight ratio. Median values (line), interquartile range (boxes), and min to max values (whiskers) are shown, n = 5 mice per group. Distinct lowercase letters indicate significant differences between groups ($P < 0.05$). (**F**) Hematoxylin and eosin-stained liver sections (original magnification 10X, 20X, or 40X) from the indicated treatments groups. *Scale bars*, 200 μm, 100 μm, 50 μm at 10X, 20X, and 40X, respectively). (**G**) *nor*UDCA treatment increased the excretion of endogenous bile acids and the amount of 6-hydroxylated bile acids in feces. (**H**) Pie charts for the fecal bile acid profiles. Mean values are shown for fecal samples collected from cages of group-housed mice (n = 5 mice per treatment condition).

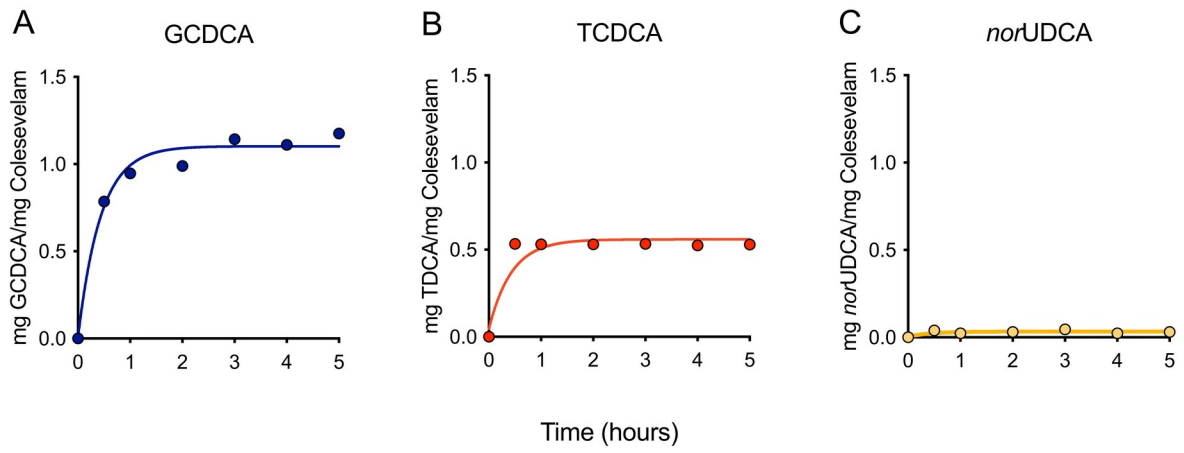

Supplemental Figure S10. In vitro binding of bile acids and *nor*UDCA to colesevelam.

(**A**) Glycochenodeoxycholic acid (GCDCA), (**B**) Taurochenodeoxycholic acid TCDCA), (**C**) *nor*UDCA. Bile acids were dissolved in simulated intestinal fluid at a concentration of 2 mM for TCDCA or 6 mM for GCDA and *nor*UDCA and incubated with 7.5 mg of colesevelam hydrochloride at 37°C. Samples were withdrawn at 0, 0.5, 1, 2, 3, 4 and 5 h, filtered through a 0.2 µm syringe filter, and the filtrate was analyzed by enzymatic assay to determine the free bile acid concentration by enzymatic assay. The difference between the initial (0 h) and unbound bile acid concentrations at each time point was used to calculate the amount of the bile acid bound per mg of colesevelam hydrochloride.

References

1. Yoon YB, Hagey LR, Hofmann AF, Gurantz D, Michelotti EL, and Steinbach JH. Effect of side-chain shortening on the physiologic properties of bile acids: hepatic transport and effect on biliary secretion of 23-nor-ursodeoxycholate in rodents. *Gastroenterology* 90: 837-852, 1986.

2. Beuers U, Trauner M, Jansen P, and Poupon R. New paradigms in the treatment of hepatic cholestasis: from UDCA to FXR, PXR and beyond. *J Hepatol* 62: S25-37, 2015.

3. Fickert P, Wagner M, Marschall HU, Fuchsbichler A, Zollner G, Tsybrovskyy O, Zatloukal K, Liu J, Waalkes MP, Cover C, Denk H, Hofmann AF, Jaeschke H, and Trauner M. 24-norUrsodeoxycholic acid is superior to ursodeoxycholic acid in the treatment of sclerosing cholangitis in Mdr2 (Abcb4) knockout mice. *Gastroenterology* 130: 465-481, 2006.

4. Fickert P, Pollheimer MJ, Silbert D, Moustafa T, Halilbasic E, Krones E, Durchschein F, Thuringer A, Zollner G, Denk H, and Trauner M. Differential effects of norUDCA and UDCA in obstructive cholestasis in mice. *J Hepatol* 58: 1201-1208, 2013.

5. Halilbasic E, Fiorotto R, Fickert P, Marschall HU, Moustafa T, Spirli C, Fuchsbichler A, Gumhold J, Silbert D, Zatloukal K, Langner C, Maitra U, Denk H, Hofmann AF, Strazzabosco M, and Trauner M. Side chain structure determines unique physiologic and therapeutic properties of norursodeoxycholic acid in Mdr2-/- mice. *Hepatology* 49: 1972-1981, 2009.

6. Moustafa T, Fickert P, Magnes C, Guelly C, Thueringer A, Frank S, Kratky D, Sattler W, Reicher H, Sinner F, Gumhold J, Silbert D, Fauler G, Hofler G, Lass A, Zechner R, and Trauner M. Alterations in lipid metabolism mediate inflammation, fibrosis, and

proliferation in a mouse model of chronic cholestatic liver injury. *Gastroenterology* 142: 140-151 e112, 2012.

7. Fickert P, Zollner G, Fuchsbichler A, Stumptner C, Weiglein AH, Lammert F, Marschall HU, Tsybrovskyy O, Zatloukal K, Denk H, and Trauner M. Ursodeoxycholic acid aggravates bile infarcts in bile duct-ligated and Mdr2 knockout mice via disruption of cholangioles. *Gastroenterology* 123: 1238-1251, 2002.
8. Fickert P, Hirschfield GM, Denk G, Marschall HU, Altorjay I, Farkkila M, Schramm C, Spengler U, Chapman R, Bergquist A, Schrumpf E, Nevens F, Trivedi P, Reiter FP, Tornai I, Halilbasic E, Greinwald R, Prols M, Manns MP, Trauner M, and European PSCnSG. norUrsodeoxycholic acid improves cholestasis in primary sclerosing cholangitis. *J Hepatol* 67: 549-558, 2017.
9. Traussnigg S, Schattenberg JM, Demir M, Wiegand J, Geier A, Teuber G, Hofmann WP, Kremer AE, Spreda F, Kluwe J, Petersen J, Boettler T, Rainer F, Halilbasic E, Greinwald R, Prols M, Manns MP, Fickert P, Trauner M, and Austrian/German N-nsg. Norursodeoxycholic acid versus placebo in the treatment of non-alcoholic fatty liver disease: a double-blind, randomised, placebo-controlled, phase 2 dose-finding trial. *Lancet Gastroenterol Hepatol* 4: 781-793, 2019.
10. Bonus M, Sommerfeld A, Qvartskhava N, Gorg B, Ludwig BS, Kessler H, Gohlke H, and Haussinger D. Evidence for functional selectivity in TUDC- and norUDCA-induced signal transduction via alpha5beta1 integrin towards choleresis. *Sci Rep* 10: 5795, 2020.
11. Zhu C, Boucheron N, Muller AC, Majek P, Claudel T, Halilbasic E, Baazim H, Lercher A, Viczenczova C, Hainberger D, Preglej T, Sandner L, Alteneder M, Gulich AF, Khan M, Hamminger P, Remetic J, Ohradanova-Repic A, Schatzlmaier P, Donner C, Fuchs

CD, Stojakovic T, Scharnagl H, Sakaguchi S, Weichhart T, Bergthaler A, Stockinger H, Ellmeier W, and Trauner M. 24-Norursodeoxycholic acid reshapes immunometabolism in CD8(+) T cells and alleviates hepatic inflammation. *J Hepatol* 75: 1164-1176, 2021.

12. Beuers U, Hohenester S, de Buy Wenniger LJ, Kremer AE, Jansen PL, and Elferink RP. The biliary HCO(3)(-) umbrella: a unifying hypothesis on pathogenetic and therapeutic aspects of fibrosing cholangiopathies. *Hepatology* 52: 1489-1496, 2010.
13. Palmer KR, Gurantz D, Hofmann AF, Clayton LM, Hagey LR, and Cecchetti S. Hypercholeresis induced by norchenodeoxycholate in biliary fistula rodent. *Am J Physiol* 252: G219-228, 1987.
14. Gurantz D, and Hofmann AF. Influence of bile acid structure on bile flow and biliary lipid secretion in the hamster. *Am J Physiol* 247: G736-748, 1984.
15. Boyer JL, and Soroka CJ. Bile formation and secretion: An update. *J Hepatol* 75: 190-201, 2021.
16. Banales JM, Prieto J, and Medina JF. Cholangiocyte anion exchange and biliary bicarbonate excretion. *World J Gastroenterol* 12: 3496-3511, 2006.
17. Li Q, Dutta A, Kresge C, Bugde A, and Feranchak AP. Bile acids stimulate cholangiocyte fluid secretion by activation of transmembrane member 16A Cl(-) channels. *Hepatology* 68: 187-199, 2018.
18. Dutta AK, Khimji AK, Kresge C, Bugde A, Dougherty M, Esser V, Ueno Y, Glaser SS, Alpini G, Rockey DC, and Feranchak AP. Identification and functional characterization of TMEM16A, a Ca2+-activated Cl- channel activated by extracellular nucleotides, in biliary epithelium. *J Biol Chem* 286: 766-776, 2011.

19. Hofmann AF, Zakko SF, Lira M, Clerici C, Hagey LR, Lambert KK, Steinbach JH, Schteingart CD, Olinga P, and Groothuis GM. Novel biotransformation and physiological properties of norursodeoxycholic acid in humans. *Hepatology* 42: 1391-1398, 2005.

20. Gurantz D, Schteingart CD, Hagey LR, Steinbach JH, Grotmol T, and Hofmann AF. Hypercholeresis induced by unconjugated bile acid infusion correlates with recovery in bile of unconjugated bile acids. *Hepatology* 13: 540-550, 1991.

21. Lipinski CA, Lombardo F, Dominy BW, and Feeney PJ. Experimental and computational approaches to estimate solubility and permeability in drug discovery and development settings. *Adv Drug Deliv Rev* 46: 3-26, 2001.

22. Dobson PD, and Kell DB. Carrier-mediated cellular uptake of pharmaceutical drugs: an exception or the rule? *Nat Rev Drug Discov* 7: 205-220, 2008.

23. Kell DB. What would be the observable consequences if phospholipid bilayer diffusion of drugs into cells is negligible? *Trends Pharmacol Sci* 36: 15-21, 2015.

24. Girardi E, Cesar-Razquin A, Lindinger S, Papakostas K, Konecka J, Hemmerich J, Kickinger S, Kartnig F, Gurtl B, Klavins K, Sedlyarov V, Ingles-Prieto A, Fiume G, Koren A, Lardeau CH, Kumaran Kandasamy R, Kubicek S, Ecker GF, and Superti-Furga G. A widespread role for SLC transmembrane transporters in resistance to cytotoxic drugs. *Nat Chem Biol* 16: 469-478, 2020.

25. Konig J, Klatt S, Dilger K, and Fromm MF. Characterization of ursodeoxycholic and norursodeoxycholic acid as substrates of the hepatic uptake transporters OATP1B1, OATP1B3, OATP2B1 and NTCP. *Basic Clin Pharmacol Toxicol* 111: 81-86, 2012.

26. Ferrebee CB, Li J, Haywood J, Pachura K, Robinson BS, Hinrichs BH, Jones RM, Rao A, and Dawson PA. Organic Solute Transporter α-β Protects Ileal Enterocytes From Bile

Acid–Induced Injury. *Cellular and Molecular Gastroenterology and Hepatology* 5: 499-522, 2018.

27. Rao A, Kosters A, Mells JE, Zhang W, Setchell KD, Amanso AM, Wynn GM, Xu T, Keller BT, Yin H, Banton S, Jones DP, Wu H, Dawson PA, and Karpen SJ. Inhibition of ileal bile acid uptake protects against nonalcoholic fatty liver disease in high-fat diet-fed mice. *Science translational medicine* 8: 357ra122, 2016.

28. Fuchs CD, Paumgartner G, Mlitz V, Kunczer V, Halilbasic E, Leditznig N, Wahlstrom A, Stahlman M, Thuringer A, Kashofer K, Stojakovic T, Marschall HU, and Trauner M. Colesevelam attenuates cholestatic liver and bile duct injury in Mdr2(-/-) mice by modulating composition, signalling and excretion of faecal bile acids. *Gut* 67: 1683-1691, 2018.

29. Dawson PA, Haywood J, Craddock AL, Wilson M, Tietjen M, Kluckman K, Maeda N, and Parks JS. Targeted deletion of the ileal bile acid transporter eliminates enterohepatic cycling of bile acids in mice. *J Biol Chem* 278: 33920-33927, 2003.

30. Temel RE, Lee RG, Kelley KL, Davis MA, Shah R, Sawyer JK, Wilson MD, and Rudel LL. Intestinal cholesterol absorption is substantially reduced in mice deficient in both ABCA1 and ACAT2. *J Lipid Res* 46: 2423-2431, 2005.

31. Beuling E, Kerkhof IM, Nicksa GA, Giuffrida MJ, Haywood J, aan de Kerk DJ, Piaseckyj CM, Pu WT, Buchmiller TL, Dawson PA, and Krasinski SD. Conditional Gata4 deletion in mice induces bile acid absorption in the proximal small intestine. *Gut* 59: 888-895, 2010.

32. Schwarz M, Russell DW, Dietschy JM, and Turley SD. Marked reduction in bile acid synthesis in cholesterol 7alpha-hydroxylase-deficient mice does not lead to diminished tissue cholesterol turnover or to hypercholesterolemia. *J Lipid Res* 39: 1833-1843, 1998.

33. Torchia EC, Labonte ED, and Agellon LB. Separation and quantitation of bile acids using an isocratic solvent system for high performance liquid chromatography coupled to an evaporative light scattering detector. *Anal Biochem* 298: 293-298, 2001.

34. Hagio M, Matsumoto M, Fukushima M, Hara H, and Ishizuka S. Improved analysis of bile acids in tissues and intestinal contents of rats using LC/ESI-MS. *Journal of lipid research* 50: 173-180, 2009.

35. Rao A, van de Peppel IP, Gumber S, Karpen SJ, and Dawson PA. Attenuation of the Hepatoprotective Effects of Ileal Apical Sodium Dependent Bile Acid Transporter (ASBT) Inhibition in Choline-Deficient L-Amino Acid-Defined (CDAA) Diet-Fed Mice. *Front Med (Lausanne)* 7: 60, 2020.

36. Love MI, Huber W, and Anders S. Moderated estimation of fold change and dispersion for RNA-seq data with DESeq2. *Genome Biol* 15: 550, 2014.

37. Li J, Witten DM, Johnstone IM, and Tibshirani R. Normalization, testing, and false discovery rate estimation for RNA-sequencing data. *Biostatistics* 13: 523-538, 2012.

38. Ueno Y, Alpini G, Yahagi K, Kanno N, Moritoki Y, Fukushima K, Glaser S, LeSage G, and Shimosegawa T. Evaluation of differential gene expression by microarray analysis in small and large cholangiocytes isolated from normal mice. *Liver Int* 23: 449-459, 2003.

39. Fiorotto R, Spirli C, Fabris L, Cadamuro M, Okolicsanyi L, and Strazzabosco M. Ursodeoxycholic acid stimulates cholangiocyte fluid secretion in mice via CFTR-dependent ATP secretion. *Gastroenterology* 133: 1603-1613, 2007.

40. Krishnaiah YS, Yang Y, Bykadi S, Sayeed VA, and Khan MA. Comparative evaluation of in vitro efficacy of colesevelam hydrochloride tablets. *Drug Dev Ind Pharm* 40: 1173-1179, 2014.

41. Kroll T, Smits SHJ, and Schmitt L. Monomeric bile acids modulate the ATPase activity of detergent-solubilized ABCB4/MDR3. *J Lipid Res* 62: 100087, 2021.

42. Krag E, and Phillips SF. Active and passive bile acid absorption in man. Perfusion studies of the ileum and jejunum. *J Clin Invest* 53: 1686-1694, 1974.

43. Mekhjian HS, Phillips SF, and Hofmann AF. Colonic absorption of unconjugated bile acids: perfusion studies in man. *Dig Dis Sci* 24: 545-550, 1979.

44. Kamp F, Hamilton JA, Kamp F, Westerhoff HV, and Hamilton JA. Movement of fatty acids, fatty acid analogues, and bile acids across phospholipid bilayers. *Biochemistry* 32: 11074-11086, 1993.

45. Hagenbuch B, and Stieger B. The SLCO (former SLC21) superfamily of transporters. *Mol Aspects Med* 34: 396-412, 2013.

46. Reichel C, Gao B, Van Montfoort J, Cattori V, Rahner C, Hagenbuch B, Stieger B, Kamisako T, and Meier PJ. Localization and function of the organic anion-transporting polypeptide Oatp2 in rat liver. *Gastroenterology* 117: 688-695, 1999.

47. van de Steeg E, Wagenaar E, van der Kruijssen CM, Burggraaff JE, de Waart DR, Elferink RP, Kenworthy KE, and Schinkel AH. Organic anion transporting polypeptide 1a/1b-knockout mice provide insights into hepatic handling of bilirubin, bile acids, and drugs. *J Clin Invest* 120: 2942-2952, 2010.

48. Fitz JG. Regulation of cholangiocyte secretion. *Semin Liver Dis* 22: 241-249, 2002.

49. Shcheynikov N, Boggs K, Green A, and Feranchak AP. Identification of the chloride channel, leucine-rich repeat-containing protein 8, subfamily a (LRRC8A), in mouse cholangiocytes. *Hepatology* 2022.

50. Florentino RM, Li Q, Coard MC, Haep N, Motomura T, Diaz-Aragon R, Faccioli LAP, Amirneni S, Kocas-Kilicarslan ZN, Ostrowska A, Squires JE, Feranchak AP, and Soto-Gutierrez A. Transmembrane channel activity in human hepatocytes and cholangiocytes derived from induced pluripotent stem cells. *Hepatol Commun* 6: 1561-1573, 2022.

51. Miethke AG, Zhang W, Simmons J, Taylor AE, Shi T, Shanmukhappa SK, Karns R, White S, Jegga AG, Lages CS, Nkinin S, Keller BT, and Setchell KD. Pharmacological inhibition of apical sodium-dependent bile acid transporter changes bile composition and blocks progression of sclerosing cholangitis in multidrug resistance 2 knockout mice. *Hepatology* 63: 512-523, 2016.

52. Baghdasaryan A, Fuchs CD, Osterreicher CH, Lemberger UJ, Halilbasic E, Pahlman I, Graffner H, Krones E, Fickert P, Wahlstrom A, Stahlman M, Paumgartner G, Marschall HU, and Trauner M. Inhibition of intestinal bile acid absorption improves cholestatic liver and bile duct injury in a mouse model of sclerosing cholangitis. *J Hepatol* 64: 674-681, 2016.

53. Hermankova E, Zak A, Polakova L, Hobzova R, Hromadka R, and Sirc J. Polymeric bile acid sequestrants: Review of design, in vitro binding activities, and hypocholesterolemic effects. *Eur J Med Chem* 144: 300-317, 2018.

54. Cabrera D, Arab JP, and Arrese M. UDCA, NorUDCA, and TUDCA in Liver Diseases: A Review of Their Mechanisms of Action and Clinical Applications. *Handb Exp Pharmacol* 256: 237-264, 2019.

55. Dutta AK, Woo K, Doctor RB, Fitz JG, and Feranchak AP. Extracellular nucleotides stimulate Cl- currents in biliary epithelia through receptor-mediated IP3 and Ca2+ release. *Am J Physiol Gastrointest Liver Physiol* 295: G1004-1015, 2008.

56. Minagawa N, Nagata J, Shibao K, Masyuk AI, Gomes DA, Rodrigues MA, Lesage G, Akiba Y, Kaunitz JD, Ehrlich BE, Larusso NF, and Nathanson MH. Cyclic AMP regulates bicarbonate secretion in cholangiocytes through release of ATP into bile. *Gastroenterology* 133: 1592-1602, 2007.

57. Sathe MN, Woo K, Kresge C, Bugde A, Luby-Phelps K, Lewis MA, and Feranchak AP. Regulation of purinergic signaling in biliary epithelial cells by exocytosis of SLC17A9-dependent ATP-enriched vesicles. *J Biol Chem* 286: 25363-25376, 2011.

58. Roda A, Hofmann AF, and Mysels KJ. The influence of bile salt structure on self-association in aqueous solutions. *J Biol Chem* 258: 6362-6370, 1983.

59. Csanaky IL, Lu H, Zhang Y, Ogura K, Choudhuri S, and Klaassen CD. Organic anion-transporting polypeptide 1b2 (Oatp1b2) is important for the hepatic uptake of unconjugated bile acids: Studies in Oatp1b2-null mice. *Hepatology* 53: 272-281, 2011.

60. van de Peppel IP, Bertolini A, van Dijk TH, Groen AK, Jonker JW, and Verkade HJ. Efficient reabsorption of transintestinally excreted cholesterol is a strong determinant for cholesterol disposal in mice. *J Lipid Res* 60: 1562-1572, 2019.

61. Balakrishnan A, Wring SA, and Polli JE. Interaction of native bile acids with human apical sodium-dependent bile acid transporter (hASBT): influence of steroidal hydroxylation pattern and C-24 conjugation. *Pharm Res* 23: 1451-1459, 2006.

62. Marchiano S, Biagioli M, Roselli R, Zampella A, Di Giorgio C, Bordoni M, Bellini R, Urbani G, Morretta E, Monti MC, Distrutti E, and Fiorucci S. Beneficial effects of

UDCA and norUDCA in a rodent model of steatosis are linked to modulation of GPBAR1/FXR signaling. *Biochim Biophys Acta Mol Cell Biol Lipids* 1867: 159218, 2022.

63. Chen ML, Huang X, Wang H, Hegner C, Liu Y, Shang J, Eliason A, Diao H, Park H, Frey B, Wang G, Mosure SA, Solt LA, Kojetin DJ, Rodriguez-Palacios A, Schady DA, Weaver CT, Pipkin ME, Moore DD, and Sundrud MS. CAR directs T cell adaptation to bile acids in the small intestine. *Nature* 593: 147-151, 2021.

64. Yang H, and Wang H. Signaling control of the constitutive androstane receptor (CAR). *Protein Cell* 5: 113-123, 2014.

65. Cattori V, van Montfoort JE, Stieger B, Landmann L, Meijer DK, Winterhalter KH, Meier PJ, and Hagenbuch B. Localization of organic anion transporting polypeptide 4 (Oatp4) in rat liver and comparison of its substrate specificity with Oatp1, Oatp2 and Oatp3. *Pflugers Arch* 443: 188-195, 2001.

66. Slijepcevic D, Roscam Abbing RLP, Katafuchi T, Blank A, Donkers JM, van Hoppe S, de Waart DR, Tolenaars D, van der Meer JHM, Wildenberg M, Beuers U, Oude Elferink RPJ, Schinkel AH, and van de Graaf SFJ. Hepatic uptake of conjugated bile acids is mediated by both sodium taurocholate cotransporting polypeptide and organic anion transporting polypeptides and modulated by intestinal sensing of plasma bile acid levels in mice. *Hepatology* 66: 1631-1643, 2017.

67. Gong L, Aranibar N, Han YH, Zhang Y, Lecureux L, Bhaskaran V, Khandelwal P, Klaassen CD, and Lehman-McKeeman LD. Characterization of organic anion-transporting polypeptide (Oatp) 1a1 and 1a4 null mice reveals altered transport function and urinary metabolomic profiles. *Toxicol Sci* 122: 587-597, 2011.

68. Oude Elferink RP, de Haan J, Lambert KJ, Hagey LR, Hofmann AF, and Jansen PL. Selective hepatobiliary transport of nordeoxycholate side chain conjugates in mutant rats with a canalicular transport defect. *Hepatology* 9: 861-865, 1989.

69. Belinsky MG, Dawson PA, Shchaveleva I, Bain LJ, Wang R, Ling V, Chen ZS, Grinberg A, Westphal H, Klein-Szanto A, Lerro A, and Kruh GD. Analysis of the in vivo functions of Mrp3. *Mol Pharmacol* 68: 160-168, 2005.

70. Zelcer N, Saeki T, Bot I, Kuil A, and Borst P. Transport of bile acids in multidrug-resistance-protein 3-overexpressing cells co-transfected with the ileal Na+-dependent bile-acid transporter. *Biochem J* 369: 23-30, 2003.

71. Chloupkova M, Pickert A, Lee JY, Souza S, Trinh YT, Connelly SM, Dumont ME, Dean M, and Urbatsch IL. Expression of 25 human ABC transporters in the yeast Pichia pastoris and characterization of the purified ABCC3 ATPase activity. *Biochemistry* 46: 7992-8003, 2007.

72. Onishi T, Sano N, and Takikawa H. Effect of colestimide on absorption of unconjugated bile acids in the rat jejunum. *J Gastroenterol Hepatol* 17: 697-701, 2002.

73. Takikawa H, Ogasawara T, Sato A, Ohashi M, Hasegawa Y, and Hojo M. Effect of colestimide on intestinal absorption of ursodeoxycholic acid in men. *Int J Clin Pharmacol Ther* 39: 558-560, 2001.

74. Rust C, Sauter GH, Oswald M, Buttner J, Kullak-Ublick GA, Paumgartner G, and Beuers U. Effect of cholestyramine on bile acid pattern and synthesis during administration of ursodeoxycholic acid in man. *Eur J Clin Invest* 30: 135-139, 2000.

75. Polter DE, Gruhl V, Eigenbrodt EH, and Combes B. Beneficial effect of cholestyramine in sclerosing cholangitis. *Gastroenterology* 79: 326-333, 1980.

76. Tian J, Brown LA, Jones DP, Levin MS, Wang L, Rubin DC, and Ziegler TR. Intestinal redox status of major intracellular thiols in a rat model of chronic alcohol consumption. *JPEN J Parenter Enteral Nutr* 33: 662-668, 2009.

77. Heuman DM. Quantitative estimation of the hydrophilic-hydrophobic balance of mixed bile salt solutions. *J Lipid Res* 30: 719-730, 1989.

78. Stravitz RT, Hylemon PB, Heuman DM, Hagey LR, Schteingart CD, Ton-Nu HT, Hofmann AF, and Vlahcevic ZR. Transcriptional regulation of cholesterol 7 alpha-hydroxylase mRNA by conjugated bile acids in primary cultures of rat hepatocytes. *J Biol Chem* 268: 13987-13993, 1993.

79. Dobin A, and Gingeras TR. Mapping RNA-seq Reads with STAR. *Curr Protoc Bioinformatics* 51: 11 14 11-11 14 19, 2015.

80. Anders S, Pyl PT, and Huber W. HTSeq--a Python framework to work with high-throughput sequencing data. *Bioinformatics* 31: 166-169, 2015.

81. Glaser S, Wang M, Ueno Y, Venter J, Wang K, Chen H, Alpini G, and Holterman A. Differential transcriptional characteristics of small and large biliary epithelial cells derived from small and large bile ducts. *Am J Physiol Gastrointest Liver Physiol* 299: G769-777, 2010.

82. Dutta AK, Khimji AK, Sathe M, Kresge C, Parameswara V, Esser V, Rockey DC, and Feranchak AP. Identification and functional characterization of the intermediate-conductance Ca(2+)-activated K(+) channel (IK-1) in biliary epithelium. *Am J Physiol Gastrointest Liver Physiol* 297: G1009-1018, 2009.

Chapter 4: Ileal Injury and Restitution of Organic Solute Transporter alpha-deficient Mice

This chapter is adapted from a manuscript in preparation:

Jennifer K. Truong[1], Anuradha Rao[1], Kimberly J. Pachura[1], Courtney B. Ferrebee[1], Saul J. Karpen[1], Paul A. Dawson[1]

[1]Department of Pediatrics, Division of Pediatric Gastroenterology, Hepatology and Nutrition, Emory University School of Medicine, Children's Healthcare of Atlanta, Atlanta, Georgia

Denotes corresponding author

Graphical Abstract

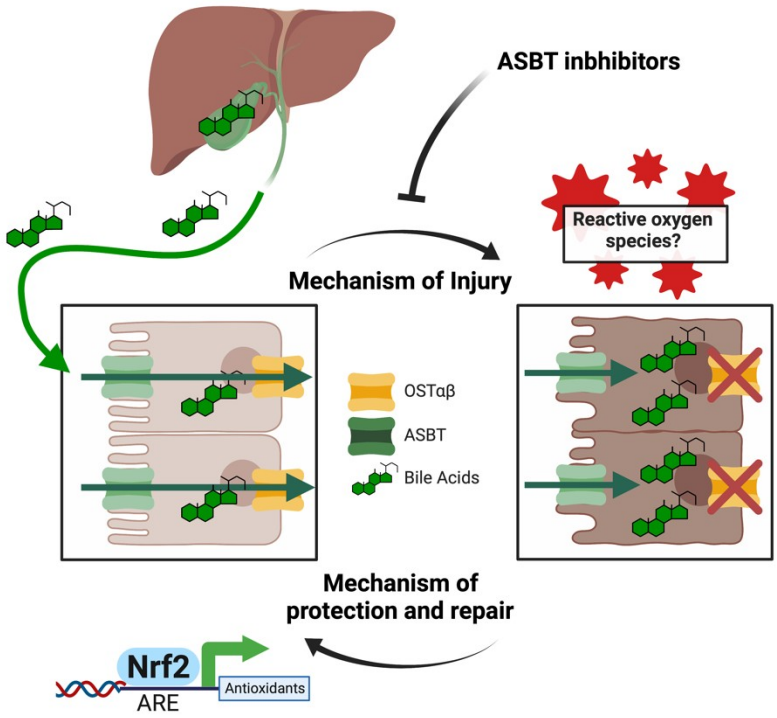

Abstract

The basolateral membrane heteromeric transporter Organic Solute Transporter alpha-beta (Ostα-Ostβ) is essential for bile acid enterohepatic cycling and is expressed at highest levels in terminal ileum enterocytes. Inactivation of Ostα or Ostβ in mice is associated with a complex phenotype that includes down-regulation of hepatic bile acid synthesis and ileal hypertrophy. Pediatric patients with mutations in the Ostα or Ostβ subunit have been identified and present with chronic diarrhea, severe fat-soluble vitamin deficiency and features of cholestatic liver disease. Recent results suggest that in addition to maintaining the enterohepatic circulation of bile acid and bile acid homeostasis, Ostα-Ostβ functions to protect the ileal epithelium against bile acid-induced injury. In this study, we investigated the molecular mechanisms underlying the hypothesized cycles of ileal bile acid retention, oxidative injury, and restitution in Ostα null mice. To understand the role of bile acid accumulation and determine whether the ileal morphological changes are reversible, we used pharmacological inhibitors of the Asbt in adult Ostα null mice to determine the temporal relationship between luminal bile acid uptake and the ileal hypertrophy. Second, we investigate the consequences of changing the bile acid composition in Ostα KO by increasing BA elimination by administration of a bile acid sequestrant and of increasing the hepatic bile acid hydrophilicity by UDCA feeding. Finally, we explore the robust induction of the antioxidant and cytoprotective target genes in Ostα KO mice to understand the role of reactive oxygen species predicted to be involved the injury and restitution response.

Introduction

Bile acids are synthesized from cholesterol in the liver and are the major organic solute found in bile. Following their synthesis, bile acids are secreted into bile and released into the small intestine where they function as natural detergents to facilitate absorption of dietary lipids, cholesterol and fat-soluble vitamins (1). Bile acids are efficiently recycled and are almost completely quantitatively reabsorbed in the intestine to be sent back in the portal circulation to the liver for uptake and resecretion into bile. This process is termed the enterohepatic circulation and is repeated 2-3 times per meal, thereby exposing the liver and gut epithelium to ~20 grams of bile acids per day in humans. The major membrane transporters that function to maintain the enterohepatic circulation of bile acids have been identified (2, 3). In the liver, bile acids are taken up across the hepatocyte sinusoidal membrane by the Na^+-taurocholate co-transporting polypeptide (NTCP; *SLC10A1*) and members of the Organic Anion Transporting Polypeptide family (OATP1B1, OATP1B3), and exported across the canalicular membrane by the Bile Salt Export Pump (BSEP; *ABCB11*). In the bile acid-transporting epithelium of terminal ileum, biliary tract and renal proximal tubules, genetic and biochemical evidence support the concept that conjugated bile acids are taken up by the Apical Sodium-dependent bile acid Transporter (ASBT or IBAT; *SLC10A2*) and exported across the basolateral membrane by the heteromeric organic solute transporter, OSTα-OSTβ (*SLC51A-SLC51B*) (4-7). In this way, the enterohepatic circulation facilitates efficient delivery of bile acid in high concentration for efficient micellization of biliary and dietary lipids, while limiting bile acid accumulation, cytotoxicity and signaling in other compartments.

The Organic Solute Transporter alpha-beta (OSTαβ) is a heteromeric protein localized to the basolateral membrane and functions as a major bile acid transporter (8). In humans, OSTαβ

is expressed at highest levels in small intestine, liver, and kidney, with highest levels of expression in enterocytes in terminal ileum. In mice, Ostαβ shows a similar pattern of expression with the exception of a lower basal expression in liver (hepatocytes). To further understand the role of OSTαβ in bile acid homeostasis and disease, the effect of mutations in the OSTα (SLC51A) and OSTβ (SLC51B) genes has been studied in patients and mouse models. Inherited mutations in the OST genes (SLC51A, SLC51B) impairs bile acid absorption and the regulation of bile acid metabolism and is associated with congenital diarrhea and evidence of hepatobiliary disease. Inactivation of Ostα in mice results in a similar complex phenotype that includes an altered gut-liver bile acid signaling and ileal hypertrophy characterized by blunted and fused villi with dysplastic crypts (9). An in-depth analysis of the phenotype of *Ostα*$^{-/-}$ mice revealed ileal enterocyte bile acid stasis that was temporally associated with the observed villous blunting, crypt hyperplasia, increased proliferation and apoptosis, as well as an increase in the number of mucin secreting cells at the villous tips. Coincident with these changes was increased expression of Nox1 and Nrf2/antioxidant response element target genes, suggesting a role for ROS and redox signaling in the intestinal phenotype of *Ostα*$^{-/-}$ mice. Based on those findings, we hypothesized that OSTαβ protects the epithelium against BA-induced injury. Loss of OSTαβ in ileal enterocytes impairs bile acid export, leading to bile accumulation, Nox1 and ROS-associated cytotoxicity, and subsequent restitution response. In this study, we used pharmacological and genetic approaches to interrogate each step in that model.

Materials and Methods

Materials

The IBAT inhibitor (IBATi) SC-435; (4R,5R)-5-[4-[4-(1-aza-4-azoniabicyclo[2.2.2]octan-4-yl)butoxy] phenyl]-3,3-dibutyl-7,8-dimethoxy-1,1-dioxo-4,5-dihydro-2H-1λ6-benzothiepin-4-ol) was received as a research gift from Shire Pharmaceuticals. Colesevelam was provided by Dr. Alan Hofmann (University of California at San Diego) and was received as a research gift from GelTex Pharmaceuticals/Genzyme. For the N-acetyl cysteine (NAC) treatment, 40 mM NAC (Sigma-Aldrich, St Louis, MO, USA) was prepared in water, pH to 7.4 with NaOH and administered in drinking water for 4 or 8 weeks. NAC water was changed twice per week. Ursodeoxycholic acid diet (sc-296407) was purchased from Santa Cruz Biotechnology and supplemented into laboratory rodent diet (13.3% of calories as fat; PicoLab Diet 20 no. 5001; catalog no. 0001319, LabDiet, St. Louis, MO).

Animals, Treatments, and Tissue Collection

All animal experiments were approved by the Institutional Animal Care and Use Committees at Emory University. The *Ostα*$^{-/-}$ mice were generated as previously described (5, 6). Nox1$^{-/-}$ (Nox1 KO) mice were obtained from Dr. Andrew Neish at Emory University (JAX stock No: 018787; conventional KO model where Nox1 exons 3-6 are replaced by a Neo cassette; backcrossed to C57BL/6J mice). *Ostα*$^{-/-}$ mice (C57BL/6J) were crossed to generate the required WT, *Nox1*$^{-/-}$, *Ostα*$^{-/-}$ and *Ostα*$^{-/-}$*Nox1*$^{-/-}$ mice. Note that Nox1 is X-linked, so the male mice are hemizygous (*Nox1*$^{+/y}$ or *Nox1*$^{-/y}$). The mice were group-housed in ventilated cages (Super Mouse 750 Microisolator System; Lab Products) containing bedding (1/8" Bed-O-Cobbs; Andersons Lab Bedding Products) in the same temperature (22° C) and light/dark cycle (12-h; 6 AM to 6 PM)

controlled room of the animal facility to minimize environmental differences. The breeding mice were maintained in cages with standard bedding (1/8" Bed-O-Cobbs; Andersons Lab Bedding Products) and pulp cotton fiber nesting material (Nestlets; Anacare), fed *ad libitum* rodent breeder chow (21% of calories as fat; PicoLab Diet 20 No. 5058; PicoLab Cat. No. 0007689), and offspring were weaned at postnatal day 20. Adult non-breeding mice were maintained on rodent chow (13% of calories as fat; PicoLab Diet 20 No. 5053, Catalog No. 0007688).

Histological Analysis

The intestinal segments were flushed with PBS to remove luminal contents and divided into five equal length segments prior to weighing, fixed overnight in 10% neutral formalin (Sigma-Aldrich), and stored in 60% ethanol until processed for histology. Each segment was cut into longitudinal strips, stacked, and encased in 2% agarose prior to being embedded in paraffin and processed by Children's Healthcare of Atlanta Pathology Services. Histological sections (5 μm) were cut and stained with hematoxylin and eosin or used for immunohistochemical analysis. Microscopy was performed in the Emory University Integrated Cellular Imaging Core.

Gene expression measurements

The intestinal segments were flushed with PBS to remove luminal contents and divided into five equal parts for histology, the remaining tissue not used for histology was flash frozen and stored at -80°C until further processing. Total RNA was extracted from the most distal segment of the intestine (segment 5) using TRIzol reagent (Invitrogen, Carlsbad, CA) and a RNeasy Mini Kit (Qiagen), and cDNA was generated using a High-Capacity cDNA Reverse Transcription Kit (Applied Biosystems). Real-time PCR (RT-PCR) was performed on a StepOnePlus 96-well

Real-Time PCR System (Applied Biosystems) using a SYBR™ Green PCR Master Mix (Applied Biosystems). Quantification of relative gene expression was conducted by calculating fold change relative to Cyclophilin D as a reference gene using the ΔΔ C(t) method. The mouse primer sets can be found in Supplemental Table 1.

Statistical Analyses

For the box and whisker plots, median values (line), interquartile range (boxes), and min to max values (whiskers are shown). The data were evaluated for statistically significant differences using ANOVA and Sidak's multiple comparisons test (GraphPad Prism; Mountain View, CA). Distinct lowercase letters indicate statistical significance at $P < 0.05$.

Results

Ileal bile acid transporter inhibition reverses ileal injury in *Ostα*$^{-/-}$ mice

To investigate whether pharmacological inhibition of the apical sodium bile acid transporter (ASBT) is protective against development of the ileal hypertrophy associated with Ostα deficiency, post-weaning (3-week old) male and female WT and *Ostα*$^{-/-}$ mice were fed chow or chow supplemented with 60 ppm ASBT inhibitor (ASBTi, SC-435, ~11 mg/kg/day) for 1, 2 or 4 weeks as outlined in Figure. 1A. Analysis of the small intestinal length and weight revealed significant increases of ileal (segment 5) weight in *Ostα*$^{-/-}$ mice at 4, 5 and 7 weeks of age compared to WT (Figure. 1B). These observations are in agreement with previously reported ileal histology in *Ostα*$^{-/-}$, where in as early as 5 days, the distal small intestine segment exhibited mild villous blunting and hypertrophy (Supplemental Figure 1) (10). Also consistent with earlier observations, the increase ileal weight is correlated to the thickening of the epithelium lining and cytoplasmic ruffling. By as early as 1 week of ASBTi treatment, ileal weight to length ratio is significantly reduced in both *Ostα*$^{-/-}$ and WT animals. Liver to body weight ratio was also reduced in male *Ostα*$^{-/-}$ mice and those treated with ASBTi after 4 weeks (Supplemental Figure 2).

Gross morphological changes observed by low magnification H&E staining demonstrated that 4-week treatment of *Ostα*$^{-/-}$ animals with ASBTi successfully, and completely reverses the changes in ileal appearance in *Ostα*$^{-/-}$ mice to indistinguishable from WT (Figure. 1C). Closer examination of the ileum by scanning electron microscopy reveals that inactivation of Ostα results in a fused morphology of the villus, which is partly reversed at a microscopic level with 4 weeks of ASBT inhibition (Figure 1D, 200X and 500X). At higher magnification, we also observe the epithelium at the tips of villi demonstrate altered morphology resembling tuft cells

and “pseudo-goblet” cells (Figure 1D, 5000X and 10000X). Similar histology has been described of the epithelium in patients affected by Barrett’s esophagus which present with columnar metaplasia of the esophagus because of chronic gastroesophageal reflux disease (11).

To determine the corresponding changes in gene expression in the ileum throughout the injury and restitution process, we examined a subset of genes related to reactive oxygen species (ROS) and Nrf2/anti-oxidant response element (ARE) target genes due to their association and responsiveness to oxidative stress and roles as a major regulator of the cytoprotective response to environmental insults (12). In particular, the Nrf2 target genes Gstα1, Gstα3, Gstα4, Gstmu1, Gstmu3 and Nqo1 were measured in male and female mice. In agreement with previously described microarray data, expression of this subset of genes were significantly elevated in Ostα KO mice up to 10-fold versus WT mice, increasing in severity from 4 to 7 weeks of age (10). Correlated with the treatment time of ASBTi, pharmacological inhibition of the bile acid transporter normalizes the changes in gene expression of the *Ostα*$^{-/-}$ animals back down to WT levels, most notably after 4 weeks of treatment (Figure 1E).

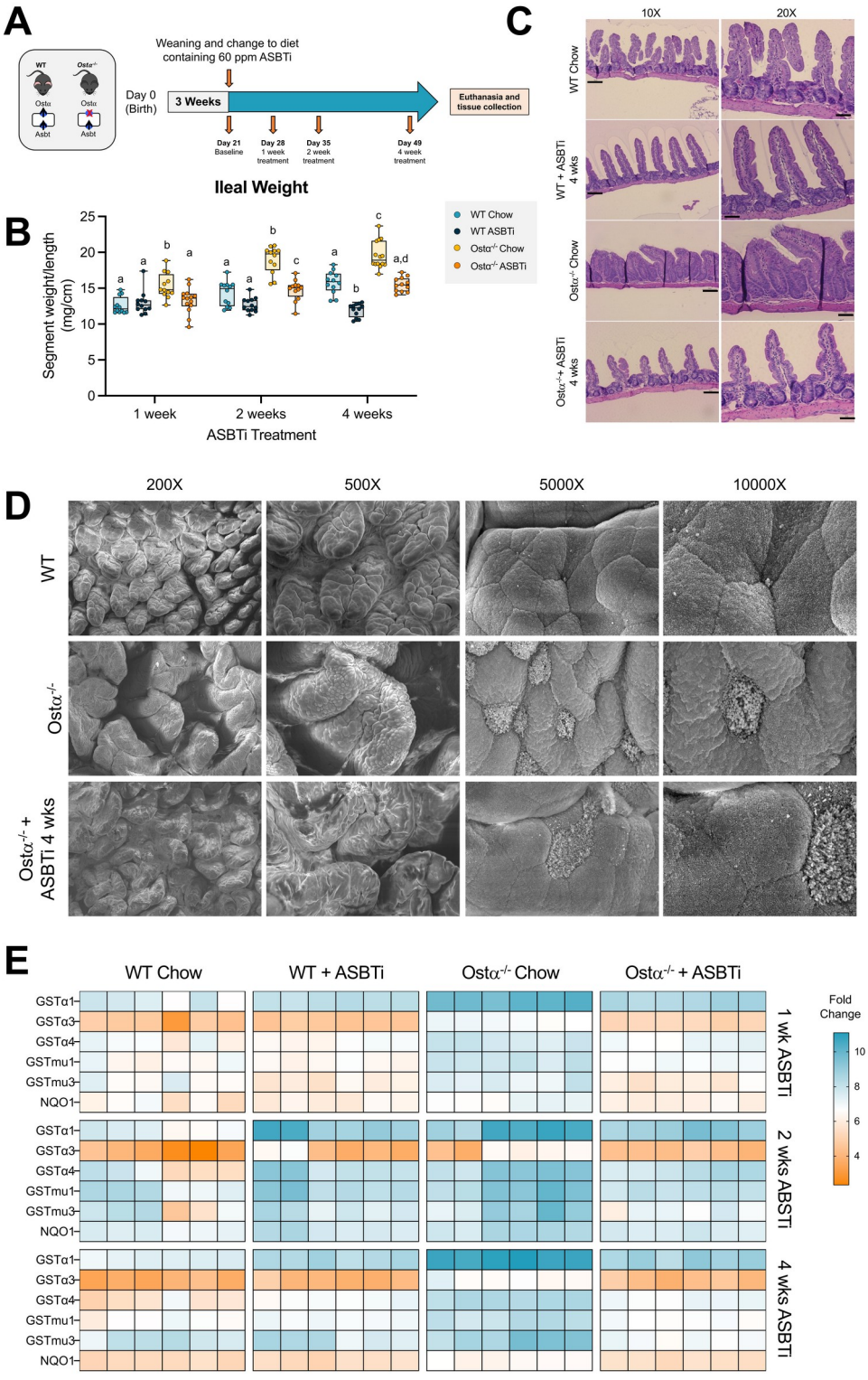

Figure 1. Ileal bile acid transporter inhibition reverses ileal injury in *Ostα*$^{-/-}$ mice

(**A**) Experimental design. (**B**) Ileal weight to length ratio (mg/cm). Median values (line), interquartile range (boxes), and min to max values (whiskers) are shown, n = 6-14 mice per group. Distinct lowercase letters indicate significant differences between groups ($P < 0.05$). (**C**) Hematoxylin and eosin-stained ileal sections (original magnification 10X and 20X) from the indicated genotypes and treatments groups (scale bar 100 μm and 50 μm, respectively). (**D**) Scanning electron microscopy of ileum (original magnification 200X, 500X, 5000X and 10000X) from the indicated genotypes and treatments groups. (**E**) Ileal expression of the indicated Nrf2 target genes in WT and *Ostα*$^{-/-}$ mice fed chow or the ASBTi-containing diet for 1, 2 or 4 weeks. Each square represents an individual mouse.

Bile acid sequestrant Colesevelam does not improve ileal phenotype in *Ostα*$^{-/-}$ mice

Following our observations of inhibition of bile acid absorption with ASBTi corrected the ileal phenotype in our *Ostα*$^{-/-}$ mice, we investigated if administering the bile acid sequestrant Colesevelam would reduce bile acid induced injury and improve the ileal phenotype caused by loss of *Ostα*. It has been shown clinically that BA sequestrants divert bile acids from enterohepatic circulation and deplete the bile acid pool by approximately 40% by increasing fecal bile acid loss (13). Colesevelam specifically is a non-absorbable polymer and second-generation bile acid sequestrant that binds bile acids with a higher affinity than first generation sequestrants such as cholestyramine and colestipol through a combination of hydrophobic and ionic interactions (14).

Male and female WT and *Ostα*$^{-/-}$ mice were fed chow or chow supplemented with 2% (w/w) colesevelam for 2 weeks at age 8-11 weeks. Details of the experimental scheme are shown in Figure 2A. During time of sacrifice (aged 12-15 weeks), *Ostα*$^{-/-}$ mice have an increased ileal weight/length ratio as previously described, with no major changes in the first 80% of the length of the mice small intestine Figure 2B. However, surprisingly, unlike ASBTi treatment, even after 4 weeks of Colesevelam feeding, there was no significant change or improvement in ileal weight in *Ostα*$^{-/-}$ mice compared to those fed chow, despite the reduction in body and liver weight upon administration of the sequestrant (Supplemental Figure S3). Upon further investigation, H&E staining revealed that 4 weeks of Colesevelam feeding indeed did not improve ileal phenotype, with the morphology of the treated *Ostα*$^{-/-}$ mice with blunted and fused villi, similar to those who which were not supplemented with the therapeutic bile acid sequestrant (Figure 2C). In agreement with the other end point measurements, there were no major changes in ileal gene

expression in the *Osta*$^{-/-}$ mice treated with Colesevelam as all the Nrf2 target genes remain elevated (Figure 2D).

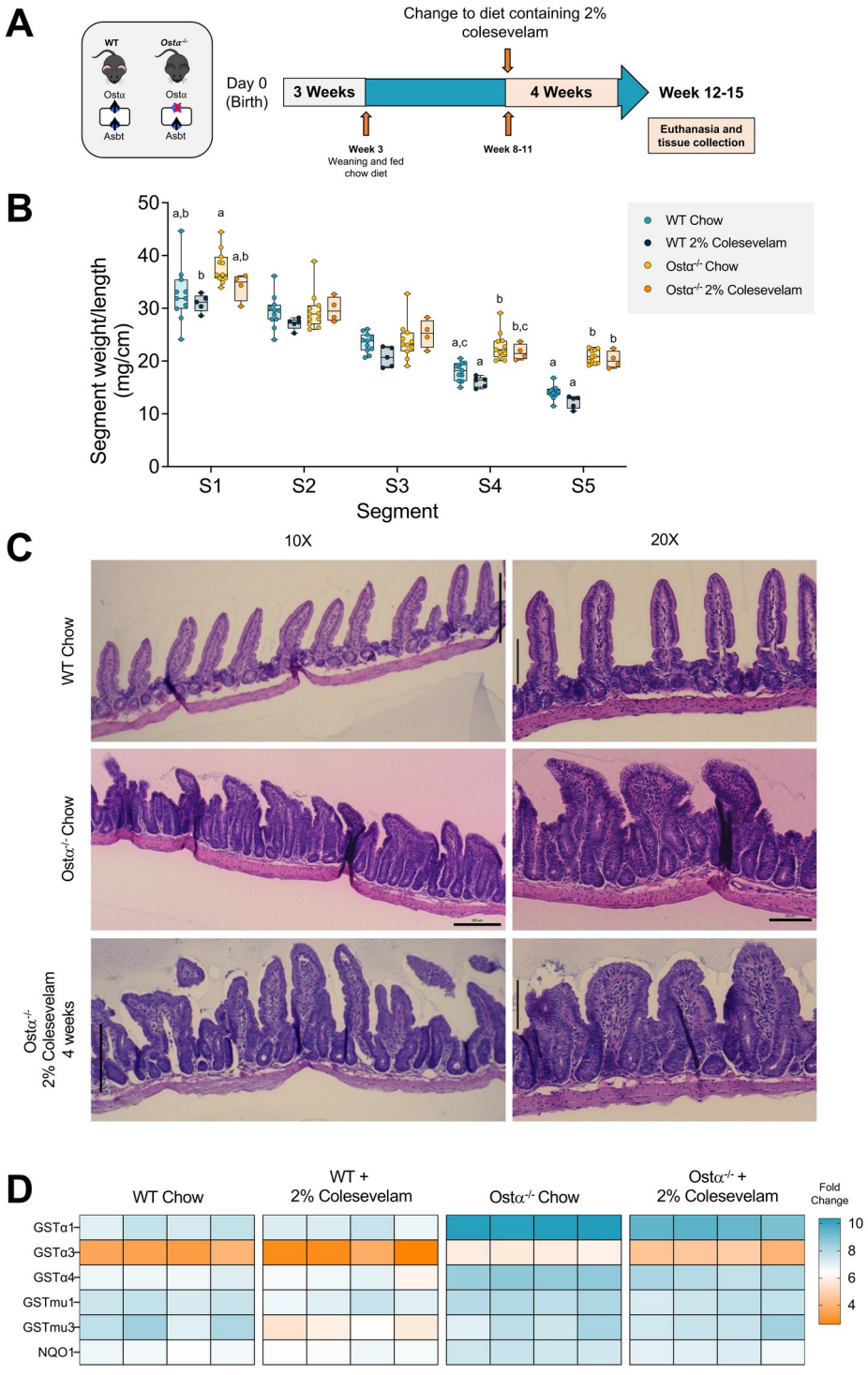

Figure 2. Bile acid sequestrant Colesevelam does not improve ileal phenotype in *Ostα*$^{-/-}$ mice

(**A**) Experimental design. (**B**) Small intestine segment weight to length ratio (mg/cm). Median values (line), interquartile range (boxes), and min to max values (whiskers) are shown, n = 4-11

mice per group. Distinct lowercase letters indicate significant differences between groups ($P < 0.05$). (**C**) Hematoxylin and eosin-stained ileal sections (original magnification 10X and 20X) from the indicated genotypes and treatments groups (scale bar 200 μm and 100 μm, respectively). (**D**) Ileal expression of the indicated Nrf2 target genes in WT and *Ostα*$^{-/-}$ mice fed chow or the Colesevelam-containing diet for 4 weeks. Each square represents an individual mouse.

Therapeutic bile acid ursodeoxycholic acid does reduce antioxidant response in *Ostα*$^{-/-}$ mice

To test our hypothesis of whether feeding the hydrophilic and therapeutic bile acid UDCA can alleviate and reverse ileal injury to a similar extent of which is observed by blocking Asbt-mediated bile acid uptake, we designed the experimental scheme shown in Figure 3A. Male and female WT and *Ostα*$^{-/-}$ pups were weaned at 3 weeks, and as previously reported by our lab, the intestinal changes in *Ostα*$^{-/-}$ mice appear as early as embryonic and can be seen and measured by histology and gene expression (10). Following weaning, WT and *Ostα*$^{-/-}$ were switched to diet containing 0.2% UDCA or continued on normal chow. After 6 weeks of UDCA feeding, animals were sacrificed, and end point measurements were collected.

The extended 6-week UDCA feeding did not decrease the ileal weight in the *Ostα*$^{-/-}$ mice compared to those fed chow (Figure 3B) and had no effect on liver and body weight (Supplemental Figure 4). This result prompted us to proceed directly to determine if there were any effects on ileal gene expression that might indicate a longer UDCA feeding may improve the ileal phenotype in the *Ostα*$^{-/-}$ mice. As suggested by the absence of changes in ileal weight and gross morphologically during tissue harvest and analysis, we report that that the gene expression signature of *Ostα*$^{-/-}$ mice treated with UDCA is not significantly different from untreated *Ostα*$^{-/-}$ and does not restore the profile towards healthy WT levels (Figure 3C).

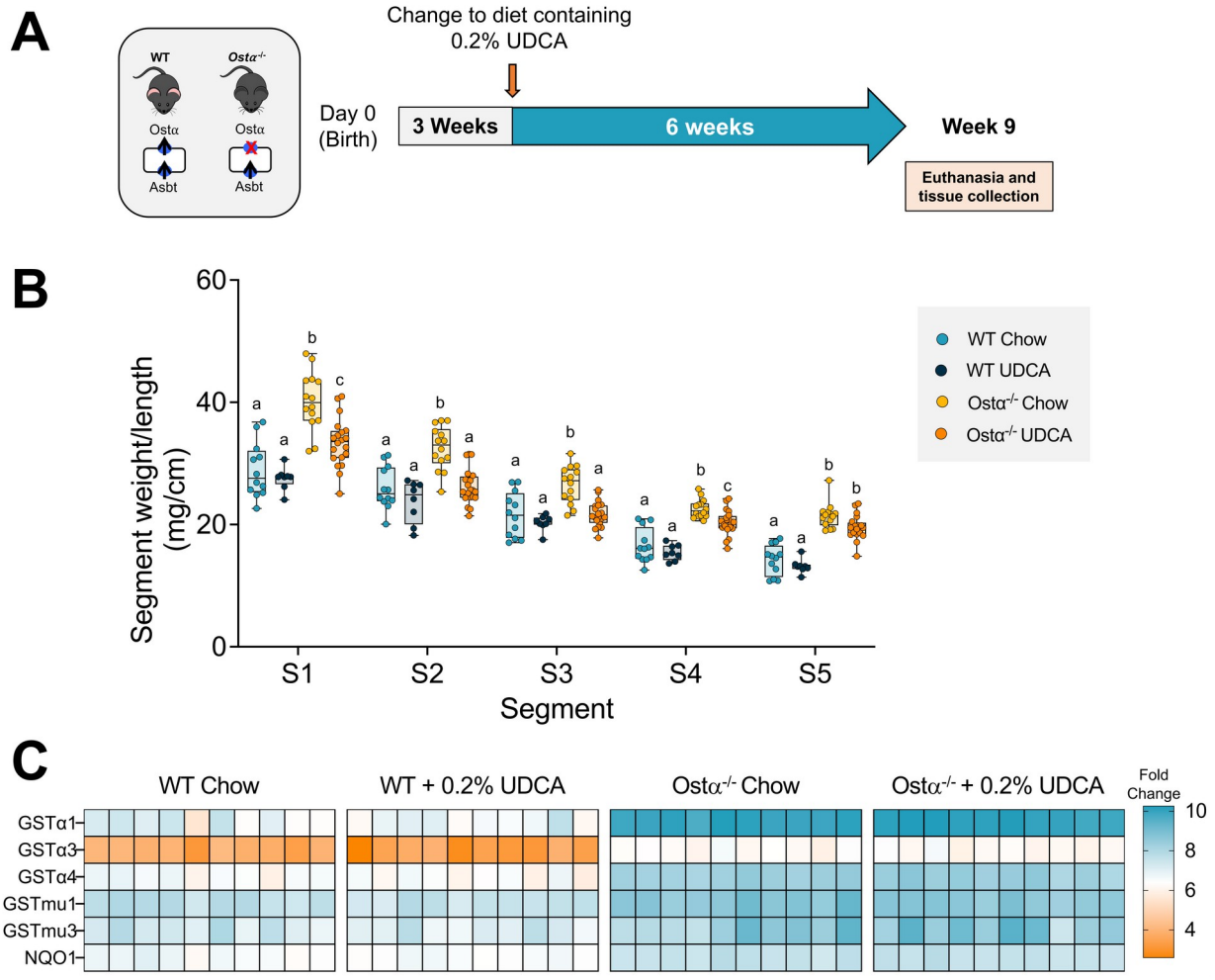

Figure 3. Therapeutic bile acid ursodeoxycholic acid does reduce antioxidant response in *Ostα*$^{-/-}$ mice

(**A**) Experimental design. (**B**) Small intestine segment weight to length ratio (mg/cm). Median values (line), interquartile range (boxes), and min to max values (whiskers) are shown, n = 10 – 12 mice per group. Distinct lowercase letters indicate significant differences between groups ($P < 0.05$). (**C**) Ileal expression of the indicated Nrf2 target genes in WT and *Ostα*$^{-/-}$ mice fed chow or 0.2% UDCA containing diet for 6 weeks. Each square represents an individual mouse.

Ileal injury in *Ostα*$^{-/-}$ mice is not dependent on NADPH oxidase 1 (Nox1)

To further interrogate the role of reactive oxygen species in the ileal phenotype reported in our *Ostα*$^{-/-}$ mouse, we bred *Ostα*$^{-/-}$/*Nox1*$^{-/-}$ double knockout (DKO) mice and evaluated the progression as described in Figure 4A. Mice of all genotypes in the study were weaned at 3 weeks on chow diet and allowed to age to 8 weeks until end point measurements were collected. Overall, *Ostα*$^{-/-}$ mice were determined to have a higher weight-to-length ratio across all segments of the small intestine while the ileal profile *Nox1*$^{-/-}$ mice appeared to be closer to WT in morphology. Other changes in liver and body weight can be found in Supplemental Figure S5. Inactivation of Nox1 in in *Ostα*$^{-/-}$ mice did not restore ileal weight/length towards WT levels, which were not significantly different from the *Ostα*$^{-/-}$ mice (Figure 4B). Ileal histology imaged by H&E staining revealed that morphologically, *Nox1*$^{-/-}$ ileum was similar in appearance to WT animals, while ileum in both *Ostα*$^{-/-}$ and *Ostα*$^{-/-}$/*Nox1*$^{-/-}$ mice displayed the same altered morphology as described throughout the previous text (Figure 4C).

At a gene expression level, *Nox1*$^{-/-}$ ileal Nrf2 target gene expression was not elevated, and similar to the profile of WT mice at a basal level. Consistent with other endpoint measurements of this study, inactivation of Nox1 in *Ostα*$^{-/-}$ mice did not reduce the elevated Nrf2 target gene expression observed in *Ostα*$^{-/-}$ mice (Figure 4D). Together, these data suggest that Nox1 is not responsible for the apparent ileal injury manifested in the *Ostα*$^{-/-}$ mice, which led us to investigate other sources of reactive oxygen species.

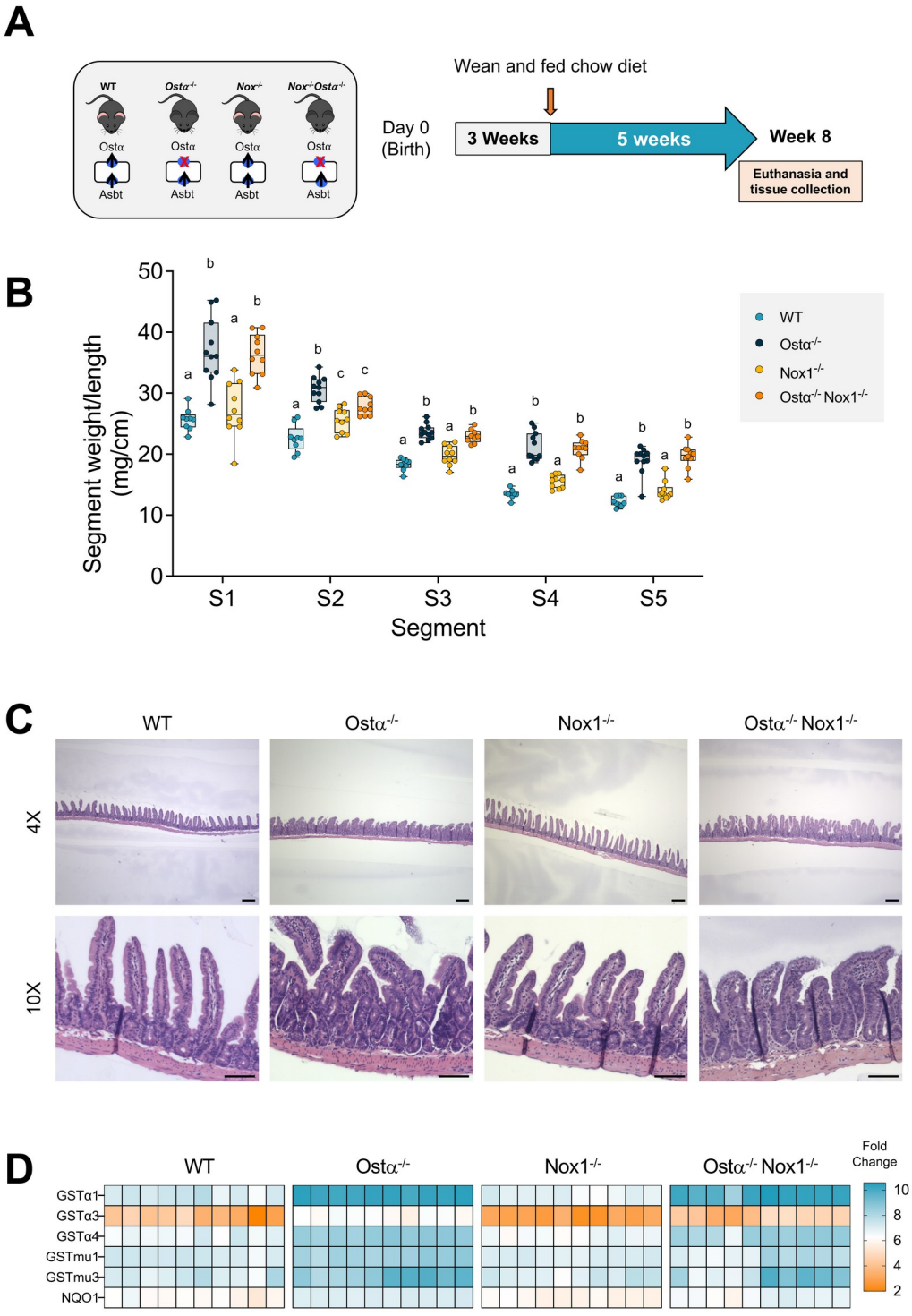

Figure 4. Ileal injury in *Ostα*$^{-/-}$ mice is not dependent on NADPH oxidase 1 (Nox1)

(**A**) Experimental design. (**B**) Small intestine segment weight to length ratio (mg/cm). Median values (line), interquartile range (boxes), and min to max values (whiskers) are shown, n = 10 – 12 mice per group. Distinct lowercase letters indicate significant differences between groups ($P < 0.05$). (**C**) Hematoxylin and eosin-stained ileal sections (original magnification 4X and 10X) from the indicated genotypes and treatments groups (scale bar 200 μm and 100 μm, respectively). (**D**) Ileal expression of the indicated Nrf2 target genes in WT, *Ostα*$^{-/-}$, *Nox1*$^{-/-}$ and *Ostα*$^{-/-}$/*Nox1*$^{-/-}$animals at 8 weeks. Each square represents an individual mouse.

Broad quenching of reactive oxygen species with n-acetylcysteine (NAC) does not rescue ileal injury in *Ostα*$^{-/-}$ mice

To investigate the role of reactive oxygen species in the ileal phenotype observed in *Ostα*$^{-/-}$ mice, WT and *Ostα*$^{-/-}$ mice were treated with the reactive oxygen species scavenger, N-acetylcysteine (NAC). At 8 weeks of age, WT or *Ostα*$^{-/-}$mice were switched to normal water or water supplemented with 40 mM NAC and then sacrificed 4 weeks or 8 weeks later as described in Figure 5A. Supplementation with NAC for 4 weeks or 8 weeks in *Ostα*$^{-/-}$ mice did not improve the gain in weight in the ileum (Figure 5B), nor did it improve ileal morphology by H&E (Figure 5C). Changes in liver and body weight can be found in Supplemental Figure S6. The same conclusion is drawn from the measured changes in gene expression as NAC feeding did not normalize the Nrf2 activated genes in *Ostα*$^{-/-}$ mice towards WT Fig. 5D).

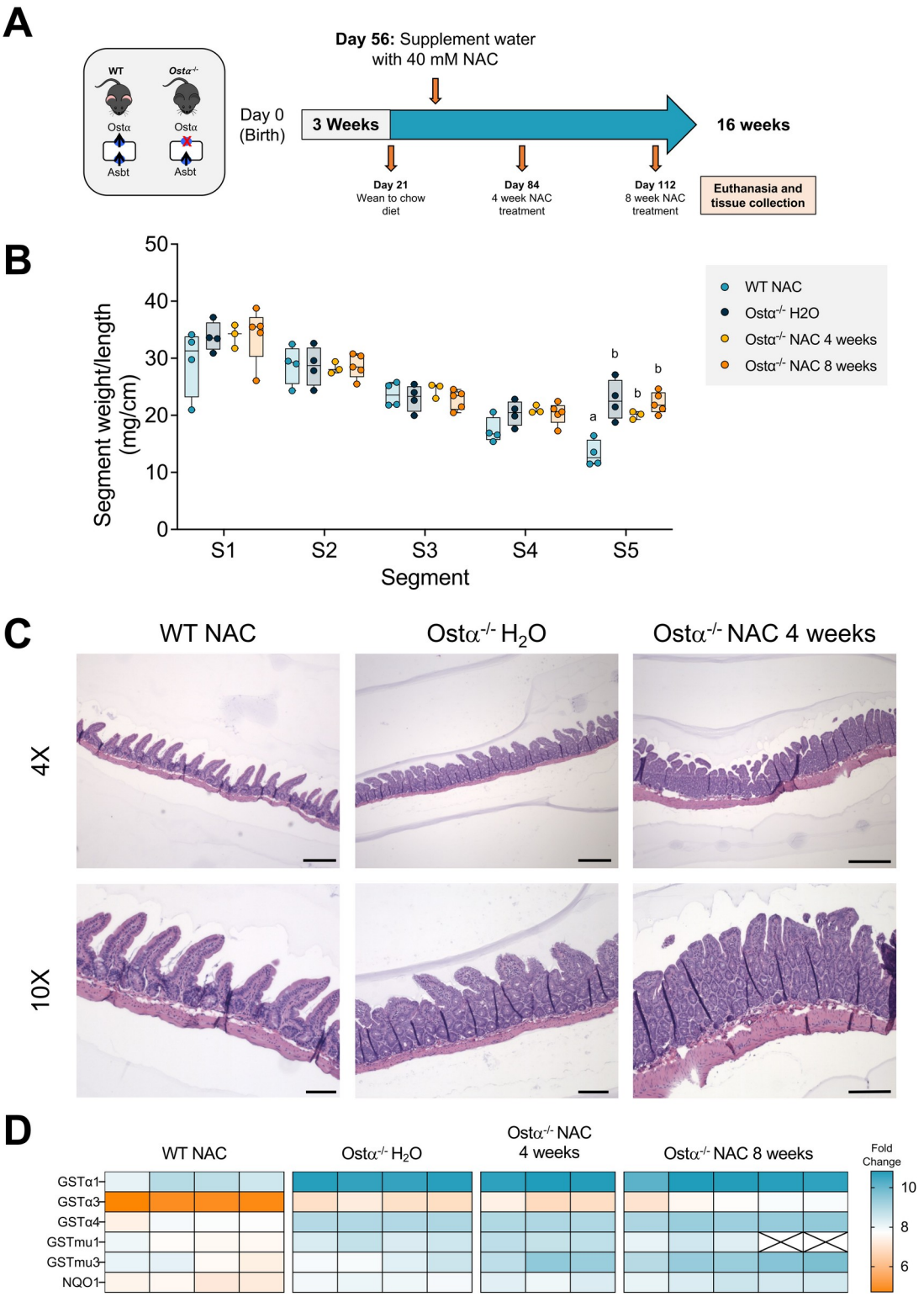

Figure 5. Broad quenching of reactive oxygen species with n-acetylcysteine (NAC) does not rescue ileal injury in *Ostα*$^{-/-}$ mice

(**A**) Experimental design. (**B**) Small intestine segment weight to length ratio (mg/cm). Median values (line), interquartile range (boxes), and min to max values (whiskers) are shown, n = 3 – 5 mice per group. Distinct lowercase letters indicate significant differences between groups ($P < 0.05$). (**C**) Hematoxylin and eosin-stained ileal sections (original magnification 4X and 10X) from the indicated genotypes and treatments groups (scale bar 200 μm and 100 μm, respectively). (**C**) Ileal expression of the indicated Nrf2 target genes in WT and *Ostα*$^{-/-}$ mice null given water supplemented with 40 mM NAC for 4 or 8 weeks. Each square represents an individual mouse.

Discussion

While the *Ostα*$^{-/-}$ ileal phenotype appears to be similar to an irritable bowel disease such as Ulcerative Colitis or Crohn's Disease, there is only a mild increase in inflammatory cells and no change in pro-inflammatory genes like TNFα or IL1β (9). This observation allows two major questions: 1. What is the source and major contributor for ileal phenotype in *Ostα*$^{-/-}$ mice? and 2. Can we alleviate or reverse the phenotype with BA-based therapeutics?

In our investigations, we explore several methods of alleviating the ileal bile acid burden in *Ostα*$^{-/-}$ mice. Our lab has reported that preventing bile acid uptake by genetic ablation of the apical sodium bile acid transporter (Asbt) has been shown to prevent ileal damage in the *Ostα*$^{-/-}$ mice. In the present studies, we utilize a pharmacologic ASBT inhibitor (ASBTi, SC-435) which has been evaluated in clinical trials as an anticholestatic therapy (15) and have demonstrated clinical benefit in children and been approved for the treatment of progressive familial intrahepatic cholestasis (PFIC) and Alagille syndrome (16, 17). Our studies demonstrate that delivery of ASBTi can reverse the ileal phenotype of *Ostα*$^{-/-}$ mice in as little as one week of treatment.

Other methods of changing the bile acid composition in *Ostα*$^{-/-}$ mice were also evaluated. Treatment with a bile acid sequestrant (18) has been shown to be therapeutic in the *Mdr2*$^{-/-}$ mouse model of cholestatic liver injury by addressing the consequences of bile acid accumulation by increasing elimination of bile acids from the system. In our experience, feeding colesevelam did not improve the ileal phenotype in the *Ostα*$^{-/-}$ mice. The kinetics of bile salts and sequestrants binding may play a role in explaining the absence of improvement in our *Ostα*$^{-/-}$ mouse model. Studies have been conducted that suggest the binding of bile salts to various BA sequestrants and resins are reversable (19). Earlier studies have demonstrated the mechanism of

action of these therapeutics are by ion-exchange which are governed by the principals of mass action and suggests bound bile salts can be displaced and replaced by endogenous competing anions in the system (20). Anions that exist physiologically, such as chloride, flux in concentration along the axis of the gastrointestinal track and can influence the binding capacity of resin by reducing the ability to sequester bile acids by occupying binding sites. Bile salts lower in concentration as we travel down the small intestine, at the terminal ileum and site of bile acid reabsorption the resins equilibrate to the bile salts and other anions (which are higher comparatively to the bile salts). It is possible that the bile salts are displaced from the resin by competing anions and consequently continue to expose the epithelium to the buildup of BA in the *Ostα*$^{-/-}$ mice. This suggests that the environment, binding capacity, and affinity of BA sequestrants play a large role in influencing their therapeutic effect (21).

Our next approach involved changing the bile acid composition by administration of the hydrophilic bile acid ursodeoxycholic acid (UDCA). UDCA is clinically used to the treat cholestatic disorders such as primary biliary cholangitis (PBC), intrahepatic cholestasis of pregnancy, and cystic fibrosis (22-24). In addition, UDCA which has been reported to have cytoprotective properties and improves portal inflammation, ductular proliferation, and fibrosis in *Mdr2*$^{-/-}$ mice as mentioned earlier (25, 26). In addition to its use for improving the outcome of hepatobiliary disease, UDCA also has been shown to provide protective effects in small intestine and colon (27, 28). To our surprise, neither of these interventions improved the ileal phenotype in our *Ostα*$^{-/-}$ mice. A potential explanation could involve the influence of UDCA on the hydrophobicity of the mouse bile acid pool. The cytochrome P450, *Cyp2c70*, was recently identified as the enzyme responsible for the synthesis of protective, hydrophilic muricholates exclusively found in murine species (29-32). Our group and others have generated and

demonstrated that the *Cyp2c70*$^{-/-}$ mouse develops early features of cholestasis as a result of a more human, hydrophobic and injurious BA pool (29, 32-34). One study demonstrated that treating *Cyp2c70*$^{-/-}$ mice with the hydrophilic BA UDCA reduced the hydrophobicity of the BA pool and normalized liver histology and hepatic injury markers (33), which prompted us to test this therapeutic approach in our *Ostα*$^{-/-}$ mouse. Our lab has previously characterized that despite a reduction in overall bile acid pool size by ~70%, the overall distribution of bile acid composition in *Ostα*$^{-/-}$ mice is not significantly different from WT as suggested from their respective hydrophobicity indexes (6). In our interrogations of the *Cyp2c70*$^{-/-}$ mouse, we evaluated the detergency profile of the hepatic BA pool in WT mice versus WT mice treated with ASBTi by calculating the hydrophobicity index and injury prolife as measured by red blood cell lysis. As expected, the WT mouse liver BA composition, which contains almost 50% hydrophilic muricholates, exhibits weak cytolytic activity in the red blood cell lysis assay and has a hydrophobic index at around -0.28. In agreement with other reported observations (35), ASBT inhibition reduced the proportion of hydrophilic TMCAs and increased TDCA and TCDCA in livers of WT mice, thereby elevating the calculated HI from -0.28 to +0.18 (36). This increase in hydrophobicity of the bile acid pool with ASBTi administration could be a possible contributor to the lack of improvement in ileal histology in our *Ostα*$^{-/-}$ mouse model.

We also followed up on the microarray data from our previous *Ostα*$^{-/-}$ characterization (10). The analysis previously identified 244 differentially expressed genes (regulated more than 2-fold $P < 0.05$); 54 that were increased and 190 genes that were decreased. Ontogeny analysis performed for differentially expressed genes revealed that pathways related to oxidation-reduction and glutathione metabolism were most highly induced, suggesting increased oxidative stress. Bile acids can induce mitochondrial ROS in hepatocytes, which promotes activation of

receptor tyrosine kinases and cell signaling pathways (37). However, the ability of bile acids to induce mitochondrial ROS is not restricted to hepatocytes, and other studies have argued that bile acids can generate ROS in various cell types (38-40). The cytotoxic effects of bile acids have been attributed to several molecular mechanisms including detergent-associated membrane damage, disruption of mitochondrial membrane potential, enhanced generation of reactive oxygen species (ROS), direct activation of cell death receptors such as CD95/Fas and TRAIL-R2, and induction of an inflammatory response (41-44). Other major sources of reactive oxygen species (ROS) in the gastrointestinal tract include the formation of free radicals by the electron transport chain in the mitochondria, NAPDH oxidases, and nitric oxide synthase (NOS) enzymes (45). Our top candidate is the NADPH oxidase enzyme Nox1 which is found to be expressed in the ileal epithelium and has been reported to be a major contributor of ROS under pathophysiological conditions (46, 47). Development of Ileitis and mucositis in mouse models has been linked to the up-regulation of oxidases and overproduction of ROS in small intestine (48, 49) and increased Nox1 activity has been linked to redox-signaling associated with epithelial repair (46, 49, 50). As described in previous studies, ileal Nox1 mRNA expression is induced almost 50-fold in male and female *Ostα*$^{-/-}$ mice, raising the argument for the Nox1 generation of ROS underlies the initial injury in our *Ostα*$^{-/-}$ mice, resulting in the induction of Nrf2-target genes and restitution response (10). To directly test this hypothesis, we generated *Ostα*$^{-/-}$*/Nox1*$^{-/-}$ mice and observed no major improvement in the ileal phenotype from the *Ostα*$^{-/-}$ mouse, suggesting that perhaps another source of ROS not generated by Nox1 is the underlying source of injury. To address this point, we administered N-acetyl cysteine (NAC) is a cell-permeable derivative of cysteine and reverses thiol oxidation in cells and tissues by scavenging reactive oxygen species and enhancing glutathione synthesis (51). Administration of NAC has been shown to protect the

small intestine and colon from injury involving oxidative stress, such as exposure to radiation, dextran sodium sulfate, and alcohol (52-54). In addition, oxidative DNA damage associated with environmental toxins or genetic manipulations in fetuses has been protected by NAC feeding to pregnant mice (55).However, supplementing the water for Ostα KO mice with NAC for 4 and 8 weeks did not improve the ileal phenotype.

The absence of improvement with *Nox1*$^{-/-}$and NAC feeding suggests that the ileal phenotype observed in *Ostα*$^{-/-}$ mice may be attributed to either reactive oxygen species generated in other locations, or other confounding factors that we have not yet investigated. In these studies, we have not addressed the outcomes of the complete ablation of the Nrf2/antioxidant response element (ARE) associated pathways. Nrf2 is a basic leucine zipper protein that plays an important role in the cellular adaptive response to counteract endogenous and exogenous oxidative stressors (56, 57). Nrf2 is regulated by Kelch-like ECH-associated protein 1 (Keap1). Under basal conditions Nrf2 is bound to Keap1 and retained in the cytoplasm and undergoes proteasomal degradation (58). In response to oxidative stress, the Nrf2-Keap1 complex is disrupted and Nrf2 translocates into the nucleus where it binds to the antioxidant response elements (AREs) of promoters to induce expression of target genes involved in GSH production, utilization and protection against oxidative insult (59-61). Furthermore, current drugs used to treat cholestasis, such as oleanolic acid and baicalin, induce Nrf2 expression (59, 62). These data suggest that the activation of Nrf2 acts on the front line to protect the cell from macromolecular damage.

Supplementary Material

Supplemental Table S1. Primers used for gene expression in mouse

Gene	Forward primer	Reverse primer
Cyclophillin	TTCTTCATAACCACAGTCAAGACC	TCCACCTTCCGTACCACATC
GSTa1	GGCAGAATGGAGTGCATCA	TCCAAATCTTCCGGACTCTG
GSTa3	AGGGAACAGCTTTTTAACAAGAAA	CCATCAAAGTAATGAAGGACTGG
GSTa4	CCCCTGTACTGTCCGACTTC	GGAATGTTGCTGATTCTTGTCTT
GSTmu1	GCAGCTCATCATGCTCTGTT	CATTTTCTCAGGGATGGTCTTC
GSTmu3	CCCGCATACAGCTCATGATA	TTGCCCAGGAACTCAGAGTAG
Nqo1	AGCGTTCGGTATTACGATCC	AGTACAATCAGGGCTCTTCTCG

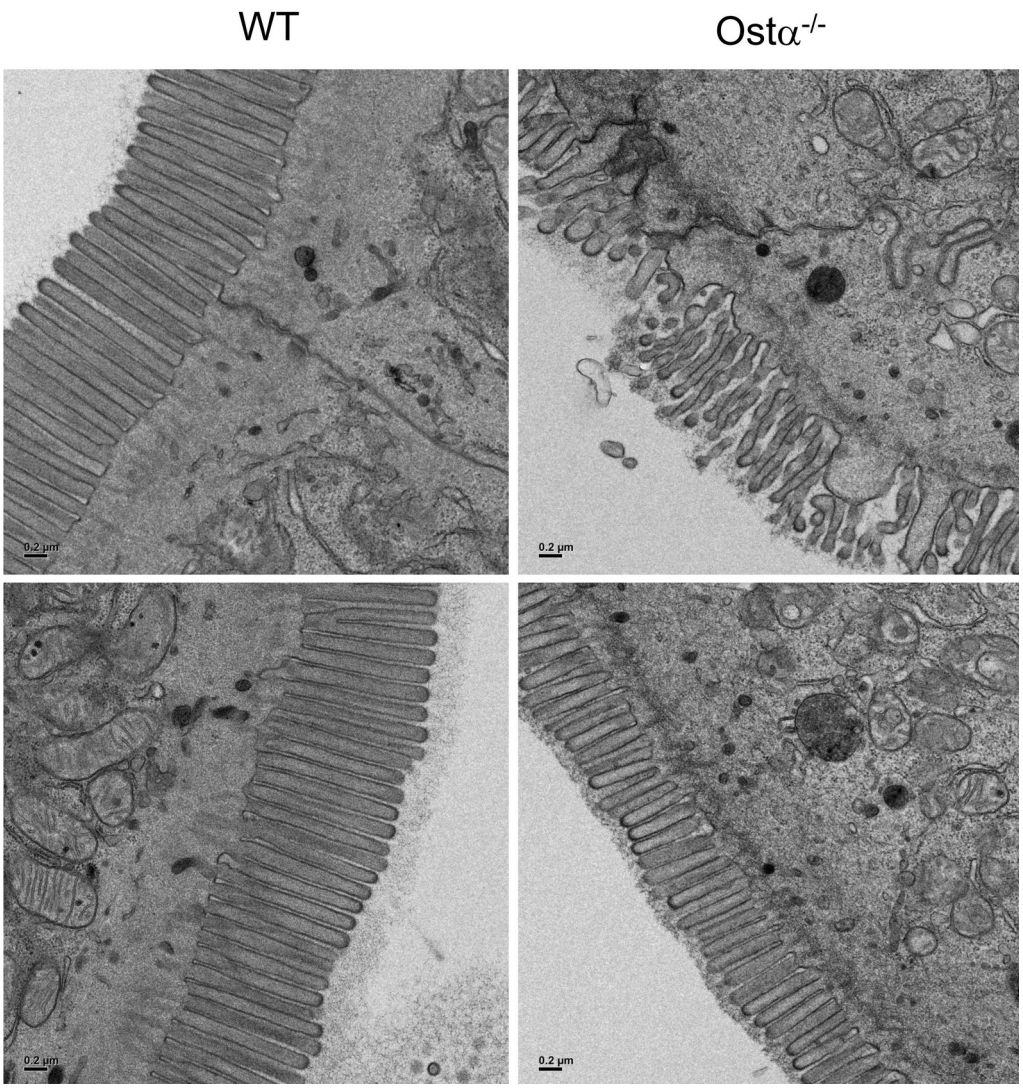

Supplemental Figure S1. *Ostα*$^{-/-}$ mice present with a shorten villus phenotype.

Transmission electron microscopy of representative *Ostα*$^{-/-}$ (right) villi morphology compared to WT (left). Scale bar 0.2 μm.

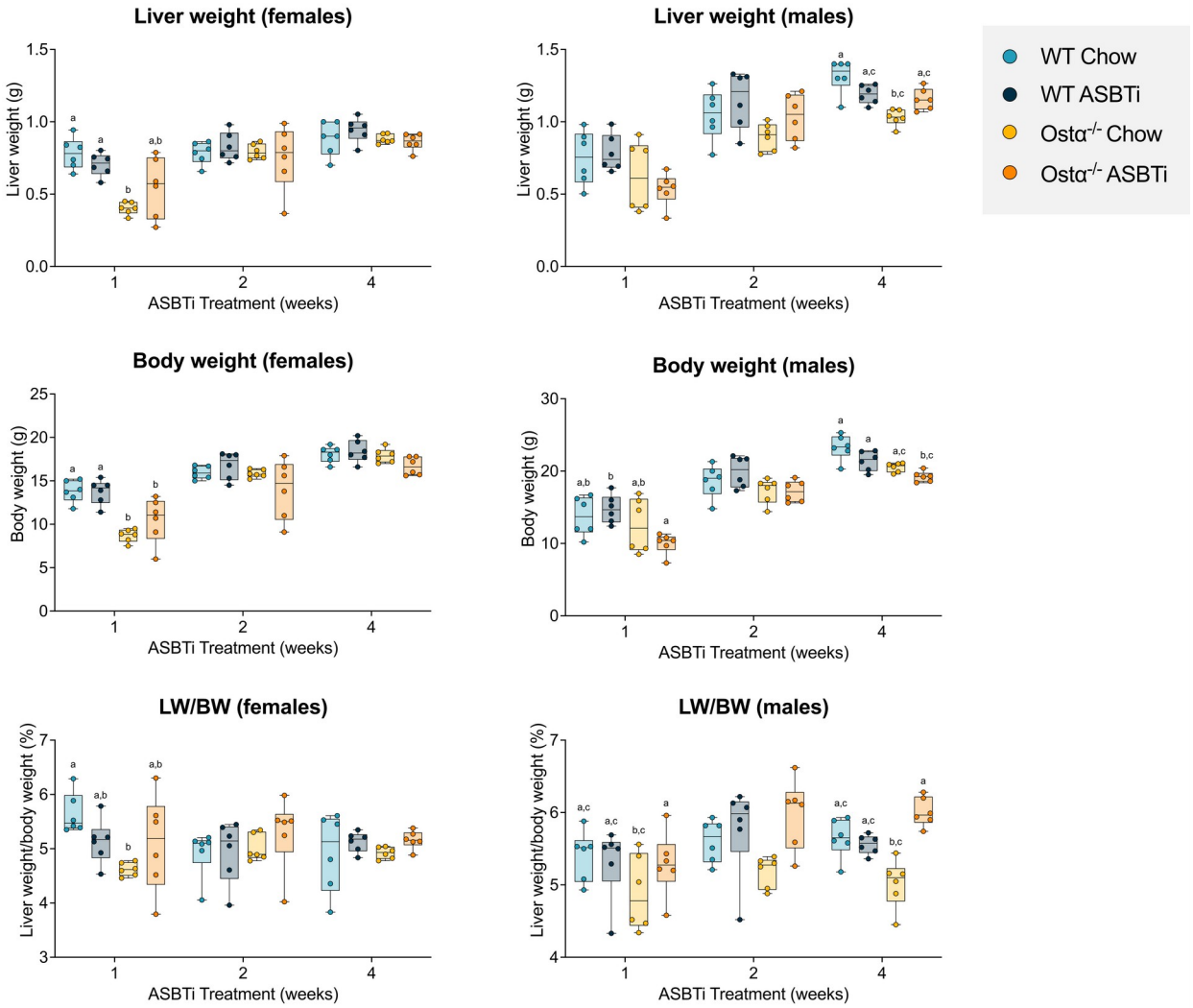

Supplemental Figure S2. Changes in liver and body weight in *Ostα*$^{-/-}$ and WT mice following 1, 2 and 4 weeks of ASBTi treatment

Median values (line), interquartile range (boxes), and min to max values (whiskers) are shown, n = 6-14 mice per group. Distinct lowercase letters indicate significant differences between groups ($P < 0.05$).

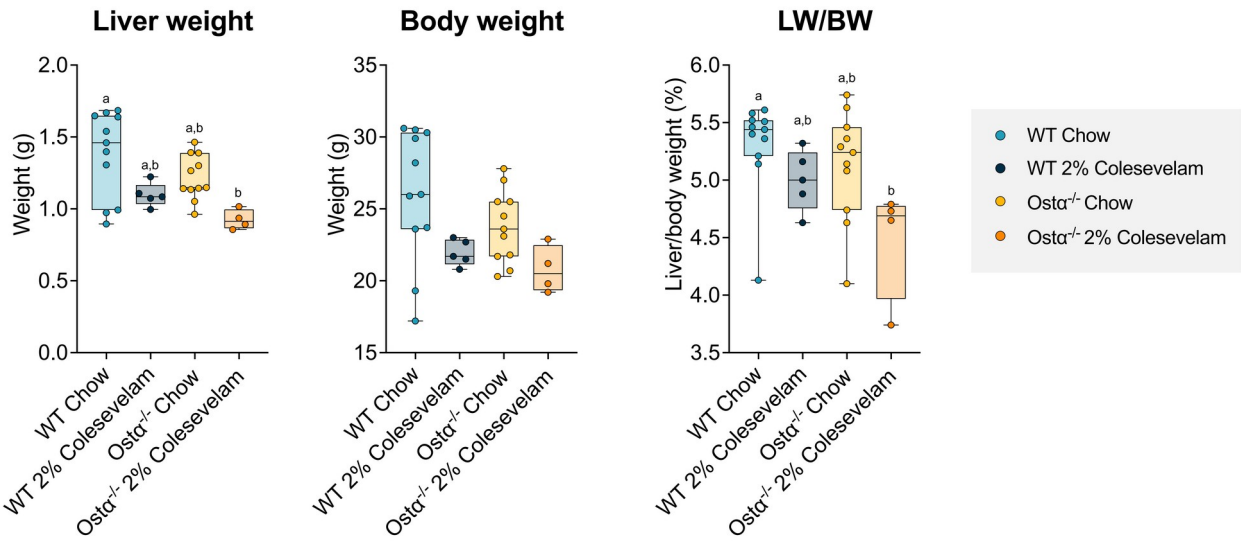

Supplemental Figure S3. Changes in liver and body weight in *Ostα*$^{-/-}$ and WT mice following 4 weeks of 2% Colesevelam feeding.

Median values (line), interquartile range (boxes), and min to max values (whiskers) are shown, n = 4-11 mice per group. Distinct lowercase letters indicate significant differences between groups ($P < 0.05$).

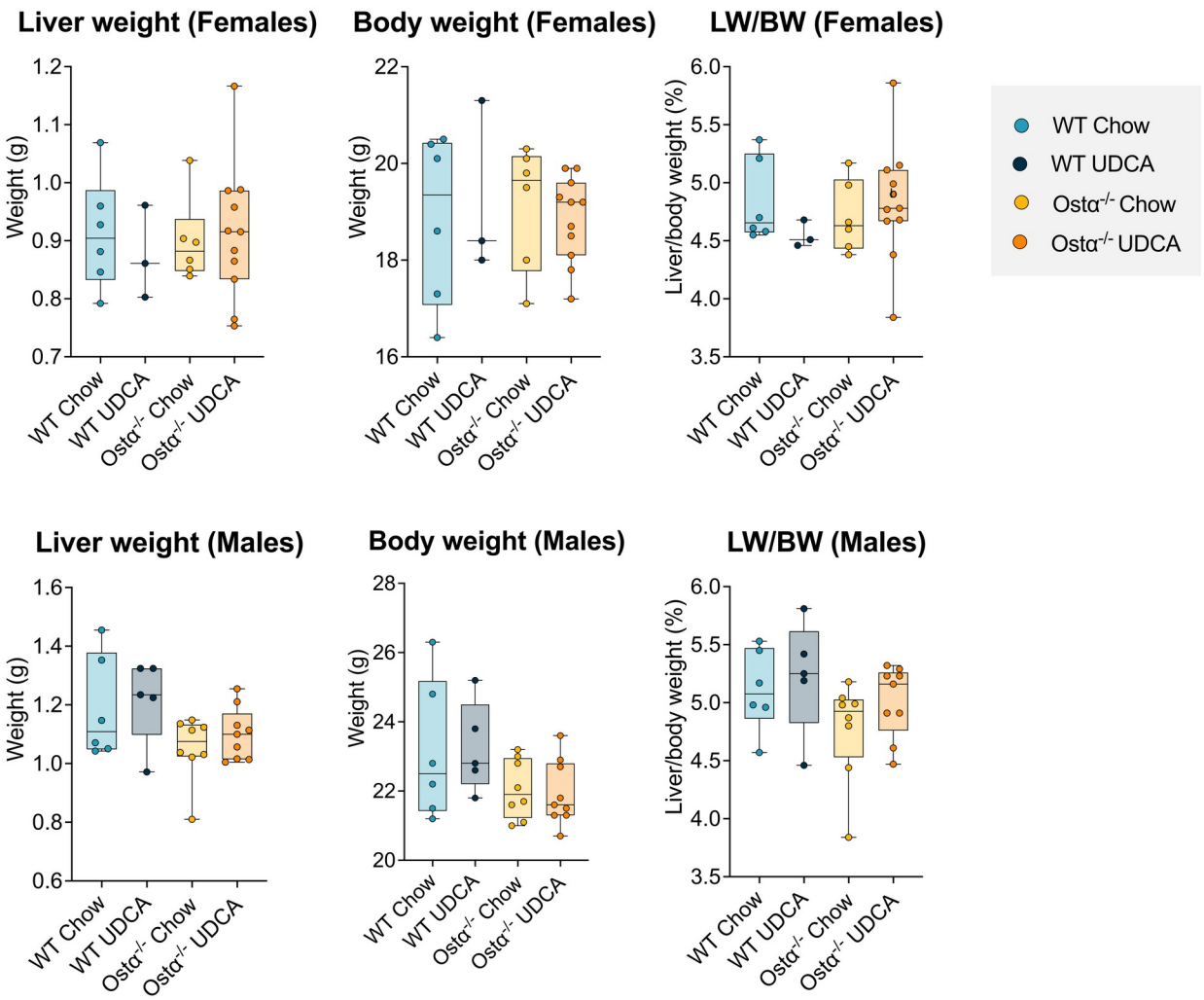

Supplemental Figure S4. Changes in liver and body weight in *Ostα*$^{-/-}$ and WT mice following 6 weeks of 0.2% UDCA feeding

Median values (line), interquartile range (boxes), and min to max values (whiskers) are shown, n = 10 – 12 mice per group.

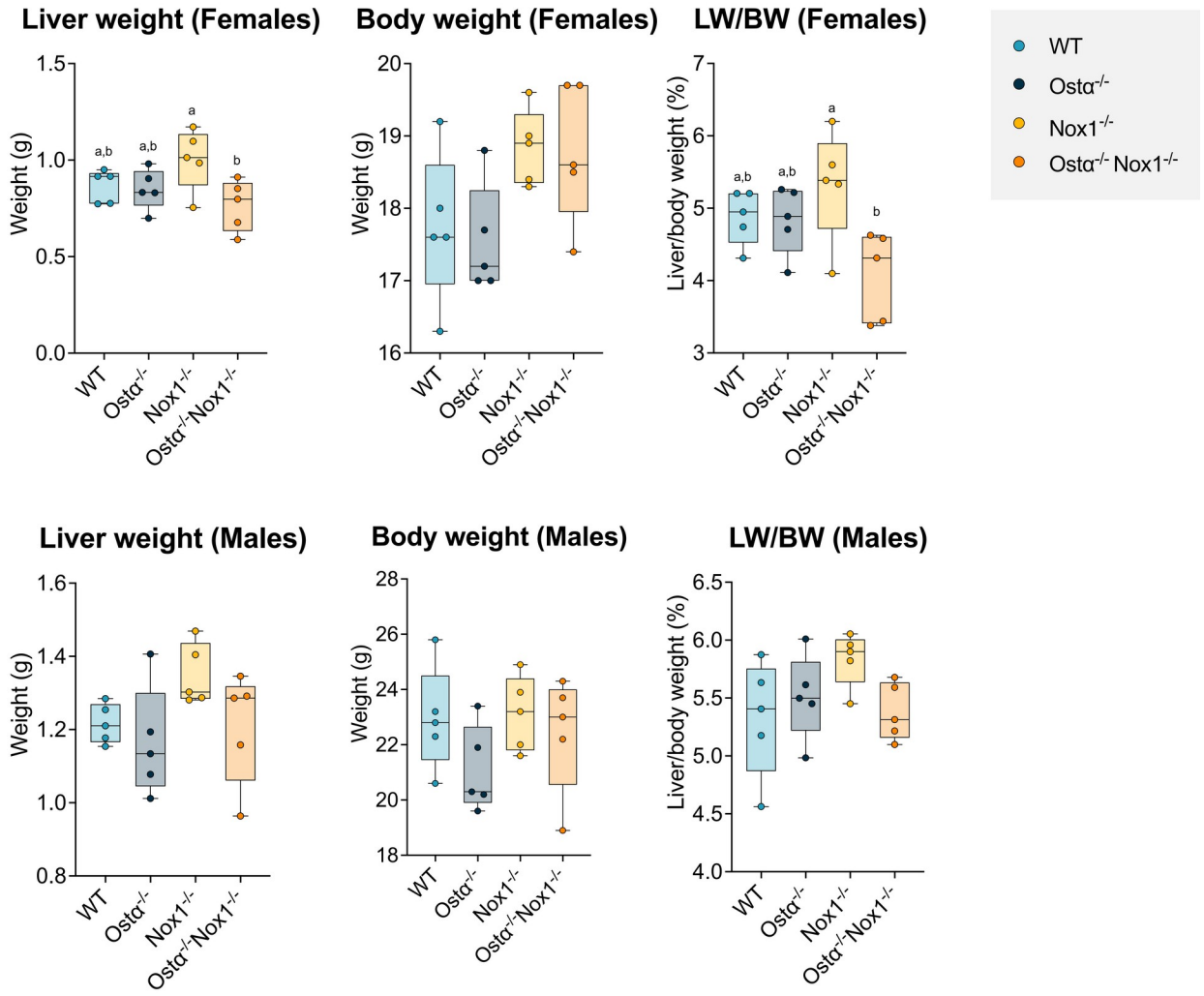

Supplemental Figure S5. Changes in liver and body weight in WT, *Ostα*$^{-/-}$, *Nox1*$^{-/-}$ and *Ostα*$^{-/-}$/*Nox1*$^{-/-}$ mice on chow

Median values (line), interquartile range (boxes), and min to max values (whiskers) are shown, n = 10 – 12 mice per group. Distinct lowercase letters indicate significant differences between groups ($P < 0.05$).

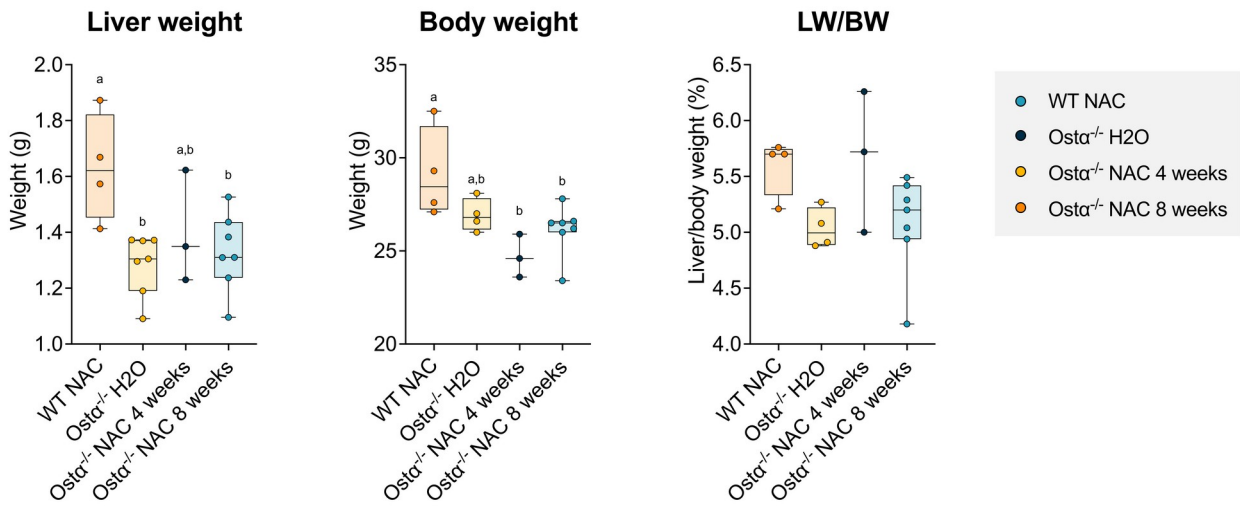

Supplemental Figure S6. Changes in liver and body weight in WT and *Ostα*$^{-/-}$ mice following NAC treatment for 4 and 8 weeks

Median values (line), interquartile range (boxes), and min to max values (whiskers) are shown, n = 3 – 5 mice per group. Distinct lowercase letters indicate significant differences between groups ($P < 0.05$).

References

1. Dawson PA, and Karpen SJ. Intestinal transport and metabolism of bile acids. *J Lipid Res* 56: 1085-1099, 2015.
2. Dawson PA, Lan T, and Rao A. Bile acid transporters. *J Lipid Res* 50: 2340-2357, 2009.
3. Halilbasic E, Claudel T, and Trauner M. Bile acid transporters and regulatory nuclear receptors in the liver and beyond. *J Hepatol* 58: 155-168, 2013.
4. Oelkers P, Kirby LC, Heubi JE, and Dawson PA. Primary bile acid malabsorption caused by mutations in the ileal sodium-dependent bile acid transporter gene (SLC10A2). *J Clin Invest* 99: 1880-1887, 1997.
5. Dawson PA, Haywood J, Craddock AL, Wilson M, Tietjen M, Kluckman K, Maeda N, and Parks JS. Targeted deletion of the ileal bile acid transporter eliminates enterohepatic cycling of bile acids in mice. *J Biol Chem* 278: 33920-33927, 2003.
6. Rao A, Haywood J, Craddock AL, Belinsky MG, Kruh GD, and Dawson PA. The organic solute transporter alpha-beta, Ostalpha-Ostbeta, is essential for intestinal bile acid transport and homeostasis. *Proc Natl Acad Sci U S A* 105: 3891-3896, 2008.
7. Ballatori N, Fang F, Christian WV, Li N, and Hammond CL. Ostalpha-Ostbeta is required for bile acid and conjugated steroid disposition in the intestine, kidney, and liver. *Am J Physiol Gastrointest Liver Physiol* 295: G179-G186, 2008.
8. Dawson PA, Hubbert M, Haywood J, Craddock AL, Zerangue N, Christian WV, and Ballatori N. The heteromeric organic solute transporter alpha-beta, Ostalpha-Ostbeta, is an ileal basolateral bile acid transporter. *J Biol Chem* 280: 6960-6968, 2005.

9. Lan T, Rao A, Haywood J, Kock ND, and Dawson PA. Mouse organic solute transporter alpha deficiency alters FGF15 expression and bile acid metabolism. *J Hepatol* 57: 359-365, 2012.

10. Ferrebee CB, Li J, Haywood J, Pachura K, Robinson BS, Hinrichs BH, Jones RM, Rao A, and Dawson PA. Organic Solute Transporter alpha-beta Protects Ileal Enterocytes From Bile Acid-Induced Injury. *Cell Mol Gastroenterol Hepatol* 5: 499-522, 2018.

11. Naini BV, Souza RF, and Odze RD. Barrett's Esophagus: A Comprehensive and Contemporary Review for Pathologists. *Am J Surg Pathol* 40: e45-66, 2016.

12. Ma Q. Role of nrf2 in oxidative stress and toxicity. *Annu Rev Pharmacol Toxicol* 53: 401-426, 2013.

13. Catapano AL, Reiner Z, De Backer G, Graham I, Taskinen MR, Wiklund O, Agewall S, Alegria E, Chapman M, Durrington P, Erdine S, Halcox J, Hobbs R, Kjekshus J, Filardi PP, Riccardi G, Storey RF, Wood D, European Society of C, and European Atherosclerosis S. ESC/EAS Guidelines for the management of dyslipidaemias The Task Force for the management of dyslipidaemias of the European Society of Cardiology (ESC) and the European Atherosclerosis Society (EAS). *Atherosclerosis* 217: 3-46, 2011.

14. Hermankova E, Zak A, Polakova L, Hobzova R, Hromadka R, and Sirc J. Polymeric bile acid sequestrants: Review of design, in vitro binding activities, and hypocholesterolemic effects. *Eur J Med Chem* 144: 300-317, 2018.

15. Karpen SJ, Kelly D, Mack C, and Stein P. Ileal bile acid transporter inhibition as an anticholestatic therapeutic target in biliary atresia and other cholestatic disorders. *Hepatol Int* 14: 677-689, 2020.

16. Gonzales E, Hardikar W, Stormon M, Baker A, Hierro L, Gliwicz D, Lacaille F, Lachaux A, Sturm E, Setchell KDR, Kennedy C, Dorenbaum A, Steinmetz J, Desai NK, Wardle AJ, Garner W, Vig P, Jaecklin T, Sokal EM, and Jacquemin E. Efficacy and safety of maralixibat treatment in patients with Alagille syndrome and cholestatic pruritus (ICONIC): a randomised phase 2 study. *Lancet* 398: 1581-1592, 2021.

17. Thompson RJ, Arnell H, Artan R, Baumann U, Calvo PL, Czubkowski P, Dalgic B, D'Antiga L, Durmaz O, Fischler B, Gonzales E, Grammatikopoulos T, Gupte G, Hardikar W, Houwen RHJ, Kamath BM, Karpen SJ, Kjems L, Lacaille F, Lachaux A, Lainka E, Mack CL, Mattsson JP, McKiernan P, Ozen H, Rajwal SR, Roquelaure B, Shagrani M, Shteyer E, Soufi N, Sturm E, Tessier ME, Verkade HJ, and Horn P. Odevixibat treatment in progressive familial intrahepatic cholestasis: a randomised, placebo-controlled, phase 3 trial. *Lancet Gastroenterol Hepatol* 2022.

18. Fuchs CD, Paumgartner G, Mlitz V, Kunczer V, Halilbasic E, Leditznig N, Wahlstrom A, Stahlman M, Thuringer A, Kashofer K, Stojakovic T, Marschall HU, and Trauner M. Colesevelam attenuates cholestatic liver and bile duct injury in Mdr2(-/-) mice by modulating composition, signalling and excretion of faecal bile acids. *Gut* 67: 1683-1691, 2018.

19. Aldridge MA, and Ito MK. Colesevelam hydrochloride: a novel bile acid-binding resin. *Ann Pharmacother* 35: 898-907, 2001.

20. Feng Y, Li Q, Ou G, Yang M, and Du L. Bile acid sequestrants: a review of mechanism and design. *J Pharm Pharmacol* 73: 855-861, 2021.

21. Luner PE, and Amidon GL. Equilibrium and kinetic factors influencing bile sequestrant efficacy. *Pharm Res* 9: 670-676, 1992.

22. Trauner M, and Graziadei IW. Review article: mechanisms of action and therapeutic applications of ursodeoxycholic acid in chronic liver diseases. *Alimentary pharmacology & therapeutics* 13: 979-996, 1999.

23. Poupon R, and Poupon RE. Ursodeoxycholic acid therapy of chronic cholestatic conditions in adults and children. *Pharmacology & therapeutics* 66: 1-15, 1995.

24. Beuers U, Boyer JL, and Paumgartner G. Ursodeoxycholic acid in cholestasis: potential mechanisms of action and therapeutic applications. *Hepatology* 28: 1449-1453, 1998.

25. Van Nieuwkerk CM, Elferink RP, Groen AK, Ottenhoff R, Tytgat GN, Dingemans KP, Van Den Bergh Weerman MA, and Offerhaus GJ. Effects of Ursodeoxycholate and cholate feeding on liver disease in FVB mice with a disrupted mdr2 P-glycoprotein gene. *Gastroenterology* 111: 165-171, 1996.

26. van Nieuwerk CM, Groen AK, Ottenhoff R, van Wijland M, van den Bergh Weerman MA, Tytgat GN, Offerhaus JJ, and Oude Elferink RP. The role of bile salt composition in liver pathology of mdr2 (-/-) mice: differences between males and females. *J Hepatol* 26: 138-145, 1997.

27. Ward JBJ, Lajczak NK, Kelly OB, O'Dwyer AM, Giddam AK, Ni Gabhann J, Franco P, Tambuwala MM, Jefferies CA, Keely S, Roda A, and Keely SJ. Ursodeoxycholic acid and lithocholic acid exert anti-inflammatory actions in the colon. *Am J Physiol Gastrointest Liver Physiol* 312: G550-G558, 2017.

28. Rodriguez VA, Rivoira MA, Perez Adel V, Marchionatti AM, and Tolosa de Talamoni NG. Ursodeoxycholic and deoxycholic acids: Differential effects on intestinal Ca(2+) uptake, apoptosis and autophagy of rat intestine. *Arch Biochem Biophys* 591: 28-34, 2016.

29. Takahashi S, Fukami T, Masuo Y, Brocker CN, Xie C, Krausz KW, Wolf CR, Henderson CJ, and Gonzalez FJ. Cyp2c70 is responsible for the species difference in bile acid metabolism between mice and humans. *J Lipid Res* 57: 2130-2137, 2016.

30. Honda A, Miyazaki T, Iwamoto J, Hirayama T, Morishita Y, Monma T, Ueda H, Mizuno S, Sugiyama F, Takahashi S, and Ikegami T. Regulation of bile acid metabolism in mouse models with hydrophobic bile acid composition. *J Lipid Res* 61: 54-69, 2020.

31. Straniero S, Laskar A, Savva C, Hardfeldt J, Angelin B, and Rudling M. Of mice and men: murine bile acids explain species differences in the regulation of bile acid and cholesterol metabolism. *J Lipid Res* 61: 480-491, 2020.

32. Oteng AB, Higuchi S, Banks AS, and Haeusler RA. Cyp2c-deficiency depletes muricholic acids and protects against high-fat diet-induced obesity in male mice but promotes liver damage. *Mol Metab* 53: 101326, 2021.

33. de Boer JF, de Vries HD, Palmiotti A, Li R, Doestzada M, Hoogerland JA, Fu J, La Rose AM, Westerterp M, Mulder NL, Hovingh MV, Koehorst M, Kloosterhuis NJ, Wolters JC, Bloks VW, Haas JT, Dombrowicz D, Staels B, van de Sluis B, and Kuipers F. Cholangiopathy and Biliary Fibrosis in Cyp2c70-Deficient Mice Are Fully Reversed by Ursodeoxycholic Acid. *Cell Mol Gastroenterol Hepatol* 11: 1045-1069, 2021.

34. de Boer JF, Verkade E, Mulder NL, de Vries HD, Huijkman N, Koehorst M, Boer T, Wolters JC, Bloks VW, van de Sluis B, and Kuipers F. A human-like bile acid pool induced by deletion of hepatic Cyp2c70 modulates effects of FXR activation in mice. *J Lipid Res* 61: 291-305, 2020.

35. Rao A, Kosters A, Mells JE, Zhang W, Setchell KD, Amanso AM, Wynn GM, Xu T, Keller BT, Yin H, Banton S, Jones DP, Wu H, Dawson PA, and Karpen SJ. Inhibition of

ileal bile acid uptake protects against nonalcoholic fatty liver disease in high-fat diet-fed mice. *Science translational medicine* 8: 357ra122, 2016.

36. Truong JK, Bennett AL, Klindt C, Donepudi AC, Malla SR, Pachura KJ, Zaufel A, Moustafa T, Dawson PA, and Karpen SJ. Ileal bile acid transporter inhibition in Cyp2c70 KO mice ameliorates cholestatic liver injury. *J Lipid Res* 63: 100261, 2022.

37. Fang Y, Han SI, Mitchell C, Gupta S, Studer E, Grant S, Hylemon PB, and Dent P. Bile acids induce mitochondrial ROS, which promote activation of receptor tyrosine kinases and signaling pathways in rat hepatocytes. *Hepatology* 40: 961-971, 2004.

38. Chu SH, Lee-Kang J, Lee KH, and Lee K. Roles of reactive oxygen species, NF-kappaB, and peroxiredoxins in glycochenodeoxycholic acid-induced rat hepatocytes death. *Pharmacology* 69: 12-19, 2003.

39. Yerushalmi B, Dahl R, Devereaux MW, Gumpricht E, and Sokol RJ. Bile acid-induced rat hepatocyte apoptosis is inhibited by antioxidants and blockers of the mitochondrial permeability transition. *Hepatology* 33: 616-626, 2001.

40. Czaja MJ. Induction and regulation of hepatocyte apoptosis by oxidative stress. *Antioxid Redox Signal* 4: 759-767, 2002.

41. Perez MJ, and Briz O. Bile-acid-induced cell injury and protection. *World J Gastroenterol* 15: 1677-1689, 2009.

42. Palmeira CM, and Rolo AP. Mitochondrially-mediated toxicity of bile acids. *Toxicology* 203: 1-15, 2004.

43. Woolbright BL, and Jaeschke H. Novel insight into mechanisms of cholestatic liver injury. *World J Gastroenterol* 18: 4985-4993, 2012.

44. Cai SY, Ouyang X, Chen Y, Soroka CJ, Wang J, Mennone A, Wang Y, Mehal WZ, Jain D, and Boyer JL. Bile acids initiate cholestatic liver injury by triggering a hepatocyte-specific inflammatory response. *JCI Insight* 2: e90780, 2017.

45. Aviello G, and Knaus UG. ROS in gastrointestinal inflammation: Rescue Or Sabotage? *Br J Pharmacol* 174: 1704-1718, 2017.

46. Lambeth JD, and Neish AS. Nox enzymes and new thinking on reactive oxygen: a double-edged sword revisited. *Annu Rev Pathol* 9: 119-145, 2014.

47. Zhdanov AV, Aviello G, Knaus UG, and Papkovsky DB. Cellular ROS imaging with hydro-Cy3 dye is strongly influenced by mitochondrial membrane potential. *Biochim Biophys Acta* 1861: 198-204, 2017.

48. Yasuda M, Kato S, Yamanaka N, Iimori M, Utsumi D, Kitahara Y, Iwata K, Matsuno K, Amagase K, Yabe-Nishimura C, and Takeuchi K. Potential role of the NADPH oxidase NOX1 in the pathogenesis of 5-fluorouracil-induced intestinal mucositis in mice. *Am J Physiol Gastrointest Liver Physiol* 302: G1133-1142, 2012.

49. Esworthy RS, Kim BW, Chow J, Shen B, Doroshow JH, and Chu FF. Nox1 causes ileocolitis in mice deficient in glutathione peroxidase-1 and -2. *Free Radic Biol Med* 68: 315-325, 2014.

50. Leoni G, Alam A, Neumann PA, Lambeth JD, Cheng G, McCoy J, Hilgarth RS, Kundu K, Murthy N, Kusters D, Reutelingsperger C, Perretti M, Parkos CA, Neish AS, and Nusrat A. Annexin A1, formyl peptide receptor, and NOX1 orchestrate epithelial repair. *J Clin Invest* 123: 443-454, 2013.

51. Samuni Y, Goldstein S, Dean OM, and Berk M. The chemistry and biological activities of N-acetylcysteine. *Biochim Biophys Acta* 1830: 4117-4129, 2013.

52. Shukla PK, Gangwar R, Manda B, Meena AS, Yadav N, Szabo E, Balogh A, Lee SC, Tigyi G, and Rao R. Rapid disruption of intestinal epithelial tight junction and barrier dysfunction by ionizing radiation in mouse colon in vivo: protection by N-acetyl-l-cysteine. *Am J Physiol Gastrointest Liver Physiol* 310: G705-715, 2016.

53. Forsyth CB, Voigt RM, Shaikh M, Tang Y, Cederbaum AI, Turek FW, and Keshavarzian A. Role for intestinal CYP2E1 in alcohol-induced circadian gene-mediated intestinal hyperpermeability. *Am J Physiol Gastrointest Liver Physiol* 305: G185-195, 2013.

54. Cha H, Lee S, Hwan Kim S, Kim H, Lee DS, Lee HS, Lee JH, and Park JW. Increased susceptibility of IDH2-deficient mice to dextran sodium sulfate-induced colitis. *Redox Biol* 13: 32-38, 2017.

55. Reliene R, Goad ME, and Schiestl RH. Developmental cell death in the liver and newborn lethality of Ku86 deficient mice suppressed by antioxidant N-acetyl-cysteine. *DNA Repair (Amst)* 5: 1392-1397, 2006.

56. Weerachayaphorn J, Mennone A, Soroka CJ, Harry K, Hagey LR, Kensler TW, and Boyer JL. Nuclear factor-E2-related factor 2 is a major determinant of bile acid homeostasis in the liver and intestine. *Am J Physiol Gastrointest Liver Physiol* 302: G925-936, 2012.

57. Suzuki T, and Yamamoto M. Molecular basis of the Keap1-Nrf2 system. *Free Radic Biol Med* 88: 93-100, 2015.

58. Li T, and Chiang JY. Nuclear receptors in bile acid metabolism. *Drug Metab Rev* 45: 145-155, 2013.

59. Chen P, Zeng H, Wang Y, Fan X, Xu C, Deng R, Zhou X, Bi H, and Huang M. Low dose of oleanolic acid protects against lithocholic acid-induced cholestasis in mice: potential

involvement of nuclear factor-E2-related factor 2-mediated upregulation of multidrug resistance-associated proteins. *Drug Metab Dispos* 42: 844-852, 2014.

60. Pang C, Zheng Z, Shi L, Sheng Y, Wei H, Wang Z, and Ji L. Caffeic acid prevents acetaminophen-induced liver injury by activating the Keap1-Nrf2 antioxidative defense system. *Free Radic Biol Med* 91: 236-246, 2016.

61. Sun W, Yan C, Frost B, Wang X, Hou C, Zeng M, Gao H, Kang Y, and Liu J. Pomegranate extract decreases oxidative stress and alleviates mitochondrial impairment by activating AMPK-Nrf2 in hypothalamic paraventricular nucleus of spontaneously hypertensive rats. *Sci Rep* 6: 34246, 2016.

62. Shen K, Feng X, Pan H, Zhang F, Xie H, and Zheng S. Baicalin Ameliorates Experimental Liver Cholestasis in Mice by Modulation of Oxidative Stress, Inflammation, and NRF2 Transcription Factor. *Oxid Med Cell Longev* 2017: 6169128, 2017.

Chapter 5: Discussion and Future Directions

Sections of this chapter are adapted from below with permission from Elsevier Science:

Truong, J. K., & Dawson, P.A. (2021) Bile Acid Metabolism. In N. Ridgway & R. McLeod (Eds). *Biochemistry of Lipids, Lipoproteins and Membranes* (pp. 395-428). Elsevier Science.

Impact and Significance

Investigation from 2015 to 2022 has uncovered additional details involving the pathways for bile acid synthesis, transport, signaling and the regulation of their metabolism. With regard to bile acid synthesis, identification of the murine enzymes responsible for the 6-hydroxylation (*Cyp2c70*) and 7-rehydroxylation (*Cyp2a12*) of bile acids represented important breakthroughs in the field (1). There are substantial differences in the bile acid pool composition between mice and humans, with mice making more hydrophilic and less-injurious bile acid species. This has long hampered our ability to use the mouse to study the role of bile acids in human disease. However, the generation and characterization of the *Cyp2c70* KO and *Cyp2c70*-*Cyp2a12* double KO mouse models have begun to address the long-standing challenge of modeling of role of bile acid retention and cytotoxicity in human cholestatic diseases. This breakthrough is predicted to yield novel insights to the connection between bile acids and human metabolic, liver, and gastrointestinal disease and to promote the development of new therapies.

The concept that cholehepatic shunting can improve delivery of therapeutic compounds to bile acid ducts has considerable potential but may restricted in part by the expression of transporters involved in their uptake by hepatocytes and biliary epithelial cells. Our studies found that the major bile acid transporters were not required for the potent bicarbonate-rich hypercholeresis induced by *nor*UDCA, and indirectly support the hypothesis that cholehepatic shunting of *nor*UDCA is mediated by passive diffusion. Moreover, our results suggest that the intestinal absorption and choleheptic distribution of *nor*UDCA is transporter-independent, with the fate of *nor*UDCA being controlled by its Phase 2 metabolism (primarily glucuronidation) and excreted in the urine or feces. Although *nor*UDCA does not behave like a native C-24 bile acid for its distribution in the enterohepatic circulation and its hepatic/intestinal metabolism, we show

for the first time that *nor*UDCA potently stimulates the Ca^{+}-activated Cl^{-} channel TMEM16A, similar to native bile acids such as TUDCA. The discovery of TMEM16A dependent *nor*UDCA-induced chloride secretion that is bile acid transporter-independent yields new insights to the superior ability of *nor*UDCA versus hydrophilic C-24 bile acids such as TUDCA to induce a bicarbonate-rich hypercholeresis. In our current model, *nor*UDCA stimulates extracellular ATP-release and P2 purinergic receptor signaling through the IP3 receptor, resulting in cytosolic Ca^{2+} release and TMEM16A Cl^{-} secretion. The Cl^{-} secreted by TMEM16 then stimulates bicarbonate secretion via the plasma membrane Cl^{-}/bicarbonate exchanger AE2 (*SLC4A2*) (2-4). Interestingly, biliary bicarbonate secretion and stimulation of biliary bile flow induced by *nor*UDCA is partly CFTR-dependent (5), suggesting that there are additional mechanisms by which *nor*UDCA may be stimulating ATP release or bicarbonate secretion.

Future Directions

I predict that the use of *Cyp2c70* KO mice as an experimental model will shed new light on the role of hydrophobic bile acids in other cholestatic diseases such as the different forms of progressive familial intrahepatic cholestasis (PFIC), primary biliary cholangitis, primary sclerosing cholangitis, Alagille syndrome, biliary atresia, and intrahepatic cholestasis of pregnancy (ICP). With regard to ICP, we and others have observed that the liver injury is more severe in female *Cyp2c70* KO mice, although the underlying cause for the sex differences remain largely unexplained. The absence of liver phenotypic differences between male and female during early postnatal development suggest the involvement of sex hormones in the more rapid and serious liver disease progression in female *Cyp2c70* KO. Male-female difference in bile acid metabolism have been reported for humans and mice but are poorly understood. An important

sex difference in *Cyp2c70* KO mice is the more significant reduction in 12-hydroxylated bile acid synthesis in the female. Interestingly, expression of the rate-limiting enzyme for synthesis of 12-hydroxylated bile acids, *Cyp8b1*, has been shown to be repressed by estrogen (6), providing clues to the potential mechanism. In addition, females have a larger bile acid pool size per unit body weight versus males. As such, if there exists a hepatic bile acid content threshold to induce liver injury, females may exceed that boundary more readily than males. In humans, approximately a quarter of pregnant woman develop ICP, which is commonly diagnosed after hormones are elevated in the third trimester and resolves quickly after delivery when placental hormone production ceases. Pruritis (itching) is a clinically significant symptom present in ICP and other cholestatic disease patients. Despite intensive investigation, the molecular mechanisms by which bile acids trigger pruritus remain unclear. With the *Cyp2c70* KO mouse, the field will be more well equipped to answer these questions.

The studies performed in Chapter 4 demonstrating that *nor*UDCA stimulates the Ca^{2+}-activated Cl^- channel TMEM16A in mouse cholangiocytes leaves many new questions to be explored. It is not known if other side chain-shortened C-23 *nor*-bile acids behave similarly, or if *nor*UDCA can stimulate other channels such as CFTR or LRRC8A, a volume-activated Cl^- channel recently identified in cholangiocytes. The questions of how *nor*UDCA is secreted into bile or if there a role for any other membrane transporter in the uptake and export of *nor*UDCA still remain to be answered. Although we were able to successfully show that the major bile acid carriers ASBT, OSTα-OSTβ, and OATP1a/1b transporters are not required for orally administered *nor*UDCA to stimulate a bicarbonate-rich hypercholeresis, there were additional transporters whose expression was induced by *nor*UDCA treatment that we did not pursue. However, based on the physicochemical properties of norUDCA, our findings, and the weight of

evidence in the literature, we conclude that the cholehepatic shunting of norUDCA is maintained by passive membrane diffusion.

Additionally, other unexpected properties of *nor*UDCA were discovered. Unlike other bile acids that are efficiently sequestered by Colesevelam, it was surprising that *nor*UDCA showed little apparent binding to the resin, despite only a one carbon difference from the endogenous ursodeoxycholic acid. This result challenged our curiosity, and we were interested in testing if *nor*UDCA was sequestered by other bile acid resins. Early investigations I conducted suggest that *nor*UDCA does not bind to other clinically administrated sequestrants such as colestipol or cholestyramine. From that, I also discovered that unique bile acids have different binding affinities to resins and lead me to wonder what specific property was influencing the BA's ability to be sequestrated. Pilot data I generated did not show any obvious trends, but it would be interesting to follow up and explore the basis, which allows *nor*UDCA to evade being bound by these first and second generation bile acid sequestrants.

Despite our efforts described in Chapter 4, the molecular mechanisms by which enterocytes withstand bile acid injury still remain unclear. In our model of intestinal bile acid stasis, we systematically tested various therapeutic approaches to interrogate components our model for ileal phenotype in *Ostα* KO mice. The absence of a significant effect of UDCA on the villus structures in *Ostα* KO mice could be attributed to the hydrophilic muricholate-rich bile acid pool in these mice. Thus, increasing the amount of UDCA in the bile acid pool has a minimal effect on the overall hydrophobicity. This could be tested using a *Ostα*$^{-/-}$*/Cyp2c70*$^{-/-}$ mouse model, which we predict would show more severe ileal injury versus mice lacking *Ostα* alone. In our studies, ablating of Nox1 and NAC feeding did not have a large effect on the ileal phenotype in *Ostα*$^{-/-}$ mice. These data suggest that ROS is driving the ileal phenotype and other

factors may be involved in the induction of Nrf target genes and ileal phenotype observed in the *Ostα* KO mice. To approach this question, we predicted that knocking out *Nrf2* would be protective in our intestinal stasis model by interrupting the antioxidant response to protect against oxidative damage. However, early phenotyping of intestine *Nrf2*$^{-/-}$/*Ostα*$^{-/-}$ mice suggested that there was no change in *Ostα*$^{-/-}$ ileal morphology upon ablation of *Nrf2*. In the *Ostα* model, the ileal enterocytes appear to have a protective mechanism or undergo a constant injury and restitution response to protect themselves from bile acid induced damage. It is certainly possible that mice are protected from more severe bile acid injury due to the very high turnover of the intestinal epitheial cells in the ileum versus more long-lived hepatocytes or cholangiocytes.

Beyond the liver and biliary tract, there is growing evidence that bile acids play a role in the kidney injury observed in patients with high circulating levels of bile acids and liver disease (7, 8). This presents a broader application of the therapeutics currently used to treat BA-related injuries and opens the possibilities of co-treating for cholestatic liver diseases. Additionally, recent advancement in our knowledge of therapeutic molecular targets and etiologies for several liver diseases has encouraged the use of bile acid-based therapies.

Final Thoughts

With regard to bile acid transport in the enterohepatic circulation, many questions remain to be answered regarding the intracellular movement and compartmentalization of bile acids. There have been recent advances in our understanding of intracellular cholesterol transport, such as the discovery of the Aster proteins. Similar studies are needed to extend our understanding of the molecular pathways for directing lipoprotein-derived cholesterol into the bile acid biosynthetic pathway and the intracellular trafficking of bile acids, their biosynthetic

intermediates, and bile acid analogs. An exciting byproduct of this line of investigation is predicted to be further insights into the molecular mechanisms by which different bile acid species are delivered to and engage intracellular targets. These targets include nuclear receptors such as FXR, PXR, and VDR, transcription factors such as yes-associated protein 1 (YAP), and as yet unidentified mediators of bile acid signaling or cytotoxicity.

Over the next five years, high through-put sequencing technology and gene chips for cholestatic liver disease will identify additional patients with inborn errors in the major bile acid biosynthesis and transporter genes, but also identify novel genes involved in bile acid homeostasis and human disease. Other areas of future investigation will include the interaction of bile acids with the microbiome, bile acid signaling particularly in immune cells in the gut and liver, and on the complex role of bile acids in the regulation of lipid, carbohydrate, and energy metabolism. These pathways provide promising targets for pharmacological intervention in a variety of liver, gastrointestinal and metabolic diseases, and will garner considerable attention within and outside the bile acid field. Clearly, bile acids are much more than simple detergents and much remains to be discovered.

References

1. Takahashi S, Fukami T, Masuo Y, Brocker CN, Xie C, Krausz KW, Wolf CR, Henderson CJ, and Gonzalez FJ. Cyp2c70 is responsible for the species difference in bile acid metabolism between mice and humans. *J Lipid Res* 57: 2130-2137, 2016.

2. Li Q, Dutta A, Kresge C, Bugde A, and Feranchak AP. Bile acids stimulate cholangiocyte fluid secretion by activation of transmembrane member 16A Cl(-) channels. *Hepatology* 68: 187-199, 2018.

3. Boyer JL, and Soroka CJ. Bile formation and secretion: An update. *J Hepatol* 75: 190-201, 2021.

4. Dutta AK, Woo K, Doctor RB, Fitz JG, and Feranchak AP. Extracellular nucleotides stimulate Cl- currents in biliary epithelia through receptor-mediated IP3 and Ca2+ release. *Am J Physiol Gastrointest Liver Physiol* 295: G1004-1015, 2008.

5. Halilbasic E, Fiorotto R, Fickert P, Marschall HU, Moustafa T, Spirli C, Fuchsbichler A, Gumhold J, Silbert D, Zatloukal K, Langner C, Maitra U, Denk H, Hofmann AF, Strazzabosco M, and Trauner M. Side chain structure determines unique physiologic and therapeutic properties of norursodeoxycholic acid in Mdr2-/- mice. *Hepatology* 49: 1972-1981, 2009.

6. Koopen NR, Post SM, Wolters H, Havinga R, Stellaard F, Boverhof R, Kuipers F, and Princen HM. Differential effects of 17alpha-ethinylestradiol on the neutral and acidic pathways of bile salt synthesis in the rat. *J Lipid Res* 40: 100-108, 1999.

7. Fickert P, Krones E, Pollheimer MJ, Thueringer A, Moustafa T, Silbert D, Halilbasic E, Yang M, Jaeschke H, Stokman G, Wells RG, Eller K, Rosenkranz AR, Eggertsen G,

Wagner CA, Langner C, Denk H, and Trauner M. Bile acids trigger cholemic nephropathy in common bile-duct-ligated mice. *Hepatology* 58: 2056-2069, 2013.

8. Krones E, Pollheimer MJ, Rosenkranz AR, and Fickert P. Cholemic nephropathy - Historical notes and novel perspectives. *Biochim Biophys Acta* 2017.